A STUDY OF CALCIUM CARBONATE FORMATION

IN BIOLOGICAL SYSTEMS

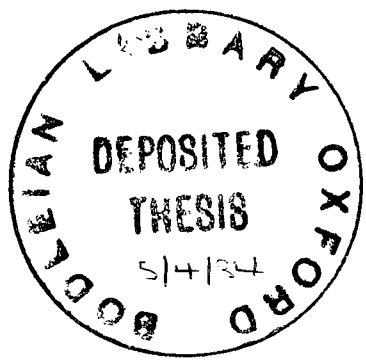

A thesis submitted in partial fulfilment of the requirement for the degree of Doctor of Philosophy

Stephen Barry Parker

Wolfson College

Oxford

1983

Abstract

A STUDY OF CALCIUM CARBONATE FORMATION

IN BIOLOGICAL SYSTEMS

Stephen B. Parker, Wolfson College, Oxford

Submitted for the Degree of Doctor of Philosophy

Trinity Term, 1983

This thesis has studied aspects of biomineralisation, covering the inorganic mineral, the organic matrix, the possible use of phospholipid bilayer vesicles to control mineralisation, calcium and other metal binding to an antibiotic ionophore, Lasalocid-A and a study of a known inhibitor of biomineralisation, the glycopeptide antifreeze found in the plasma of fish which live under polar conditions. The mineral systems studied have been calcium carbonate formations in otoconia and otoliths, crystals which form part of the balance organs of the inner ear, and coccoliths, the earliest eukariotic formation of calcium carbonate, from an alga. Both these systems have been studied by ultra-high resolution electron microscopy with the observation that both types of structures grow in a unique manner, quite distinct from their geological counterparts; indeed the coccolith system involves two distinct mechanisms of growth for different partsof its structure, which is only 2 μm in diameter. Mechanisms of growth of both biominerals are proposed. The study of the organic matrix was less successful in that it was not possible to fully characterise an acidic matrix protein, but it has been shown that the soluble matrix consists of many polypeptide chains cross-linked together, which undergo a conformational change on dissolution from the insoluble matrix on which they lie *in vivo* and consequently give *in vitro* results which do not mimic the *in vivo* condition. Equally, the use of vesicles to control the formation of calcium carbonate was shown to be possible on occasion, but lipids are very unstable in the presence of calcium and no means of stabilising the system to produce consistent results was determined.

Two studies were made by ^{1}H-nmr, the metal-ion complexes of the ionophore Lasalocid-A and the antifreeze glycopeptide of polar fish, in order to demonstrate principles of the handing of isolated ions and of crystallisation inhibition. In both cases, the biological action of the system was mimicked and followed by nmr and a mechanism for their function proposed.

Acknowledgements

I would like to thank my supervisor, Professor R.J.P. Williams, FRS, for his advice and encouragement throughout this work.

Dr A.J. Skarnulis helped with electron microscopy and advice on all crystallographic aspects of the project; Dr S. Mann introduced me to electron microscopy.

Two academic visitors worked with me on different parts of the work, Professor M.D. Ross and Professor G.W. Everett; I would like to express my appreciation to them both for their stimulating contributions.

Many people in the RJPW and HAOH research groups have contributed with practical help and suggestions. In particular, I would like to thank David Dalgarno, Monika Green, Joe Bannister, Barry Levine, Fraser Armstrong, who introduced me to 'Chrono-' techniques of protein preparations, and all in the 'Friday-lunchtime seminar group'.

Tina Diggines happily coped with the second generation in typing this thesis.

The SERC provided me with a research studentship to support this work.

Finally, I would like to thank my parents and Su for all their support, particularly when the going was tough.

Dedication

To

my parents

and,

in memoriam

Dr. S. Leonard Simpson MA, MD (Cantab), FRCP

1901-1983

ERRATA

There are no pages 55 and 175.

Contents

Chapter 1

Introduction

Chapter 2

Instrumental Techniques

Chapter 3

Ultrastructural Study of Otoconia and Otoliths

Chapter 4

Ultrastructural Study of Coccoliths

Chapter 5

Preliminary Investigation of Organic Components of Biominerals

Chapter 1

Introduction

The problem of control of the formation of a solid phase is one which has attracted attention in many fields of research. Factors which have been studied are the production of crystallites of a controlled size (1) and morphology (2), the problems of nucleation (3) and inhibition (4) and the nature of epitaxial growth (5). This work is reflected in developments in industries such as cement (6), glass (7) and plastics (8). There has also been a great deal of interest in the examples of solid structures in biology, which are functionally strong and suitable for skeletal function, yet, in many cases, are also constructed in intricate, repeatable, shapes. Biologically formed minerals use four main classes of compound; silica, which is always amorphous in biology; calcium carbonates; calcium phosphates and iron oxides. Much work has been carried out by Lowenstam in identifying the various classes of biominerals and a recent summary presents the current level of understanding of the occurrence of biomineral (9). A part of a table, relating to the occurrence of calcium carbonate as a biomineral, is reproduced as Figure 1.1.

1.1 Mechanisms of Biomineralisation

At present, three mechanisms for biomineralisation have been proposed; Biologically Induced mineralisation which is found in some green and brown algae and also bacterial species. This process results in the growth of minerals with similar crystal habits to those formed by chemical precipitation. The opposite

FIGURE 1.1

Diversity and Phylum Distribution of Calcium Carbonates in Extant Organisms. After Lowenstam (9).

Kingdom	Phylum	Calc	Arag	Vat	MHC	AmHC
Monera		+	+		+	
Protocista	Dinoflagellata	+				
	Haptophyta	+	?			
	Phaeophyta		+			
	Rhodophyta	+	+	+		
	Chlorophyta		+			
	Siphonophyta	+	+			
	Charophyta	+				
	Forminifera	+	+			
	Mixomycota	+				
Animalia	Porifera	+	+			
	Coelenterata	+	+			
	Platyhelminthes	+				+
	Ectoprocta	+	+			
	Brachiopoda	+				
	Annelida	+	+			
	Mollusca	+	+	+	+	+
	Arthropoda	+	+	+		+
	Sipuncula	+	+			
	Echinodermata	+				
	Chordata	+	+	+	+	+
Plantae	Bryophyta	+				
	Trachaephyta	+	+	+		

Key to Figure 1.1

Polymorphs of calcium carbonate:

Calc	:	Calcite
Arag	:	Aragonite
Vat	:	Vaterite
MHC	:	Monohydrocalcite
AmHC	:	Amorphous Hydrogen Carbonate

to this is Organic Matrix Mediated mineralisation in which complete control over the mineral formation is exercised by an organic matrix synthesised by the organism. Thus, ultimately, the type of mineral, direction of growth and the morphology of the structure are under genetic control (9). It should be noted that this control may be applied in two ways; by epitaxial promotion of crystal growth or by selective inhibition of crystal growth in unwanted directions (10). Williams (11) has proposed a third mechanism which is Vesicle Limited mineralisation. This method is particularly exemplified in the choanoflagellate *Stephanoeca diplocostata* Ellis which forms a basket comprised of amorphous silica strips (12,13). Each strip is formed by pumping silica into a vesicle which then hardens and is exported out of the cell to be constructed. The characteristics of this mechanism are that there may be structure on the outside, as dictated by the constraints placed upon the vesicle at the time of hardening, but there is no internal structure. Vesicle limited mineralisation appears to apply only to amorphous solids; crystalline materials require a far greater control if they are to be utilised to full effect. All three examples of mineralisation have been reviewed by Degens (14).

The organic control of mineralisation has interested workers from several fields for many years and observations have been made from the macroscopic to the molecular level. This work, and the increasing level of understanding of the materials have been successively reviewed (15-21). The nature of the various types of minerals involved and the increasing complexity of the systems as a whole meant that the whole range of crystalline biominerals formed a problem too large for a long-term research

programme. As a consequence, the work presented here limits itself to the question of biomineralisation involving calcium carbonate in chosen systems. This mineral was chosen as being convenient for study in the electron microscope, the major method available, since it forms anhydrous structures, unlike calcium phosphates, and are thus less likely to be susceptible to electron beam damage. The organic matrix, however, is less well defined than that of most calcium phosphate biominerals, such as bones and teeth, although it has been widely assumed to be simple. Recent work by Bevelander and Nakahara (22) and Weiner (23) on different aspects of the matrix, however, indicated that this is not the case, and one of the aims of this work has been to investigate the properties of the matrix in certain systems.

1.2 Promotion and Control of Biomineralisation

The formation of biological minerals has been studied from many viewpoints and many theories have been proposed to account for the observed structures. These theories have to explain the fact that structures are often formed from thermodynamically unfavourable polymorphs, for example the otoliths from the inner ears of fish are formed from the high-temperature stable form of calcium carbonate, aragonite, whilst mammals have similar structures (otoconia) formed from the low-temperature stable calcite (see chapter 3 below). Indeed, in marine gastropods, it is normal to find different polymorphs of calcium carbonate - including the normally unstable vaterite - in different parts of the shell (24,25). The major system chosen for my study is the balance organ structures of the inner ear,

from different species with different polymorphs and crystalline forms. A different calcitic biomineral is also studied, the coccolith formed by unicellular algae, which is of great significance since it provides the greatest quantity of biogenic mineral on earth; the substantial limestone layer which extends under the English Channel and commonly recognised as the 'white cliffs' of Dover is constructed entirely of coccoliths which have compressed over a geological timescale. A second example of geological structures originating from coccoliths can be found in the Red Sea in the form of a mat of coccoliths some thirty square miles across and one metre in depth which has entrapped a large quantity of oil due to the open structure formed. The ultrastructural work discussed in chapter 4 below, together with work carried out in the State University of Leiden, Holland, has led to a new hypothesis of biomineralisation (26).

The promotion of inorganic crystal growth in calcium carbonate-forming biominerals depends on the action of the organic matrix; we attempted to isolate and study a group of such proteins from gastropod shells, but the study was not conclusive. This work is discussed at greater length in chapter 5 below.

1.3 Limitation and Inhibition of Biomineralisation by Organic Molecules

The control of crystal growth has already been referred to, but, as yet, no substance has been identified as acting as a growth inhibitor of calcium carbonate *in vivo*. This is not the case for calcium phosphate, in which the γ-carboxyglutamic acid (gla)- containing "Bone Gla Protein" (or "Osteocalcin") has been

recognised as inhibiting unwanted bone growth (27). The method of inhibition of calcium carbonate formation appears to be the surrounding of each crystallite with an organic matrix, resulting in a bricks-and-mortar construction (22). I have studied certain examples of this formation of growth, which is illustrated in Figure 1.2

An alternative method of controlling crystal growth is to limit the concentration of ions allowed into an enclosed system. To do this, one might picture a bilayer vesicle system, containing carbonate (or hydrogen carbonate) ions, outside of which calcium is added. Providing that the calcium does not interact with the vesicle itself, and, in the case of phosphatidylcholine vesicles, it clearly does (28), the calcium will not cross the vesicle until some form of ionophore is added which complexes the calcium and carries it into the interior of the vesicle, whereupon it can form ion-pairs with the carbonate and then precipitate as calcium carbonate when the solubility product is exceeded. This hypothesis has been approached from two directions; (i) experiments with various vesicle systems, and (ii) a ^{1}H-nuclear magnetic resonance spectroscopy study of various complexes of the ionophore Lasalocid (X-537A). The passage of the metal-ionophore complex across a membrane was simulated by the use of both polar and non-polar solvents.

The role of the organic matrix in biomineralisation has yet to be conclusively demonstrated, but certain small proteins and glycoproteins have been shown to have physiological roles of inhibition of crystal growth. One of these is "Statherin", a phosphoprotein found in saliva which inhibits the formation

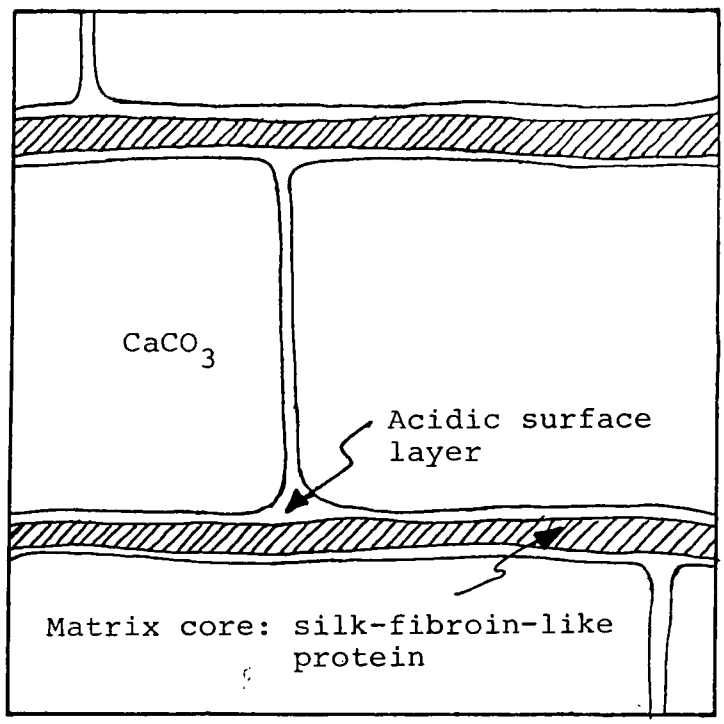

Figure 1.2

A schematic representation of a section through a mollusc organic matrix layer showing the "framework" core overlain by the surface acidic proteins (After Weiner).

of hydroxyapatite on the teeth (saliva is supersaturated with respect to calcium and phosphate) (29). Another family is that of the peptides and glycopeptides isolated by DeVries (30,31) which act as an inhibitor of ice formation for fish which live in arctic and antarctic waters with temperatures of about - 1.9°C. This is over 1°C below the freezing point of a typical marine teleost and the difference arises from the non-colligative action of these polypeptides. The mechanism of inhibition has been studied in this thesis by ^{1}H-nmr spectroscopy in both one- and two-dimensions. This has led to some understanding of another biomineralisation process.

1.4 A New Hypothesis on Biomineralisation

During the course of this work, a hypothesis has been formulated to explain the manner of construction of biominerals. It was originally applied to otoconia and otolith formation, but we believe that it can be applied to all calcium carbonate biominerals and also has value in considering all crystalline structures in biology. The hypothesis is summarised in Figure 1.3 and is as follows. The final biomineral may have the appearance of a geological crystal, but more often, it has a unique morphology which is not obviously crystalline. This final structure is composed of aggregations of crystals surrounded by an organic matrix of some form. We have termed these aggregations "Composite Crystallites". Each composite crystallite is held in place in the biomineral by a layer of organic matrix, but these constructions, in their turn, are composed of both inorganic and organic components. The organic matrix contained within the composite crystallites may be the same as, or different from, that surrounding each structure; the inorganic phase contains no organic material, but may be of two forms. The first is a "Single Crystallite" as determined by ultra-high resolution

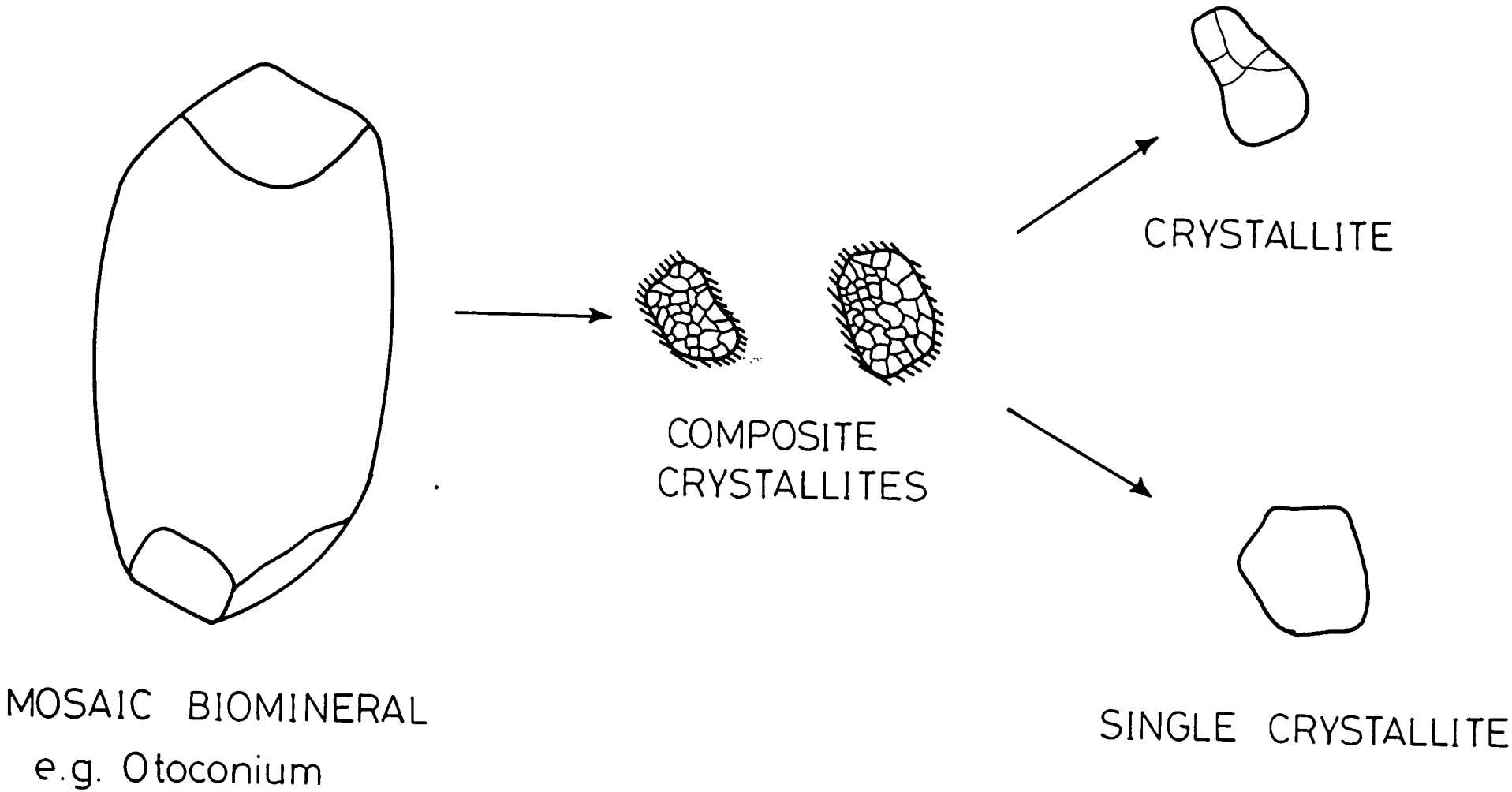

Figure 1.3

Summary of the hypothesis of biomineral construction

electron microscopy; the second is comprised of microdomains and is distinguished from the first case by the title "Crystallite In our definition this is a quite specific name and not a default term. Reducing the scale of both components leads to the unit cell of the mineral. This hypothesis will be referred to in more specific terms in discussion of the ultrastructures of the biominerals below.

1.5 The Scope of This Thesis

This project covers the inorganic mineral, aspects of the organic matrix in the formation of the structure and various methods of controlling growth, either wanted or unwanted; vesicles, ionophores or inhibitors.

1.6 REFERENCES

1. Matijevic, E. *Acc. Chem. Res.* 14, 229-237, (1975)
2. Kitano, Y., Kanamori, N. and Tokuyama, A. in *'Organic Matter in Natural Waters'* ed. D.W. Hood, 413-445, (1970). Pub. Inst. Marine Sci., University of Alaska
3. de Jong, E.J. in *'Industrial Crystallization 78'* eds, E.J. de Jong and S.J. Jancic, 3-17, (1979). Pub. North-Holland Publishers, Amsterdam
4. Bosky, A.L., Goldberg, M.R. and Posner, A.S. *Calc. Tiss. Int.* 27, 83-88, (1979)
5. Koutsoukos, P.G. and Nancollas, G.H. *J. Cryst. Growth* 53, 10-19, (1981)
6. Birchall, J.D., Howard, A.J. and Kendall, K. *Chem. in Brit.* 18, 860-863, (1982)
7. Bunnell, L.R. *Ext. Absr. Program - Bienn. Conf.* Carbon 12, 333-334,(1975)
8. Han, K.S. *Composites* 14, 145-150, (1983)
9. Lowenstam, H.A. *Science* 211, 1126-1131, (1981)
10. Pak, C.Y.C., Ohata, M. and Holt, K. *Kidney Int.* 7, 154-160, (1975)
11. Mann, S., Parker, S.B., Perry, C.C., Ross, M.D., Skarnulis, A.J. and Williams, R.J.P. *'Biomineralisation and Biological Metal Accumulation'* P. Westbroek and E.W. de Jong (eds), 171-183, (1983) pub. D. Reidel
12. Leadbeater, B.S.C. *Protoplasma* 98, 241-262, (1979)
13. Mann, S. and Williams, R.J.P. *Proc. Roy. Soc. Lond. B* 216, 137-146, (1982)
14. Degens, E.W. *Top. Curr. Chem.* 65, 1-112, (1976)
15. Wilbur, K.M. and Simkiss, K. in *'Comprehensive Biochemistry'* eds. Florkin and Stotz 26A 229-295, (1968)

16. Schiffmann, E., Martin, G.R. and Miller, E.J. in *'Biological Calcification : Cellular and Molecular Aspects'* ed H. Schraer, pp 27-67, (1970), pub. North-Holland Publishing Company, Amsterdam

17. Simkiss, K. in *'Calcium in Biological Systems'* ed. C.J. Duncan. Symposia of the Society for Experimental Biology, 30, 423-444, (1976). Pub. Cambridge University Press

18. Krampitz, G. and Witt, W. *Top. Curr. Chem.* 78, 57-144, (1979)

19. Glimcher, M.J. in *'The Chemistry and Biology of Mineralised Connective Tissues'* ed. A. Veis. 617-673, (1981). Pub. Elsevier North-Holland Inc.

20. Crenshaw, M.A. in *'Biological Mineralisation and Demineralisation'* ed. G.H. Nancollas, 243-257, (1982). Pub. Springer-Verlag, Berlin

21. Mann, S. *Structure and Bonding* 54, 125-174, (1983)

22. Bevelander, G. and Nakahara, H. in *'The Mechanisms of Biomineralisation in Animals and Plants'* ed. M. Omori and N. Watabe, 19-27, (1980). Pub. Tokai University Press, Tokyo

23. Weiner, S. *Calc. Tiss. Int.* 29, 163-167, (1979)

24. Taylor, J.D., Kennedy, W.J. and Hall, A. *Bull. Br. Mus. nat. Hist. (Zool.)*, Suppl. 3, 1-125, (1969)

25. Taylor, J.D., Kennedy, W.J. and Hall, A. *Bull. Br. Mus. nat. Hist. (Zool.)* 22, 255-294 (1973)

26. de Jong, E.W., Borman, A.H., de Vrind, J.P.M., Kok, D.J., Parker, S.B. and Westbroek, P. *Proc. R. Soc. Lond.* (1983), in press

27. Price, P.A., Lothinger, J.W., Bankol, S.A. and Reddi, A.H. *J. Biol. Chem.* 156, 3781-3784, (1981)

28. Duzgunes, N. and Ohki, S. *Biochem. Biophys. Acta* 467, 301-308, (1977)

29. Schlesinger, D.H. and Hay, D.I. *J. Biol. Chem.* 252, 1689-1695, (1977)

30. DeVries, A.L. and Wohischlag, D.E. *Science, N.Y.* 163, 1074-1075, (1969)

31. Duman, J.G. and DeVries, A.L. *Comp. Biochem. Physiol.* 533, 375-380, (1976)

Instrumental Techniques

2.1 Introduction

This project used two major techniques; electron microscopy (EM) and nuclear magnetic resonance spectroscopy (nmr). In addition, several minor techniques were used for various experiments. The major techniques are covered at sufficient length in this chapter for the ensuing discussion to be self-explanatory; the minor techniques are described in a more cursory manner. In addition, various preparative procedures and analytical techniques were followed for the study of the organic matrix; these preparations are described in this discussion.

2.2 Analytical Electron Microscopy

2.2.1 Routine Electron Microscopy

Routine electron microscopy was carried out on a Jeol-100CX Temscan instrument in the Department of Chemical Crystallography, University of Oxford. This instrument operates at a maximum accelerating voltage of 100 KeV in the following modes: transmission (TEM), scanning (SEM) and scanning transmission (STEM). These last two modes were operated via an ASID-4D control attachment. In addition, electron diffraction and transmission were possible by using a selected area aperture. The range of magnification possible is x 330 to x 250 000 in the normal mode and x 3 300 to x 66 000 using the selected area aperture. Selected area electron diffraction could be carried out at camera lengths between 20 cm and 260 cm. In practice, TEMs were recorded in the normal mode up to a magnification of x 160 000, since the exposure time became very long at the highest magnification, and

diffraction patterns were obtained with camera lengths of 76 cm or 120 cm. Transmission images were recorded onto Kodak electron microscope film 4489 using the plate camera built into the base of the microscope.

Scanning images could theoretically be obtained at magnifications from x10 to x200 000 at an optimum resolution of 30 Å in the SEM mode and from x300 to x300 000 at a resolution of 15 Å in the STEM mode. In practice, images were of an unacceptable quality above magnifications of x100 000 and photographic images were poor above x 50 000. Photography of scanning images was carried out on the recording unit of the EM-ASID-4D unit via a Mamiya 6 x 7 camera back using Ilford FP4, 120 format film.

The Jeol JEM-100CX is an analytical electron microscope and incorporates a Link Energy Dispersive X-ray Spectrometer (EDAX) unit. This comprises a lithium-drifted silicondetector capable of a resolution of 150 eV. This is connected to a Nova 290 computer which analyses the X-ray signals, thus allowing X-ray microanalysis of selected samples to be carried out. The spectrum obtained can be displayed on a 625-line monitor and plotted on a Bryans Model 294 X-Y plotter. The areas under selected peaks can be measured and the data printed on a Data Dynamics 390 printer terminal. Storage of the spectra can be carried out on single-density floppy discs. The detector is separated from the microscope column (and thus the sample under analysis) by a beryllium window. As a consequence, all signals from atoms of lower relative atomic mass than sodium are absorbed and cannot be detected by this technique. One further complication is that the amount of white radiation, or 'bremstrahllung' tends to obscure

the peaks at low electron voltage in the spectrum; thus this technique is particularly sensitive for high relative atomic mass species and results from low mass elements should be approached with caution, particularly when attempting to quantify the values.

The normal operating parameters for the Jeol JEM-100CX electron microscope arise from an accelerating voltage of 100 keV, which gives rise to a saturated filament with a current of 90 - 100 μA. This saturation can be controlled by adjusting the filament emission and gun bias to an optimum value. In the TEM mode, which is capable of a theoretical point-to-point resolution of 7.0 Å with the ASID unit attached, the condenser spot size is set to its maximum and a condenser aperture of 300 μm inserted into the column. In the scanning modes the condenser aperture remains unchanged, but the spot size is reduced to its mimimum value.

Samples were prepared for the electron microscope by dropping suspensions in either water or trichloromethane on to carbon-coated, formvar covered copper grids and then air-dried. As is common in analytical microscopes, the specimen was inserted into the microscope column by a eucentric side-entry goniometer stage with a maximum tilt angle of $\pm 60^{\circ}$. The actual holder could rotate the grid if electron diffraction patterns were to be obtained; if not, a simple holder was used which merely tilted with the stage. The speed of both tilts and rotations were variable and controlled via foot pedals.

Chromatic aberration was minimised by aligning the beam tilts and astigmatism corrected by observing the carbon grains on the grid at a magnification of x250 000. Astigmatism

was always checked before photographs were taken. The contrast of the images was enhanced by inserting an objective aperture of either 120 μm or 60 μm into the column; this was centred by correcting around the central beam in the selected area diffraction mode.

Electron diffraction patterns were obtained by focusing on the object of interest in the selected area mode. The objective aperture was removed and a selected area aperture introduced into the column. These apertures have diameters of 1000, 250, 80 and 20 μm and the required aperturewas positioned to enclose the sample under study and exclude all other particles. The mode was then changed to selected area diffraction and the pattern adjusted with the focus and condenser controls. If the sample of interest is a single crystal, then the diffraction pattern has to be aligned using the microscope tilt and rotate controls. This process can be followed by observing the decrease of the so-called 'Laue zones' (see below) and increase of a symmetrical series of spots around the central, non-diffracted beam. It is common to de-focus the diffraction pattern during such adjustments, which allows one to follow the sample in the small central spot. When the sample is microcrystalline, however, no single pattern can be obtained (the area covered during selected area diffraction is a circle of diameter 20 μm). In such cases a 'powder pattern' of concentric circles about the central spot is obtained. This arises from the various particles in the beam being orientated in different directions. As the number of particles increases, the observed pattern moves from being discrete spots to obvious spots around a circle. As the number of orientations tends to infinity, so the circles become complete and of equal intensity. Samples studied here, however,

comprised too few particles for this end-point to be reached, and the powder patterns are normally of spots around circles.

Powder electron diffraction patterns can be assigned by calculating the d-spacings for each circle from the following formula:

$$d = \frac{\lambda . L}{R} \qquad (2.1)$$

where L is the camera length in cm

λ is the relativistic wavelength of the electron (0.0037 nm at 100 keV)

R is the reciprocal lattice spacing in cm

Thus measurement of the radius of each circle leads to a value of the d-spacings which is accurate enough to enable assignment from the Powder Diffraction File (1). In practice, though, this method is not accurate, largely because the camera length given by the microscope is only a nominal value and also because the accuracy of R is limited by the method used to measure the circle radius. This formula can, however, be used to analyse diffraction patterns taken in conjunction with ultra-high resolution TEMs and this will be discussed below.

The X-ray microanalysis enabled a comprehensive study of a specimen to be made; imaging, either transmission if the sample is thin enough, or secondary electron imaging (SEI) if not, electron diffraction to determine the crystallinity and microanalysis to discover its composition. The Jeol-100CX Temscan microscope is designed to facilitate easy movement between the various instrument modes and such a study can easily be made; the only problem lying in the ability of the sample to withstand the effect of the electron beam.

X-ray microprobe analysis was carried out by tilting the sample to an angle of 40^{o} towards the detector and selecting the area to be analysed. This had to be in the quarter of the grid nearest to the detector to enable a high enough count rate for significant results to be obtained. Microprobe analysis is a qualitative technique, but it can be quantified in one of two ways. The first is to determine corrections for atomic number effects (C_Z), absorption (C_A) and fluorescence (C_F). These corrections apply to individual microscopes, but are constant within one instrument. These corrections (called 'ZAF' corrections) can then be used to determine the concentration of an element, c_x from the intensity of its emission line in the X-ray spectrum, I_x as follows:

$$c_x = \frac{k.I_x}{C_Z.C_A.C_F} \qquad (2.2)$$

where k is a constant (2). The alternative is to use the ratio method of Cheetham and Skarnulis (3) in which, in the thin crystal limit, the corrections become negligible and all that is required is a constant for the two elements under study, obtained from a stoichiometric sample containing both elements. This ratio method is discussed at greater length in section 3.3.2 below. In microprobe analysis, care had to be taken that the nature of the specimen was not changing. Several different substances are known to be affected by an electron beam (4), and such changes would invalidate subsequent imaging and diffraction studies.

2.2.2. The Jeol JEM-1200EX Temscan Electron Microscope

Several advances have been made in electron microscope design since the development of the Jeol JEM-100CX instrument which allow scanning techniques and microprobe analysis to be carried out at a much better resolution and sensitivity. This improvement arises from a new design of vacuum system, known as a dry vacuum, which comprises a sputter ion pump to evacuate the specimen chamber and electron gun chamber of the microscope and a turbo molecular pump which evacuates the viewing and camera chambers, resulting in a total pressure in the system of 1.2×10^{-5}Pa. In addition, the magnification capabilities have been increased to a maximum of x500 000 with a point-to-point resolution of 4 Å with the ASID-10 scanning unit attached. The scanning performance is x10 to x800 000 with a resolution of 30 Å in SEM and x200 to x800 000 with an optimum resolution of 15 Å in STEM mode. The instrument operates at a maximum accelerating voltage of 120 keV. The microscope also includes a specimen protection system of exposing it to a mimimum dose of the electron beam during field selection, focusing and photography.

The instrument used was the property of Jeol (U.K.) Ltd, and sited at Jeol House, Grove Park, Colindale, London NW9. It was operated by Dr A C Brown. The SEM and X-ray microanalysis modes were used, the former on gold-sputtered samples. The improvements to the vacuum system resulted in microprobe analyses of increased sensitivity and a very low background level. Photographs were taken using the ASID-10 recording unit fitted with a Polaroid back and Polaroid type 55 positive/negative film, rated at 50 ASA (18 DIN).

2.3 Ultra-high Resolution Electron Microscopy

Ultra-high resolution electron microscopy was carried out using a Jeol JEM-200CX electron microscope in the Department of Metallurgy, University of Oxford. This microscope was fitted with a high-brightness LaB_6 filament, giving a point-to-point resolution of 2.46 Å. At these conditions, the chromatic aberration constant was measured as 1.4 mm and the spherical aberration constant measured as 1.2 mm. In order to achieve the highest possible resolution, a top-entry stage comprising a specimen holder magazine and specimen exchange knob was fitted to the microscope. This system accepts grids of a 2.3 mm diameter (side-entry stages accept 3 mm grids). All ultra-high resolution work was undertaken with Dr A Jerome Skarnulis, Department of Chemical Crystallography, University of Oxford.

Lattice imaging was carried out using a condenser aperture of 200 μm and objective aperture of 40 μm. Under these conditions and for the aberration constants quoted above, the optimum defocus condition was -650 Å. Focusing increments were 500 Å per step on the fine focus control and 31 Å per step on the ultra-fine focus control. The microscope had to be allowed to equilibrate for about two hours after the sample was inserted into the column.

The normal procedure of investigation was to search around the grid for a particle that gave an electron diffraction pattern. This was aligned and photographed. After this, the crystallite was focused in the normal mode, normally by adjusting to the Gaussian image plane, which is the minimum focus on a hole in the carbon film. The optimum focus was then achieved by defocusing to -650 Å, at first by counting focus

steps as calibrated above, but, in later experiments, by following a digital meter attached to the focussing controls. Once the optimum focus had been achieved, it was normal practice to take a series of three photographs. In certain samples, it was not possible to fully align the electron diffraction pattern, either because a powder pattern was obtained from intra-vesicular precipitates, or because the structure under investigation was made up of unaligned crystallites.

Lattice images and electron diffraction patterns were recorded on Agfa-Gevaert Scientia film in the plate camera housed in the base of the microscope.

2.4 ^{1}H Nuclear Magnetic Resonance Spectroscopy

2.4.1 Spectrometers

^{1}H-NMR spectra were recorded on a Bruker WH-300 spectrometer equipped with an Oxford Instruments superconducting magnet using a 5 mm ^{1}H probe and an Aspect 2000 computer. This spectrometer operates in the Fourier Transform (FT) mode. Two-dimensional correlated spectra (COSY) (5) were run on a 470 MHz ^{1}H-spectrometer equipped with a Nicolet 1180 computer and an Oxford Insrument magnet. Both of these spectrometers belong to the Oxford Enzyme Group. On the 300 MHz spectrometer, Free Induction Decays (FIDs) were acquired over 8K data points and a 4 000 Hz sweep width, and the instrument was operated using quadrature detection. For normal spectra a 70^{o} flip angle was used (a 7.0 μs pulse). Spectra were stored as FIDs. For protein samples 512 scans were acquired; fewer scans were required for vesicles and metal-ion complexes.

'Fully relaxed' spectra, in which the signals show their true intensity were recorded by inserting a relaxation delay

between acquisitions. For protein species in D_2O, a delay of 5 s was needed (the delay time is approximated to 5 x T_1, the spin-lattice relaxation time); small molecules, particularly when in $CDCl_3$ have a T_1 of about 3 s and thus a delay of up to 15 s is required. Fully relaxed spectra were recorded without solvent suppression (see below) since this can perturb the relaxation times by affecting resonances close to the water peak.

2.4.2 Data Manipulation

For normal spectra the FID was routinely multiplied by an exponential function. This has the effect of reducing the noise at the tail of the FID, which improves the signal to noise ratio (S/N), but at the expense of resolution. In practice, a 1.0 Hz excess line-width was employed in this procedure.

Resolution enhancement was carried out in one of two ways: convolution difference (CD) or by a Gaussian (sine-bell) multiplication. The CD procedure was first described by Campbell et al (6) and was performed by subtracting an FID line-broadened by 4 Hz from the same FID line-broadened by 1 Hz, using a subtraction constant of -0.98. Less harsh CD spectra used smaller subtraction constants.

Gaussian resolution enhancement was carried out by multiplying the FID by the following function (from Ernst, 7):

$$\exp(-at - bt^2)$$

where: $a = \pi . LB$

$$b = \frac{-a}{(2^{*}GB^{2}AQ)}$$

The parameters used were LB = -12 and GB = 0.15.

2.4.3 Pulse Sequences

i) Solvent Suppression

Solvent suppression was carried out routinely, in order to reduce the intensity of the residual HDO peak (δ = 4.7 ppm at ambient temperature). This was achieved by applying a pre-acquisition irradiation pulse of 0.3s at the HDO resonance position, causing partial saturation of the HDO signal.

ii) Nuclear Overhauser Enhancement (NOE) Experiments

NOE experiments were carried out using an automatic difference programme. Cycles of 16 scans were used; in each scan a pre-acquisition irradiation time of 1.0 s was used. For 8 scans of the cycle, this pulse was on-resonance and for the other 8 the pulse was off-resonance. Normally 32 such cycles were acquired. This cycling procedure compensates for long-term instrumental drift. The power level of the pre-acquisition pulse was determined by following the extent of saturation of the peak under study in a normal spectrum of a small number of scans before the difference procedure was used. This practice also revealed the degree of selectivity of the irradiation since the line-shape and saturation of peaks close together could be followed.

This technique can, in theory, yield quantitative information about the distance apart of protons within a structure; however, such analysis is only attempted if a crystal structure is known for the system, and even then the results tend to be ambiguous due to the effects of the solution. The qualitative application of the technique is a valuable one for protein study, but it was found that the effects were consistently gross for the metal-ion complexes and the shorter-range spin-decoupling technique was

used in that case.

iii) J-Decoupling

In molecules which have sufficiently long T_2 values, the scalar, or J-coupling can be observed in the resonances. This will show protons which lie on adjacent carbon atoms along the backbone of the structure. This experiment could be run as a difference spectrum between irradiated and blank spectra as described above, but it was found that Bloch-Steigert shifts were easily introduced into the spectra which led to poor differenc and a consequent difficulty in interpreting the spectra. This problem could be overcome in automatic difference spectra by keeping the on-resonance irradiation and the off-resonance irradiation as close together as possible, or alternatively by acquiring normal spectra, which often showed the decoupling effects and taking a manual difference with a blank spectrum if required.

iv) Spin-Echo Spectra

The spin-echo sequence was originally described by Hahn (8) and modified by Carr and Purcell (9). By adjusting the lengths of time (τ) in between pulses in a (90° - τ - 180° - τ - AQ) sequence to 60 ms (= 1/2J) (10), it is possible to obtain a spectrum in which singlet and triplet resonances appear upright and doublets are inverted. This experiment was carried out after measuring the length of time corresponding to a 90° pulse on each occasion as this can vary slightly.

The pulse train can be combined with specific decoupling to produce spin-echo spectra showing NOE effects (11). This technique is known as "Spin-Echo Double Resonance" and is visualise

as difference spectra since Bloch-Steigert effects to not arise.

2.4.4 Preparation of Samples for NMR Spectroscopy

i) Vesicle Preparation

The preparation of vesicles for study by NMR was identical to that for other methods and is described at length in the relevant chapter. In this case, however, D_2O was used for all solutions and purification steps. A total of 500 µl was added to a Wilmad type 507pp NMR tube and 5 µl of 3 (trimethylsilyl)-1-propane sulphonic acid (DSS) was added as an external reference. The total concentration of the vesicle solution was about 17 mM.

ii) Lasalocid Preparation

Lasalocid samples were weighed into an NMR tube and dissolved in 500 µl of d-trichloromethane ($CDCl_3$). The solution was degassed by exchanging the air above the solution for argon for a few minutes; oxygen dissolved inthe trichloromethane was ignored. This is because the lasalocid can be slowly oxidised and as a consequence, fresh samples were always prepared before study. 5 µl of Tetramethysilane (TMS) was added to act as an external reference for the spectrum. The final concentration of the solution was about 10 mM.

iii) Protein Preparation

Protein samples were prepared for spectroscopy by dissolving the sample in and lyophilising from D_2O twice before final dissolution. This procedure exchanges labile protons, such as exposed -NH groups and also exchanges adventitiously bound water for D_2O. This is necessary in order to reduce the intensity

of the residual HDO peak in the spectrum and was particularly important for the glycopeptide antifreeze since the resonances from the saccharide protons lie close to this peak and can be obscured if the sample is too 'wet'. For final preparation for spectroscopy, the protein was weighed into an NMR tube and then 400 µl of 99.7% D_2O (Merck, Sharpe and Dohme, Canada Ltd.) was added using an adjustable sample^r with disposable tips (Gilson). 5 µl of DSS was added to act as the external reference (both TMS and DSS give a reference peak at δ = 0.00 ppm). The pH of the solution was measured with a Radiometer pHM 26 or Radiometer pHM 84 pH meter connected to a Pye Ingold combination microelectrode which enabled the pH* of the solution to be measured inside the NMR tube. All pH values used in experiments and quoted below are those read directly from the meter and no adjustment has been made for the effect of measuring D^+ rather than H^+ in solution since isotope effects on ionisation are likely to compensate for electrode effects (12). The pH meter was standardised before use with commercial buffers (BDH Chemicals Ltd) of pH = 9.2 and pH = 4.(in water. Adjustments to the pH of the protein solutions were made with microlitre aliquots of stock solutions of DCl and NaOD in D_2O. Concentrated acid (35%) was supplied by Merck, Sharpe and Dohme, Canada Ltd. and concentrated alkali (40%) by Ciba-Geigy.

2.5 Computing Methods

2.5.1 Prediction of Electron Microscope Results

A computer program written by Dr A Jerome Skarnulis, Department of Chemical Crystallography, University of Oxford, was used to predict the electron diffraction patterns and lattice images obtained from the minerals and biominerals observed in the ultra-high resolution electron microscope. This is an interactive program (13) capable of relating the symmetry of the crystals

under study (see below) to the microscope directly, and is not limited to orthogonal cases. The predictions from the program were used to identify the electron diffraction patterns of the minerals, to scale accurately both lattice images and diffraction patterns (by re-arranging the formula given above) and to interpret two-dimensional lattice images.

2.5.2. Computer Graphics

The crystal structure of the barium salt of lasalocid ($Ba(LAS)_2$) (14) was used as input for the CHEMGRAF program suite, written by Mr E Keith Davies (15) and implemented on a Vax 11/750 computer in the Department of Chemical Crystallography, Oxford University, linked to a Sigma graphics terminal (model TG680) and Calcomp 81 plotter. Mr Davies assisted in the creation of archive files as convenient data handling devices. Photographs of the structures were obtained from the screen on an Olympus OM2n 35 mm camera in automatic mode and using Kodak Kodacolor II Professional film (speed 125 ASA) or Ilford FP4 film, speed 125 ASA.

The specific program used to display the structure was MODEL which enables the user to select particular features of the molecule, rotate in space and zoom in and out. Furthermore, the user can display the molecule in a number of formats, calculate and modify geometry and perform energy minimisation calculations.

2.6 REFERENCES

1. Powder Diffraction File: Inorganic Phases. 1980. Ed. W.F. McClune. Pub. JCPDS International Centre for Diffraction Data, Pennsylvania, U.S.A.
2. Reed, S.J.B. *"Electron Microprobe Analysis"*. Pub. Cambridge University Press, Cambridge. 1975.
3. Cheetham, A.K. and Skarnulis, A.J. *Anal. Chem.* 53, 1060-1064, (1981)
4. Mann, S. D. Phil Thesis, Oxford University, (1982)
5. Jenner, J. Meier, B.H., Bachmann, P. and Ernst, R.R. *J. Chem. Phys.* 71, 4546-4553, (1979)
6. Campbell, I.D., Dobson, C.M., Williams, R.J.P. and Xavier, A.V. *J. Mag. Res.* 11, 172-181. (1973)
7. Ernst, R.R. *Adv. Mag. Res.*2, 1-136 (1966)
8. Hahn, E.L. *Phys. Rev.* 80, 580-594, (1950)
9. Carr, H.Y. and Purcell, E.M. *Phys. Rev.* 94, 630-638, (1954)
10. Campbell, I.D., Dobson, C.M., Williams, R.J.P. and Wright, P.E. *FEBS Lett.* 57, 96-99 (1975)
11. Campbell, I.D. and Dobson, C.M. *J.C.S. Chem. Comm.* 750-751, (1975)
12. Glasgoe, P.K. and Long, F.A. *J. Phys. Chem.* 64, 188-191, (1960)
13. Skarnulis, A.J. *J. Appl. Crystallogr.* 12, 636-638, (1979)
14. Johnson, S.M., Herrin, J., Liu, S.J. and Paul, I.C. *J. Am. Chem. Soc.* 92, 4428-4435. (1970)
15. Davies, E.K. D. Phil Thesis, University of Oxford, (1983)

Chapter 3

Ultrastructural Study of Otoconia and Otoliths

3.1 Introduction

Otoconia are found within the utricle and saccule of the inner ear of mammals and the utricle, saccule and lagena of amphibians. They are formed of calcium carbonate; the amphibian structures being aragonite, the mammalian, calcite. Otoliths are massive structures of aragonite which are found within the saccule of fish. Calcified structures have been observed within the inner ears of lower vertebrates, including the lamprey, although these structures are largely calcium phosphate (1). The composition of otoconia in animals lower than fish tends to be variable, since the inner ears are open to the surrounding medium, usually sea-water; indeed cray-fish have been found to scoop up grains of sand into their inner ears to supplement their otoconia. Because their structures are open, these invertebrates change their otoconia whenever they undergo ecdysis. This is in distinct contrast with the behaviour of the higher vertebrates, which will be discussed below.

3.1.1. The Anatomy of the Macula

The otoconia and otoliths form part of the gravity receptors of the vertebrates, although certain other functions have also been observed. They will respond to dynamic linear acceleration and also to acoustic (vibratory) stimulation in some cases. Recent work on the otoliths of fish (2,3) has identified an angular component in the auditory response, due to the strongly directional response of the otoliths to oscillatory motion. Thus they will play an important role in direction finding.

Figure 3.1

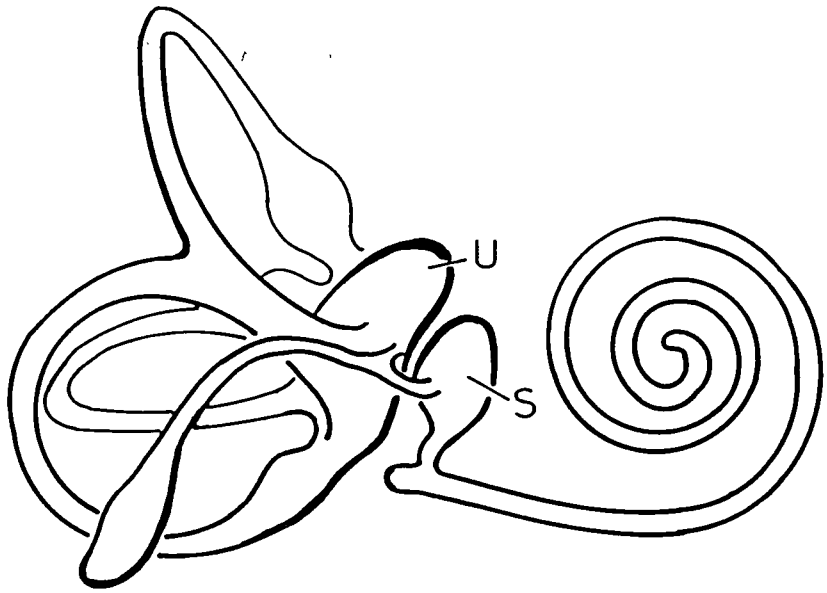

The anatomy of the mammalian inner ear showing the relative positions of the utricle (U) and saccule (S) from (33).

Figure 3.2

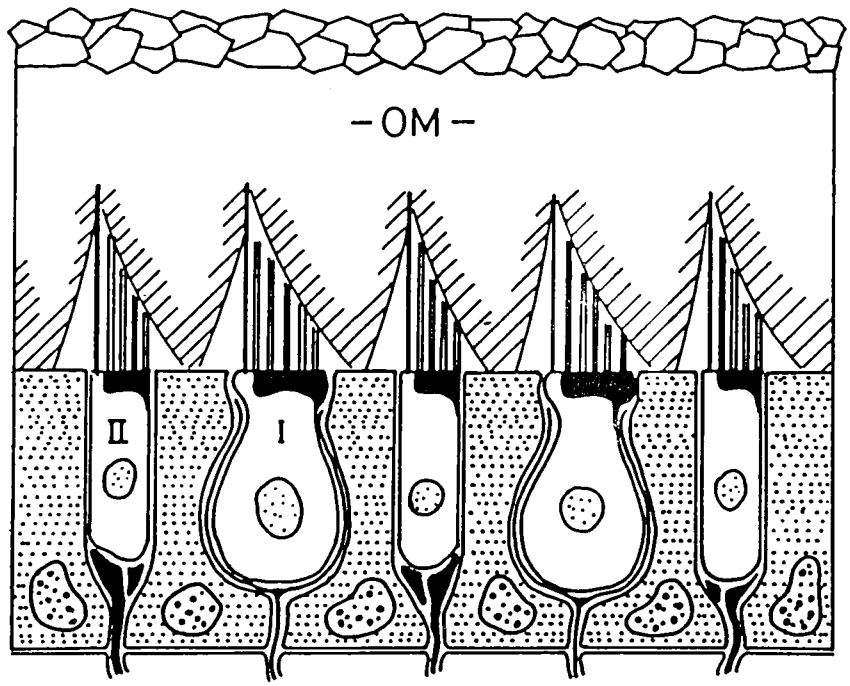

The end-organ containing both the otoconia and the neuroepithelium which contains two types of receptor hair cells I and II. OM is the otolithic membrane which forms a connection between the otoconia and the cilia and the neuroepithelium (33).

The cavities of the inner ear containing the balance organs in mammals are illustrated in Figure 3.1. The anatomy of the organ in the fish and amphibian is related, but also contains the lagena, a third, peripheral cavity. All three cavities are filled with perilymph and contain the end-organ which forms the gravity receptor. This end-organ is illustrated in Figure 3.2. It will be seen to comprise the otoconial complex which comprises the calcium carbonate otoconia embedded in a proteinaceous otoconial membrane lying on a patch of neuroepitheliu which contains receptor hair cells. The mass of the otoconia markedly increases the sensitivity of these hair cells to gravitational and dynamic linear acceleration.

3.1.2. The Morphology of Otoconia and Otoliths

The morphology of the otoconia varies between the different classes of vertebrates, although there seems to be no great species dependence, particularly in the mammals and birds, in which the polymorph of the structures is calcite. These otoconia are barrel-like structures with smooth, prismatic end-faces and slightly curved bodies which may show signs of waisting,particularl in the saccular crystals. Exceptions to this morphology, which is shown in Figure 3.3, have been found, indicating that the mechanism of growth is not perfect.• This is not surprising since the growth of the crystals is very fast (4). The otoconia from the amphibians, which are aragonitic, show a less regular morphology. Samples from frogs are usually shaped like a rugger ball,which is to say, ovoid in four panels (Figure 3.4). As the downward evolutionary trend is continued, however, a large number of perfectly straight-edged crystals are observed. It is impossible to tell from the morphology whether these crystals are

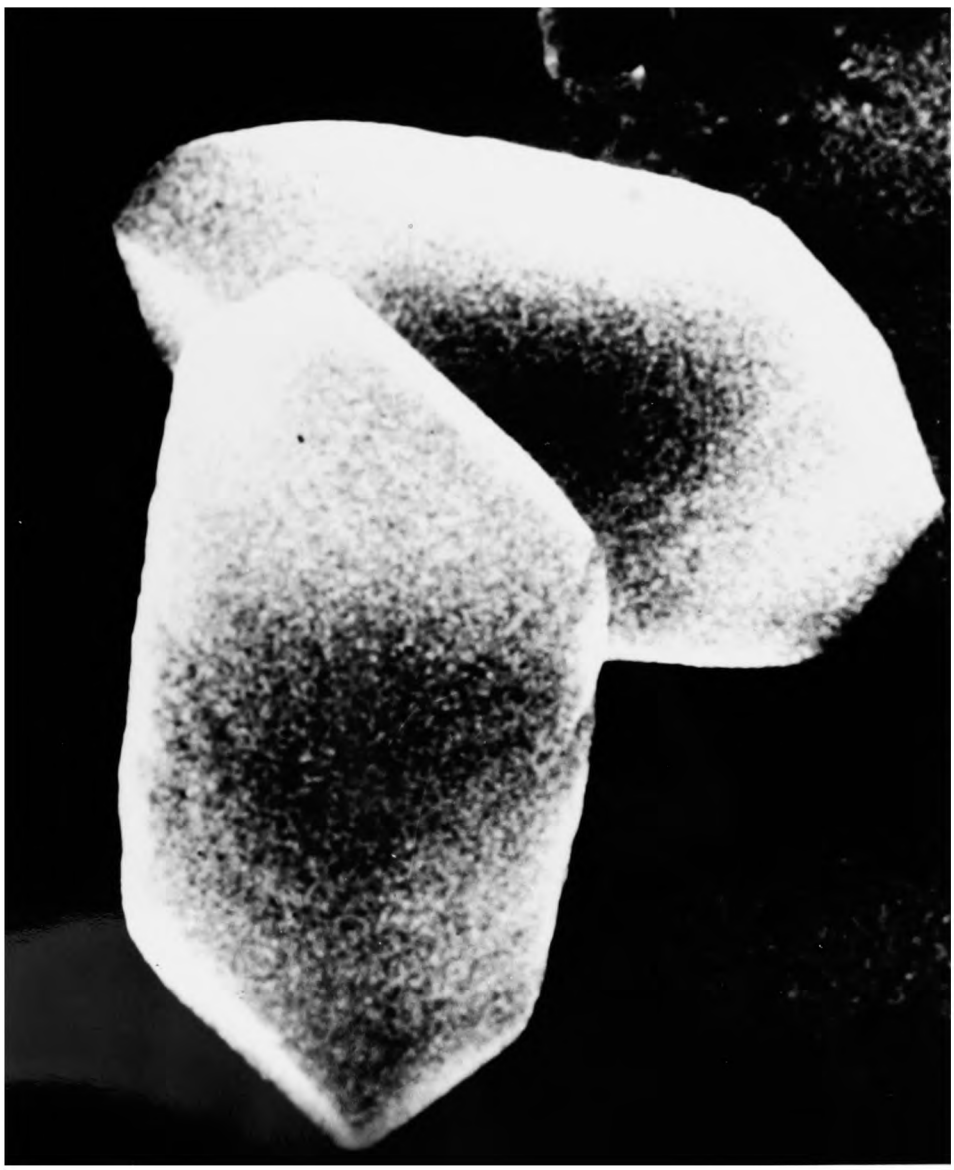

Figure 3.3

Utricular otoconia showing typical rhombohedral end-faces and curved bodies. This sample is from rat. Magnification x 20 000

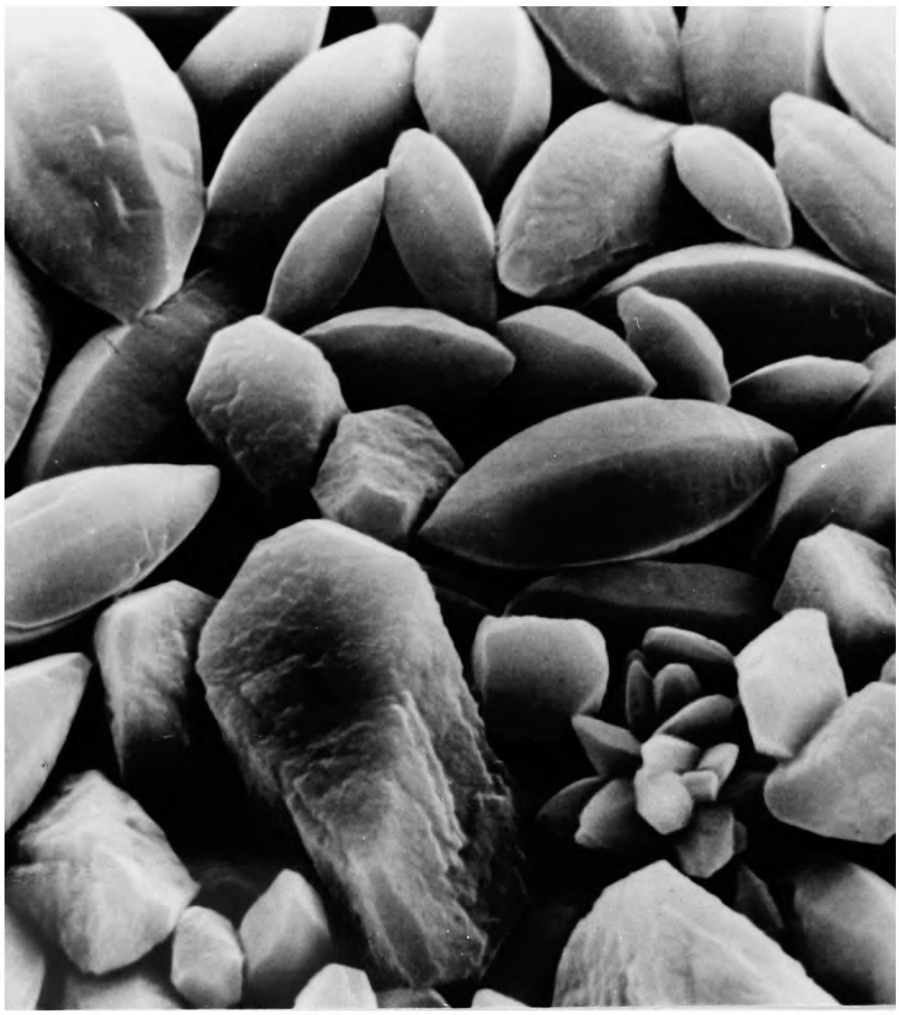

Figure 3.4

Scanning electron micrograph otoconia from the inner ear of frog. Magnification x 3520.

single crystals or grown under the influence of the organic matrix normally associated with biomineralisation phenomena. The size distribution of these crystals is large, and they tend to be interspersed with large, curved crystals similar to those seen in frog. Thus, the morphology of the otoconia can reveal very little about their biogenesis and mechanism of growth and this can only be determined by studying the ultrastructure of the interior in some way.

The morphology of fish otoliths is quite different and highly species-dependent. This is illustrated for four species of teleost fish in Figure 3.5. Much classic work was carried out on the morphology of these structures by Frost (5-16). It is interesting to note that the size of the otolith is not related to the size of the fish; the cod family (gadoids) tend to have large otoliths, but the huge 'game' fish of the Bahamas have very small structures. The growth of the otoliths is time dependent and they grow throughout the life of the fish; indeed the most accurate method of ageing a fish is to extract and section the otoliths and count the growth rings. Irie (17) followed this growth by autoradiography and established the seasonal growth pattern throughout the year, with alternate matrix-rich and mineral-rich bands giving rise to the growth rings.

3.1.3 Previous Work on the Ultrastructure of Otoconia

Much work has previously been carried out on the ultrastructure of otoconia. The first identification of the polymorph of the mammalian otoconia as calcite was made by Carlström et al in 1953 (18). By using X-ray crystallography, this study was extended to further species with both calcitic

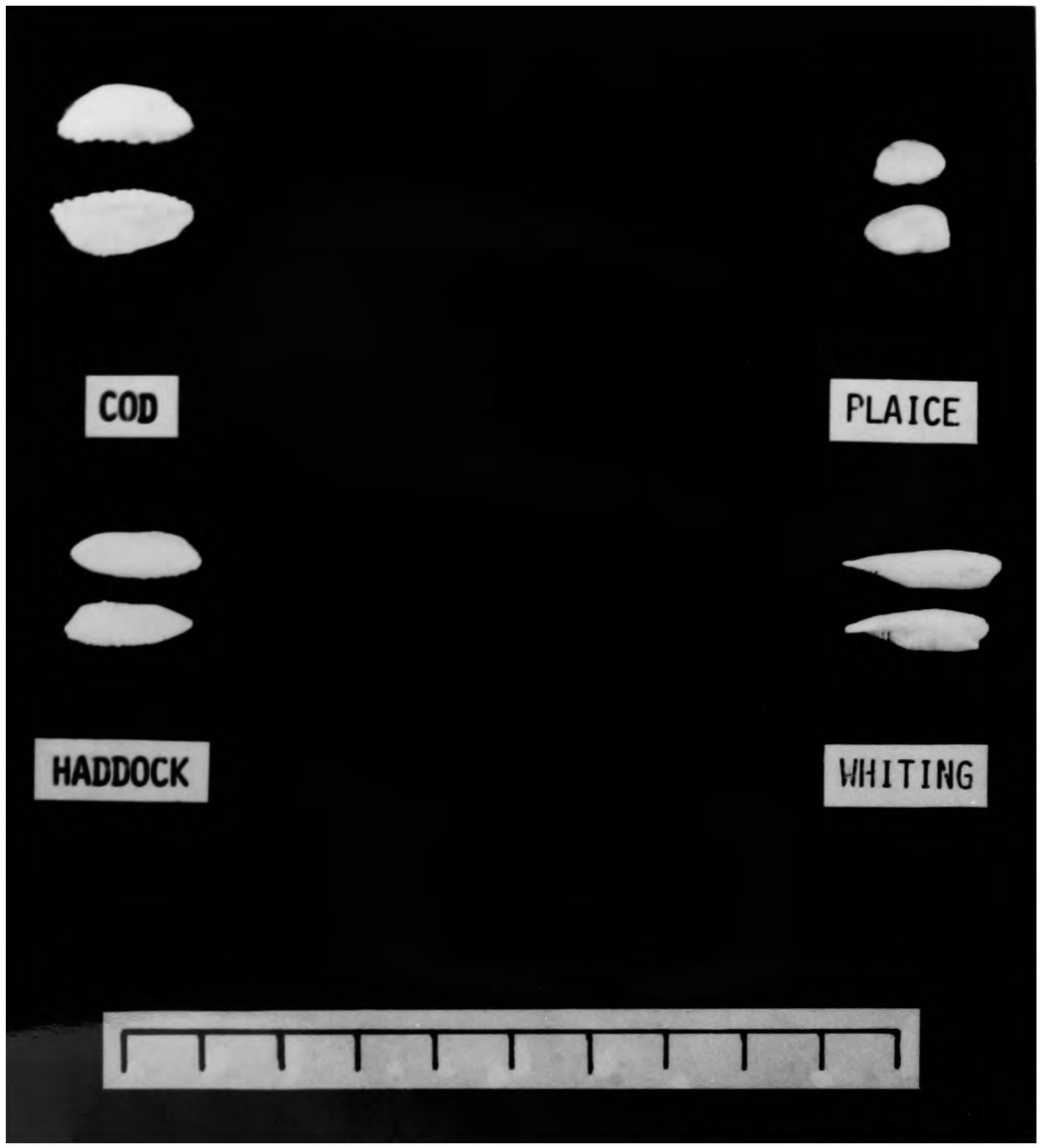

Figure 3.5

The morphology of otoliths from four species **of bony fish.** The scale bar is in centimetres

and aragonitic otoconia being studied (19) and ultimately extended to all classes of vertebrates (1). His ultimate conclusion was that the otoliths are polycrystalline structures, but the otoconia are single crystals of either calcite or aragonite. This conclusion is at variance with the earlier observation (19) that crushing human otoconia produced a series of well-formed hexagonal platelets which, they suggested, packed together to form the entire structure. Carlström's diagram summarising the evolutionary pattern of the structures is reproduced as Figure 3.6. This work remains of importance because of the very large number of species sampled. It should be noted, however, that the analysis was carried out by powder X-ray diffraction, light microscopy and polarised light microscopy, the last two on ground thin sections of otoliths and whole otoconia to determine size, shape and texture. In the absence of electron microscopy techniques (scanning microscopy, elemental analysis and electron diffraction) the amount of information obtainable is inevitably limited. Powder X-ray diffraction, by definition, cannot determine the long-range order of a crystalline sample and light microscopy is dependent on the wavelength of visible light for its maximum resolution.

Marco and co-workers (20) studied the otoconia from guinea pigs and observed differing zones within thin sections from the structure, with the body being very dense with a low density centre and the extremities consisting of low density filamentous granules. They concluded from these observations that the otoconia have a micro-crystalline constitution. A later paper from the same laboratory (21) sub-divided the centre region into a low-densit centre, surrounded by an intermediate zone before the high-density

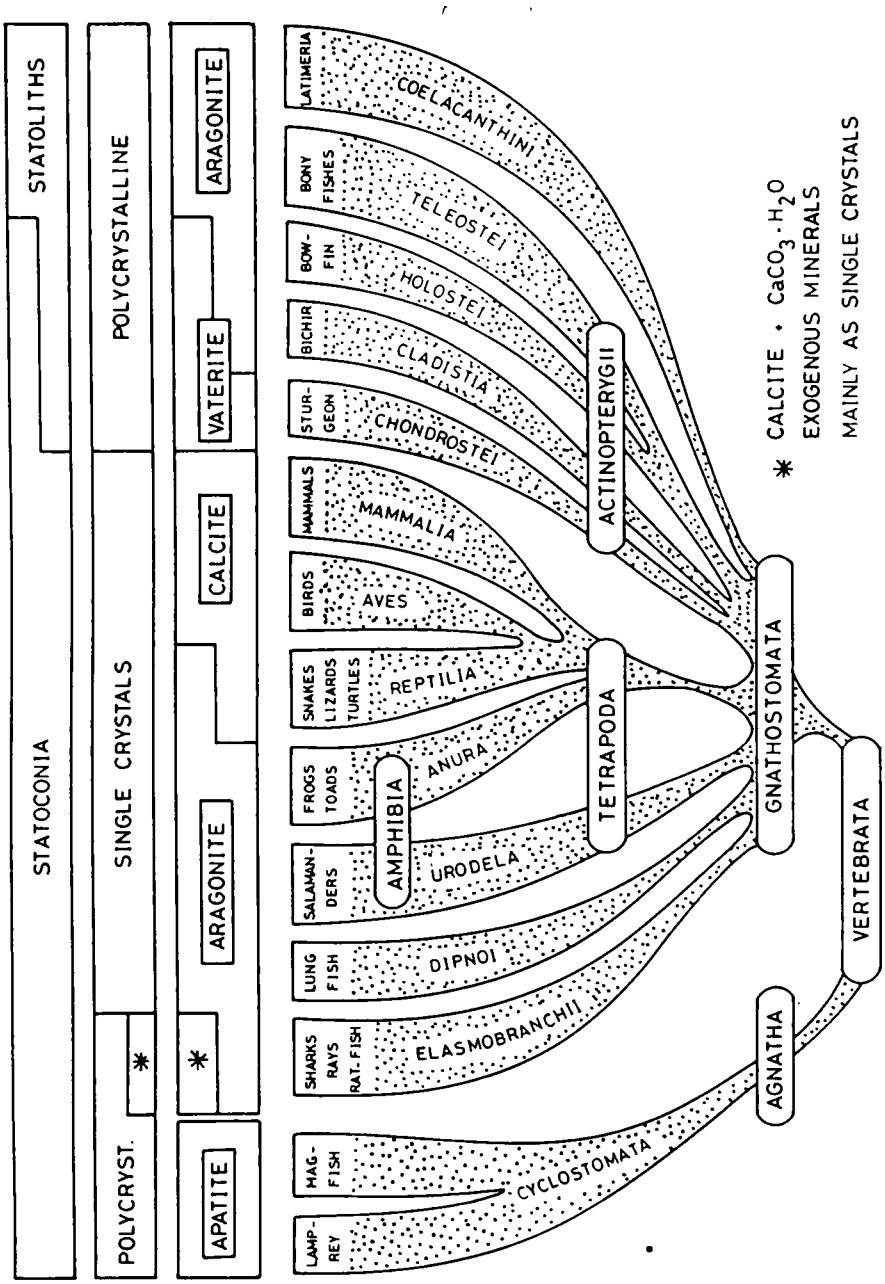

Figure 3.6

Diagram reproduced from the work of Carlstrom (1) of the evolutionary pattern of the balance organs of the inner ear.

peripheral zone was encountered. This concept of differing regions within the otoconia was taken up by Lim (22) in a scanning and transmission electron microscopy study, using guinea pigs, cats and squirrel monkeys. He found that when the calcium was removed with EDTA, the structure collapsed without being etched, eventually leaving an amorphous substance which varied in density throughout the structure, but was very condensed in the centre, forming a proposed nucleus for growth. He suggested that this substance is morphologically similar, if not identical, to the proteinaceous layer of otoconial matrix which surrounds the crystals. He further assumed that this layer dictates the general growth pattern of the otoconia and ascribed the curved bodies of the structure to the pressure exterted by this matrix.

This view of the ultrastructure of the otoconia has not met with uniform acceptance. Ross and Peacor (23) described several morphologies other than that commonly observed from the study of young rats. These immature otoconia differ in many properties from the adult form, such as the ease of the cleavage, fracture and etching. They observed, however, a central core in one fortuitously cleaved juvenile otoconium which, on decalcificatio revealed a great deal of organic matter in the centre core, but which also extended to the surface of the structure. Ross and Peacor preferred to ascribe the rounded body of mature otoconia to chemical inhibition of growth in this area, with normal growth at the end-faces. These theories were subject to change with later observations; Ross et al (24) appeared to move away from the general opinion of otoconium growth by microcrystal accumulation. This arose from the single crystal X-ray analysis carried out by Peacor on a pathologically enlarged otoconium from a human sample. He was able to identify the end faces of the crystal as being

(100) faces of calcite and further drew the conclusion that the entire otoconium was a single crystal. This view was challenged by Nakahara and Bevelander (25) in a transmission electron microscope study of ultrathin sections of mouse otoconia. They observed an aggregation of organic clusters in the saccule after 15.5 days in the foetus, which are modified to the typical hexagonal shape in the next two days. They named this purely organic structure a 'preotolith' and regarded it as the template for consequent calcite formation which was first observed one day after the birth of the mouse. The growth began with the formation of minute tube-like structures in which needle crystals of calcite developed. Initially this process occurred at the ends of the hexagon, but then extended throughout the structure. Nakahara and Bevelander named the needle-like crystallite structure a 'multi-iso-orientated-crystal'. This paper was criticised by Peacor et al (26) on the grounds that they had found no evidence in work on rat otoconia of a preotolith; they also restated their claim that the otoconium is a single crystal of calcite. This critique was followed by a paper from the same laboratory (4) on the otoconial formation in the foetal rat in which they showed scanning and transmission electron micrographs of the foetal otoconia, clearly showing the existence of calcium in the structures. One consequence of this paper, however, was a weakening of the argument which Peacor had initited for the single crystal nature of the structure; certain transmission micrographs clearly showing the sort of rod-like crystallites that Nakahara and Bevelander had spoken of.

3.1.4 Previous Work on the Ultrastructure of Otoliths

The ultrastructure of fish otoliths has not received the same attention as the otoconia, but several interesting observations have been made about the growth of the structure. Irie (27, 28, 17) has carried out extensive investigations on the growth rates in differing regions of the otolith over the course of the year. He suggested that the growth was dependent on calcium uptake from both food and sea-water, and that as this varied by the seasons, so the rate was enhanced or suppressed. As a consequence of these observations, Irie postulated that the measurement of the growth rings of the otolith would give an accurate life-history of one particular fish. Later work by Bagenal (29) revealed that the rings observed in ageing fish were due to varying concentrations of protein bound up in the structure, but the discovery of daily ring growth in teleost otoliths (30,31) focused interest on the otolith as a good mechanism for the study of biomineralisation. This daily growth was confirmed for certain species by Brothers et al (32) and Taubert and Coble (33) by counting the increments in fish of known age. The list of species studied has increased with contributions from Barkman (34): (Atlantic Silverside, *Menidia menidia*); Townsend and Graham (35): (Atlantic Herring, *Clupea harengus harengus*); Brothers (36), a general discussion on reef fishes and Radtke and Dean (37) (see below). Dunkelburger et al (38) made the first ultrastructural study of the otolithic membrane in a teleost, the juvenile Mummichog, *Fundulus heteroclitu* and determined that the gelatinous region is composed of tightly arranged fibrous material and is restricted to the sensory region of the macula, lying between the otolith surface and the tips of a mechanoreceptor, being intimately connected to the otolith.

A further, non-structured, zone which is composed of fibres in very loose networks covers the entire macula. In the sensory region, some of this material is in contact with the otolith through pores in the gelatinous material. Dunkelburger et al suggested that it is this material which is incorporated into the otolith as the organic matrix. Close inspection of sectioned otolith revealed that many mineralised layers are incomplete and further, that the point of nucleation, in the centre of the structure is composed of concentric layers, whilst slightly further out, secondary layers begin to grow in selected directions. This accounts for the overall morphology of the otoliths. High magnification scanning micrographs revealed that there is a distinct arrangement in layers of the organic matrix and the mineral which is laid down in rounded subunits, giving rise to the appearance of peaks and troughs in sections where the organic matrix has been removed.

3.1.5 Piezoelectic Properties of Otoliths

Morris and Kittleman (39) made an important contribution to the understanding of the part played by the otoliths in the physiology of the inner ear when they found that they have piezoelectric properties. Otoliths were extracted from a nototheneid fish, *Trematomus bernacchii*, a catfish, *Ictalurus nebulosus* and a flatfish from the Pacific, *Parophrys vetulus*. All these otoliths gave a strong positive result, although quantitative results were not obtainable. Interestingly, the otolith from *T. bernacchii* oscillated over a range of 300 to 8 000Hz, whilst the otolith from *P. vetulus*, oscillated over the large range of 1 to 15 000Hz. This difference must be a consequence of the markedly different lifestyle of the two

species; sound at the sea-bed will have very low frequencies indeed. Morris and Kittleman demonstrated that the composition of the otoliths was not as would be expected for pure aragonite: 40% Ca, 12% C, 48% O. They found a consistent value of 36.9% Ca, a 7.5% deficiency. Analysis for sodium revealed that they contained 2.31% and potassium analysis was zero. These results were for otoliths taken from *T. bernacchii* and although the quantitive values varied, the qualitative observation of sodium replacing calcium in the otolith was found to be true for each of the three species analysed. They thus concluded that the substitution of sodium for calcium, together with the required substitution of hydrogen carbonate (HCO_3^-) for carbonate (CO_3^{2-}), gave rise to the observed piezoelectric properties. This topic is of increasing importance in the understanding of the physiology of the end-organs, and will be further discussed in the results of the present work.

3.1.6 The Organic Matrix of Otoconia and Otoliths

The analysis of the organic matrix associated with the otoconia and otoliths is much less advanced than the study of the mineral. In the case of otoconia, this is due to the difficulties of obtaining a large enough pool of crystals to facilitate the isolation of the matrix. Work has begun in the laboratory of Ross, in Michigan, to isolate these proteins as part of the overall work to understand the physiology of the otoconial matrix. A preliminary report, discussing the electrophoresis of a protein sample has appeared (40). This work found a series of protein bands with molecular weights of about 16 500 and 46 000 daltons with other bands at 56 000, 80 000 and over 100 000 daltons. These

gels were run under reducing conditions and thus dimerisation should not occur. Problems which occur when running gels of highly acidic proteins, which, in common with most soluble proteins from calcium carbonate biominerals, this is (Ross, personal communication) are discussed in the chapter of this work dealing with the study of the organic matrix; these problems would indicate that this report should be regarded as a preliminary finding. More recent work from the same laboratory (41) indicates that the amino acid composition for this protein has been determined. Uniquely, for a protein of this type, it is believed to contain γ-carboxy glutamic acid (GLA) (Ross, personal communication), although this result, too, is a preliminary finding. The study of the otolith proteins has progressed further (42), but this work will be discussed at some length in the chapter dealing with the isolation of otolith proteins carried out as part of this study.

3.1.7 The Aim of this Study

In summary, the crystalline nature of both otoconia and otoliths remains uncertain. A solution to the problem is important generally since there is little understanding of the mechanism of crystal growth in biological systems and new well-defined cases must be helpful. In this thesis it was the intention to determine unequivocally the nature of otoconia crystals and to find how similar the basic sub-unit is to the sub-unit which forms the continuous growth in otoliths. This study will use an ultra-high resolution electron microscope in an analysis of the crystallinity of crushed biominerals in comparison with crushed samples of geological minerals.

3.2 Materials and Methods

This study was carried out using the otoconia from Sprague-Dawley rats (*Rattus norvegicus*) and frogs (*Rana pipiens*) and the otoliths from plaice (*Pleuronectes platessa*). The otoconia were collected by Professor Muriel D. Ross in the University of Michigan, Ann Arbor, Michigan, U.S.A. as follows (40): adult rats and frogs were decapitated and their bullae were removed to small dishes for microdissection. This microdissection was initially carried out in double distilled, deionised water, but later artificial endolymph was used to mimic the conditions found in the bullae. This artificial endolymph was prepared according to the following formula:

AE: 1.0 mM NaCl; 148 mM KCl; 10 mM $KHCO_3$; 1 mM $MgCl_2$;
1.5 mM $CaCl_2$, pH=7.4-7.8

The tissue was moved to fresh fluid several times and the otoconial complexes washed with AE before being picked up with a micropipette; this washed away any contaminating proteins. The saccular and utricular complexes were kept separate and centrifuged to separate the otoconia from the supernatant AE. Otoliths were obtained from Dr. R W Blacker of the Ministry of Agriculture, Fisheries and Food, Fisheries Laboratory, Lowestoft, Suffolk NR33 OHT. These had been extracted from freshly caught specimens of plaice, in order to reduce the degradatory process that occurs within the saccule after death, cleaned of attendant organic material and supplied as matched pairs of crystals. Otoconia for study under the scanning electron microscope were then resuspended in chloroform and mounted onto holey-carbon covered copper grids which were then gold-sputtered to a thickness of approximately 100 Ångstroms. Scanning electron microscopy was either carried out in Professor Ross' laboratory in Michigan or on a Jeol-100CX Temscan electron microscope in Oxford. This

electron microscope is capable of operating in the following modes; transmission, scanning, scanning transmission, electron diffraction and X-ray microanalysis. Given suitable conditions of sample, it is possible to use several of these techniques at one time in the study of a system. (see chapter on instrumental techniques). Otoliths were too large to be studied whole by scanning electron microscopy due to the great tendency to charge at the high accelerating voltages used; the morphology of the structures were not part of the aim of this study since it was considered that much was already understood about this aspect of otoliths (37). Samples to be studied by ultra-high resolution electron microscopy were further prepared as follows: a fresh sample of otoconia was crushed in a pestle and mortar or between glass slides in order to apply a gentle force. This method was chosen over others, which included ion beam-thinning and crushing under liquid nitrogen because samples thus prepared showed fewer faults in the electron microscope. There was a great tendency to produce shear faults and gross deformations, visualised as Moire fringes in the other preparative methods; the results obtained by the other methods which led to the final choice of preparation are discussed at length below. The electron microscope used for ultra-high resolution work was a Jeol-200CX transmission electron microscope in the Department of Metallurgy, University of Oxford (see chapter on instrumental techniques). These biological specimens were compared with geological speciments of calcite and aragonite, supplied by the University Museum, University of Oxford. The aragonite originated from Aragon, Spain, and the calcite was in the form of Iceland Spar, and showed the typical characteristics of birefringence associated with the mineral. Both these minerals were analysed by atomic

absorbtion spectroscopy and standard carbon, nitrogen and hydrogen analysis on a Carlo Erba 1106 elemental analyser and gave the predicted analysis of Ca: 40%; C: 12% and O: 48% by difference. No trace nitrogen or hydrogen was detected. These were not studied by scanning microscopy, but were prepared for study in the Jeol-100CX and Jeol-200CX electron microscopes in exactly the same way as the biological minerals described above. Analysis of the otoconia was not undertaken due to the very small size of the crystals and the consequently large mass required for significant results; a qualitative analysis was carried out on the Jeol-100CX Temscan electron microscope. Analysis of the otoliths was undertaken, however, in an attempt to follow the work of Morris and Kittleman (39). This was performed as above, with the addition of analysis for phosphorus, which was achieved by a quantitative application of the X-ray microanalysis facility of the Jeol-100CX electron microscope (43). This analysis was extended to thermogravimetric analysis (T.G.A.) which was performed on 10 mg samples of mineral aragonite and powdered fish otolith on a Stanton Redcroft TG770 thermobalance Thus a typical pattern of study for each of the minerals might be, study on the Jeol-100CX during which the morphology of the otoconia would be studied, study of crushed minerals on the Jeol-100CX in order to establish which crystal faces are exposed by crushing; this is carried out using the electron diffraction capability of the microscope and finally a study of the crushed mineral on the Jeol-200CX high resolution microscope. As detailed above, the otolith samples were, in addition, subjected to elemental analysis.

The identification of the electron diffraction patterns was carried out by comparison with patterns generated by a computer program written by Dr A J Skarnulis, Chemical Crystallography Laboratory, University of Oxford (see chapter on instrumental techniques).

3.3 Results

3.3.1 The Morphology of Otoconia

The published work up to 1980 gave no conclusive evidence of the crystalline nature of otoconia. Two schools of thought were clearly evident, that they were single crystals or else microcrystalline aggregates, but neither hypothesis had been proven. In order to finally establish the ultrastructure of the otoconia, Professor Muriel D. Ross came to Oxford on sabbatical leave for four months in 1981. All otoconia samples were supplied from her laboratory in Michigan (see above) and whole otoconia were studied by scanning electron microscopy as a prelude to the work. The otoconia were taken from rat and were separated by their source (utricle or saccule) onto copper grids for the electron microscope. These samples were not coated; this resulted in a decrease in the quality of micrographs obtainable, but eliminated one source of artefact and also made X-ray microanalysis of the crystals possible.

The otoconia from both utricle and saccule were generally found to be rhombohedra with clearly defined end-faces comprising three planes and rounded bodies which normally showed no morphological features typical of a geological crystal. The two end-faces were related by a two-fold reflexion-rotation axis of symmetry. These features are illustrated in Figure 3.7. A certain number of features were observed, however, which indicate that the structure may have been imperfectly formed or unstable when removed from in vivo conditions. This is important since it has been assumed that the degeneration of otoconia occurs due to physiological changes within the vestibule and not due to the removal of the samples, which has been regarded as a non-artefact-

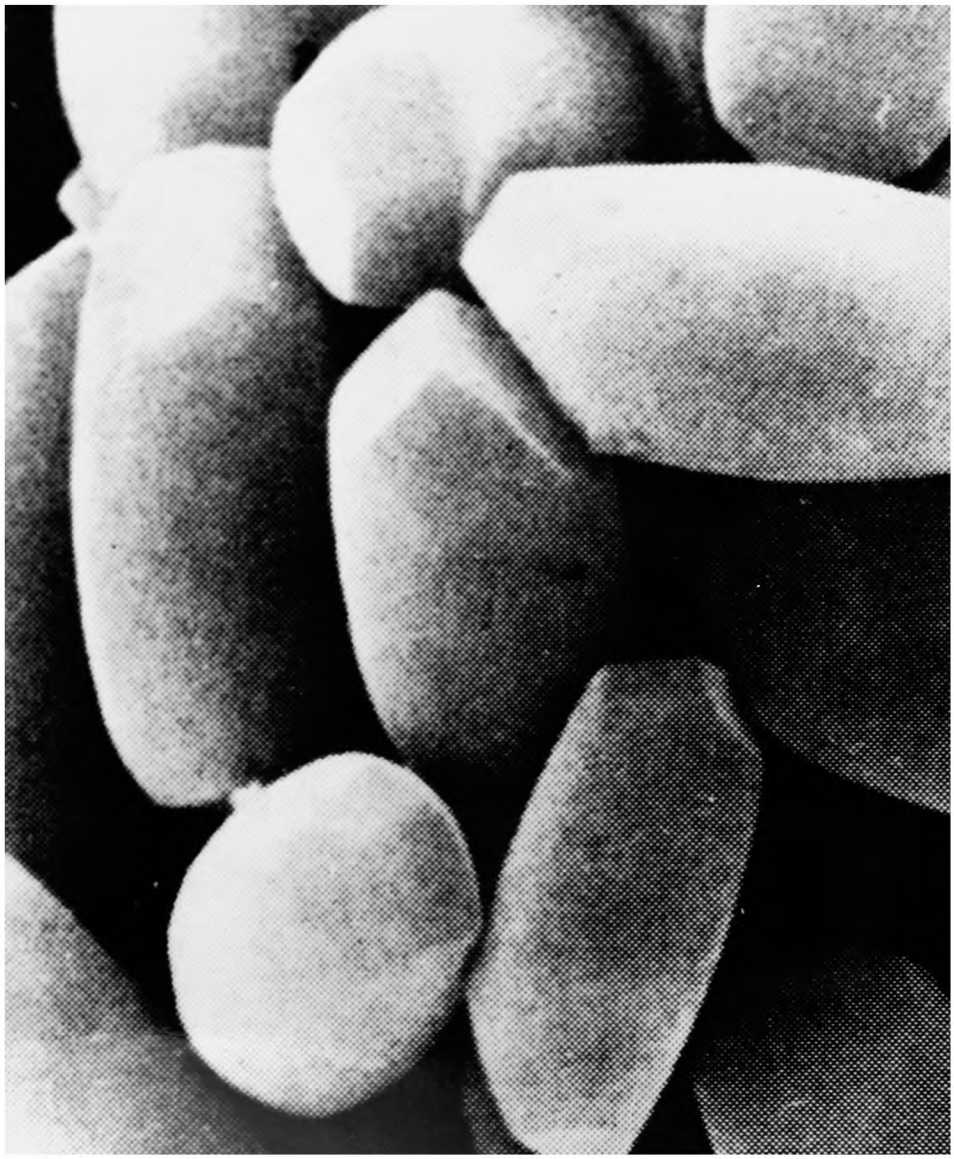

Figure 3.7

Human saccular otoconia from a young adult.

The rhombohedral end-faces can clearly be seen.

Magnification = x 7 000 (24)

inducing procedure (23).

Occasional freak growths of calcite were observed in which crystals had grown together and one example in which the growth is entirely circular, with the final morphology resembling a doughnut. These freak growths contained calcium as analysed in the microscope. Many of these observations are not reproducible and it is difficult to assign any process to the growth, other than the general observation that the normal control which is exercised in the biomineralisation process has malfunctioned in some way. The growths of otoconia in a star-shape (see, for example, 40) or in the forms seen in Figures 3.8a, 3.8b and 3.8c could arise from mineral twinning, which is common in geological specimens, but the round growth seen in Figure 3.8d could not be accounted for in this way.

A more common occurrence was the indication of crystallites comprising the body of the otoconia. This sort of change was often seen in the saccular otoconia, which have long been regarded as more labile (23) but was also observed in samples from the utricle as well. The original observation, above, was induced by soaking a saccular otoconial sample in acetate buffer, pH = 5.5, for one hour, and it was concluded that the maintenance of physiological conditions was vital for the preservation of the otoconia. These samples, however, were dissected under artificial endolymph (see above), which was regarded as a physiological medium.

The saccular otoconia exhibit one characteristic change from the usual morphology which is a fissure in the equatorial plane, giving a 'waisted' structure. This may arise from a twin

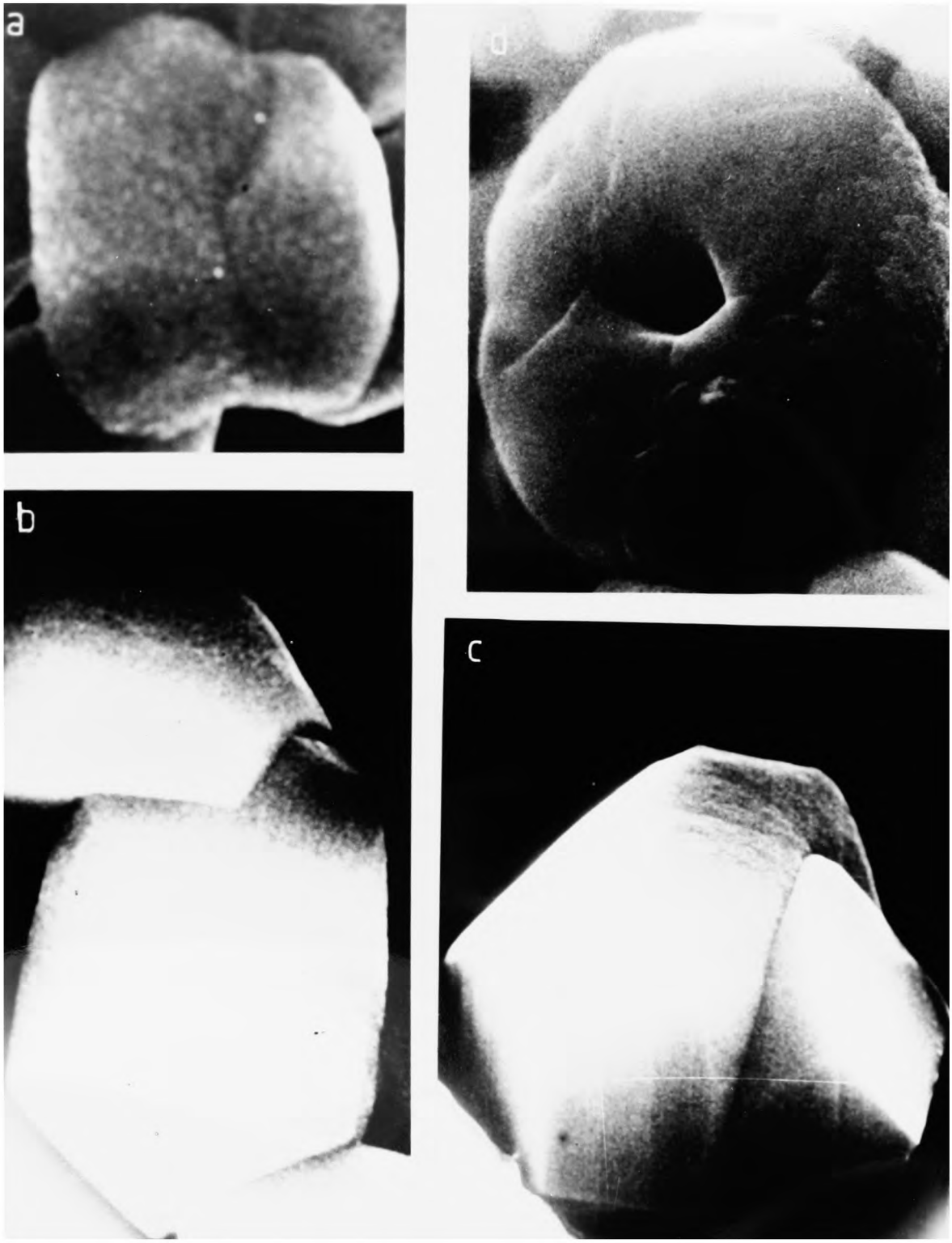

Figure 3.8

Faults in the growth of otoconia. (a), (b) and (c) could arise from mineral twinning. Magnifications: (a) x 14 000 (b) x 6150, (c) x 11 050, (d) x 10 000

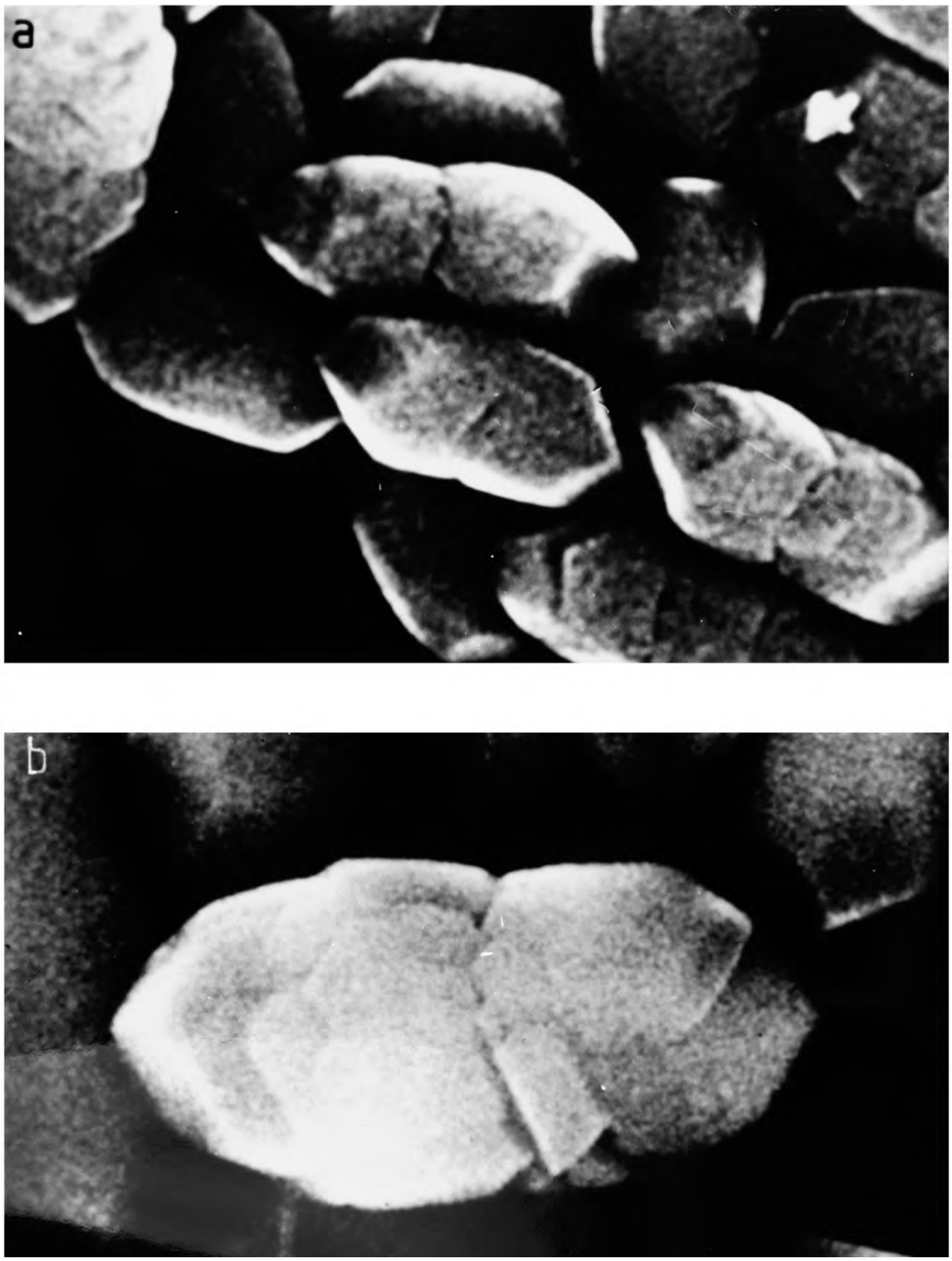

Figure 3.9

Saccular otoconia from rat showing 'waisting' at the equatorial plane. Magnification (a) x 5 440, (b) 10 700

plane in the equator of the crystal, but is more likely to be a factor arising from the positioning of the organic material which runs inside the otoconium and is known to be concentrated in this area (23). Apart from this crack, a series of surface fissures may be observed giving the overall appearance of a structure comprised of microcrystals which would be in the order of 1μm in length. Saccular crystals are shown in Figure 3.9 a and b

The utricular otoconia may show the waist seen in the saccular crystals, but this is not a regular feature (Figure 3.10). Two very interesting aspects of utricular otoconia are the various forms of growth that are revealed in the morphology. The first lies in the formation of the end-faces. Figure 3.11a shows a perfect end-face of calcite in the fore-ground, but lying beneath it is an otoconium which has formed improperly in that it has grown one set of rhombohedral end-faces and then continued the growth in a slightly mis-aligned manner. It should be noted that this extension of growth has a rounded body as would be expected for an otoconium and another set of end-faces at the end of the crystal. A related, but less marked example is shown in Figure 3.11b. This sample shows a line running parallel to the end-faces which may be a fresh growth up the side of the structure which has been inhibited by some means and thus failed to grow. It is also interesting to note that a similar inhibition has occured at the other end of the crystal giving a deformed character to the end with the body inhibited about two-thirds of the way through the growth. These two faults are probably examples of the same phenomenon viewed normal to each other and indicate that this arises from an error in the controlling organic matrix, rather than an inorganic crystal growth phenomenon.

Figure 3.10

Utricular otoconia showing occasional signs of waisting and dissolution into component crystallites.

Magnification x 9 126

Figure 3.11

Utricular otoconia showing controlled faults in the growth process. These are probably due to substitutions in the organic matrix. Magnifications (a) x 10 700 (b) x 12 000

The other aspect of otoconium growth which may be best observed in utricular crystals is the strongest indication so far observed that these structures are not single crystals. Figure 3.12a shows a utricular otoconium which has developed surface cracks and a central waist. These cracks seem to surround areas which are approximately otoconia-shaped in themselves as if the growth has occured by a packing together of minature crystals. If one considers a highly magnified area of this sample, however, (Figure 3.12b), one can see that each of these crystals are themselves composed of microcrystallites. This is particularly evident in the shadowy areas of the central fissure. The microcrystallite composition appears to extend over the entire structure, including the end-faces (arrow). There is no apparent long-range ordering of the packing of the crystallites which have the appearance of spherules at this resolution. The fact that these crystallites remain as distinct spherules rather than growing together into a single crystal, or even smaller microcrystals which could then comprise the whole structure, suggests that some form of organic matrix is surrounding each inorganic crystallite and acting as a kind of cement. This concept is of great importance when discussing biomineralisation phenomena and this observation, in conjunction with the work at ultra-high resolution discussed below led us to formulate an hypothesis of crystal packing in biominerals which is proposed above and, in the light of the work on otoconia, below. The problem left from the scanning microscopy observations concerned the nature of the component spherules of otoconia; to solve this, a transmission ultra-high resolution electron microscopy study was carried out.

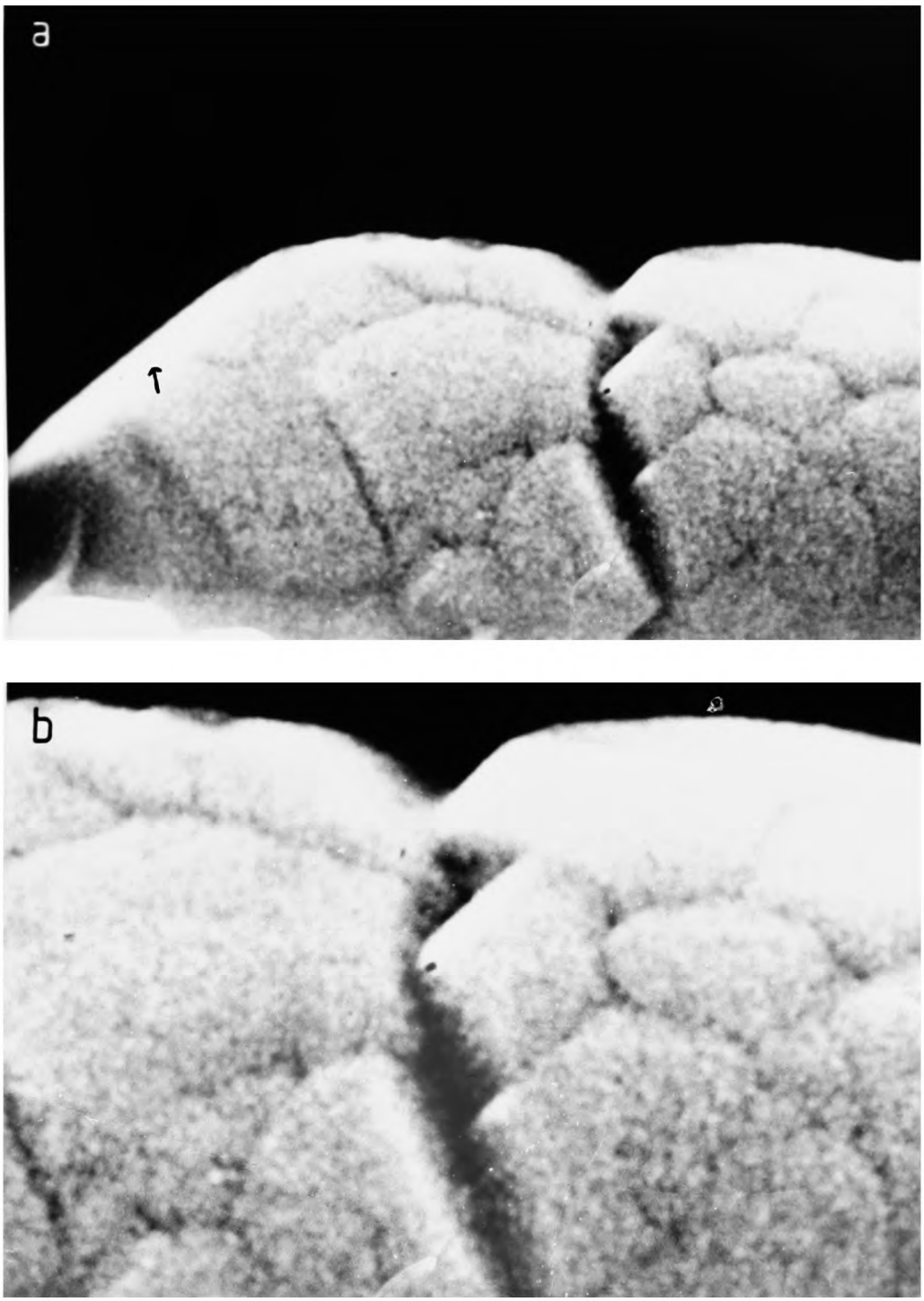

Figure 3.12

SEM of a saccular otoconium showing the component crystals and microscopic spherule structure.

(a) magnification x 18 325 (b) magnification x 32 000

3.3.2 X-ray Microanalysis of Otoconia

The X-ray detection facility on the Jeol-100CX Temscan electron microscope was used to carry out a qualitative analysis of rat otoconia. This showed that otoconia from both saccule and utricle contained trace quantities of magnesium, phosphorus and sulphur; chlorine was observed occasionally. This observation leads one to believe that the crystals themselves contain trace quantities of these ions and that they do not arise from trace quantities of artificial endolymph, which contains these ions, except phosphate. However, chloride is the major anion and one would expect it always to be present in analysis if this was the case. It will be observed from Table 3.II below that phosphorus was the most abundant trace element and this may be approximately quantified by the ratio method of Cheetham and Skarnulis (43). It should be noted that this procedure is accurate only for thin crystals, when corrections for atomic number effects, absorption and fluorescence become negligible; however, these crystals have a fairly constant thickness and thus will act as a guide of constancy of phosphorus concentration. The method involves a ratio for two elements involving their concentration, c_x and c_y, their intensities, I_x and I_y and the constant k_{xy}, which holds for the two elements in any particular piece of equipment (Cheetham, personal communication). The general equation is:

$$c_x/c_y = k_{xy}.I_x/I_y$$

Thus rearranging the equation, for calcium and phosphorus, we can obtain a value for the constant k_{CaP}:

$$k_{CaP} = \frac{c_{Ca}.I_P}{c_p.I_{Ca}}$$

TABLE 3.I

Determination of Calcium: Phosphorus constant by the method of Cheetham and Skarnulis (43). Values are the number of counts under the named peaks.

Standard used: $Ca_3(PO_4)_2$

	K_α(Ca)	K(P)
	59364	28559
	69921	33442
	36507	17694
	89203	42824
$\bar{x}$	63749	30630

Now:

$$\frac{c_{Ca}}{c_p} = k_{CaP} \frac{I_{Ca}}{I_p}$$

(see text)

Thus:

$$k_{CaP} = \frac{c_{Ca} \cdot I_p}{cp \cdot I_{Ca}} .$$

$$= \frac{3 \ . \ 30630}{2 \ . \ 63749}$$

$$= 0.72(1)$$

TABLE 3.II

X-ray Microanalysis of Otoconia from Utricle and Saccule of rat. Values are the intensities of the K_α peak and have the baseline count subtracted.

Utricle

Ca	P	S	Mg	Cl	K
49744	309	50	--	--	--
162278	4466	1507	--	1267	--
234112	1774	511	--	226	--
129094	313	180	--	--	--
45395	141	127	25	120	--
62893	173	98	57	62	--
32560	69	128	34	31	--

Saccule

Ca	P	S	Mg	Cl	K
138002	1336	814	--	--	--
92236	746	--	125	738	--
412204	852	224	98	5248	212
158534	1336	814	224	570	--
197585	2217	791	176	2247	--

This constant may be determined by calculation involving various parameters of the X-ray detector or by experimental measurement of the intensities of the calcium and phosphorus peaks from a sample of known stoichiometry. In this case, Calcium Orthophosphat $Ca_3(PO_4)_2$ was used and a k_{CaP} value of 0.72 obtained as detailed in Table 3.I.

The X-ray emission spectra obtained from both utricular and saccular samples reveals the presence of several trace elements, chief among which is phosphorus. The two types of otoconia reveal no significant differences in their spectra, typical examples of which are illustrated in Figures 3.13a and 3.13b. Table 3.II reveals that there is no constant pattern of composition, with the exception that phosphorus is always present. Magnesium was found in all except one of the saccular crystals analysed but less than half of the utricular samples; sulphur was absent only once, in a saccular crystal, but by contrast, potassium was detected on just one occasion. Sodium was never present in significant quantities and this and the widely changing values of chlorine led to the conclusion that the presence of these trace elements is a property of the crystals and not just an artefact.

The calcium and phosphorus values were quantified in Table 3.III, which reveals that the ratio is never stoichiometric. The widely varying values of phosphorus concentration in both utricular and saccular samples indicates that the phosphorus is present as a trace element. It should be noted, however, that the figures shown in Table 3.III were, in part obtained from crystals in which the $K_\beta:K_\alpha$ ratio was lower than the expected 12%-13% for thin crystals (43) which indicates that

Figure 3.13

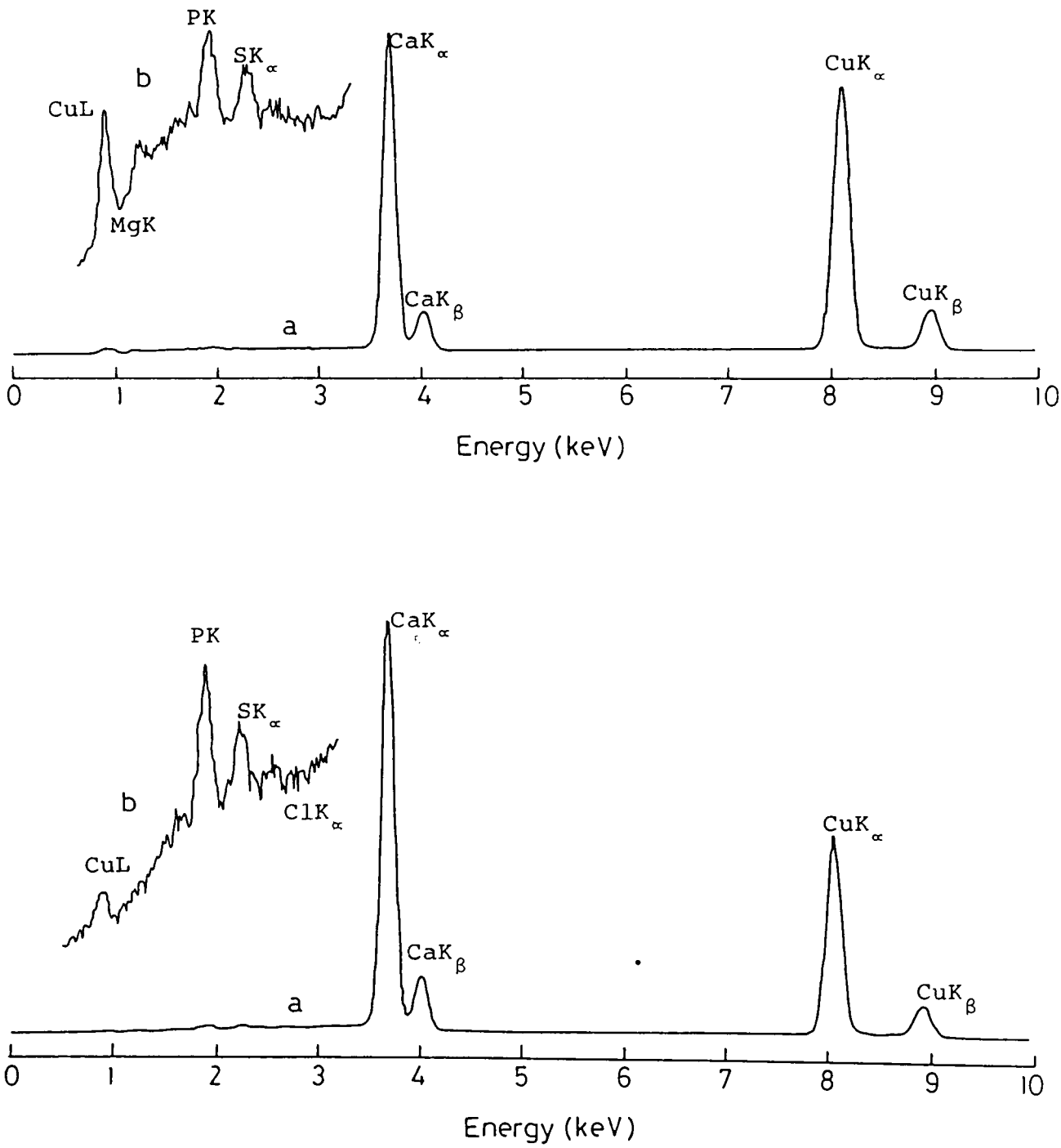

X-ray microprobe analysis of (top) saccular and (bottom) utricular otoconia from rat. Trace b is x16 in each case.

TABLE 3.III

Quantification of Calcium: Phosphorus Ratio in Utricular and Saccular Otoconia. The values in parentheses are clearly anomalous and have been excluded from the calculation.

Utricle

	K_{α}(Ca)	$k_{CaP}.K_{\alpha}$(Ca)	K(P)	Ca:P
	49744	35815.68	309	115.91
	(162278	116840.16	4466	26.16)
	234112	168560.64	1774	143.58
	129094	93051.06	313	297.29
	45395	32684.40	141	231.80
	62893	45282.96	173	261.75
	32560	23443.20	69	339.76
$\bar{x}$	92299.67	66472.88	463.17	231.68

Saccule

	K_{α}(Ca)	$k_{CaP}.K_{\alpha}$(Ca)	K(P)	Ca:P
	138002	99361.44	1336	74.37
	92236	66409.92	746	89.02
	412204	296786.88	852	348.34
	158534	114144.48	1336	85.44
	197585	142261.20	2217	64.17
$\bar{x}$	199712.20	143792.78	1297.40	110.83

some absorbtion is occurring. The $K_\beta:K_\alpha$ ratio data are listed in Table 3.IV. More analyses of thin crystals would be required to obtain statistically significant data.

The qualitative observations of otoconia composition are of great interest when one considers that they are formed in vivo in a endolymph-filled cavity and are then extracted with artificia. endolymph, neither of which fluid fully accounts for the observations. The comparison with the quantitative determination of fish otolith composition is of great interest, particularly when one considers the sodium content of each biomineral and the suggested physiological purpose of its presence in otoliths. This observation will be discussed at greater length below.

3.3.3 Methods of Preparation of Samples for Ultra-High Resolution Electron Microscopy

One problem with the study of biological tissues by electr microscopy is the preparation of samples which are suitable. This involves obtaining a sample which is thin enough to allow the transmission of electrons through yet robust enough not to be destroyed by the heat generated by the transmission of electrons. There are various methods which are used, when the biological sample is a tissue, which involve fixing, dehydrating and staining the sample, and then sectioning with an ultra-microtome to obtain a very thin specimen (44). When studying minerals, however, a different set of problems arise. The sample does not need to be dehydrated or fixed and staining is detrimental to obtaining an ultra-high resolution micrograph; in this respect, preparation is easier. However, it is not easy to obtain sections which are

TABLE 3.IV

Determination of the area of the K_β peak as a percentage of the area of the K_α peak for calcium in Otoconia samples.

Utricle

K_α(Ca)	K_β(Ca)	K_β as % K_α
414314	49873	12.04
129094	12569	9.74
45395	4387	9.66
62893	6047	9.61
49744	4641	9.33
32560	3000	9.21

Saccule

K_α(Ca)	K_β(Ca)	K_β as % K_α
138002	16568	12.01
412204	44765	10.86
92236	8596	9.32

thin enough for study. At the beginning of our study, a variety of preparative methods were attempted and the success of the method judged from the amount of artefact visible under the electron microscope. These methods included ion-beam thinning, sectioning, crushing under liquid nitrogen and crushing gently between glass microscope slides or in a small pestle and mortar.

Ion-beam thinning produced acceptable diffraction patterns, although certain zones were identified by this method and no other (see below). This arose from the fact that it is impossible to align the otoconia in the resin before thinning takes place; thus it is not likely that one will obtain reproducible results since the otoconia will be thinned at whatever angle they are constrained at. Furthermore, it was found that the images were very hazy due to the resin which tended to overlap the sample. Whilst one might obtain recognisable patterns and images from the Jeol-100CX electron microscope, this would certainly not be the case in the Jeol-200CX high resolution microscope, since the obscuring resin would degrade the resolution obtainable. A typical diffraction pattern and micrograph from an ion-beam thinned sample is illustrated in Figure 3.14.

Sectioning using an ultra-microtome was attempted at the University of Michigan. This technique is probably the most difficult of all preparative techniques of mineralised tissues since the mineralised tissue is of about the same hardness as the surrounding resin, or even greater. The consequence of this is that the sample tends to bounce out of the resin when struck by the sectioning knife. As a result, Spurr's resin is commonly used (45,46). This is a low-viscosity epoxy resin with variable hardness which can be made suitable for various mineral samples.

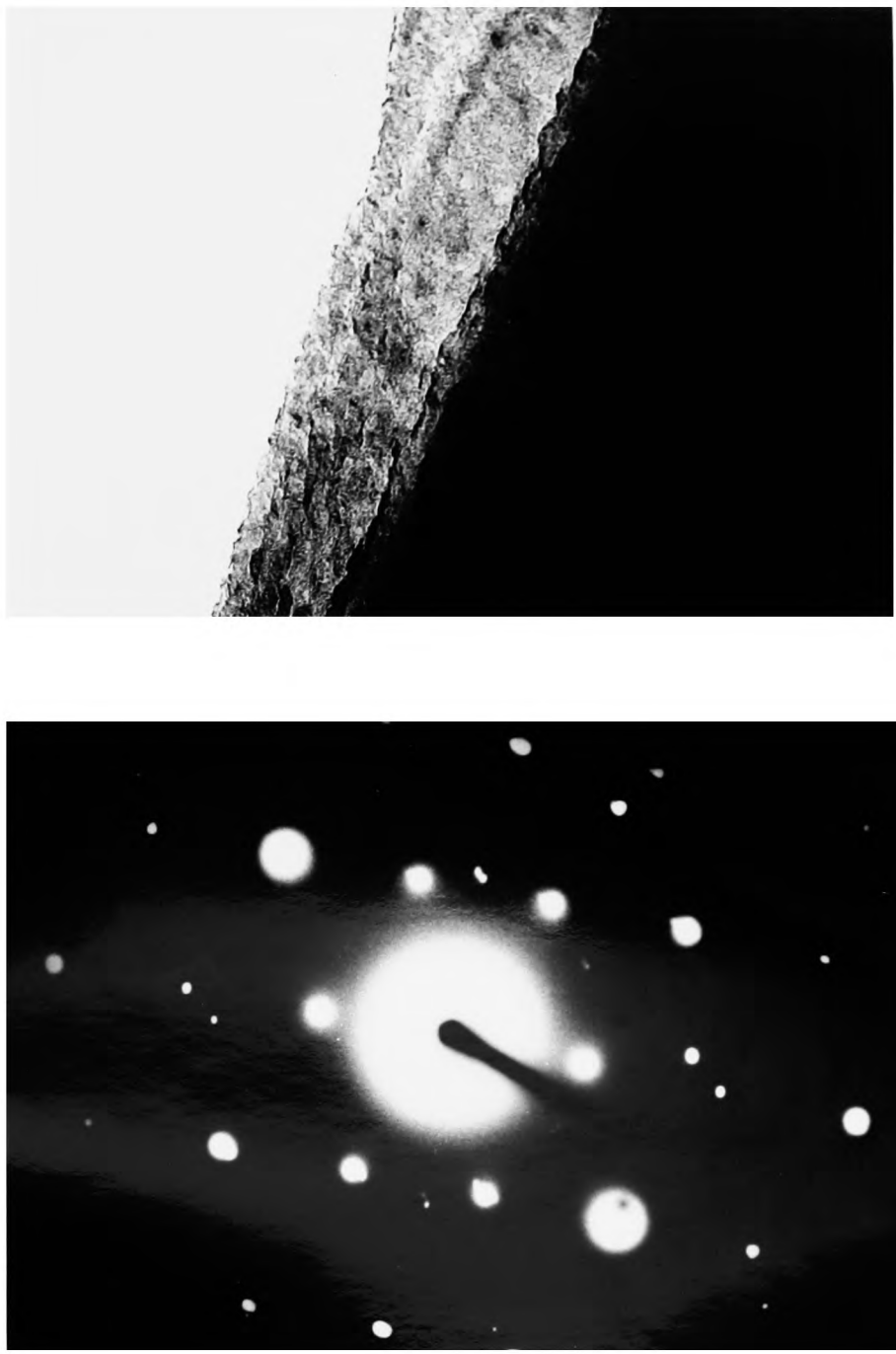

Figure 3.14

(a) TEM and (b) electron diffraction pattern of an ion-beam thinned sample of rat otoconia. The zone revealed is a [201] zone of calcite. Magnification = x320 000

Spurr's resin is most suitable for bone samples, which are not as brittle as calcium carbonates. We found that no high quality sections were obtainable; those which were sectioned proved to be highly disfigured by the process. An example of a sectioned otoconial sample is illustrated in Figure 3.15.

Crushing was attempted, firstly in liquid nitrogen as it was feared that the heat generated within the crystal lattice would cause faults to appear which would be observed in the high-resolution microscope; it was found, however, that the liquid nitrogen caused damage, the samples crushed in this way showing shear faults and also gross Moiré fringes. This may be seen in the sample illustrated in Figure 3.16. Consequently, it was decided to prepare all samples by crushing gently between glass slides or in a pestle and mortar; all micrographs of otolith and otoconia samples and their respective mineral counterparts illustrated below are prepared in this way.

3.3.4 Electron Diffraction Studies of Otoconia, Otoliths and their Geological Counterparts

The first transmission electron microscopy work, carried out on the Jeol-100CX electron microscope, on the crushed samples included a study of the various electron diffraction patterns obtained from the fragments of minerals. It was reasoned that crushing causes a mineral to fracture along the lines of least strength and a comparison of the zones exposed when crushing a biomineral and its geological counterpart would give an indication of whether they had the same ultrastructure or not. The results of the work are presented in Table 3.V below. If the aragonitic minerals are considered first,it will be seen that the mineral

Figure 3.15

High resolution micrograph of a sectioned otoconium. Damage to the sample is visualised by the presence of Moiré fringes. Magnification = x1 500 000

Figure 3.16

High resolution micrograph of rat otoconia crushed under liquid nitrogen. Distortions are clearly visible.

Magnification = x1 950 000

TABLE 3.V

The identification of Various Crystal Faces of Calcium Carbonate from the Geological and Biological Minerals Under Discussion

Face...	001	010	011	100	111	211	401	421	42$\bar{1}$
Aragonite	---	5	---	---	---	---	---	---	---
Fish	3	4	---	---	---	---	---	---	---
Frog	4	4	3	1	---	---	---	---	---
Calcite	2	---	---	---	---	4	3	5	2
Rat	10	---	---	---	3	3	---	1	---

Note: 3 (201) faces were also observed, but only in ion-thinned samples and were thus discounted for reasons explained above.

always fractured to expose the [010] zone; there is rather more spread in the results from the frog otoconia and fish otolith, but the [010] zone remains prominent, particularly in the fish otolith. The comparison of the rat otoconia and Iceland Spar shows more marked differences; the calcite always fracturing to reveal high index zones, with [421] particularly common. The otoconia, however, shattered in a completely different way, with low index zones showing (although occasional high index zones were observed).

The interpretation of this data gave a further indication that the otoconia were not single crystals, and enabled a working hypothesis to be constructed for the ultrastructure of both otoconia and otoliths. When mineral aragonite is fractured, it breaks along the twin plane, which is the [010] zone; where the polycrystallite fish otolith is shattered, it breaks along the organic matrix which binds each crystallite together, revealing much the same zones since these are the ones which tend to be on the outside of a crystal as it grows normally. Thus,essentially the same process is happening in the aragonitic mineral and biomineral. In the calcitic minerals, however, a different phenomenon occurs. Calcite is not so prone to twin as aragonite (although it is known). When Iceland Spar is crushed, a single crystal is broken open; the [421] and other high index faces obviously being comparatively weak. In the otoconium, however, low index figures are revealed. This indicates that once again the fracture is taking place along lines of organic matrix revealin the faces that normally lie on the outside of calcite crystals. The only explanation to fit the observations is that otoconia are composed of microcrystals which are surrounded by organic matrix which binds them together and also orients each crystallite

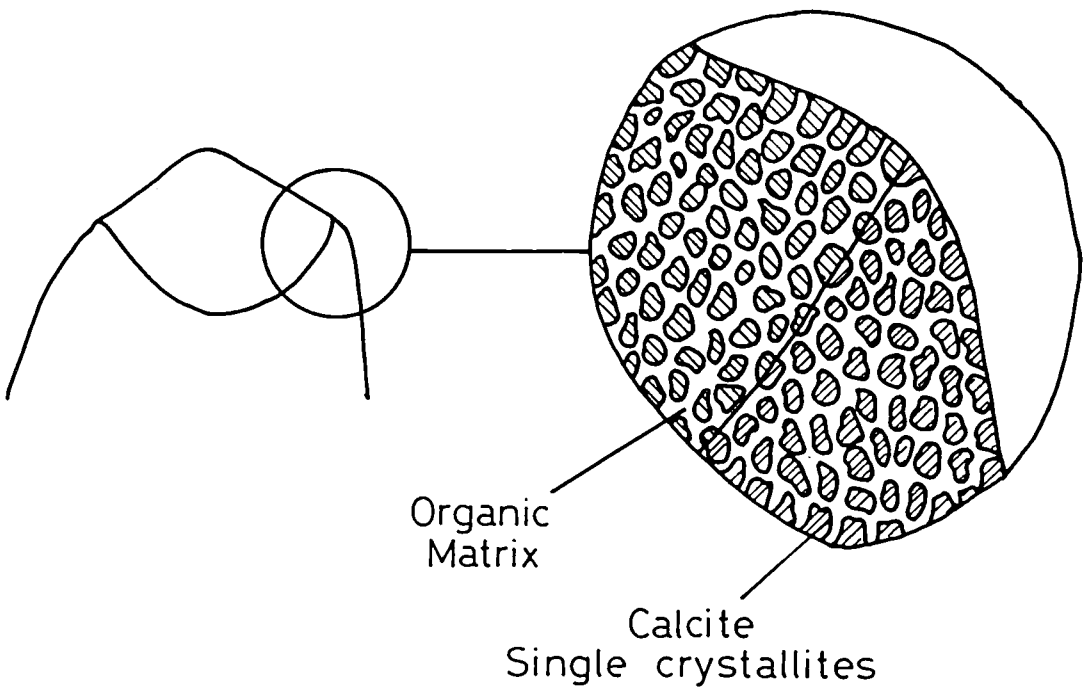

Figure 3.17

Diagram illustrating the relationship between the mineral crystallites and the organic matrix in otoconia

so that they face in approximately the same direction. This is illustrated diagrammatically in Figure 3.17.

3.3.5 Ultra-High Resolution Electron Microscopy of Calcite

Iceland Spar was studied as the model system for mammalian otoconia. When samples were crushed as described above, small plate-like particles were produced which had straight sides and flat angles. This is characteristic of a shattered inorganic crystal. A sample, photographed by both transmission and scanning electron microscopy, is illustrated in Figure 3.18. Despite the poor image, the sample was not gold sputtered,but the SEM clearly shows the layers making up the crystal. For a sample to be of use in ultra-high resolution TEM, a layer must be separated from the crystal mass so that its maximum thickness is not more than about 20 nm. In practice, it was commonly found that suitable images were obtained from the edges of crystals in which the bulk was too thick for imaging. One very good example of such a crystal is illustrated in Figures 3.19 and 3.20. The diffraction pattern shown in Figure 3.20b was identified from the computer-generated pattern (figure 3.20c) as a [421] zone. The most intense reflections from this zone are the $0\bar{1}2$, $01\bar{2}$, $\bar{1}12$ and $1\bar{1}\bar{2}$, which all have a d-spacing of 3.85 Å. It will be observed from Figure 3.20c that these reflections are the four closest to the centre point of the pattern, and these give rise to the pattern of lattice fringes observed on the image. By knowing the absolute value of the d-spacing, the magnification can be calculated with great accuracy, and is given in the figure legends.

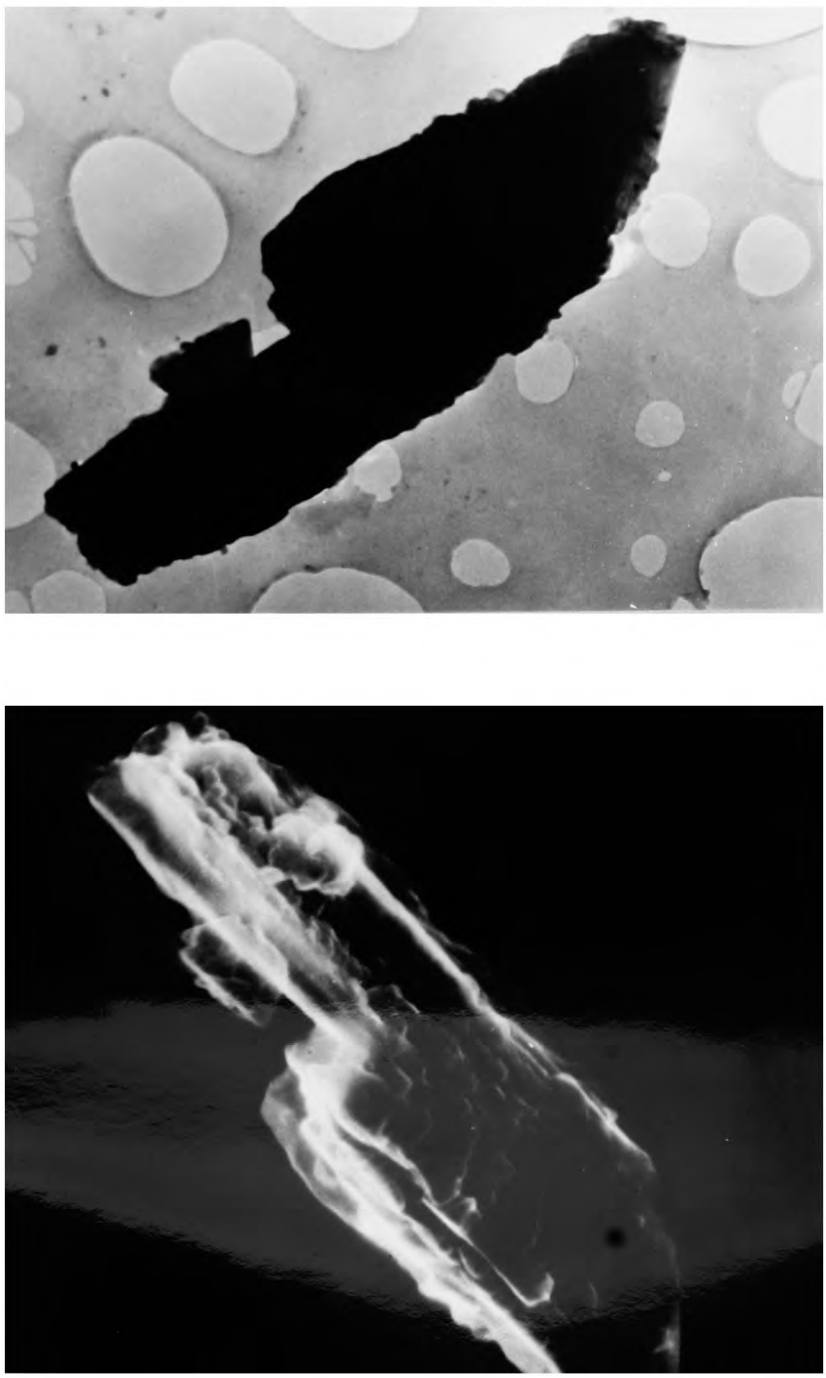

Figure 3.18

(a) TEM and (b) SEM of a sample of crushed calcite. The two images are photographed from opposite sides of the crystal. Magnification = x27 000

Figure 3.19

Ultra-high resolution micrograph of a sample of crushed calcite, revealing a [421] zone.

Magnification = x1 050 000

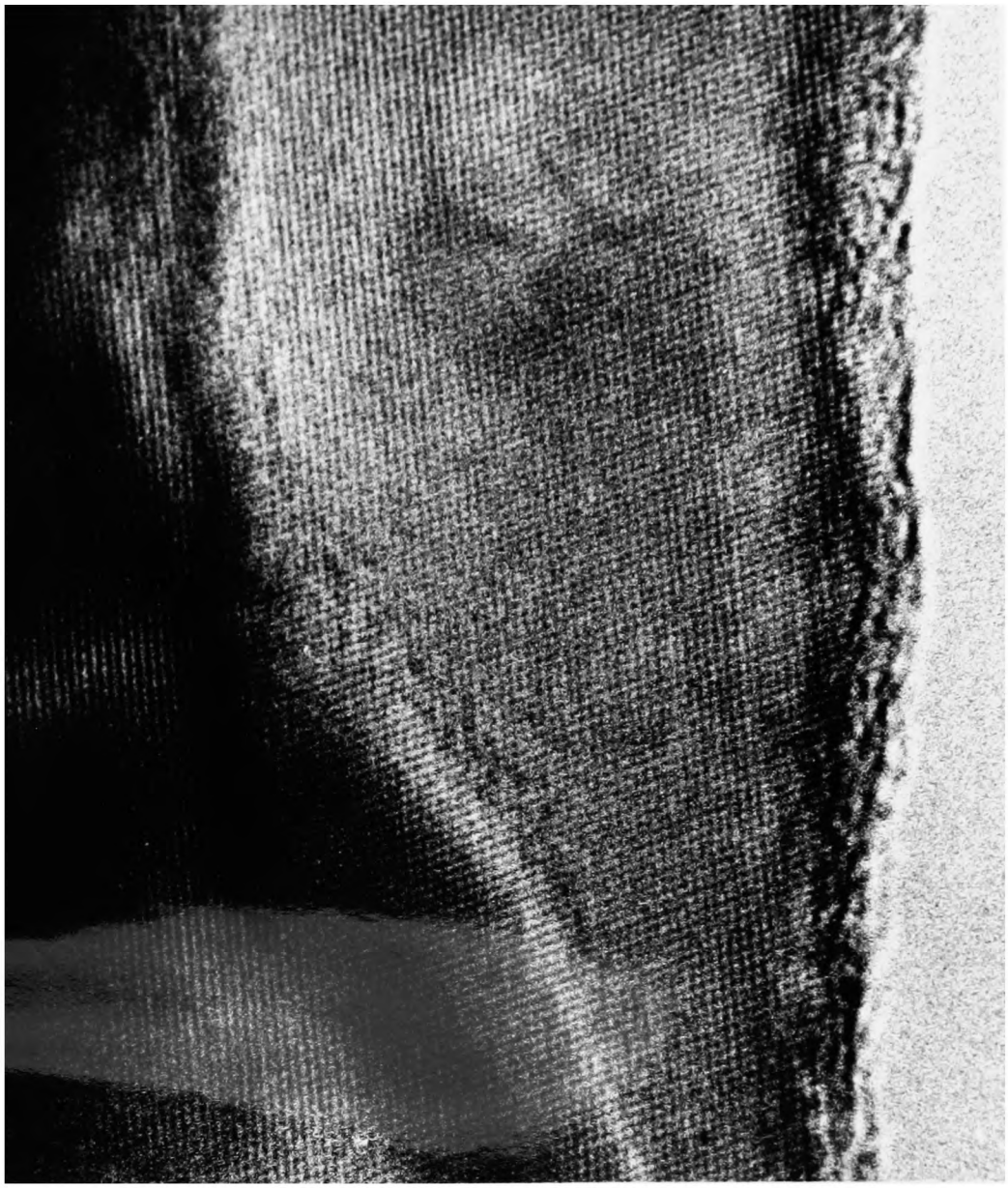

Figure 3.20a

Enlargement of the sample shown in Figure 3.19, showing the lattice fringes extending in two directions.

Magnification = x3 600 000

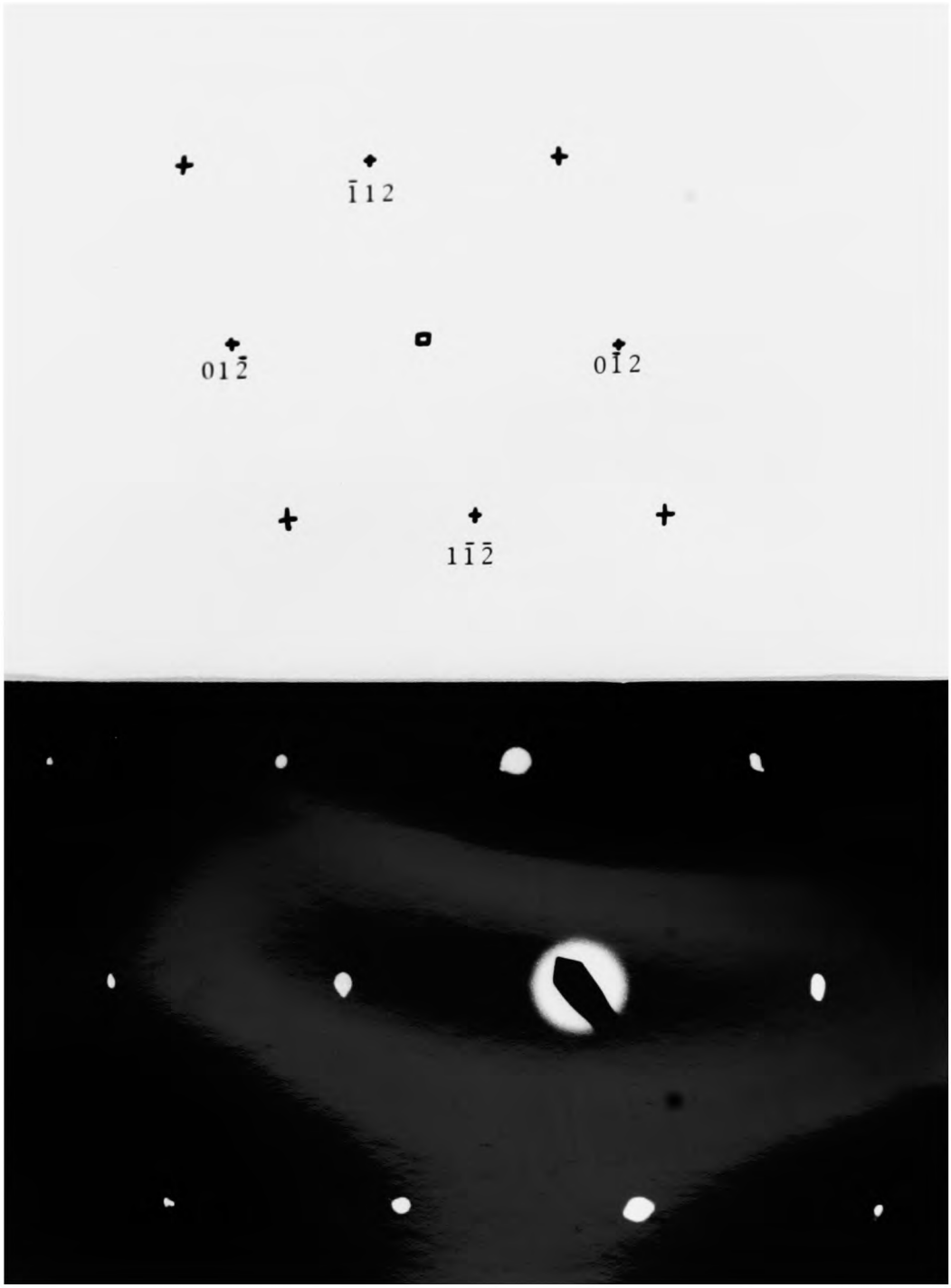

Figure 3.20b

Theoretical and experimental electron diffraction pattern of a [421] zone of calcite obtained from the sample shown in Figure 3.19. The theorectical pattern shows the reflections giving rise to the lattice image.

The electron micrographs reveal that the crystal is very well-formed, with a very high incidence of correct periodicity; occasional faults may be observed, however, and Figure 3.21 illustrates some of these observed in an Iceland Spar sample, together with a graphical version of a plane dislocation. The quality of a sample may be seen readily by combining the techniques of electron diffraction and ultra-high resolution TEM. Figure 3.22 shows a sample of calcite prepared by crushing which has not proved to be suitable for imaging. This sample has been broken into many crystallites by the preparation and possibly also by beam damage. Consequently, the electron diffraction pattern is that of a calcite powder and the lattice image confirms that it is comprised of shattered crystallites; the presence of Moiré fringes throughout the sample support the hypothesis that the damage was caused by preparation and was not present in the original system. The sample shown in Figure 3.23 is of interest in that it demonstrates that the lattice is maintained almost to the edge of the crystal, at which point it collapses completely to give what appears to be an amorphous outer coating of about 30-50 Å. This sample is shown from the diffraction pattern to be a [401] zone and the lattice fringes lie 4.32 Å apart. Many of the properties noted for the geological sample can be contrasted with the calcite formed in the biological system, which, since it is formed very quickly, might be thought to be much less well-formed and unstable. This comparison will be made after the micrographs of calcite from rat otoconia have been discussed.

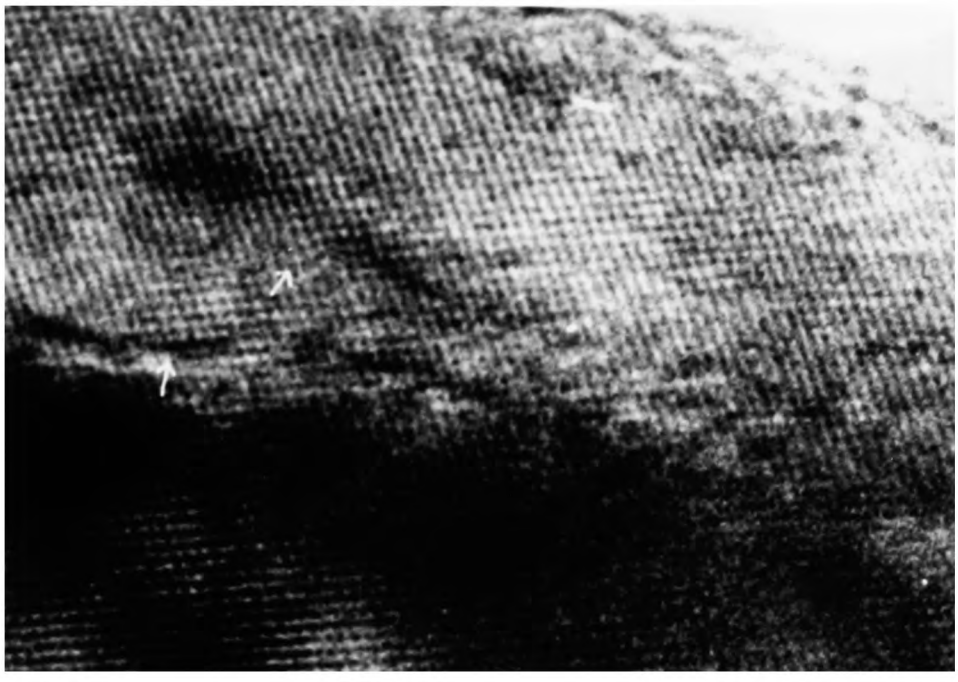

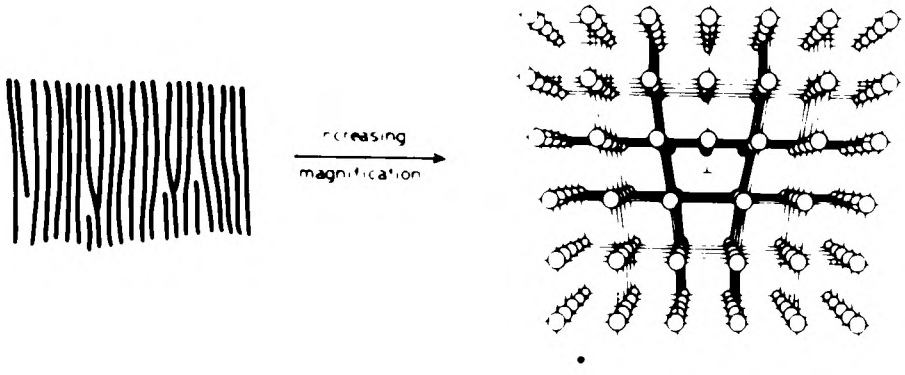

Figure 3,21

(a) Faults in a sample of calcite are rare, but may occasionally be observed. Arrows mark discontinuities in the lattice. Magnification = x4 700 000

(b) A diagrammatic representation of a plane dislocation in a lattice.

Figure 3.22

Sample of crushed calcite which has shattered into many crystallites and also shows gross Moiré fringes.

Magnification = x1 050 000

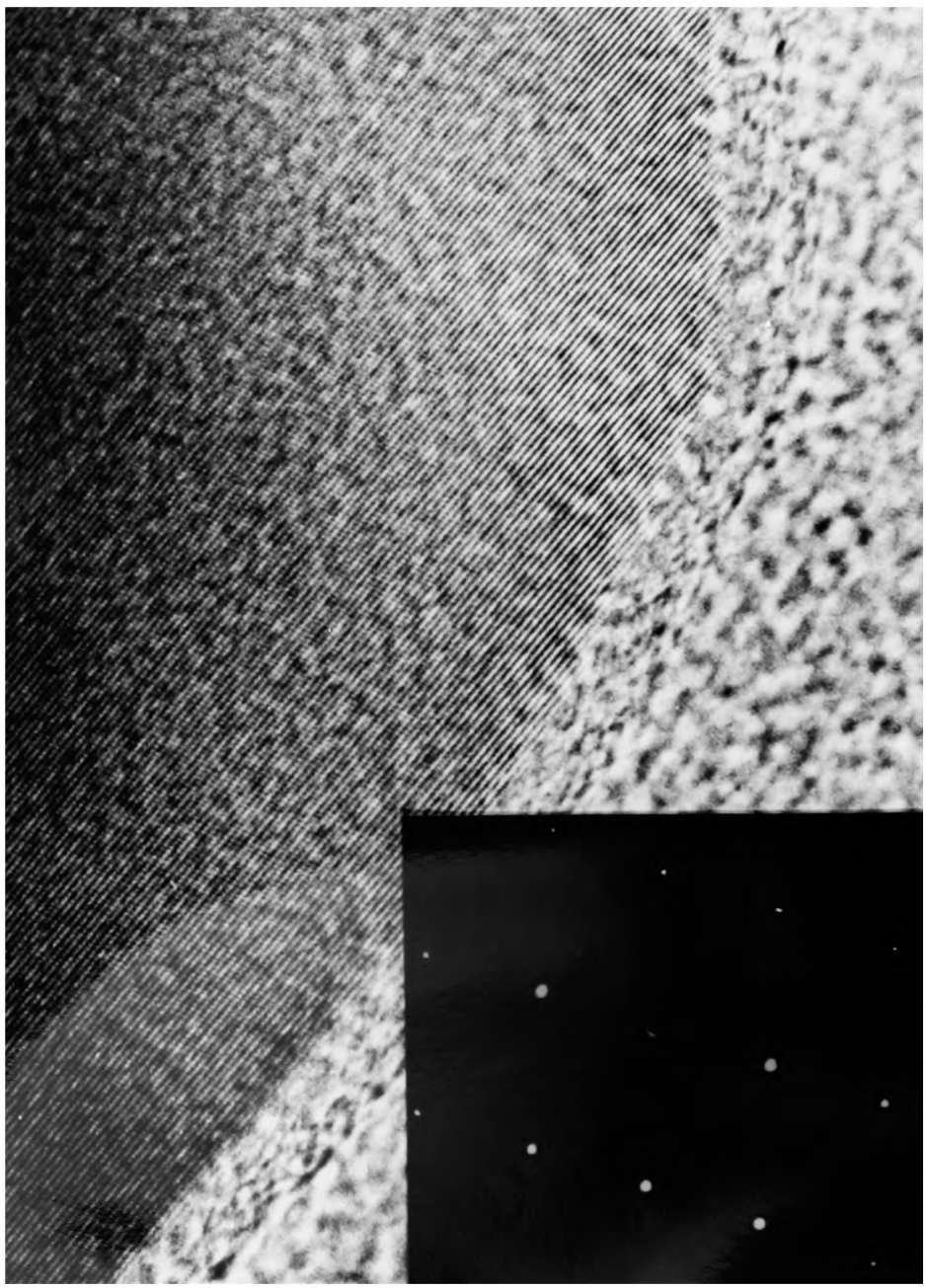

Figure 3.23

HRTEM and (insert) electron diffraction pattern of crushed calcite. Magnification = x2 200 000

3.3.6 Ultra-High Resolution Electron Microscopy of Geological Aragonite

Aragonite proved to be more difficult to crush without producing artefacts, even without the presence of liquid nitrogen. It was found to shatter in plate-like structures, which are particularly apparent in Figure 3.24. The sample, and its diffraction pattern shown in Figure 3.25 are good examples of a damaged crystal from the preparation, with crystalline areas clearly visible, but with no overall orientation and the diffraction pattern going to powder from its original [010] zone. The best result, which is shown in Figure 3.26, is of great interest, partly because of the high quality of the image, but also because shear faults are apparent running through the sample. This results in the rather messy quality of the electron diffraction pattern, but Figures 3.26 and3.27 give a good illustration of the benefits of using diffraction and transmission microscopy in tandem. The sets of fringes visible on the sample are due to two reflections, the 200, with a d-spacing of 3.50 Å, and the 100 with a d-spacing of 4.96 Å. The observation of this reflection is of considerable importance in that it is nominally forbidden. The computer-calculated diffraction pattern for an [010] zone of aragonite is shown in Figure 3.27a and the pattern obtained from this sample in Figure 3.27b. This is due to the double diffraction of certain reflections in the pattern, resulting in a very intense 100 reflection. The phenomenon of double diffraction will be discussed below. Enlargements of certain areas of Figure 3.26 reveal the quality of the crystalline areas of the structure, and in particular, the nature of the faults running through the crystal. Aragonite was found to be quite stable in the electron

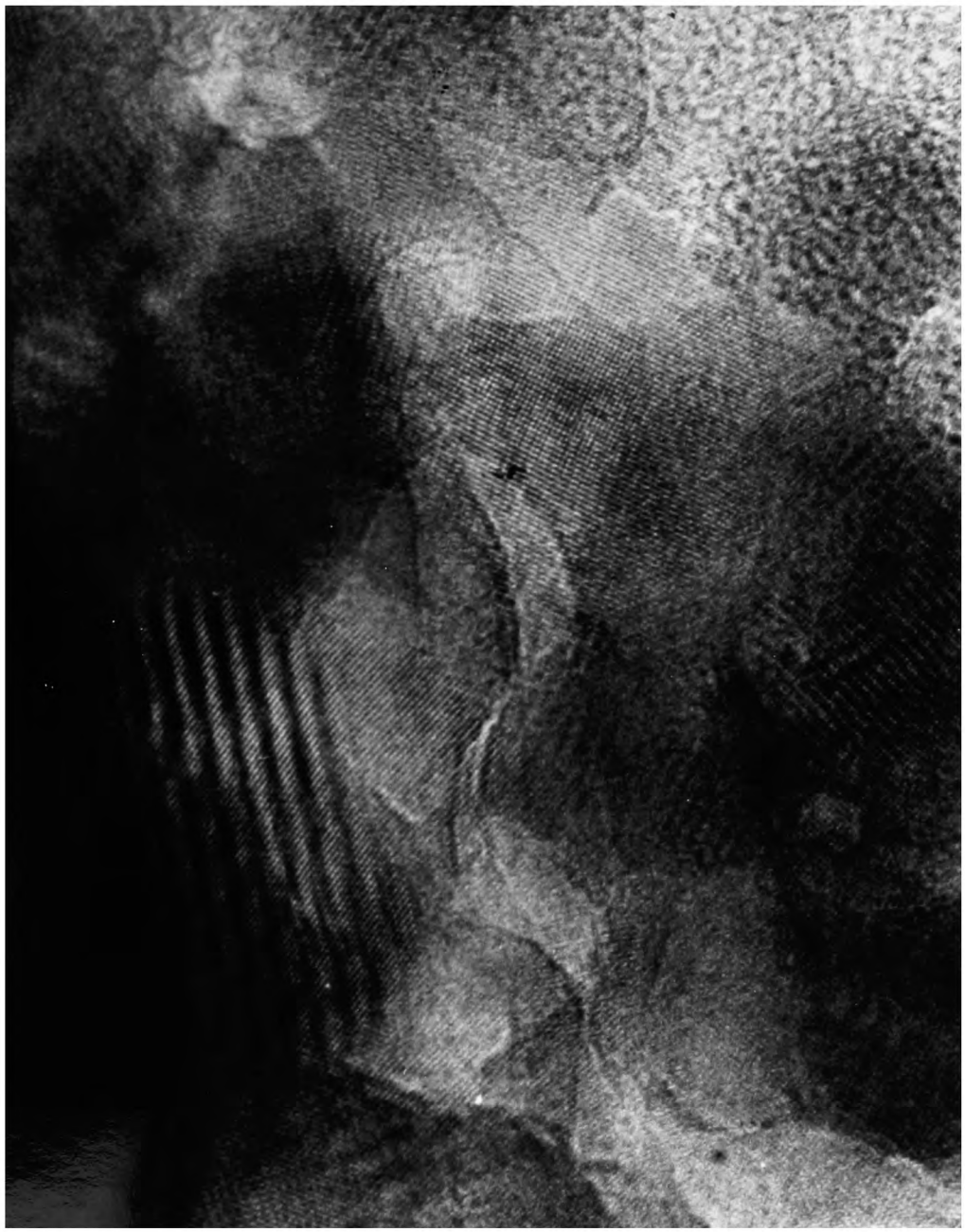

Figure 3.24

Sample of crushed aragonite, showing the plate-like structure of the mineral.

Magnification = x2 700 000

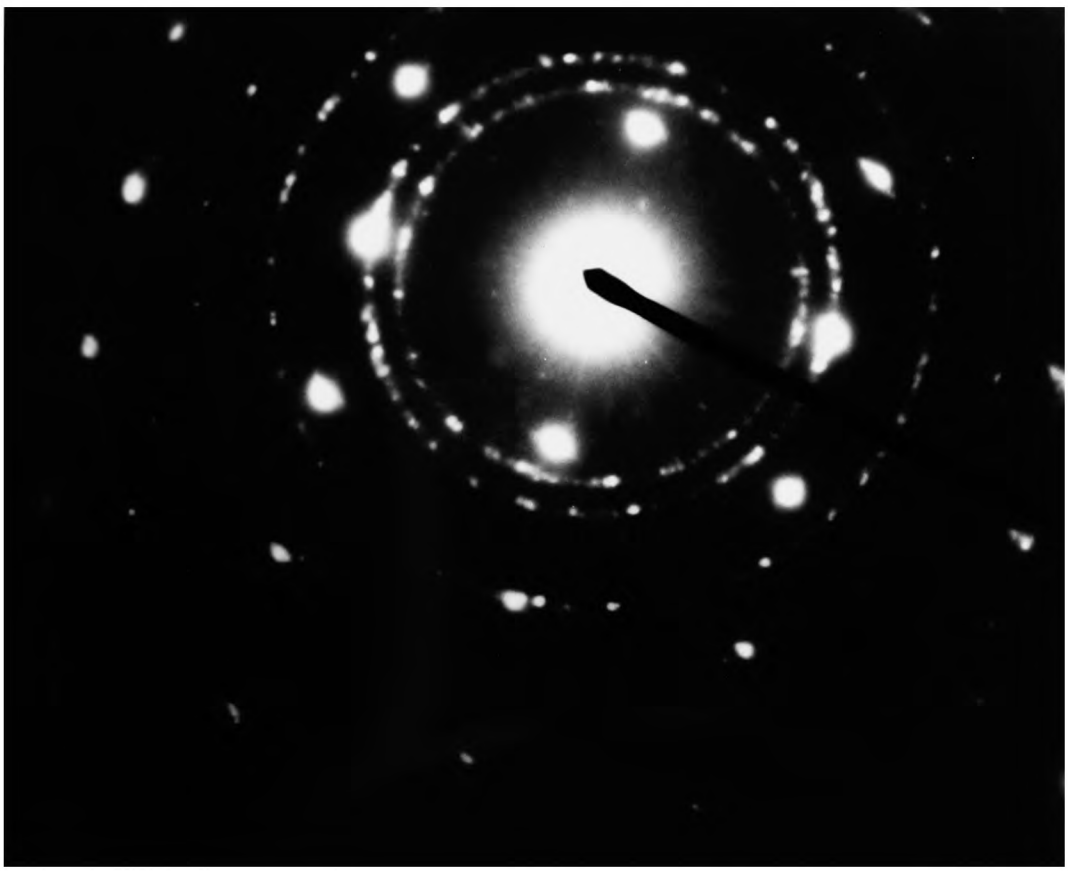

Figure 3.25

Electron diffraction pattern of the sample shown in Figure 3.24, showing the extent of damage seen in the lattice image. The pattern is an [010] zone of aragonite going to powder.

Figure 3.26

HRTEM of crushed aragonite. The diffraction pattern from this sample is shown in Figure 3.27. Arrows mark the points of dislocations through the sample.

Magnification = x1 060 000

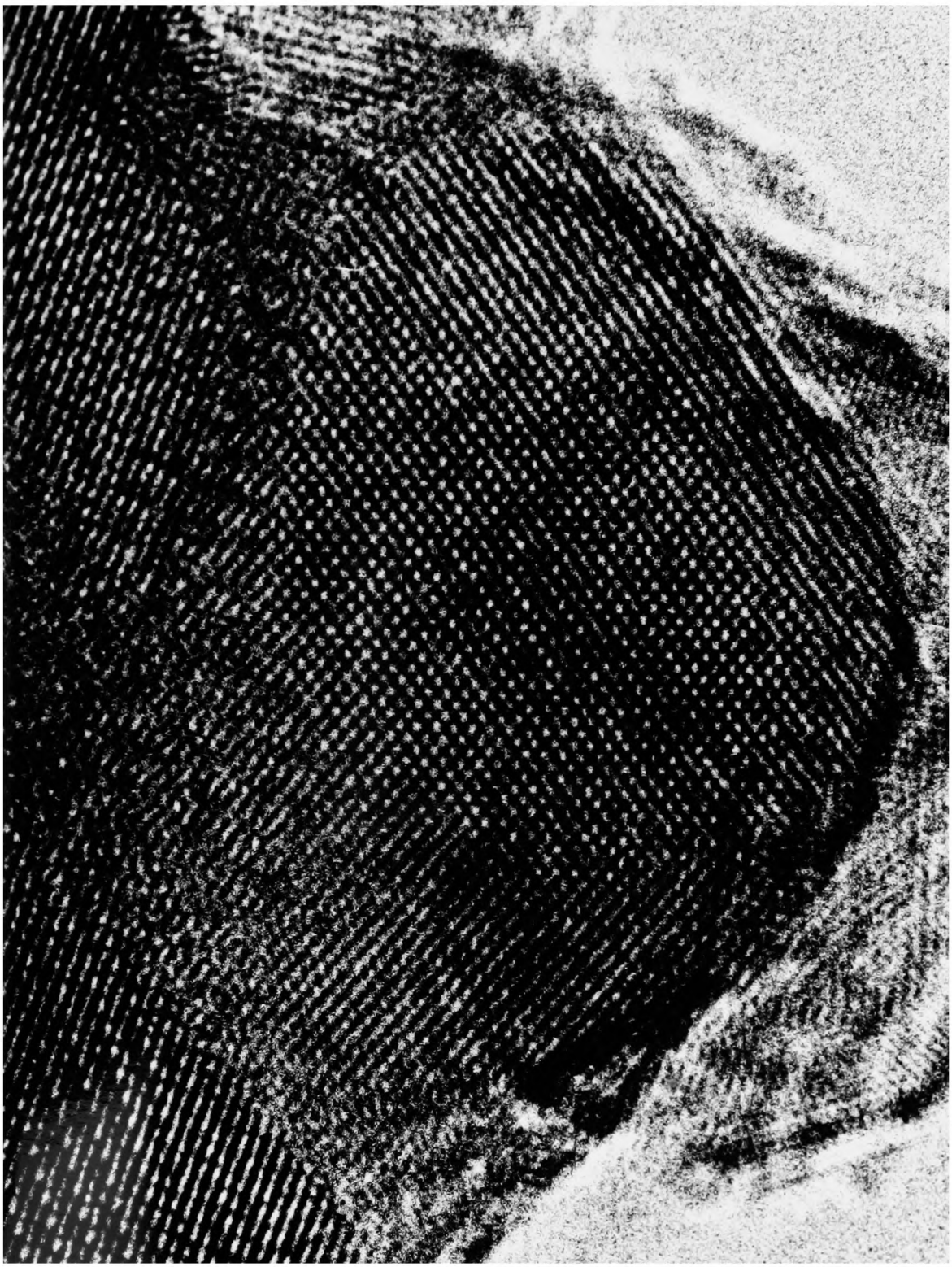

Figure 3.26b

Enlargement of part of Figure 3.26a, showing the quality of the lattice and the two sets of d-spacings (bottom left-hand corner).

Magnification = x7 600 000

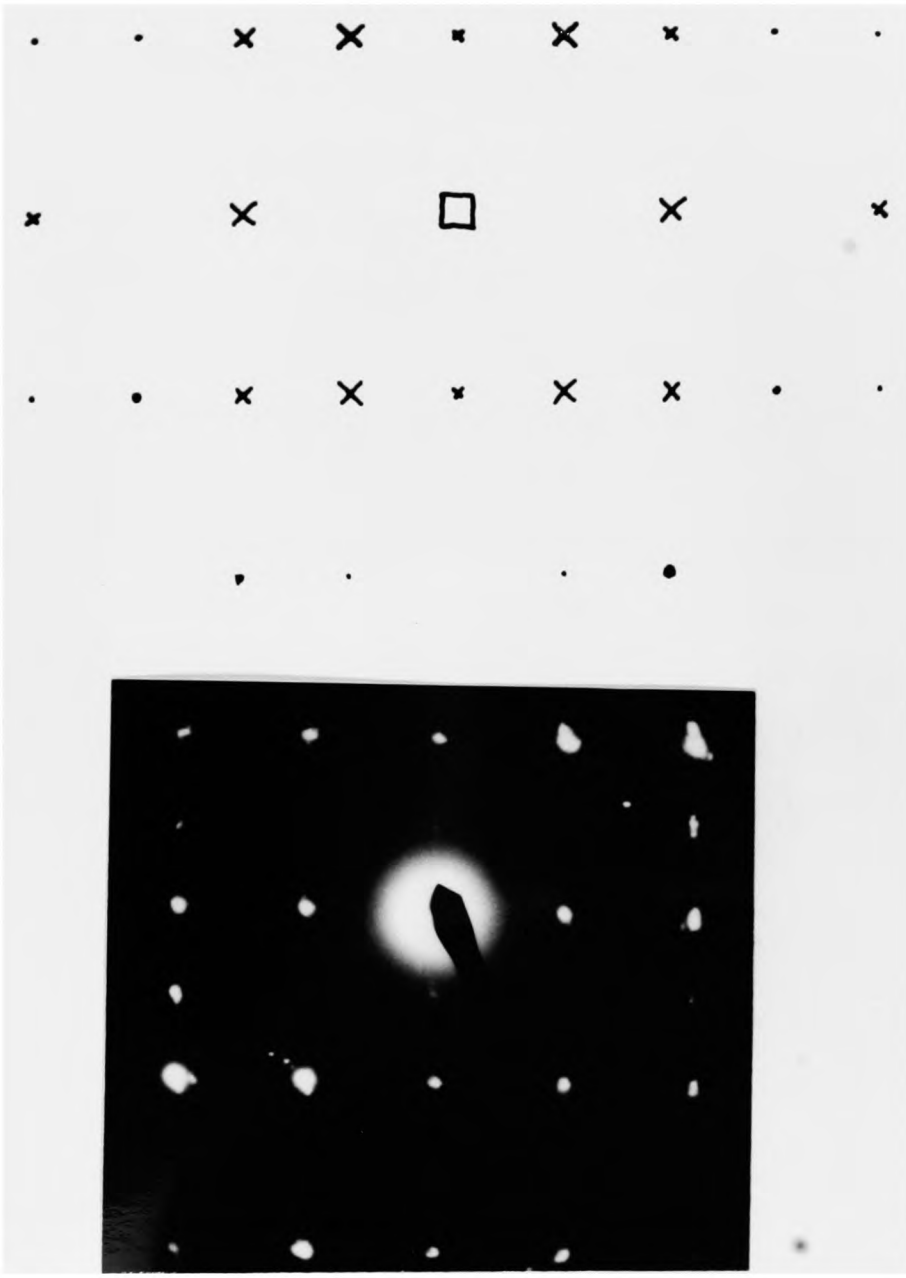

Figure 3.27

(a) computer prediction and (b) experimentally obtained electron diffraction pattern of an [010] zone of aragonite. Note the presence of nominally forbidden reflections.

beam, only showing signs of degradation after several minutes and then collapsing to a powder diffraction pattern.

3.3.7 Ultra-high Resolution Electron Microscopy of Rat Otoconia

Calcitic samples from rat otoconia proved to be stable under the electron beam, thus allowing high quality images to be obtained. As with all of these samples, the crushing preparatic gave several types of particles, many of which were too thick for high resolution study. One such particle is shown in Figure 3.28. This appears to be a large particle made up of several small crystallites of calcite; the significance of such a particle will be discussed below. Many particles of much smaller dimensions were found after crushing, but, again like the other minerals, some of these had been damaged during the preparation which had heavy Moiré fringes over them (see, for example, Figure 3.29). These were rejected in favour of crystallites which gave a single crystal electron diffraction pattern.

A study of those crystallites which met this criterion revealed a striking contrast to the fragments of Iceland Spar. The crystallites generated from otoconia were small (up to about 800 Ångstroms across) and were rounded, although some had a flat side. Most particles revealed an [001] zone by electron diffractio although one gave a [421] pattern. The shape of this crystallite proves it to be related to the others observed. Two of these crystallites are illustrated in Figures 3.30 and 3.31, the latter being a particularly fine example with no discernable structural faults and the fringes lying 4.32 Å apart due to the 110 and $\bar{1}\bar{1}0$ reflections, which, although having the same d-spacing as the $\bar{1}00$, $0\bar{1}0$, 010 and 100 reflections, are by far the most intense. This is illustrated by the predicted diffraction pattern for this zone,

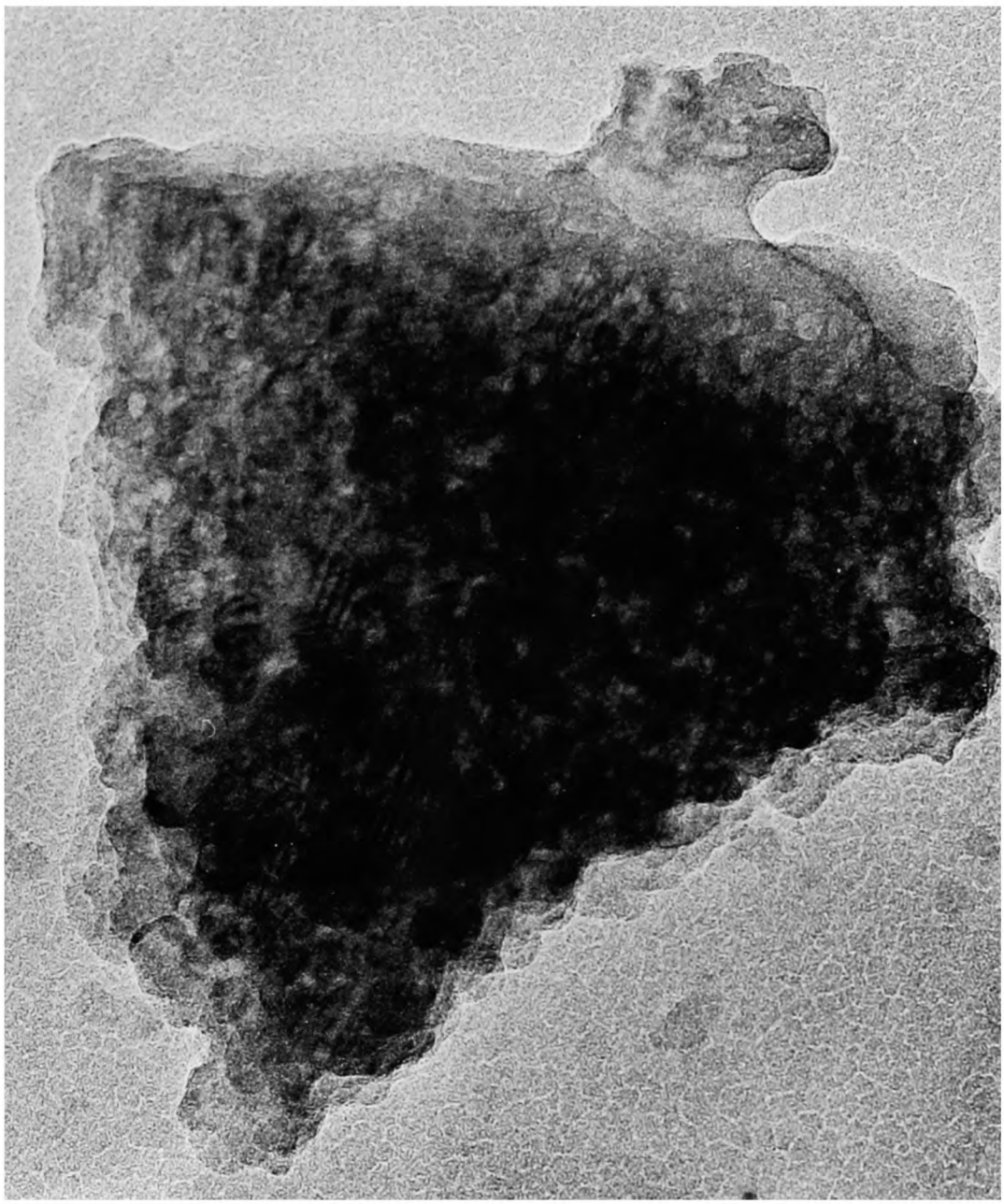

Figure 3.28

Mass of crystallites from crushed otoconia. The layer structure is apparent. This type of particle might be a composite crystallite.

Magnification = x160 000

Figure 3.29

High resolution micrograph of crushed rat otoconia. This sample shows lattice fringes extending in several directions which may be due to the sample comprising several single crystallites packed together. Magnification = x120 000

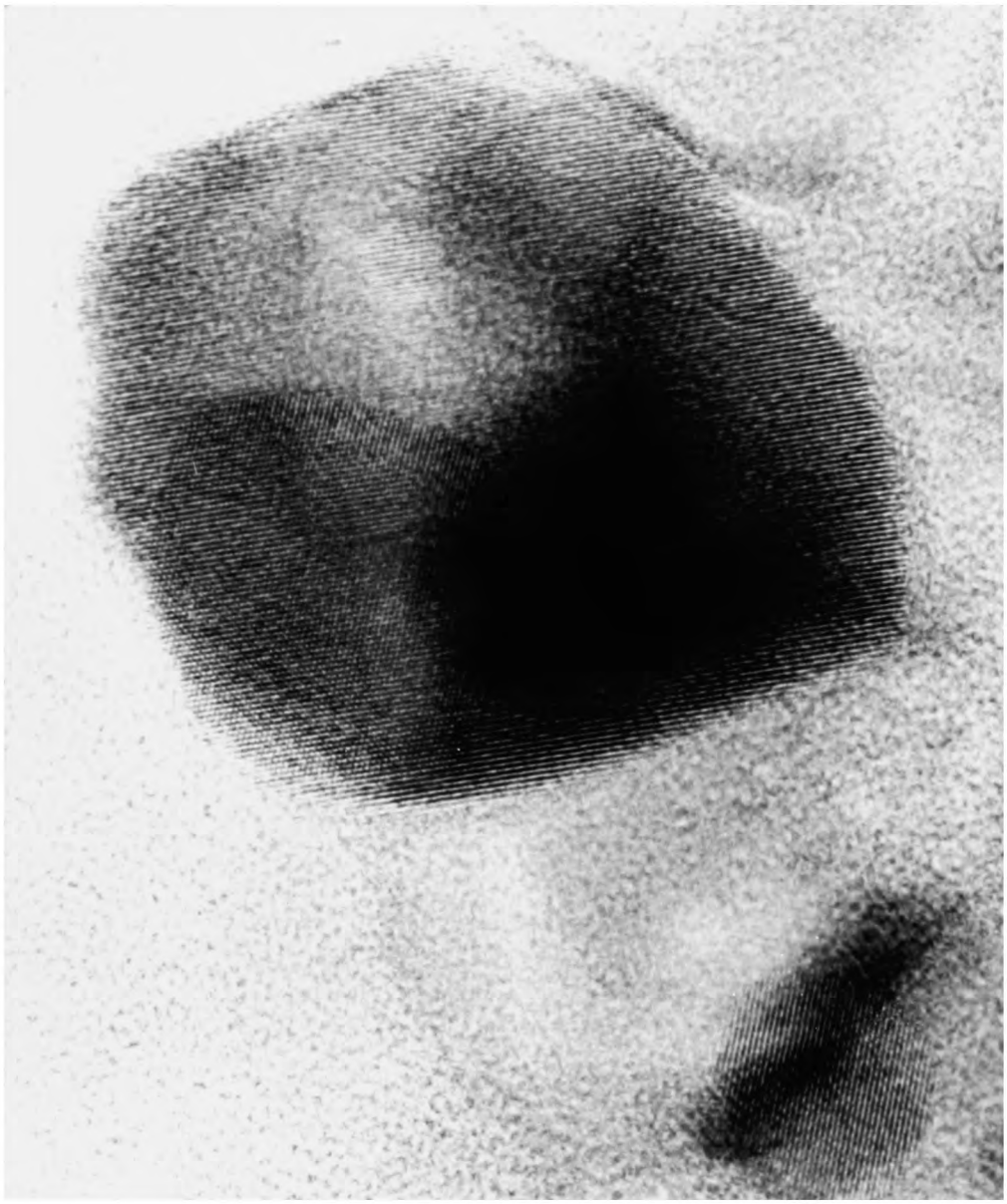

Figure 3.30

Lattice image of a single crystallite from a crushed rat otoconium. No diffraction pattern was obtainable. Magnification = x2 200 000

Figure 3.31

(a) HRTEM of a single crystallite from crushed rat otoconia showing an [001] zone of calcite. Magnification = x1 750 000

Figure 3.31

(b) Theoretical electron diffraction pattern for an [001] zone of calcite. Note the intense reflections from the $\bar{1}10$ and $1\bar{1}0$ positions.

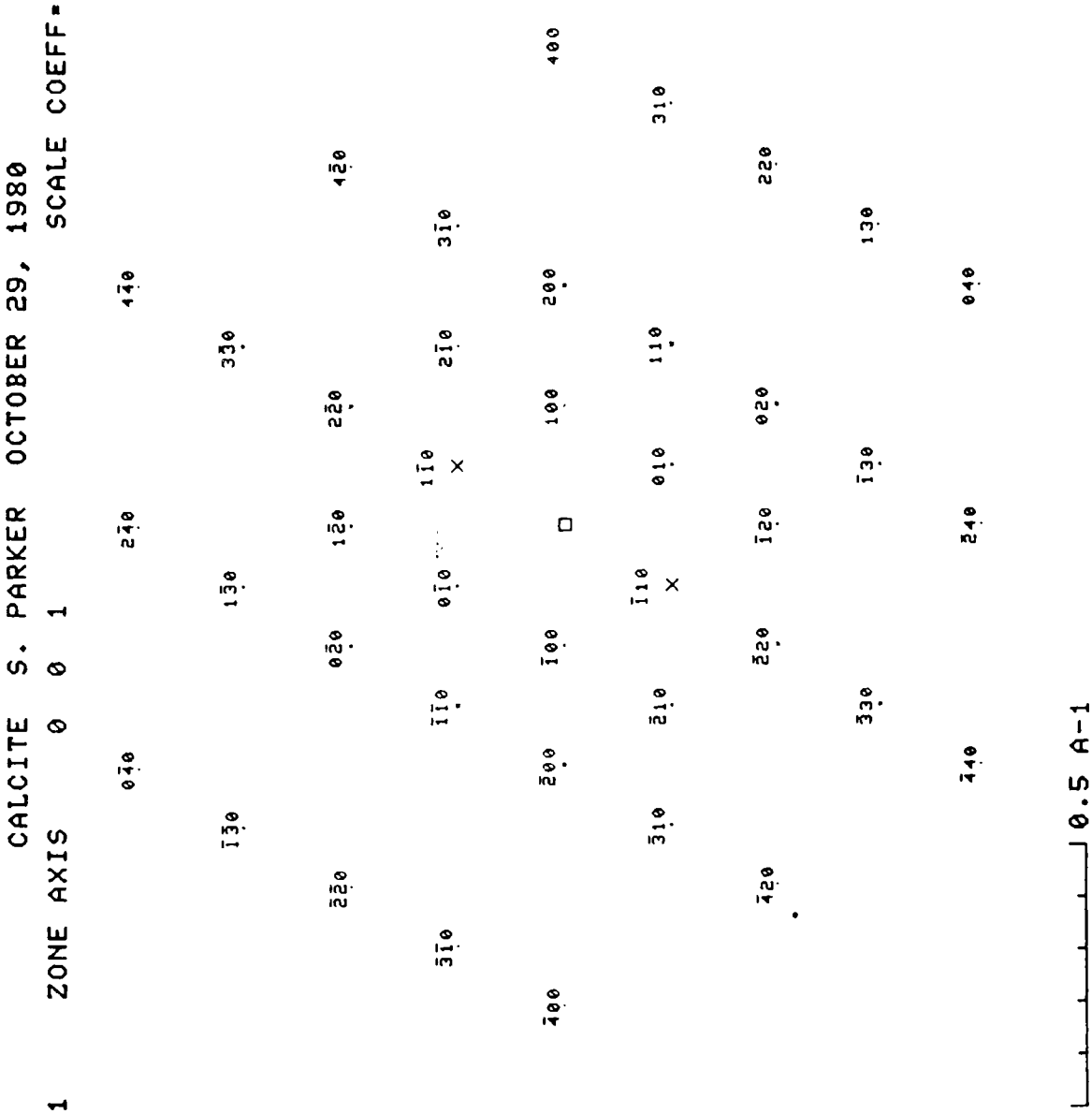

shown in Figure 3.31b. This is proven in the image by observing a lattice running in one direction only, in contrast to the lattice obtained from a [421] zone.

Figures 3.32-3.34 illustrate the crystallite observed to have the [421] zone. Unlike those previously described, this shows no straight edges and seems at first sight to be comprised of several smaller crystals. The electron diffraction pattern (Figure 3.33a) indicates that the sample is a single crystal, however, and the magnified sections of the crystal, particularly across the meridian, clearly show that the lattice fringes do not break as they run from the top to the bottom of the structure (Figure 3.34) although there is a point in this region where the crystal becomes sufficiently thin to allow a two-dimensional lattice image to be observed, rather than the usual one-dimensional lattice fringes. The lattice in this case arises from the four reflections $0\bar{1}2$, $01\bar{2}$, $\bar{1}12$ and $1\bar{1}\bar{2}$ giving a d-spacing of 3.85 Å (see Figure 3.33b).

These crystallites are clearly composed of single crystals of calcite, but it is difficult from a crushed sample to visualise what relevance these observations may have to the observed morphology of the structure. This problem will be discussed at some length below, but the question is aided by two fortuitous observations made at conventional resolution on the Jeol-100CX electron microscope and illustrated in Figure 3.35. The first of these (Figure 3.35a) shows a thin crystal from a rat otoconium. This has straight edges at the top of the crystal but a rather curved body which is not reminiscent of a fragment from a geological specimen. The second sample, however, (Figure 3.35b) consists of three crystallites joined together. The size of the three particles

Figure 3.32

Single crystallite of crushed rat otoconia showing a [421] zone.

Magnification = x1 715 000

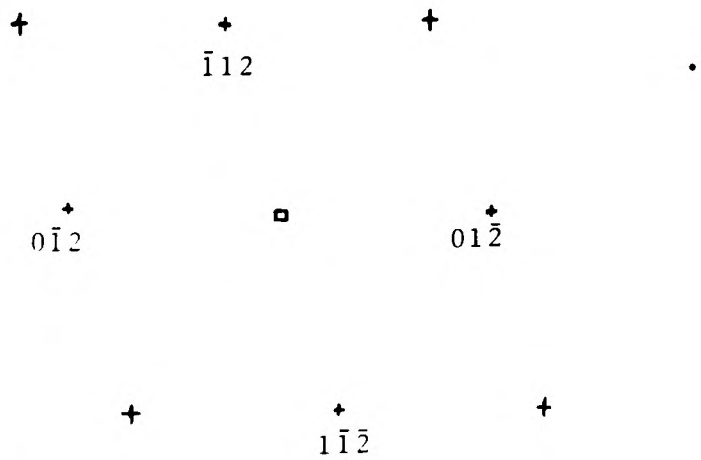

Figure 3.33

(a) Experimental and (b) theoretical diffraction pattern from the sample of rat otoconia 3.32. This is a [421] zone.

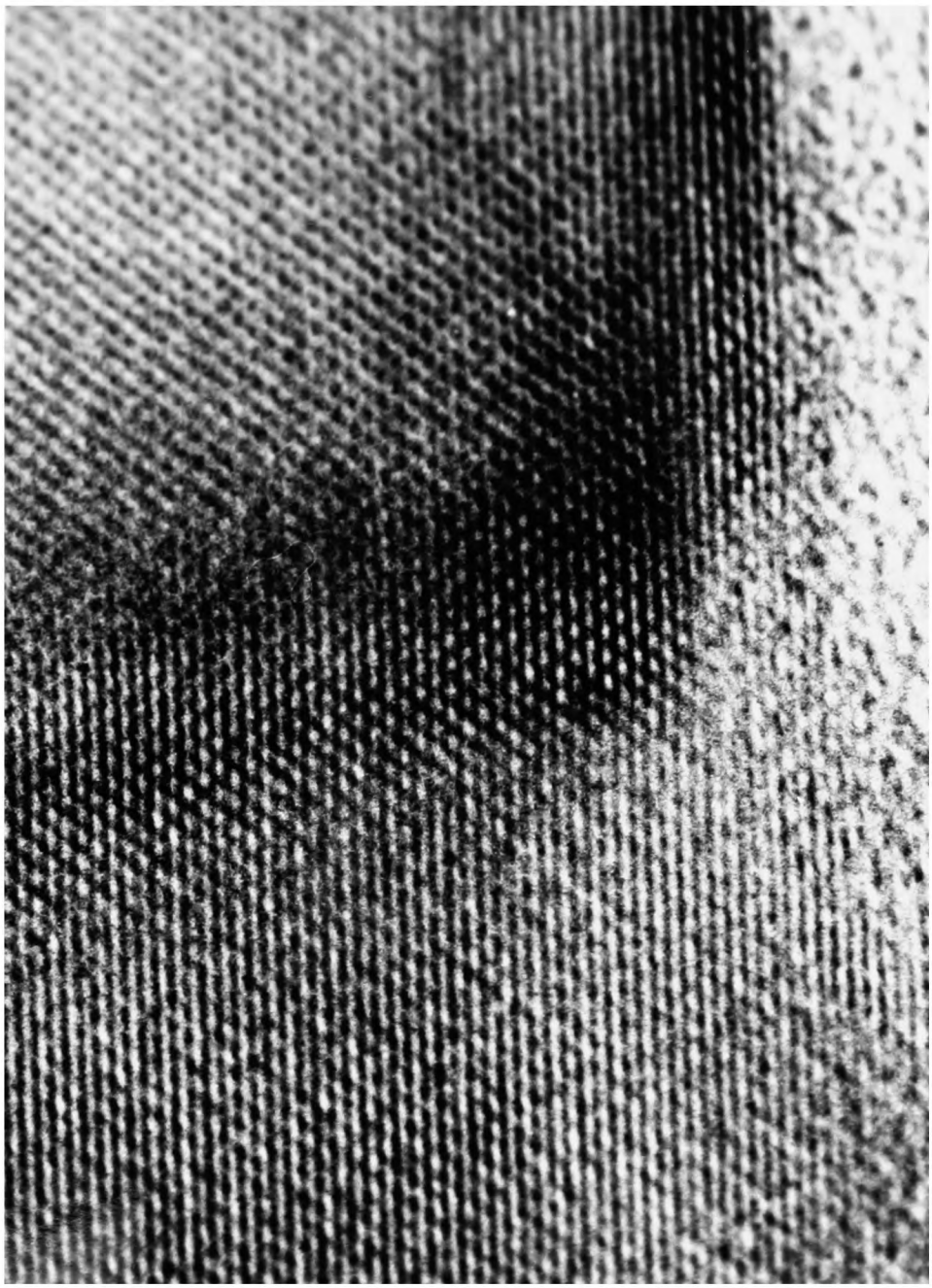

Figure 3.34

Enlargement of a portion of Figure3.32 to show the continuation of the lattice fringes through the dark centre of the crystal. Note the two-dimensional lattice pattern at the central point. Magnification = x5 250 000

from top to bottom, are approximately 550 Å x 750 Å, 900 Å x 1200 and 800 Å x 750 Å. This is in good agreement with the sizes of the particles observed at ultra-high resolution, which all lie between 500 and 1000 Ångstroms in diameter. The fascinating aspect of this sample is the way that the three particles lie together. Although they have straight edges, which is not a common observation for particles of these dimensions, there is a clear band where they join and this leads one to hypothesise that this band is the site for the organic matrix which acts as a template for the epitaxial growth of two crystals against each other. The straight edges of these particular crystals and also the single straight sides of some of the crystallites seen at high resolution lead to the suggestion that these crystals may somehow be involved in forming the outer layer of the otoconium and, particularly, the end-faces. Much work remains to be carried out, however, before this suggestion can be confirmed. It is apparent, however, that the final structure is somehow comprised of these crystallites which are orientated into approximately the same direction to produce a final crystal which may be mistaken for a single crystal by X-ray technique.

3.3.8 Ultra-high Resolution Electron Microscopy of Fish Otoliths

The otoliths used for this study were entirely from Plaice, although stones from several species were available. It was found that the otoliths did not crush to give suitable samples for high-resolution work with any regularity and most of the images obtained came from the thin edges of thicker crystals, in much the same fashion as the geological specimens. The main observation about the otolith aragonite was that it proved to be unstable in

Figure 3.35

Crystallites from crushed otoconia. Magnification = x425 000

the electron beam, in contrast with the geological sample. This made it very difficult to obtain good images, but also gave rise to a very interesting observation. One sample, which was thin enough for part of it to be imaged, gave an [010] zone electron diffraction pattern (Figure 3.36a), confirmed by the computer prediction (Figure 3.36b). The high resolution micrograph of the sample is shown at three differing lengths of exposure to the electron beam in Figures 3.37 and 3.39. It can clearly be seen that the lattice fringes present in Figure 3.37 are replaced by larger, more distinct lines by the last exposure (Figure 3.39). The electron diffraction pattern taken after the sequence of TEMs reveals that the sample has degenerated to a primitive lattice, in which no reflections are forbidden (Figure 3.40a). This is confirmed by the computer-generated pattern of all possible reflections which is shown in Figure 3.40b. This is a significant result in that it shows that the crystal has degenerated in a controlled manner and not just collapsed to powder; indeed, the calcium ions in the lattice which give rise to most of the electron density can be seen to have 'breathed' slightly, but not moved to any significant extent. This type of behaviour has been observed before, in the rare-earth oxides (47), but not in a biological system. The observation is further discussed below, in the light of the elemental analysis carried out on the otolith samples.

Generally, the otolith samples were found to be unstable and were easily damaged by the electron beam, sometimes to the extent of being destroyed. This is in contrast to the mineral aragonite sample, discussed above.

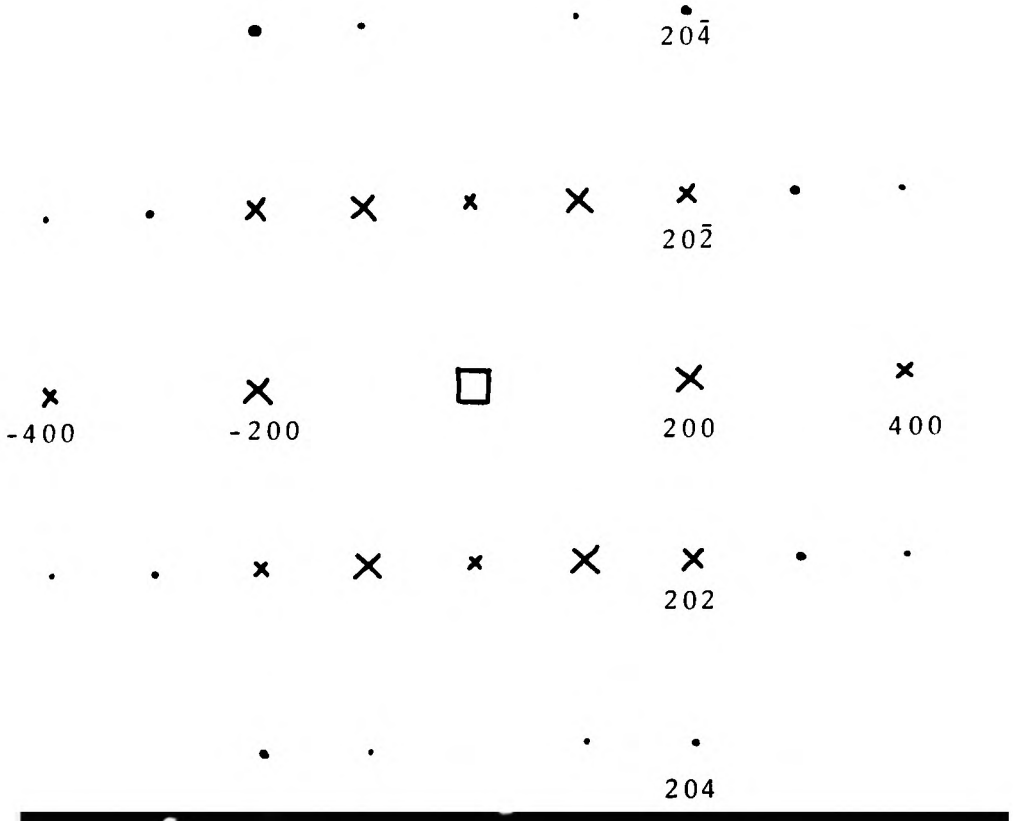

Figure 3.36

Experimental and obtained electron diffraction pattern from fish otolith before exposure to the electron beam.

Figure 3.37

Plaice otolith before gross exposure to the electron beam.

This sample gives an [010] diffraction pattern.

Magnification = x1 650 000

Figure 3.38

Plaice otolith showing changes to the lattice due to exposure in the electron beam

Magnification = x1 650 000

Figure 3.39

Lattice image of plaice otolith after long exposure to the electron beam.

Magnification = x1 350 000

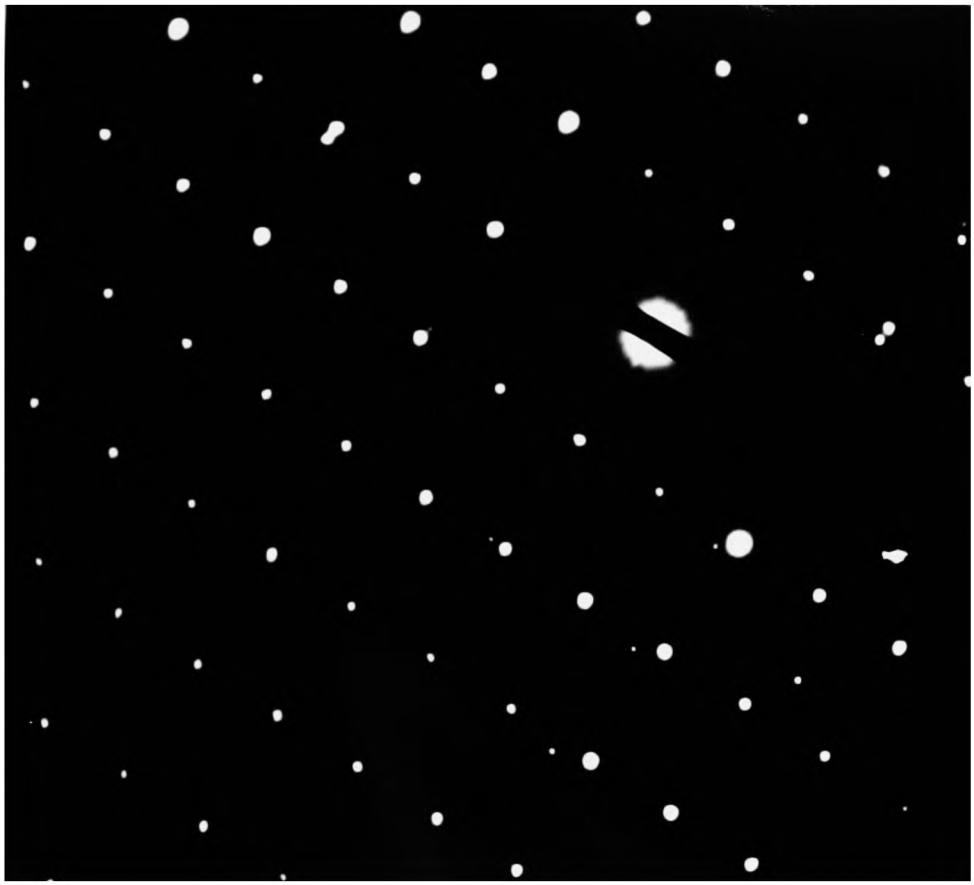

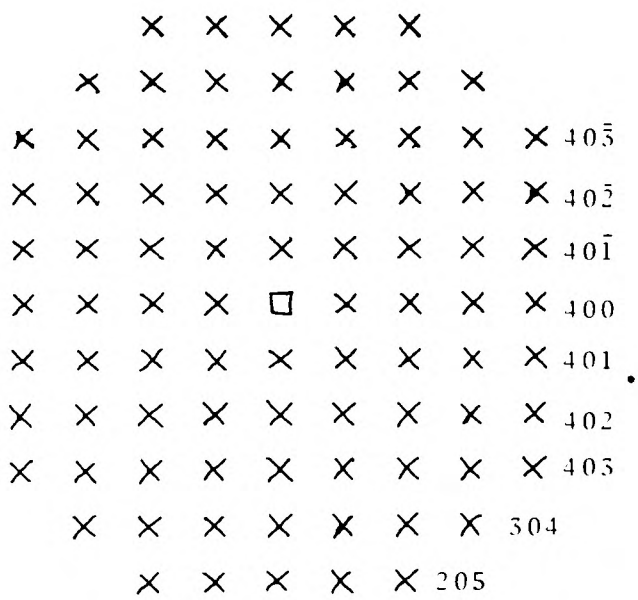

Figure 3.40

Experimental and theoretical electron diffraction patterns from the sample of plaice otolith after gross exposure to the electron beam. The pattern now shows all possible reflections.

3.3.9 Analysis of Fish Otoliths

Elemental analysis was carried out on crushed samples of Plaice otolith by three methods; standard mineral analysis by carbon, nitrogen and hydrogen elemental analyser and also atomic absorption spectroscopy for metals, the quantitative application of the X-ray emission analysis facility of the Jeol-100CX electron microscope discussed above and also Thermogravimetric Analysis (TGA). The analysis arose from an observation that the analysis of fish otoliths carried out by Morris and Kittleman (39) did not account for the entire composition; indeed, only calcium and sodium were identified. Early results by atomic absorption spectroscopy confirmed the Morris and Kittleman observation that otoliths were low in calcium by comparison with mineral aragonite. We observed a mean value of 36.35%, 3.65% below the predicted composition. In order to try to account for this result, analysis for several other ions was carried out and positive results obtained for sodium, potassium, strontium and magnesium. Analysis by C,H,N analyser showed a slightly elevated carbon value (12.15%) and positive values for nitrogen and hydrogen. This was assumed to arise from the protein known to be involved in the otolith structure. Analysis for oxygen was not possible, but phosphorus was analysed in the electron microscope, a typical spectrum being shown in Figure 3.41. In order to ascertain the nature of the impurity, a sample of powdered Plaice otolith was then heated to 600°C for several hours and reanalysed for the major components. This revealed that the hydrogen and nitrogen content had disappeared and the carbon composition dropped to 12.02%. This change in composition was accounted for in two ways; the burning up of the organic matrix and the decomposition of hydrogen carbonat HCO_3^-, ions into carbon dioxide and water. The hydrogen carbonate

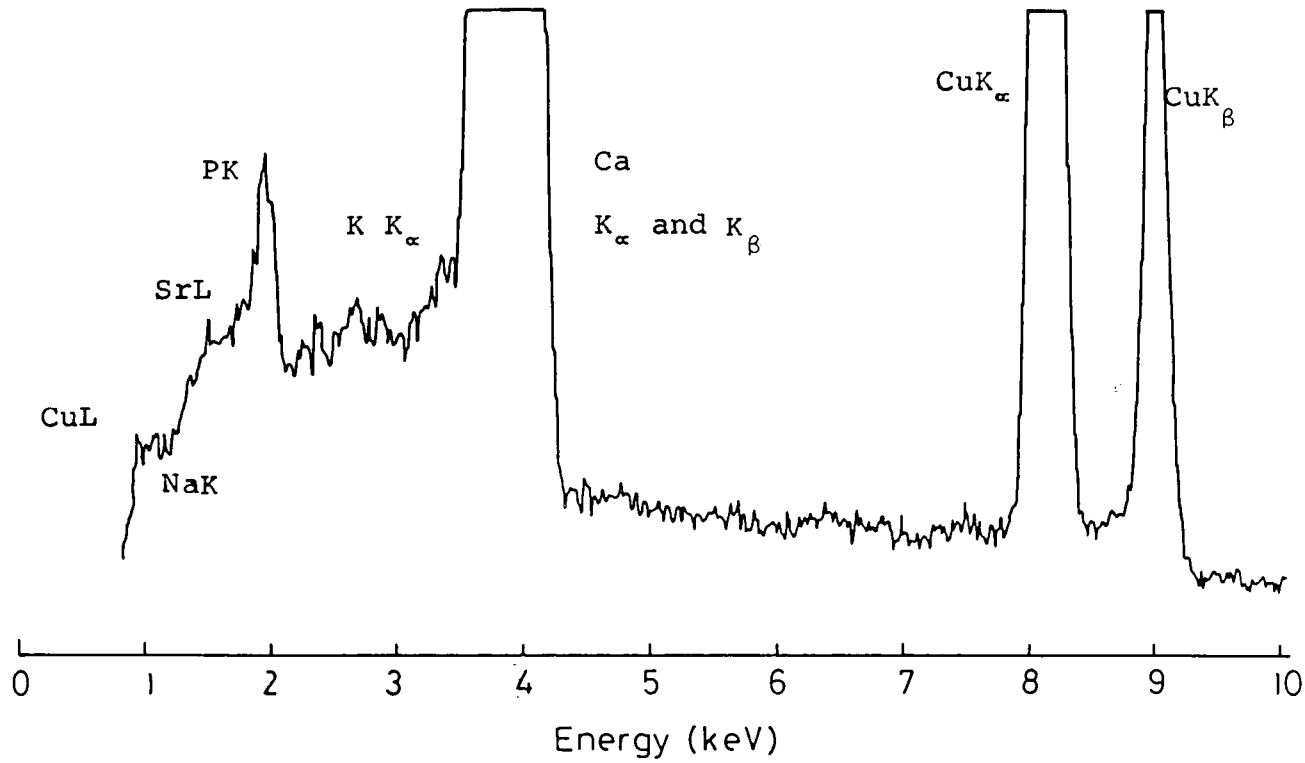

Figure 3.41

X-ray emission spectrum of a crushed sample of plaice otolith

TABLE 3.VI

Estimated Percentage Composition of (a) Plaice Otolith and (b) Heated Plaice Otolith

	Otolith	Heated Otolith
Ca	36.35	38.68
C	12.15	12.02
N	0.077	0.00
H	0.128	0.00
Na	0.375	0.236
K	0.050	0.029
Sr	0.215	n.a.
Mg	0.185	n.a.
P	0.283*	n.a.
O	49@	49@
	98.69%	99.97%

* : Result estimated from secondary X-ray emission spectrum

@ : Result estimated from stoichiometry of $CaCO_3$

was assumed to be present, rather than carbonate, to balance the charge of the Na^+ ion which is substituted for the Ca^{2+} to a small extent. This experiment was repeated under controlled conditions by TGA. The results for mineral aragonite and Plaice otolith are shown in Figure 3.42. The mineral is stable to its decomposition point at about 700°C and then falls rapidly to a new plateau at about 56% of its original composition. This transition is, in fact, to calcium oxide, which is very stable at high temperatures:

$$CaCO_3 \longrightarrow CaO + CO_2$$

The sample of otolith behaved quite differently, with a small mass loss which began at about 200°C and continued at a fairly steady rate until the normal decomposition of carbonate to oxide began at about 650°C. At this point, the total mass loss was about 2.25% ($\pm$0.25%). The loss of these impurities clearly had nothing to do with the oxide formation, but arose from the various impurity compounds contained within the biomineral As detailed above, these were the protein which forms the organic matrix for crystal growth and the HCO_3^- which balances the charge deficiency induced by the presence of sodium in the lattice. The decomposition temperature of a pure sample of $NaHCO_3$ is 270°C and one would expect that this temperature would be lower for an impurity spread throughout a mineral, which is found to be the case. It is probable that the effect observed in the electron microscope, in which the impurities are burned out of the sample by the heat of the electron beam is due to the hydrogen carbonate; if it was the protein, this would be a conclusive arguement for the presence of organic matrix within the mineral to a very high level, for example, surrounding spherules of calcium carbonate about

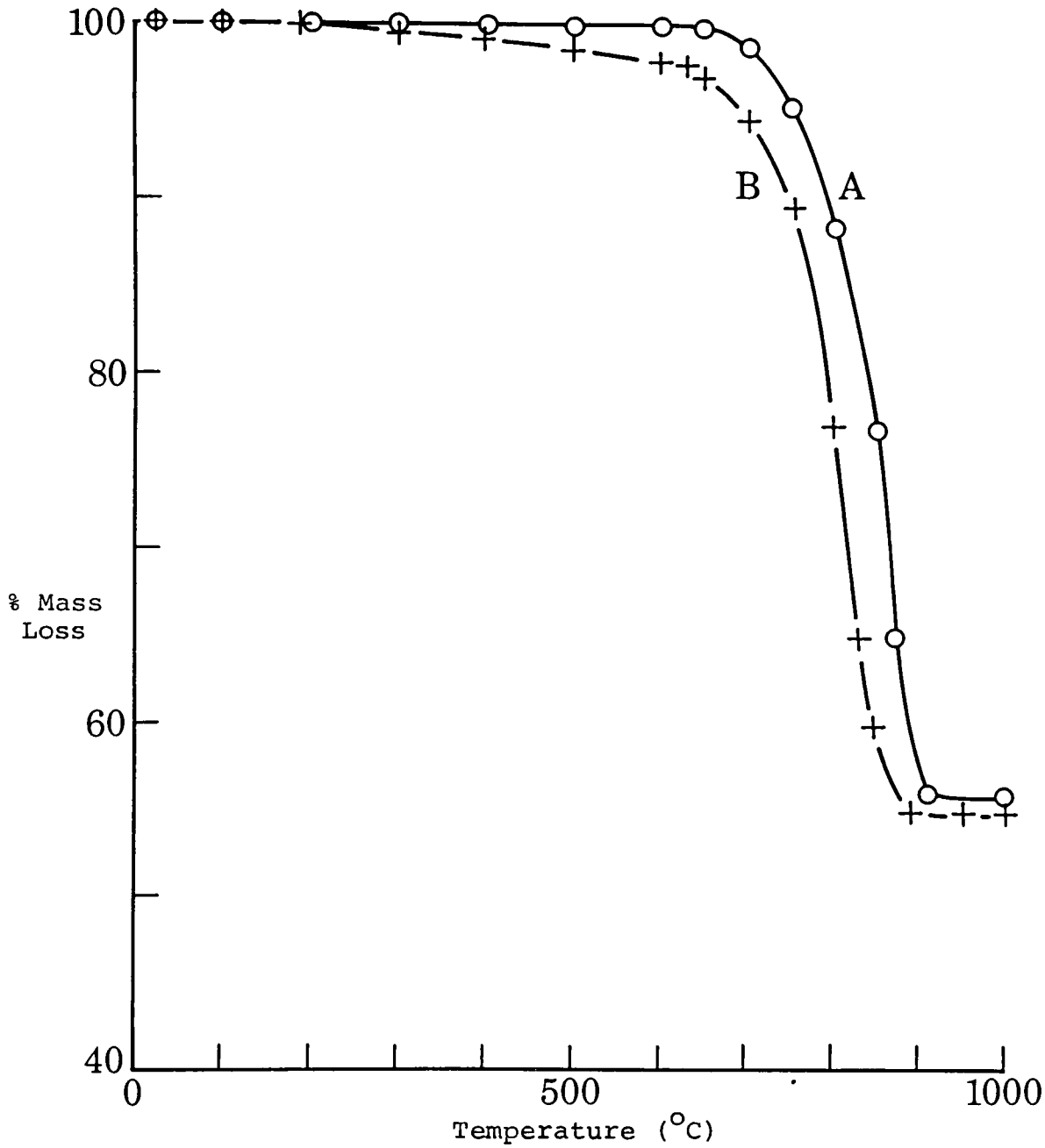

Figure 3.42

Thermogravimetric analysis of (A) mineral aragonite and (B) Plaice otolith.

50 Ångstroms in diameter. The possibility of this phenomenon is recognised within the field of biomineralisation, but, as yet, such an intimate relationship between inorganic and organic components has not been identified, and the weight of opinion would state that the organic and inorganic elements in a biomineral are separate entities below about 500 Å. The observations in the electron microscope can be best accounted for by the loss of a small component, rather than a large one such as a protein, since the loss of a large component would be unlikely to give rise to a very controlled adjustment of the lattice.

The comparison of this otolith data with the otoconia data discussed above, together with the relevance of the data to physiological processes of the inner ear will be made below.

3.3.10 Ultra-high Resolution Electron Microscopy of Frog Otoconia

The aragonitic otoconia from frog proved to be the least satisfactory of all the biominerals to study by high resolution electron microscopy. Single crystal electron diffraction patterns could be obtained from thin crystals (Figure 3.43a) and good micrographs with lattice fringes visible were sometimes possible, but the normal observation was for the crystals to turn to powder very rapidly after being exposed to the electron beam. The sample shown in Figure 3.44 is a crystal identified as an [001] zone from the diffraction pattern shown in Figure 3.43a with the lattice fringes 4.95Å apart due to the 100 reflection (Figure 3.43b). Areas of about 50Å diameter may be observed within the structure that are amorphous (arrows) and this degenerative process rapidly increases until the sample becomes a powder. This instability is in clear contrast to that observed in fish otoliths.

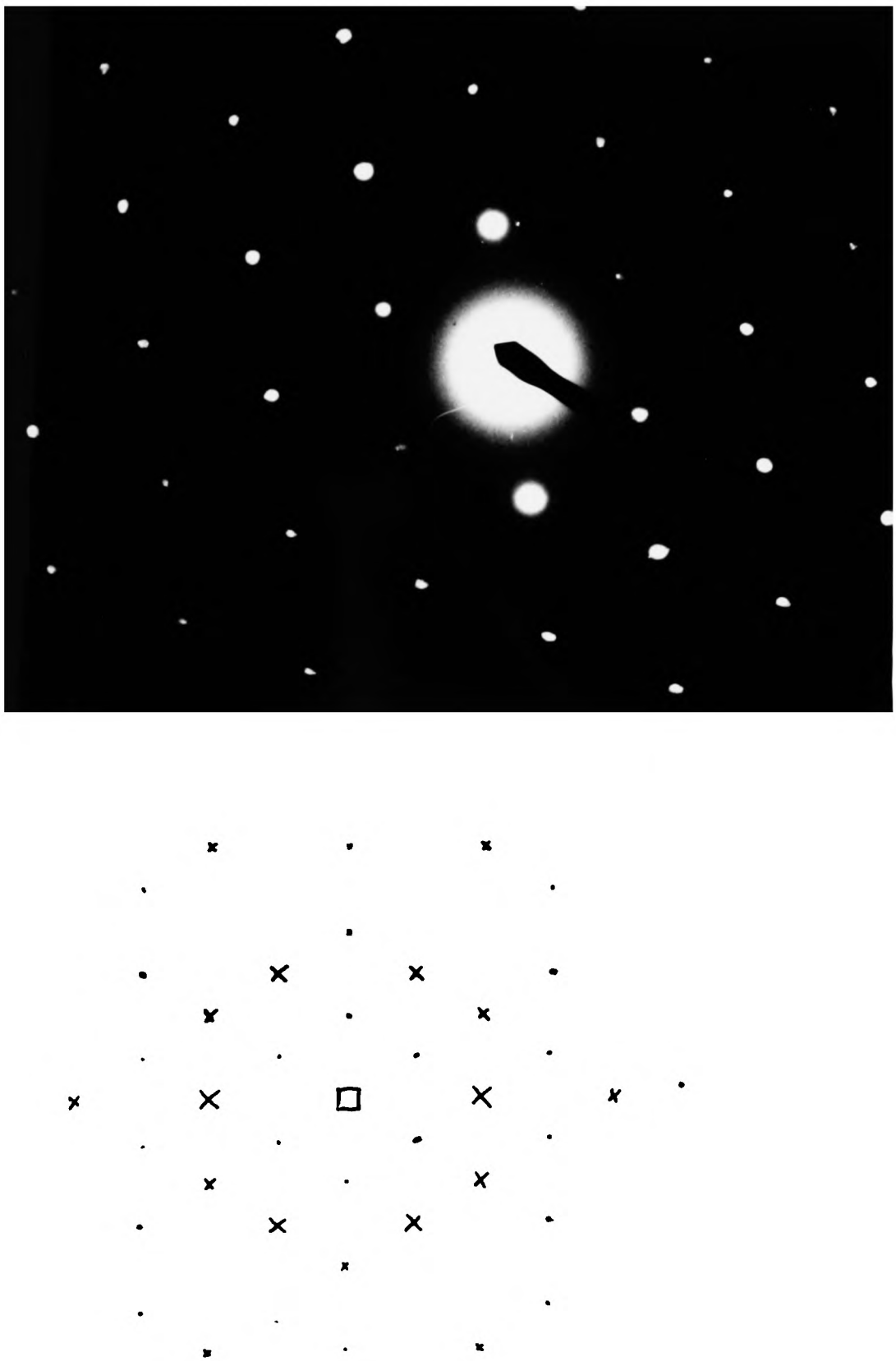

Figure 3.43

Experimental and theoretical diffraction patterns for an [001] zone of aragonite. The experimental pattern was obtained from the sample of frog otoconia seen in Figure 3.44

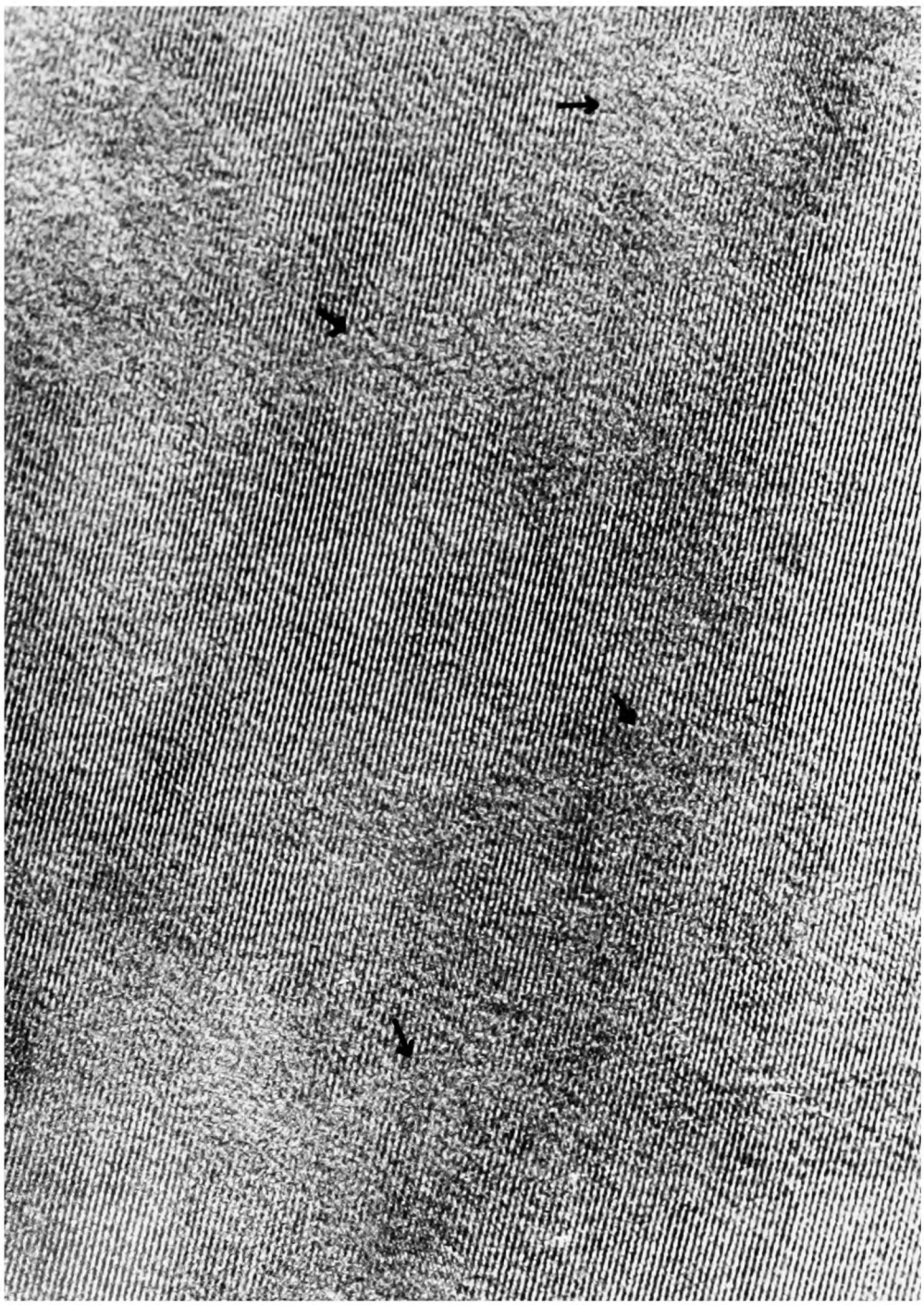

Figure 3.44

Ultra-high resolution lattice image from crushed frog otoconia. Arrows mark areas becoming amorphous under the electron beam. Magnification = x 2 040 000

There is some evidence that the structure of frog otoconia is different from that of either fish otolith or rat otoconia. Certain regions of thin crystals show evidence that the crystallites are composed of small domains which may or may not be ordered. These are not of regular shape, although some may be interpreted as hexagons. Figures 3.45 and 3.46 illustrate some of these structures. If they are genuine, then there is some explanation of the unstable nature of the system. The crystals may have a diameter as small as about 50Å, which is approaching the stability limit of a crystal. In this case, the observed amorphous spots of about the same diameter arise from metastable crystals being exposed to the electron beam and disintegrating as a consequence.

Figure 3.45

Lattice image of crushed frog otoconia showing circular or hexagonal regions of crystallites within the structure. These regions have a diameter of about 50 to 100 Å.

Magnification = x1 650 000

Figure 3.46

Lattice image of the same sample as that in Figure 3.45, taken after the sample had been exposed to the electron beam for some time. The amount of amorphous character has increased, causing distortions in the remaining lattice. Magnification = x1 650 000

3.4 Discussion

3.4.1 The Ultrastructure of Otoconia

The use of ultra-high resolution transmission electron microscopy has conclusively demonstrated that otoconia are not single crystals, which confirms the indications given by both scanning electron microscopy and electron diffraction. Although the chosen method of preparation means that we can know nothing about the construction of specific areas of the structure, such as differences between the end-faces and the body, or the centre and the outside, we are able to determine the basic constituents of the biomineral. Scanning micrographs (e.g. Figure 3.12b) indicate that both the body and end-faces are made up of the small crystallites observed in the high resolution micrographs and one may conjecture that those crystallites observed with flat edges and sharp corners are situated on an outer face, whereas those which appear rounded are located within the mass. These crystallites may be thought of as the basic unit of mineralisation; the micrographs demonstrate that they are single crystals of calcium carbonate, without any sign of containing an organic matrix or being sub-divided into domains. By recalling the hypothesis proposed earlier, and illustrated in Figure 3.47, one may understand the ultrastructure of the otoconium.

In the case of rat otoconia, the high-resolution micrographs indicate that the fundamental unit within the structure is a 'single crystallite'. These single crystallites are packed together in clumps with an organic matrix between each particle to hold them together. There are strong indications that the influence of this matrix aligns the

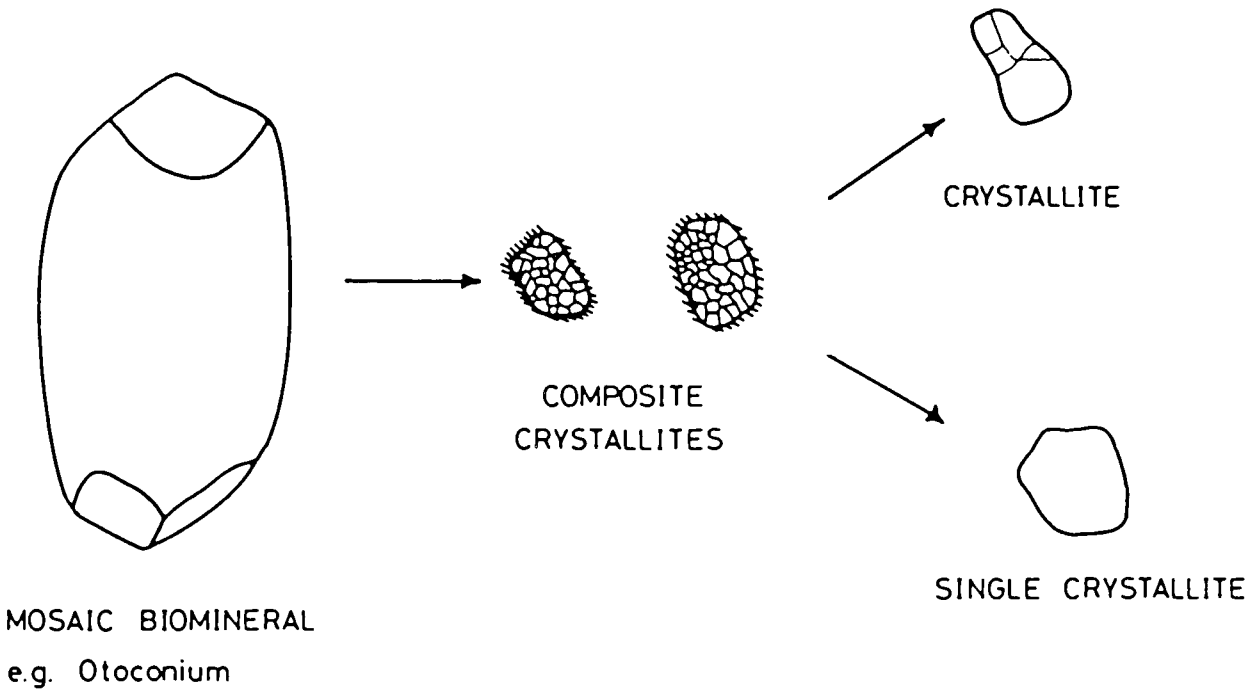

Figure 3.47

Diagram to illustrate the proposed components of a biomineral

particles to give an overall appearance of a single particle with the same orientation but the preparative methods used here do not allow a definite conclusion on this point. The results obtained in this study, however, would tend to cast doubt on the extent to which this alignment actually occurs; no other study has made use of techniques capable of atomic resolution and whenever a sample containing more than one particle of calcite is imaged, the corresponding diffraction pattern tends away from single to polycrystalline. This may be clearly seen in Figure 3.28. Such an orientation problem within a small component of the biomineral would not necessarily result in an overall polycrystalline structure, which would also be determined by the direction of crystalline growth.

Each of these clumps is, in turn, surrounded by an organic matrix, which may be the same, or different, from that surrounding the single crystallites. This matrix determines the final morphology of the biomineral. We have termed these larger groupings 'composite crystallites' in order to reflect the combination of organic and inorganic material contained within them. Photographic evidence for the existence of such composite crystallites is not easy to obtain since they are often too large to allow the transmission of electrons, but the sample shown in Figure 3.28 has the appearance of comprising many small particles which are bound together; such a particle would be an example of a composite crystallite. It is interesting to note, in the light of the above discussion, that the diffractio pattern corresponding to this particle is of a polycrystalline powder. These composite crystallites are then bound together by their surrounding organic matrix to form the final biomineral.

Thus the structure is controlled by the organic matrix. This hypothesis leads to a proposed mechanism for nucleation, which will be discussed in conjunction with that of fish otoliths.

The observation of the shattered fragments of otoconia from frog give some indication that the structure is different from the calcitic otoconia of mammals in two ways. One is in their stability, which is not good even when compared with mineral aragonite, and the other is in the observation of small hexagonal patches within the crystallites revealed by the preparative method. If these hexagons are genuine, and they are seen in many frog specimens before they disintegrate completely, then the other pathway of the hypothesis is followed (see Figure 3.47) in which the crystallites contain ordered microdomains within them. The significance of this apparent change in ultrastructure is not known.

3.4.2 The Relationship Between Single Crystallites and the Overall Morphology of Otoconia

The understanding of the ultrastructure cannot be complete without some knowledge of the way in which the component single crystallites form together to produce the overall biomineral. Although this knowledge cannot be obtained directly from our observations, one can try to relate the results given above to a stylised otoconium, such as that shown in Figure 3.48. This is a single crystal containing (100) end-faces, as observed in the biomineral, and $(10\bar{1})$ faces forming the body (after Dana, 76). One needs to relate the observed structures to one of these faces to account for the observed morphology of the otoconia.

The particles observed in the ultra-high resolution TEM were single crystallites which gave a diffraction pattern corresponding to an [001] zone of calcite (with one exception).

Diagram to show the theoretical crystal faces in otoconia

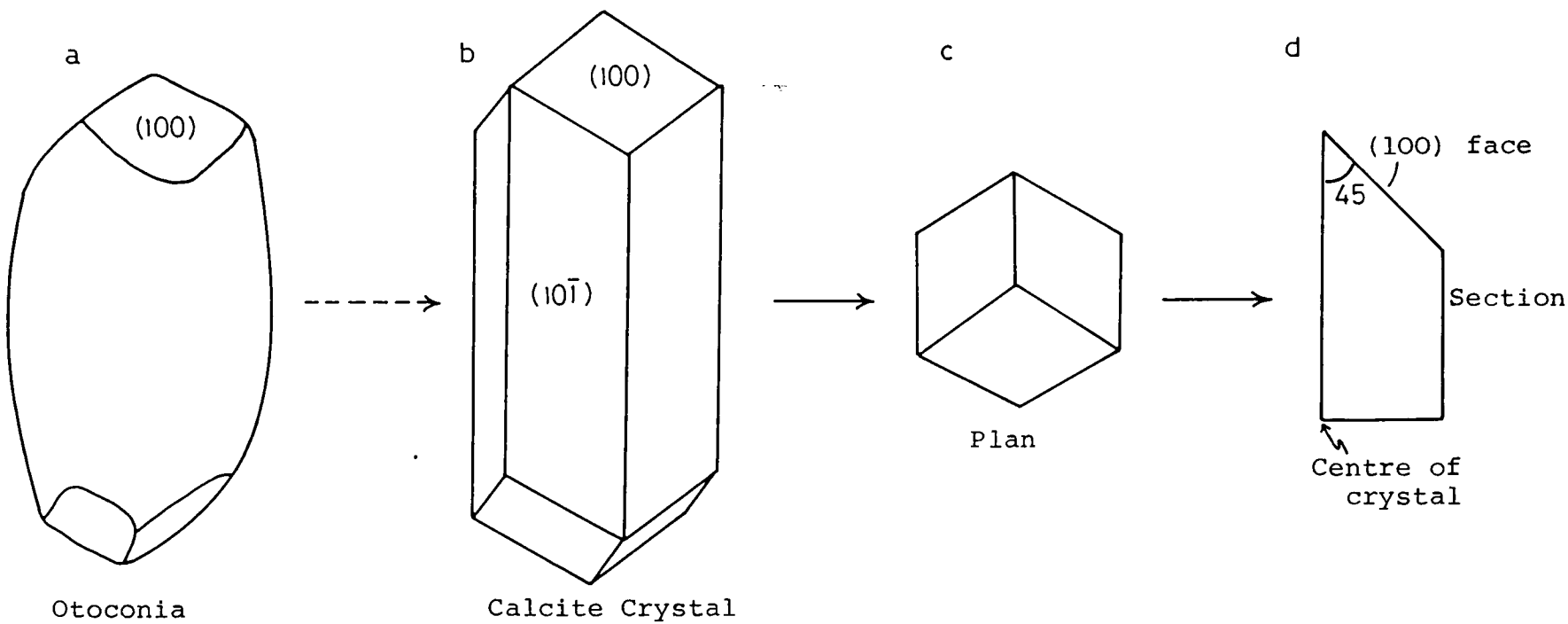

If these particles have crystal faces and zones normal to them, then the faces may be calculated from the following equation (77):

$$\frac{h}{2u - v} = \frac{k}{2v - u} = \frac{l}{2w\ (c/a)^2}$$

This equation applies to hexagonal systems and it apparent that no solution can be obtained for the [001] zone of calcite. It is likely, however, that the growth has taken place along the [001] zone and that the crystals are so arranged that the (100) face is exposed. This may be carried out through chemical inhibition of unwanted faces. The growth may be seen in Figure 3.49 and is discussed at some length below. It is thus possible that the crystallites imaged have grown from the nucleation point towards the end-face of the crystal, which may account for the common observation of a flat side to the crystallites.

Calculations of the inter-face angles, based on data from Andrews, Dyson and Keown (77), reveals that the angle between the (100) and (10$\bar{1}$) faces is 46.30°. This means that a straight growth back from the (100) face will not pass through the origin of the crystal (see Figure 3.48). It is at this point that the single-crystal model breaks down, since the broken otoconium shown in Figure 3.49 clearly shows that the growth of the three colums from the centre of the crystal curve towards the end-faces and do not extend in a straight line. Thus the calculations from the crystallites agree with the observed structures within the otoconia. It is, then, some organic matrix which is laid down in close relationship with the apparent crystal that generates the overall appearance. This is summarised in Figure 3.50.

Figure 3.49

Scanning electron micrograph of one end of a human otoconium from a patient 65 years old which has broken open during age-related degradation to reveal from the inside the tripartite growth of calcite towards the three end-faces. Magnification = x 25 500

3.4.3 The Ultrastructure of Otoliths

The structures of otoliths and otoconia are obviously different at the morphological level, but our investigations indicate that the ultrastructures of the two biominerals have much in common. Both structures comprise small crystallites of calcium carbonate in one or other of the major polymorphs surrounded by an organic matrix of some form. This interpretation of the ultra-high resolution micrographs forms the first indication of a related evolutionary basis for the two systems. The micrographs of fish otoliths may best be understood by studying them in the light of the findings of Panella (30,31) and the various workers who enlarged on his findings (32-37). By this interpretation, the particles released by crushing derive from the individual crystals of aragonite seen in the scanning micrographs of the otoliths (42). These crystals can be as thick as 3 μm and thus are far too thick for transmission microscopy as they are and have to be crushed themselves in order to obtain a suitable sample. Thus, successful high resolution micrographs are usually obtained from the thin edges of thick crystals or from thin fragments which closely resemble those obtained from crushing mineral aragonite. Thus the electron diffraction patterns for the aragonite minerals are very similar; crushing produces the same faces since aragonite crystals are being fractured in all cases, which is not the case for the calciti minerals.

The understanding of the close relation of the ultrastructures of both otoconia and otoliths, despite their widely differing morphologies, enables us to propose the evolutionary trend of the inner ear in a very basic way. The

differences lie in the organic matrix present in each type of biomineral, in the nucleation points of the crystals and in inhibitory control. This is summarised in Table 3.VII and Figure 3.50. Essentially, we suggest that the organic matrix is laid down to act as a template for calcium carbonate growth in certain directions in the case of otoconia and radially for otoliths. The concentration of calcium then increases markedly in both systems, with the carbonate ions known to be present in the inner ear (49). The morphologies of the two minerals are already markedly different; the otoconia are like dumb-bells with a very knobbly surface (4) and the otoliths already with a recognisable 'adult' morphology (50). The otoconia mature by completely filling out the body of the structure and then growing towards a point on the end-faces where an inhibition of some kind occurs which stops the growth at a specific face of calcite, observed to be the (100). The termination of growth is probably in part due to the formation of a single crystal face, which removes the steps on which crystal nucleation commonly occurs. However, it is not reasonable to assume that the termination is a spontaneous process, rather than being brought about by an inhibitor. The otolith growth continues through the laying down of fresh organic material and aragonite daily, giving a continuous and increasing number of nucleation sites on the structure. This growth continues throughout the life of the fish.

This hypothesis depends on the organic matrix exercising a tight control over the polymorph of calcium carbonate laid down in the nucleation sites, but recent work in the related area of mollusc shells indicates that this is possible. (This work is discussed in the chapter concerned with the organic matrix). An indication that the method of growth is correct, however, comes

TABLE VII

BIOMINERALISATION OF THE BALANCE ORGANS

	Otoliths	Otoconia
Nucleation point	Multiple (unrestricted)	Limited
Organic matrix	Constantly formed	formed only once
Growth inhibitors	no	yes

OTOCONIA

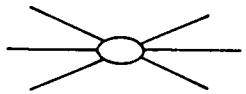

increasing calcium →

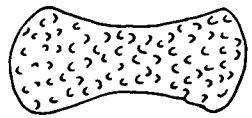

maturing + inhibition →

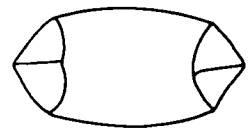

1. Nucleation and initial growth directions.

2. Fetal stage with obvious spherules In-filling of body commences.

3. Mature otoconia. End-faces formed through inhibition and removal of nucleation steps

OTOLITHS

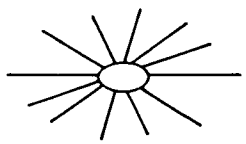

daily formation of organic matrix →

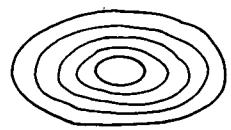

continuing daily growth →

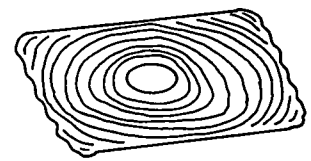

1. Nucleation. Growth allowed in all directions.

2. Growth favoured in x and y directions over z.

3. Mature otolith. Edge decoration often occurs, but growth continues.

Figure 3.50

from a fortuitous observation in the laboratory of Professor Muriel Ross, of a human otoconium which had degraded with age and exposed the internal growth, clearly showing three spikes of calcium carbonate growing from the centre of the biomineral towards the end-faces. The specimen is shown in Figure 3.49 and indicates that the end-faces are more stable than the body of the structure, which would be expected since the former are recognisible crystal structures whereas the latter is clearly composed of some kind of packing together of crystallites without the stability that arises from the formation of a crystal lattice.

3.4.4 Recent Developments in the Understanding of Otoconia and Otoliths

Research on various aspects of otoconia has managed to build a much more complete picture about the ultrastructure and function of the crystals. Nakahara et al (51) produced further evidence that each otoconium of the mouse is a polycrystalline structure, although they still argued for the initial formation of a preotolith before calcification at multiple nucleation sites commenced. One micrograph, of a section from a seven day old mouse shows the crystal growth to be occuring in a roughly radial manner, although some of their conclusions about a crystal-free region in the centre must be treated with caution due to the danger of hard crystals being prised from an ultrathin section by the diamond knife during cutting. The concept of a nucleus of organic material within the otoconia was supported by Anniko (52) who carried out decalcification of the entire membraneous labyrinth using trichloroacetic acid injected into the labyrinth of decapitated guinea pigs. Gross changes were observed

to many structures within the labyrinth, including extensive decalcification of the otoconia leaving a hexagonal-shaped organic mass.

Recent work by Wright and Hubbard (53) on human otoconia during the first three months of gestation has revealed that a few calcium-containing otoconia are present in the utricle by the end of the seventh week. By the eighth week, they were present in both utricle and saccule and at twelve weeks, the maculae were covered by the otoconial membranes and newly-formed otoconia were seen on the inferior utricular wall. X-ray analysis revealed that calcium had been rapidly increasing in the otoconia during the five week period. At twelve weeks, the otoconia were approaching maturity, with the end-faces in the process of being formed. One interesting aspect of the photograph of such an otoconium is the granular nature of the body with the end-faces resembling the ends of needle-shaped crystals. Wright and Hubbard concluded that this indicates the presence of longitudinally-orientated internal elements. This work is important as it helps to solve the problem of the presence of a 'preotolith'. It is apparent from this work that the mechanism of otoconia growth proposed by Nakahara and Bevelander (25) is incorrect.

There has been a great deal of recent interest in pathological conditions of the otoconia and also the effect of ageing. Wright et al (54) have found that it is possible to disrupt the formation of the otoconia by certain drugs. Two cases were found in which pregnant women, suffering from juvenile-onset rheumatoid arthritis, had taken prostaglandin-synthetase inhibiting drugs during pregnancy. One case was an infant, the other a second trimester foetus. In both cases, the vestibular maculae were covered in otoconia composed of vaterite which have the

appearance of bi-convex lenses composed of many tiny spherules. X-ray diffraction analysis revealed that the saccular otoconia were pure vaterite, while the sample from the utricle was a mixture of vaterite and apatite. They concluded that the apatite structures were buried beneath the vaterite ones and probably arose from the collapse of the surrounding temporal bone. Other defects of the otoconia were identified by Johnsson et al (55,56) which were induced by streptomycin. In this case, the otoconia had already formed, but administration of the drug caused dissolution of the structures, reducing them to hollow shells, resembling the structures found in man during the ageing process (57).

The effects of weightlessness have attracted the attention of both Russian and American space programmes and Vinnikov et al (58) reported on the alteration of the size and shape of the otoconia of rats during a 20 day flight abroad the sputnik "Kosmos-782". Changes were observed to the receptor cells, some of which were destroyed, and also to the joining of the otoconia to the receptor surface. The changes to the otoconia and receptor were assumed to arise from the interuption of the calcium exchange process which are known to occur in the vestibule (59-62). It should be noted, however, that a subsequent report of a later experiment (63) claimed that there were no deleterious effects to either rats or frogs which had been fertilised and developed during the course of the space flight. Preparations are underway for similar experiments to be carried out in the American scientific space shuttle programme. The emphasis of this work will try to establish the nature of the potentials set up in the utricle and saccule during normal function (41,64). This system will benefit particularly from research under conditions

of low gravity since it is believed to be the major controlling force on the end-organ; this involves studying whether the otoconia are piezoelectric, as would be predicted from results with fish otoliths (39) and how this corresponds with the generated chemical potentials in the system. Results relevant to this problem are discussed above. Lim (65) has reviewed the development and structural aspects of the otoconia as part of a major study of the inner ear.

Work on the fish otolith has enabled a good understanding of the mechanisms involved in the daily incremental growth found in this system. Mugiya et al (66) carried out uptake experiments using ^{45}Ca on the goldfish, *Carassius auratus*. They showed that there is a diurnal rhythm in the formation of the otolith with calcium uptake slowing down or stopping at sunrise and resuming three hours later. They also found that the plasma calcium level increased towards sunrise and fell significantly in the succeeding three hours and that this increase corresponded with a period of rapid decrease in the surrounding tank water. These results are in close agreement with studies carried out on the deposition of shell in bivalve gastropods, which has been shown to be temperature and tide-dependant (67-73). Recent work by Haake et al (50) and Radtke and Dean (37) has been concerned with the growth of the otolith in larval fish. The study of *Fundulus heteroclitus* showed that the otolith within the saccule of the fish is the first calcified tissue to develop and that two to three increments were laid down before hatching. The increment formation is initiated by light and controlled by the 24 hour photoperiod. This increment formation was disrupted by periods of darkness or by a shortened photoperiod. They also confirmed that the rate of growth is strictly one increment per day. A recent contribution from Dean et al (48) demonstrated that the observed patterns within the otolith are present in all forms of

teleost and has no dependence on type of water that the fish inhabits, its physiology of reproducing (live bearing or egg laying) nor its size. Indeed, the only two factors that vary in the otoliths are the final morphology of the structure and the onset of otolith growth within the saccule. The comprehensive nature of the data provided by a study of the otolith, however, provides a wealth of data for the fish ecologist which even Irie cannot have expected.

3.4.5 The Piezoelectric Properties of Otoconia and Otoliths

There is currently a good deal of interest in the physiology of the inner ear in general and the role of the otoconia in the function of the vestibule in particular. The recent literature in this area is discussed below, but parts of the work reported here are relevant to the current discussion. Ross et al (59-62) have shown that there is a flux of calcium into and out of the otoconia, indicating an active role for the mineral. This is in contrast to the otoliths, in which there is believed to be no resorption of calcium (Dean, personal communication).

At present, the piezoelectric properties of otoconia are unknown, due to the very small size of the crystals, although the possibility of positive effects has been noted in a recent hypothesis concerning the physiological action of the otoconial complex (64).

Otoliths have long been known to be piezoelectric (and, hence, pyroelectric, since they operate in fluid-filled compartments and Morris and Kittleman ascribe this property to the presence of sodium in the lattice, causing charge differences in certain areas (39). It is interesting to note, although the point was not made in the original report, that the probable mode of action

would be due to the presence of protons from the HCO_3^- counter-ions which could move around the lattice in response to local field gradients. There are two results in the current study which lead one to be wary of attributing the same properties to the otoconia as the otoliths. The first concerns the stability of the otoconia under the electron beam compared with the changes observed for fish otoliths, the second, the X-ray emission spectra of otoconia, which failed to detect any sodium in the samples, although several trace elements were present. A possible explanation for these differences may lie in the differing crystal structures of calcite and aragonite, with the former havin a coordination number of 6 and a density (ρ) of 2.710 and the latter a coordination number of 9 and ρ=2.930. This increase in coordination number gives aragonite a much more open structure which would facilitate the movement of protons; this would be more difficult in the calcite lattice. The X-ray data does not support any substitution on a large scale, although the presence of phosphorus is surprising since, although carbonate is commonly known to substitute into apatite structures, the reverse substitution is not common, although it has been reported (74). One answer to the problem may lie in considering the otoconia in conjunction with the rest of the end-organ structure, since it has been suggested that a permanent charge separation exists across the otolithic membrane (64); this would not necessarily require the otoconia themselves to have piezoelectric properties.

It is possible that the presence of piezoelectric properties in otoliths have no physiological relevance whatsoever; indeed, recent work (3) indicates that the otoliths can detect and discriminate between sound waves from different distances over three dimensions rather than being concerned with the detection

of pressure changes, which is thought to be a function of the Xth Cranial Nerve (Vagus) running down the lateral line of the fish. These two mechanisms are independent. One possible explanation for the piezoelectric property might lie in the ability of the otolith to trap ions irreversibly. This would mean that the otolith is a perfect sink for toxic elements or others which were not required in the vestibular area. To support this hypothesis, consider the percentages of the following ions: Ca^{2+} : 36.35%, Na^{+} : 0.375% and Mg^{2+} : 0.185%. Correcting these figures for molarities, they read, Ca^{2+} : 91%, Na^{+} : 2% and Mg^{2+} : 1%. This difference is very small in the context of the number of calcium ions being substituted, yet if all the substitutions had been by magnesium, the system would not have been piezoelectric at all. Thus there is no positive indication that the otolith has to maintain a certain ionic balance in order to function. It is worth noting that the molarity-corrected percentage of strontium in the system is 2.53×10^{-3}% and the value of potassium 1.28×10^{-3}%. so that the total monovalent: divalent substitution ratio is 1.70, even less than that obtained for sodium and magnesium alone.

The presence of both magnesium and strontium is of some interest, since magnesium is known to inhibit calcite formation in favour of aragonite (75) and strontium is known to substitute readily into the aragonite lattice. Thus, one cannot dismiss the possibility that the crystal form obtained in otoliths arises from the presence of these inorganic trace elements as well as, or instead of, the organic matrix known to be bound in the structure.

REFERENCES

1. Carlstrom, D. *Biol. Bull.* 125, 441-463, (1963)
2. Enger, P.S., Hawkins, A.D., Sand, O and Chapman, C.J. *J. Exp. Biol.* 59, 425-435, (1973)
3. Schuif, A. and Hawkins, A.D. *Nature, Lond.* 302, 143-144, (1983)
4. Salamat, M.S., Ross, M.D. and Peacor, D.R. *Ann. Otol. Rhinol. Laryngol.* 89, 229-238 (1980)
5. Frost, G.A. *Ann. Mag. Nat. Hist. Series 9*, 15, 152-153, (1925)
6. Frost, G.A. *Ann. Mag. Nat. Hist. Series 9*, 15, 553-561, (1925)
7. Frost, G.A. *Ann. Mag. Nat. Hist. Series 9*, 18, 81-85 (1926)
8. Frost, G.A. *Ann. Mag. Nat. Hist. Series 9*, 18, 465-482 (1926)
9. Frost, G.A. *Ann. Mag. Nat. Hist. Series 9*, 18, 483-490 (1926)
10. Frost, G.A. *Ann. Mag. Nat. Hist. Series 9*, 20, 298-305, (1927)
11. Frost, G.A. *Ann. Mag. Nat. Hist. Series 10*, 1, 451-456, (1928)
12. Frost, G.A. *Ann. Mag. Nat. Hist. Series 10*, 2, 328-331, (1928)
13. Frost, G.A. *Ann. Mag. Nat. Hist. Series 10*, 4, 120-130, (1929)
14. Frost, G.A. *Ann. Mag. Nat. Hist. Series 10*, 4, 257-264, (1929)
15. Frost, G.A. *Ann. Mag. Nat. Hist. Series 10*, 5, 231-239, (1930)
16. Frost, G.A. *Ann. Mag. Nat. Hist. Series 10*, 5, 621-627, (1930)
17. Irie, T. *Bull. Fac. Fish. Anim. Husb. Hiroshima Univ.* 3, 203-221, (1960)
18. Carlstrom, D., Engstrom, H. and Hjorth, S. *Laryngoscope*, 63, 1052-1057, (1953)
19. Carlstrom, D. and Engstrom, H. *Acta Otolaryngol. (Stockh).* 45, 14-18, (1955)
20. Marco, J., Sanchez-Fernandez, J.M. and Rivera-Pomar, J.M. *Acta Otolaryngol (Stockh).* 71, 1-8, (1971)
21. Sanchez-Fernandez, J.M., Marco, J., Rivera-Pomar, J.M. and Marquez Delgardo, R. *Acta Otolaryngol. (Stockh).* 73, 267-269, (1972)

22. Lim, D.J. *Ann. Otol.* 82, 23-35, (1973)

23. Ross, M.D. and Peacor, D.R. *Ann. Otol. Phinol. Laryngol.* 84, 22-37, (1975)

24. Ross, M.D., Johnson, L.-G., Peacor, D.R. and Allard, L.F. *Ann. Otol. Rhinol. Laryngol.* 85, 310-326, (1976)

25. Nakahara, H. and Bevelander, G. *Anat. Rec.*193, 233-241, (1979)

26. Peacor, D.R., Rouse, R.C. and Ross, M.D. *Anat. Rec.* 197, 375-376, (1980)

27. Irie, T. *Bull. Fac. Fish. Anim. Husb. Hiroshima Univ.* 1, 1-8, (1955)

28. Irie, T. *Bull. Fac. Fish. Anim. Husb. Hiroshima Univ.* 1, 311-317, (1957)

29. Bagenal, T.E. *"The Ageing of Fish"* ed. T.E. Bagenal, pub. Unwin Bros., pp234, (1974)

30. Panella, G. *Science N.Y.*, 173, 1124-1127. (1971)

31. Panella, G. in *"The Ageing of Fish"* ed. T.E. Bagenal, pub. Unwin Bros., p28-39, (1974)

32. Brothers, E.B., Mathews, C.P. and Lasker, R. *Fish. Bull.* 74, 1-8, (1976)

33. Taubert, B.D. and Coble, D.W. *J. Fish. Res. Bd. Can.* 34, 332-340, (1977)

34. Barkman, R.C. *Trans. Am. Fish. Soc.* 107, 790-792, (1978)

35. Townsend, D.W. and Graham, J.J. *Fish. Bull.* 79, 123-130, (1981

36. Brothers, E.B. in *"The Biological Bases for Reef Fishery Management"*, NOAA Tech. Memorandum. NMFS-SEFC-80. NMFS Beaufort, N.C., U.S.A. G.R. Huntsman, W.R.Nicholson and W.W. Fox, Jr. (eds), pp3-23, (1982)

37. Radke, R. and Dean, J.M. *Fish. Bull.* (1982) in press

38. Dunkelburger, D.G., Dean, J.M. and Watabe, N. *J. Morph.* 163, 367-377, (1980)

39. Morris, R.W. and Kittleman, L.R. *Science, N.Y.* 153, 368-370, (1967)

40. Ross, M.D., Pote, K.G., Rarey, K.E. and Verma, L.M. *Ann. N.Y. Acad. Sci.* 374, 808-819, (1981)

41. Ross, M.D. and Pote, K.G. *Proc. R. Soc. Lond. B* (1983) in press.

42. Degens, E.T., Deuser, W.G. and Haedrich, R.L. *Marine Biol.* 2, 105-113, (1969)

43. Cheetham, A.K. and Skarnulis, A.J. *Analyt. Chem.*, 53, 1060-1064, (1981)

44. *Practical Methods in Electron Microscopy*, A.M. Glauert (ed.), Vols 3 and 5 Elsevier/North Holland Publishing Company, Amsterdam, (1975-1977)

45. Spurr, A.R. *J. Ultrastructure Res.*, 26, 31-43, (1969)

46. Xipell, J., Makin, H. and McKinnon, P. *Stain Technology* 49, 69-76, (1974)

47. Kunzmann, P. and Eyring, L. *J. Solid State Chem.*, 14, 229-237, (1975)

48. Dean, J.M., Wilson, C.A., Haake, P.W. and Beckman, D.W. in *"Biomineralisation and Biological Metal Accumulation"* P. Westbroek and E.W. de Jong (eds.). Pub. D. Reidel, Holland. pp 353-359, (1983)

49. Erulkar, S.D. and Maren, T.H. *Nature, Lond.* 189, 459-460, (1961)

50. Haake, P.W., Wilson, C.A. and Dean, J.M. in *"Proceedings of the Fifth Annual Larval Fish Conference"*, 12-15, (1982). C.F. Bryan, J.V. Conner and F.M. Truesdale (eds.). Pub. LSU Press, Baton Rouge, Louisiana, U.S.A.

51. Nakahara, H. Kakei, M. and Kunii, S. *Bull. Josai Dent. Univ.* 10, 333-336, (1981)

52. Anniko, M. *Micron*, 12, 267-278, (1981)

53. Wright, C.G. and Hubbard, D.G. *Acta Otolaryngol (Stockh).* 94, 7-18, (1982)

54. Wright, C.G., Rouse, R.C., Johnsson, L.-G., Weinberg, A.G. and Hubbard, D.G. *Ann. Otol.* 91, 193-199, (1982)

55. Johnsson, L.-G., Wright, C.G., Preston, R.E. and Henry, P.J. *Acta Otolaryngol (Stockh).* 89, 93-104, (1980)

56. Johnsson, L.-G., Wright, C.G., Preston, R.E. and Henry, P.J. *Acta Otolaryngol (Stockh).* 89, 401-406, (1980)

57. Ross, M.D. in *"Special Senses in Ageing, a current biological assessment"*, eds. S.S. Han and D.H. Coons. Pub. Univ. Michigan Press 163-167 (1977)

58. Vinnikov, Ya.A., Gazenko, O.G., Titova, L.K., Bronstein, A.A., Govardovskii, V.I., Gribakin, F.G., Pevzner, R.A., Aronova, M.Z., Kharkeevich, T.A., Tsirulis, T.P., Pyatkina, G.A., Lichakov, D.V., Pal'mbach, L.P. and Andanina, V.O. *Acta Otolaryngol (Stockh).* 87, 90-96, (1979)

59. Ross, M.D. *Adv. Oto-Rhino-Laryng.* 25, 26-33, (1979)

60. Ross, M.D. and Williams, T.J. *Physiologist* 22 Supp, S63-S64, (1979)

61. Ross, M.D., Pote, K.G., Cloke, P.L. and Corson, C. *Physiologist* 23 Supp, S129-S130, (1980)

62. Ross, M.D., Corson, C., Pote, K.G. and Cloke, P.L. *in Adv. Physiol. Sci.* 19, *Gravitational Physiology"* J. Heideg and O. Gazenko (eds), pp243-246, (1980)

63. Vinnikov, Ya.A., Lichakov, D.V., Pal'mbach, L.R., Govardovskii, V.I., Andanina, V.O., Allakhverdov, B.L. and Pogorelov, A.G. *J. Evol. Biochem. Physiol. (Leningrad),* 16, 574-579, (1980)

64. Ross, M.D. in *"Advances in Space Research" vol. 3 R.* Holmquist (ed), (1983), in press

65. Lim, D.J. in *"Ultrastructural Atlas of the Inner Ear"* (1983) in press

66. Mugiya, Y., Watabe, N., Bean, J.M., Dunkelburger, D.G. and Shimizu, M. *Comp. Biochem. Physiol.* 68A, 659-662, (1981)

67. Richardson, C.A., Crisp, D.J. and Runham, N.W. *Malacologia* 18, 277-290, (1979)

68. Crisp, D.J. and Richardson, C.A. *Marine Biol.* 33, 155-160, (1975)

69. Richardson, C.A., Crisp, D.J., Runham, N.W. and Gruffydd, Ll. D. *J. Mar. Biol. Ass. U.K.* 60, 977-989, (1980)

70. Richardson, C.A., Crisp, D.J. and Runham, N.W.J. *Mar. Biol. Ass. U.K.* 60, 991-1004, (1980)

71. Richardson, C.A., Crisp, D.J. and Runham, N.W. J. *Mar. Biol. Ass. U.K.* 61, 465-476, (1981)

72. Yule, A.B., Crisp, D.J. and Cotton, I.H. *Marine Biology Letters* 3, 273-2-8, (1982)

73. Ekaratne, S.U.K. and Crisp, D.J. *Proc. R. Soc. Lond. B* 214, 305-323, (1982)

74. Kitano, Y., Okumura, M. and Idogaki, M. *Geochemical Journal,* 12, 29-37, (1978)

75. Kitano, Y., Park, K. and Hood, D.W. *Geophysical Journal* 67, 4873-4874, (1962)

76. Dana, J.D.*"The System of Mineralogy" Volume 2,* Seventh edition, rewritten and enlarged by C. Palache, H. Berman and C. Frondel. Pub. J. Wiley and Sons, Inc., New York, (1951)

77. Andrews, K.W., Dyson, D.J. and Keown, S.R.*"Interpretation of Electron Diffraction Patterns"* Second edition 1971, Plenum Press, New York p94ff.

Chapter 4

Ultrastructural Study of Coccoliths

4.1 Introduction

The formation of minerals occurs in all forms of life, both animal and plant, including bacteria. Calcium carbonate formation, although present as the pure mineral in some prokaryotes (1), however, is first observed in conjunction with an organic matrix in coccolithophorids, which are monocellular, photosynthetic marine algae in the class Haptophyceae Park and Dixon (2). These algae will form scales of calcium carbonate (usually calcite, although aragonite is known) which are generally round or oval and act as a protective layer or coccosphere, around the cell. This is illustrated, for *Emiliania huxleyi* (Lohmann) Kamptner, in Figure 4.1.

4.1.1 The Significance of Coccoliths to Biomineralisation

Coccolithophores have been used as a simple model for biomineralisation due to their unicellular structures. This has led to the assumption that the mineralisation process utilised within the cell is simple and much work has been carried out on both the cellular processes involved and the coccoliths themselves. The work reported here reveals that the biogenesis of the coccoliths is not simple; within a vesicle in the cell of the alga, two entirely different mechanisms are used to construct the final structure. This observation, considered with work carried out at the University of Leiden by Drs. Peter Westbroek and Elisabeth de Jong, is of great significance for the understanding of the physiology of coccolithophoridae and also of biomineralisation processes generallly. In order to facilitate a full discussion

Figure 4.1

Coccoliths surrounding a cell of *Emiliania huxleyi* (Lohmann) Kamptner. This structure is known as a coccosphere. Scale bar = 1 μm

of the relevance of this work, I have reviewed the biology of coccoliths more fully than is necessary for an understanding of this, ultrastructural,work.

4.1.2 The Discovery of Coccoliths

Coccoliths were first observed by light microscopy in 1836 by C.G. Ehrenberg, who was studying samples of chalk from the Baltic. They were first recognised as biogenic formations in 1861, by H.C. Sorby (3). At a similar time, T.H. Huxley and G.C. Wallich investigated the first samples of deep-sea ooze to be raised from the Atlantic Ocean and observed many of these rounded structures, both individually, which Huxley first named, and as the coccosphere (4). Later they found coccospheres swimming freely near to the surface of the ocean. Subsequent work has shown that coccolithophorids are found in tropical and sub-tropical as well as arctic waters (5). Many different types of coccoliths have now been found and it is apparent that the morphology of the structures is species dependent (6,7).

Most research has concentrated on one species of coccolithophorid, *Emiliania huxleyi*, which was previously named *Coccolithus huxleyi* and this study used the form *Emiliania huxleyi* (Lohmann) Hay and Mohler.

4.1.3 The Morphology of Coccoliths of E. Huxleyi

Coccoliths from *E. huxleyi* were first observed in an electron microscope by Braaud and Nordli (8,9). They used a sample from *E. huxleyi* (Lohmann) Kamptner as a model system for electron microscopy and described the structure as consisting of two discs; an upper disc with a large number of radial spokes

which form a connection at their inner end with a thin lower disc which has no central opening. Later work showed that this lower disc was comprised of as many segments as there are spokes in the upper disc and that the upper and lower discs always lie so that a spoke sits above and in the centre of a lower disc segment. Wilbur and Watabe (10), in a paper concerned with the biogenesis of the coccoliths (see below) described these components as upper and lower elements, which are joined by a central element. This nomenclature has generally been followed in the subsequent literature and will be used in this discussion. Later work by Watabe (11), which involved the use of electron diffraction as well as transmission electron microscopy, was concerned with the ultrastructure of the coccoliths. By obtaining identical electron diffraction patterns from each of the upper, central and lower elements, as well as the joined unit itself, he concluded that the unit comprising the upper element joined to the lower element through the central element is a single crystal of calcite. Watabe acknowledged that this would be an unusual structure for a single crystal and thus suggested that one possible explanation for his results could be that each individual component of the unit was a single crystal and that these components are joined together in an ordered manner so that each crystal is aligned to produce a single crystal diffraction pattern. This view of the ultrastructure of coccoliths has been largely accepted and little further work has been carried out on the subject. One report from Outka and Williams (12) is notable in that it used light and electron microscopy to follow coccolith formation in *Hymenomonas carterae*. They noted the role played by the Golgi bodies in creating the correctly-shaped coccolith vesicle. The morphology of the coccolith from this species

differs markedly from that of *E. huxleyi*, but the process of formation is identical. Formation occurs in the Golgi apparatus from two precursors, a scale-like base and multiple granular elements, which they named 'coccolithosomes'. The cisternal membrane attaches to the base and then the coccolithosomes form an outer rim which is subsequently filled in by calcium carbonate. This general process will be discussed at further length below.

4.1.4 The Organic Matrix of Coccoliths

In common with all calcium carbonate-forming systems, the coccoliths contain an organic matrix which is known to play a role in controlling growth. The presence of an extracrystalline matrix was first detected by Watabe in 1970 (13), but an intracrystalline fraction was found by Westbroek et al (14) which was soluble and acidic. Analysis showed that the soluble intracrystalline fraction (SIF) was a protein-free polysaccharide containing about 26% uronic acid. The analysis was extended in a later paper from the same laboratory (15). This showed that the polysaccharide contains two forms of calcium-binding acidic residues; the uronic acids and a stronger binding form which was not identified. The dissociation constant for calcium binding to the two sites was determined by flow-rate dialysis. The high-affinity sites were present in a concentration of 0.38 $\pm$ 0.04 µmol mg^{-1} polysaccharide with a K_d value of 2.2 $\pm$ 1.0 x 10^{-5} M for calcium and the low affinity sites, K_d for Ca^{2+} = 111 $\pm$ 39 x 10^{-5} M, in a concentration of 0.74 $\pm$ 0.11 µmol mg^{-1} polysaccharide. Calcium is bound preferentially even in the presence of a hundred-fold excess of sodium and magnesium, although an equivalent excess of strontium inhibited binding and an equimolar

concentration of lanthanum totally inhibited calcium binding. The polysaccharide was further characterised by structure analysis and graded acid hydrolysis (16-19). A second acidic residue was found, 3-O-methyl-D-galacturonic acid, in the side chains of the structure. The polysaccharide proved to be unusually complex, with a backbone of about 80% of (1⟶3)-linked D-mannosyl residues. The balance of the backbone comprises terminal D-ribosyl or L-arabinosyl groups and short side-chains of two or three D-galactosyluronic acid residues. Ester-bound sulphate groups are also scattered along the backbone. The complex side-chains consists of D-xylose and L-rhamnose, which is highly substituted. One of these substitutions is by an oligosaccaride composed of 2,3-di-O-methyl-L-rhamnose, 3-O-methyl-D-galactouronic acid, 6-O-methyl-L-mannose, D-galactouronic acid, L-mannose and L-rhamnose. The acid groups and the sulphates account for the acidic nature of the polysaccharide.

The relevance of the organic matrix for coccolith formation has been studied (20). In common with many other soluble organic matrices (21,22), it has been found to inhibit calcium carbonate crystal formation *in vitro*. This effect is striking and is dependant on the ions bound to the acid groups; Na^+ bound polysaccharide will cause total inhibition for a period up to six hours, but Ca^{2+}-bound polysaccharide is much less effective. If 1% ethanol is added to the solution, the inhibition effect is substantially reduced, presumably due to the altering of the polysaccharide conformation. The calcium-binding was shown to be due to the uronic acids since desulphation has no effect on the Ca^{2+} binding capacity. Recent work from the same laboratory (23) has shown that a related polysaccharide, alginic

acid (polymannuronic-guluronic acid), will inhibit $CaCO_3$ formation to the same extent as the native polysaccharide, but when immobilised to either Bovine Serum Albumin (by carbodiimide) or the Sepharose-4B beads (by cyanogen bromide), the polysaccharide has a stimulatory effect on $CaCO_3$ precipitation. This is consistent with a general observation by Crenshaw (24) that immobilisation of biomineralisation organic matrix components changes their properties towards $CaCO_3$ formation and arises from the conformation necessary to bind calcium effectively; there is no logical reason why a biological polymer, whether polysaccaride or protein, should retain the same conformation in solution as it has when bound to a substrate, either organic or inorganic. This is discussed at further length elsewhere in this report. This experiment has not been successfully repeated with the native polysaccharide, since the number of acidic residues is far smaller than in alginic acid and the coupling reaction tends to use them all.

4.1.5 The Biosynthesis of Coccoliths

Wilbur and Watabe (10) studied coccolithophoridae cells and observed coccoliths within 'coccolith vesicles' close to the nucleus inside the cell. These coccoliths were seen at various stages of growth. Just before calcification commenced, the vesicle took on the shape of the coccolith, with finger-like projections extending outwards. They observed that calcification began at the point where the upper element is joined to the lower element (in the region now described as the central element) and proceeds upwards and outwards to form the central and upper elements, and laterally in both inwards and outwards directions to form the basal element (see Figure 4.2). As one follows the

Figure 4.2

(a) A coccolith from *Emiliania huxleyi*, comprising several segments.

(b) A single segment from a coccolith, in which the following elements can be distinguished:

l.e.: flattened radially oriented lower element; u.e.: hammer shaped upper element;

c.e.: central element and m.e.: medially directed element

growth of the upper elements, one sees that they extend outwards, and finally, when they have achieved a certain, predetermined length, they grow in a lateral direction, forming "hammer-like" heads. There is no set number of elements in a coccolith; Kamptner in 1956 reported between 26 and 34 (25). Wilbur and Watabe reported that these head units eventually fuse together to form a structure reminiscent of a rim of a wheel. Klaveness (26) reported that the cell is only capable of constructing one coccolith at a time and that the coccolith vesicle is probably formed from the fusion of Golgi vesicles. Within this vesicle and before coccolith growth a series of membranes develop, firstly as a basal structure parallel to the vesicle base and then bending upwards into the space to be occupied by the upper elements This membraneous structure probably forms a complete coating of the final structure. De Jong et al (27) associated coccolith formation with the uptake of hydrogen carbonate and galactose. They developed a technique for removing the newly-formed calcium carbonate from within the cell and measuring the radioactive labels taken up from the surrounding medium. By successively labelling $^{45}Ca^{2+}$, $H(^{14}C)O_3^-$, D-(1-^{14}C) galactose and $(^{35}S)O_4^{2-}$, they managed to follow the various metabolic pathways and obtain a hypothesis for coccolith formation, which is reproduced as Figure 4.3. Interestingly, non-calcifying, or 'naked' cells were also analysed and it was found that they are unable to take up galactose and calcium. No satisfactory explanation of this phenomenon has yet been postulated, but it is thought that the ability to photosynthesise is closely linked to coccolith production (28).

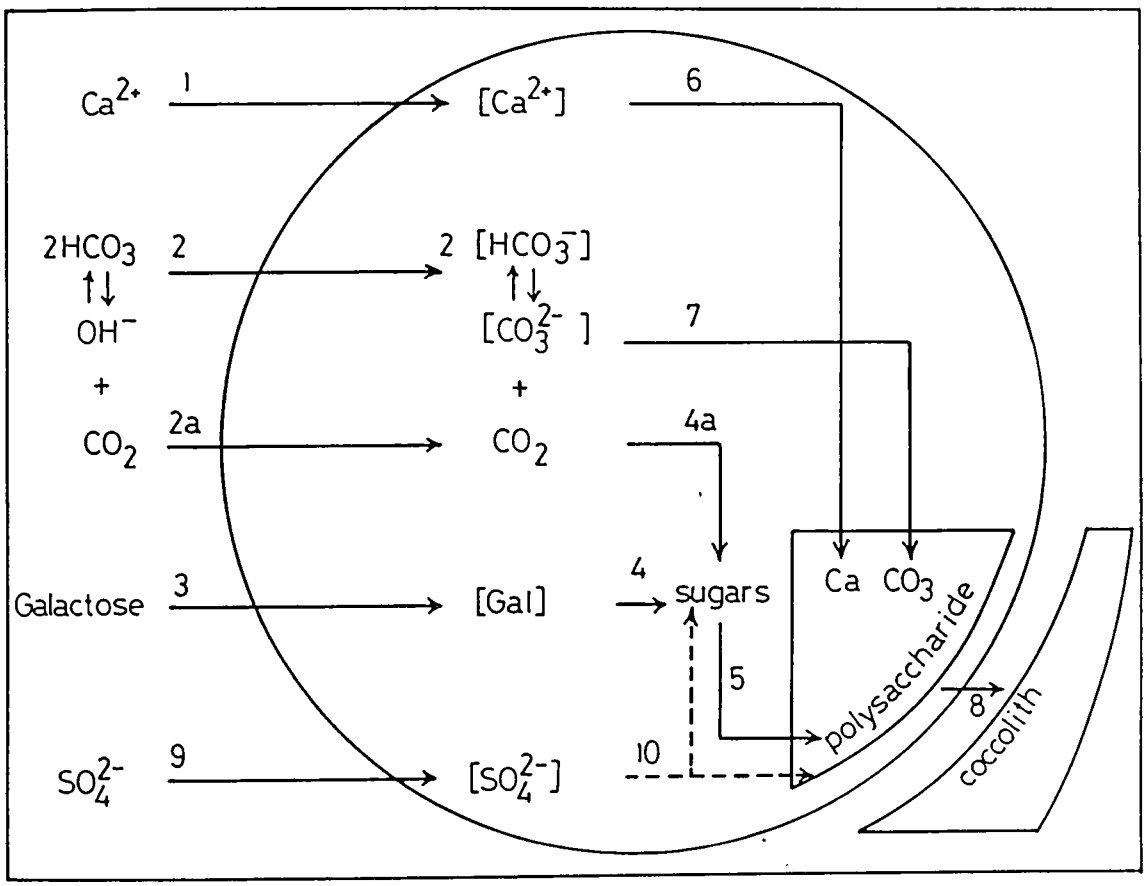

Figure 4.3

Hypothesis of the biochemical pathways leading to coccolith formation. Numbers represent the order of the process. After de Jong et al (9).

4.1.6 The Aim of this Study

The ultrastructural study carried out by Watabe (11) in 1967 has been accepted and used as a basis for hypotheses of coccolith formation by various workers since that time. It was felt, however, that the unlikely nature of those original conclusions, coupled with the author's own uncertainty as to the exact ultrastructure, made it necessary to apply ultra-high resolution electron microscopy to the system. It is particularly important to have a good understanding of coccolith structures as they have often been used as a simple system for modelling biomineralisation processes; thus much research work in the field reflects accepted theories for the coccolith system. The work was carried out in close collaboration with Drs. Peter Westbroek and Elisabeth de Jong at the University of Leiden and Dr. A. Jerome Skarnulius at the University of Oxford.

4.2 Materials and Methods

Samples of coccoliths were obtained by Drs. Westbroek and de Jong. They were prepared by farming the species of coccolithophoridae used, in this case *E. huxleyi* (Lohmann) Hay and Mohler, strain A92, originally provided by Dr. J.P.M. de Vrind, Department of Biochemistry, State University of Leiden, The Netherlands. Farming is carried out in a substantial tank since the algae cannot survive in conventional culture conditions (28). The isolation of the coccoliths from the cells was carried out in Leiden by the method of de Jong et al (15).

Coccoliths were prepared for examination in the ultra-high resolution electron microscope by sonicating the suspended pellet in an MSE probe sonicator for 5 minutes. This broke the

structure up into its component parts which were thin enough for imaging. After lyophilising to remove the water, the sample was resuspended in chloroform by bath sonication, dropped onto a 2.3 mm holey-carbon coated copper grid and dried in air. The electron microscope used for the ultra-high resolution study was a Jeol-200CX instrument in the Department of Metallurgy, University of Oxford. Identical operating conditions were used as for the study of otoconia and otoliths which have been described above.

Initial observations were made at conventional resolution using a Jeol-100CX Temscan electron microscope operating at 100 keV. Qualitative X-ray microanalysis was carried out using the Link facility on the microscope.

Scanning electron micrographs were obtained from a Jeol-1200CX analytical electron microscope situated at Jeol House, Grove Park, Colindale, London NW9. The micrographs were obtained with the assistance of Dr. A.C. Brown of Jeol (U.K.) Ltd. This microscope was operated at 60 keV and the sample used was gold-sputtered to a thickness of about 100 Ångstroms to aid resolution. This microscope was fitted with a y-modulation facility to enhance the three-dimensional aspects of the structures under study.

The electron diffraction patterns obtained from this study were interpreted by comparison with computer-generated patterns of calcite from an interactive image calculation program designed to predict both electron diffraction patterns and the ultra-high resolution lattice images. This program plots and calculates an image based on a projected structure, no matter what kind of symmetry is involved. It will handle non-orthogonal axes and produces both diffraction patterns and

projections which can be related directly to the images seen in the microscope.

4.3 Results

4.3.1 Scanning Electron Microscopy of Coccoliths

The use of scanning electron microscopy enables a careful study of the morphology of the coccoliths to be made. Study of coccolith morphology by electron microscopy is not new but my study was made to take particular advantage of a new technology electron microscope, the Jeol-1200EX. This microscope is capable of achieving a very good resolution at high magnification and also to produce a photograph with y-modulation which emphasises three-dimensional structure within the subject (although reducing overall depth of field). The sample studied was a gold-sputtered mount of *E. huxleyi* (Lohmann) Hay and Mohler. Figure 4.4 shows a series of four photographs of coccoliths at varying angles emphasising the different aspects of the morphology. Of particular note is the curved nature of the structure. This arises from the construction of the coccolith within the coccolith vesicle which lies closely apposed to the nucleus. The curvature is an indication that the structure is not a simple crystalline arrangement since minerals always grow with straight edges.

Figure 4.5 is of interest since it views the coccolith from an edge and gives a clear view of the nature of the central element connecting the upper and lower elements. The y-modulated SEM (Figure 4.5b) gives a clear impression of the spatial relationship between the upper elements and the lower elements which extend into the centre of the structure. In this micrograph the latter appear as ridged structures which meet in the middle as a solid block of calcium carbonate. This impression is

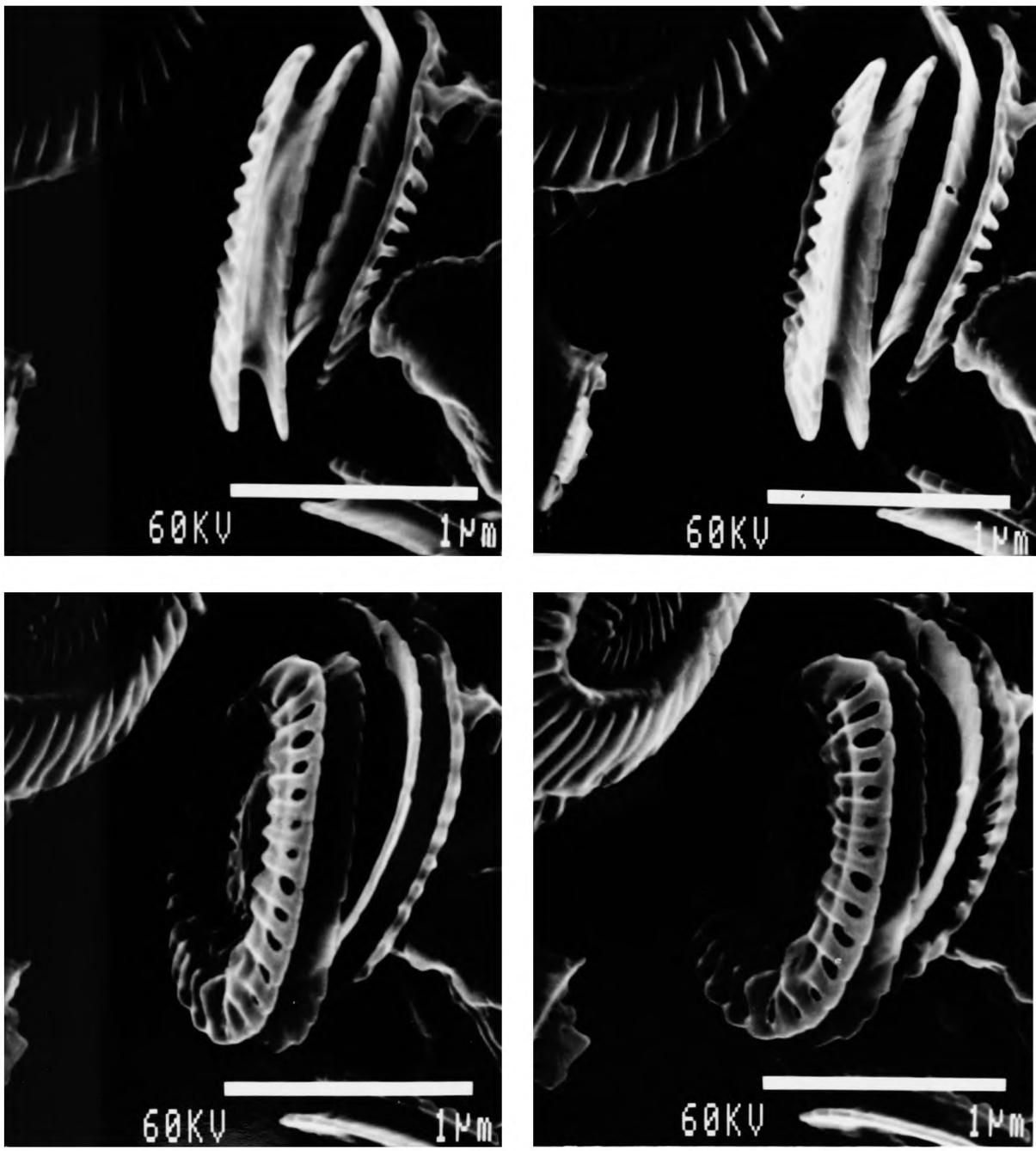

Figure 4.4

SEMs of a pair of coccoliths from *E. huxleyi* viewed at a) 0^{o}, b) 5^{o}, c) $25^{o}$and d) 35^{o}. Magnification given by scale bars.

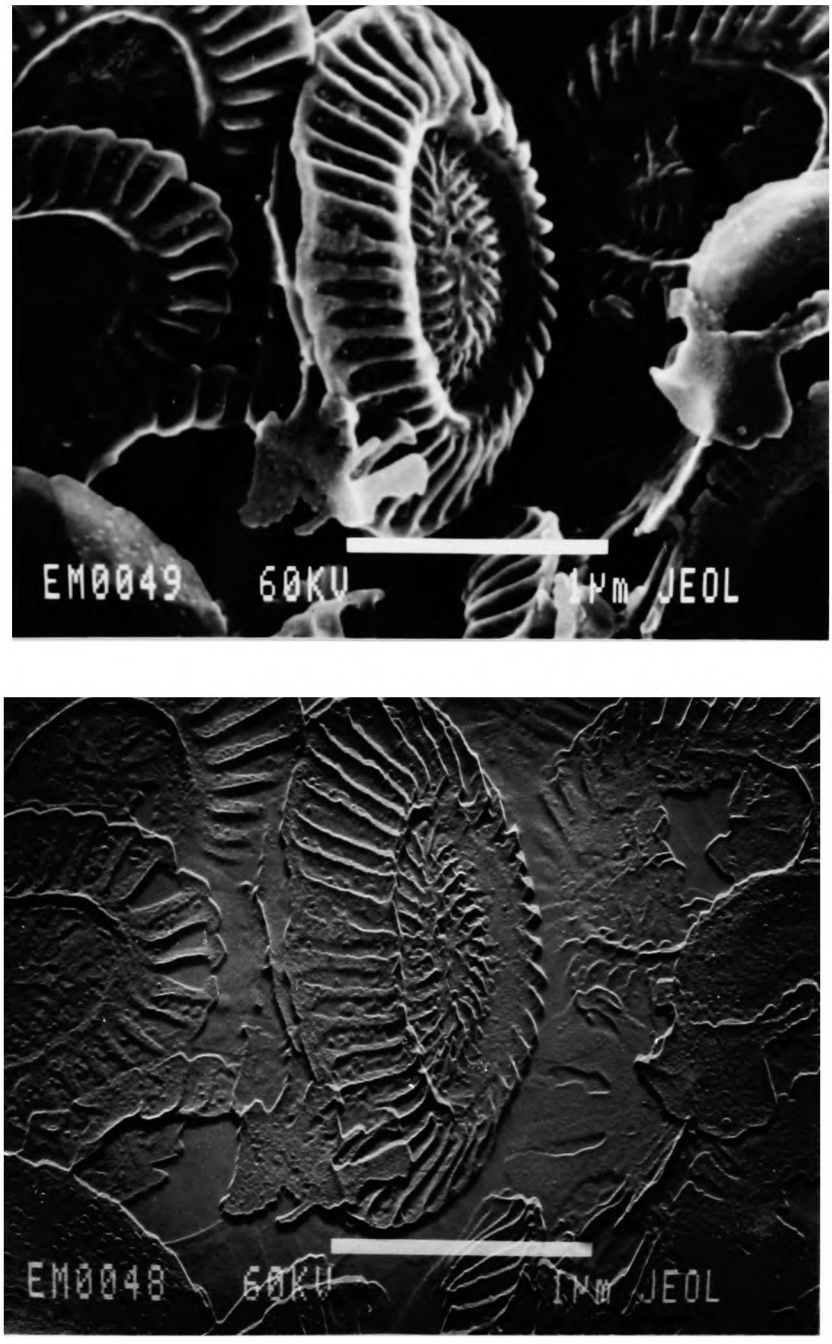

Figure 4.5

(a) SEM and (b) y-modulated SEM of coccoliths from *Emiliania hexleyi* (Lohmann) Hay and Mohler, showing the relationship between the lower and upper elements, through the central element

confirmed by the y-modulated image. As Figure 4.4 indicates, this is unusual in that the central portion is not a solid, but has a slit along it. Figure 4.6a shows that the central portion is very thin. It is inclined to snap in preparation. The coccolith with its base in view indicates that the central area is a flat continuation of the basal element from the base; structure appears to be in the top region only.

The coccoliths can redissolve as they age and this process is illustrated in Figure 4.6b. The process commences at the tips of the upper elements. As the central element dissolves, the structure becomes more apparently comprised of crystals packed together in a regular pattern. This sort of arrangement is observed in coccoliths from other species as well and is illustrated in Figure 4.7 for *Hymenomonus carterae*.

4.3.2 Elemental Analysis of Coccoliths

Analysis was carried out on coccoliths from *E. huxleyi* by X-ray microanalysis. Since the samples were so thin, analysis was made difficult by the tendency of the electron beam to punch a 10 nm hole through the structure. As a consequence the analysis was either carried out in the selected area mode of the scanning microscope, or in transmission mode, making use of the high angle detector fitted to the microscope. In both these cases, the area under analysis is larger and it was not possible to obtain analyses of the individual elements of the coccoliths. Figure 4.8 illustrates a typical spectrum for a coccolith sample. The trace elements present are phosphorus and sulphur, both in very small quantities. The sulphur probably arises from the sulphated polysaccharide and the phosphorus may

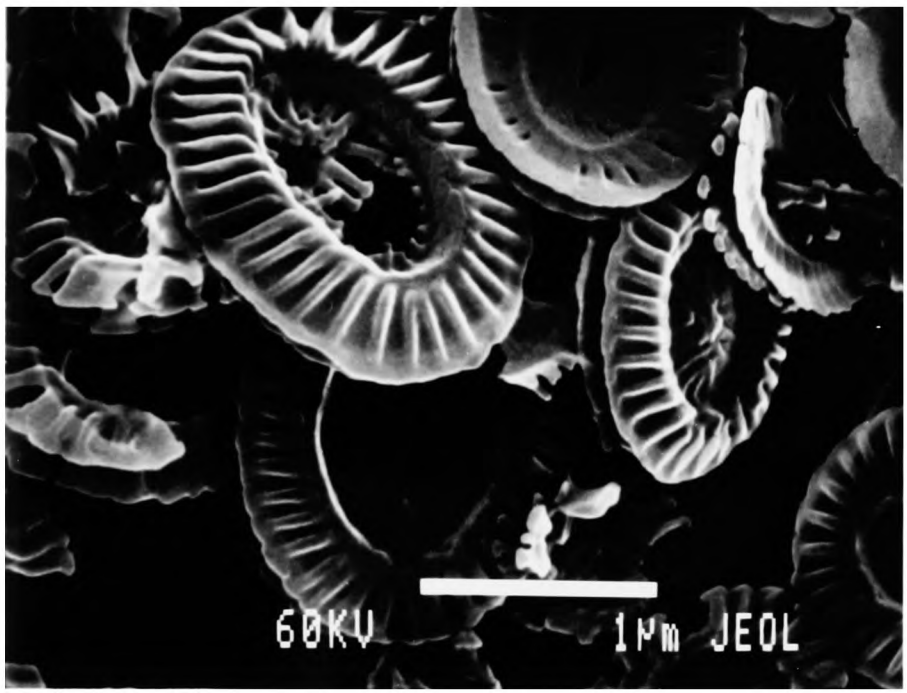

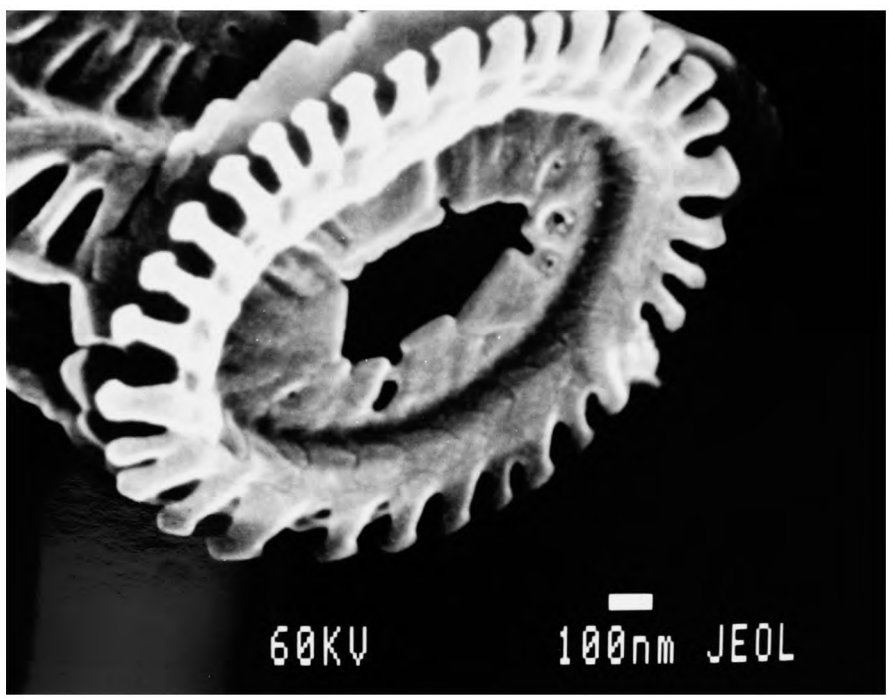

Figure 4.6

a) SEM of coccoliths showing as pects of the growth. Note the basal plate with a membrane-like appearance at top right.

b) SEM of redissolving coccolith. This process is most apparent at the ends of the upper elements. Scale bars are on the figures.

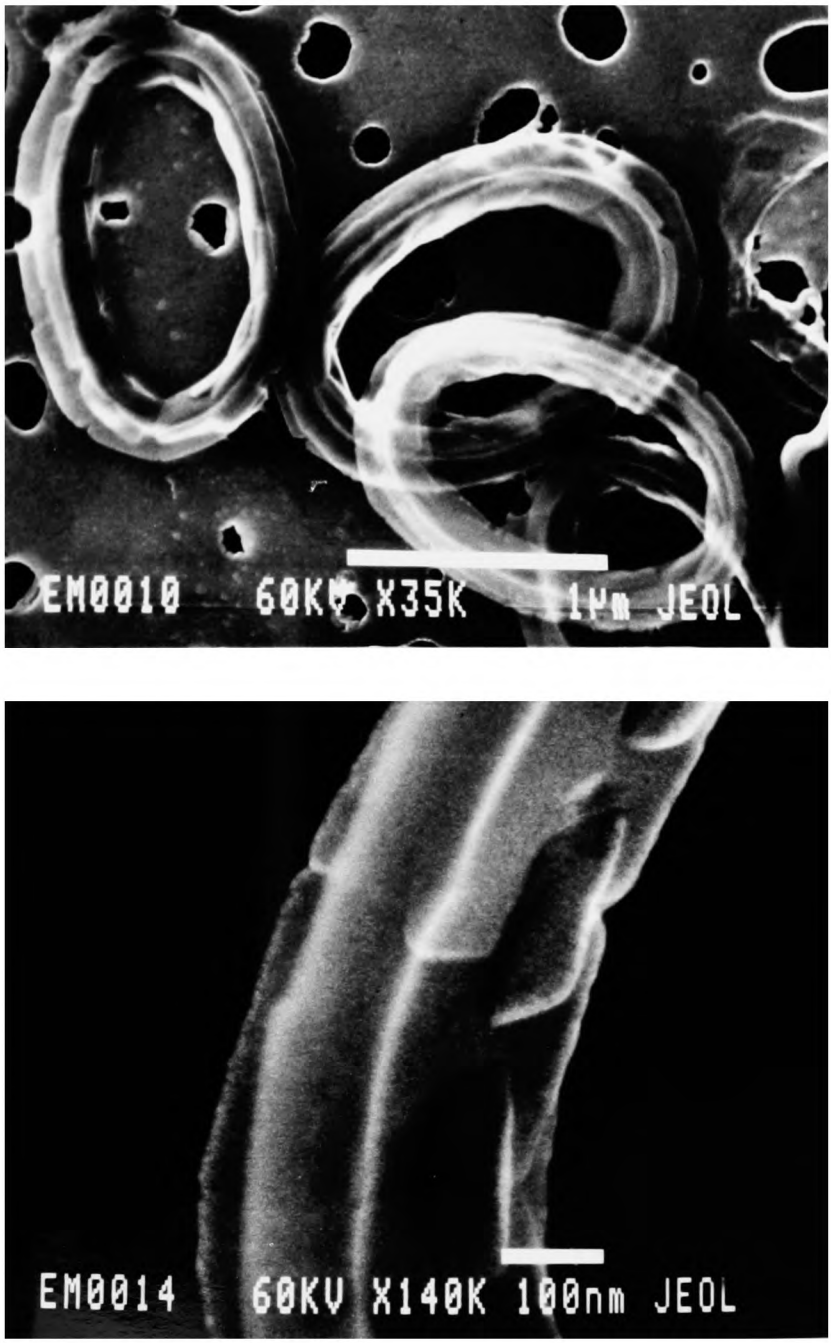

Figure 4.7

Coccoliths from *Hymenomonas carterae* showing the arrangement of calcite plates around the circle. Magnification in prints.

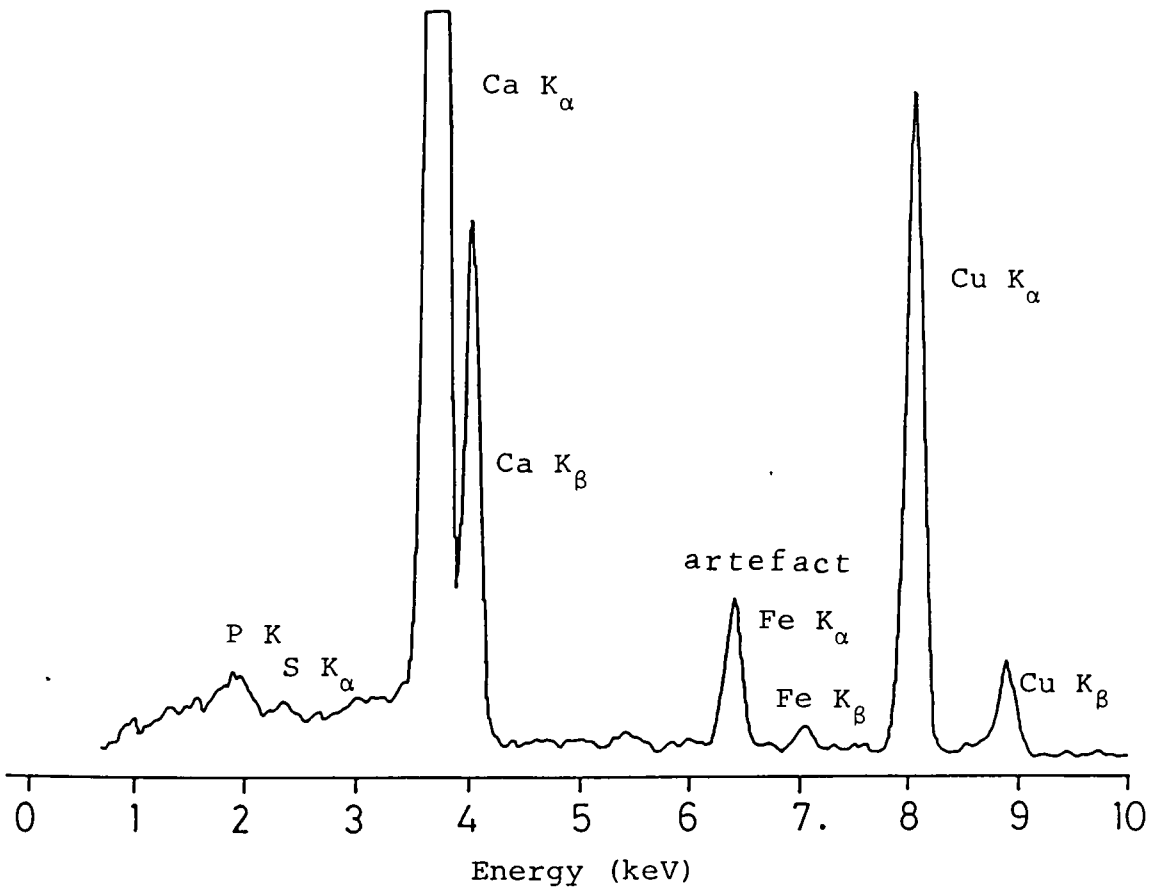

Figure 4.8

X-ray microprobe analysis of coccoliths from *E. huxleyi* (Lohmann) Hay and Mohler.

be due to the lipid vesicle which the coccolith grows in. One possible interpretation of this result is that the lipid remains as an outer coating around the structure after it is exocytosed. This would be unusual and it is possible that there is a phosphated component in the coccoliths which is as yet unknown. The specific areas of element concentration were determined by constructing an elemental analysis map over an area of the grid containing a few coccoliths. This is achieved by scanning the sample in the normal manner when photographing but arranging for a spot on the photograph whenever the element in question is detected. The result is shown in Figure 4.9. A clear correlation is found between coccolith position and calcium (Figure 4.9b); phosphorus and sulphur (Figures 4.9c and d) also show a slight correlation, but this is not obvious due to the very low count rate for the two elements. It can be seen, however, by considering Figures 4.8 and 4.9 in conjunction, that the three elements are all intimately related to the coccolith structure.

4.3.3 Ultra-High Resolution Electron Microscopy

Ultra-high resolution electron microscopy was carried out on a coccolith sample that had been sonicated to break it up into its component parts. This led to an unambiguous study of the biomineral and the extreme thinness of the sample allowed micrographs of very high quality to be obtained. In common with the practice described for the otoconia study, electron diffraction patterns were obtained with the lattice images wherever possible; in this case, though, the limited scope for tilting the sample (10^{o} in x- and y-directions) meant that the upper elements did not yield electron diffraction patterns.

The lower element broke into extremely thin sheets which gave electron diffraction patterns of single crystals. A

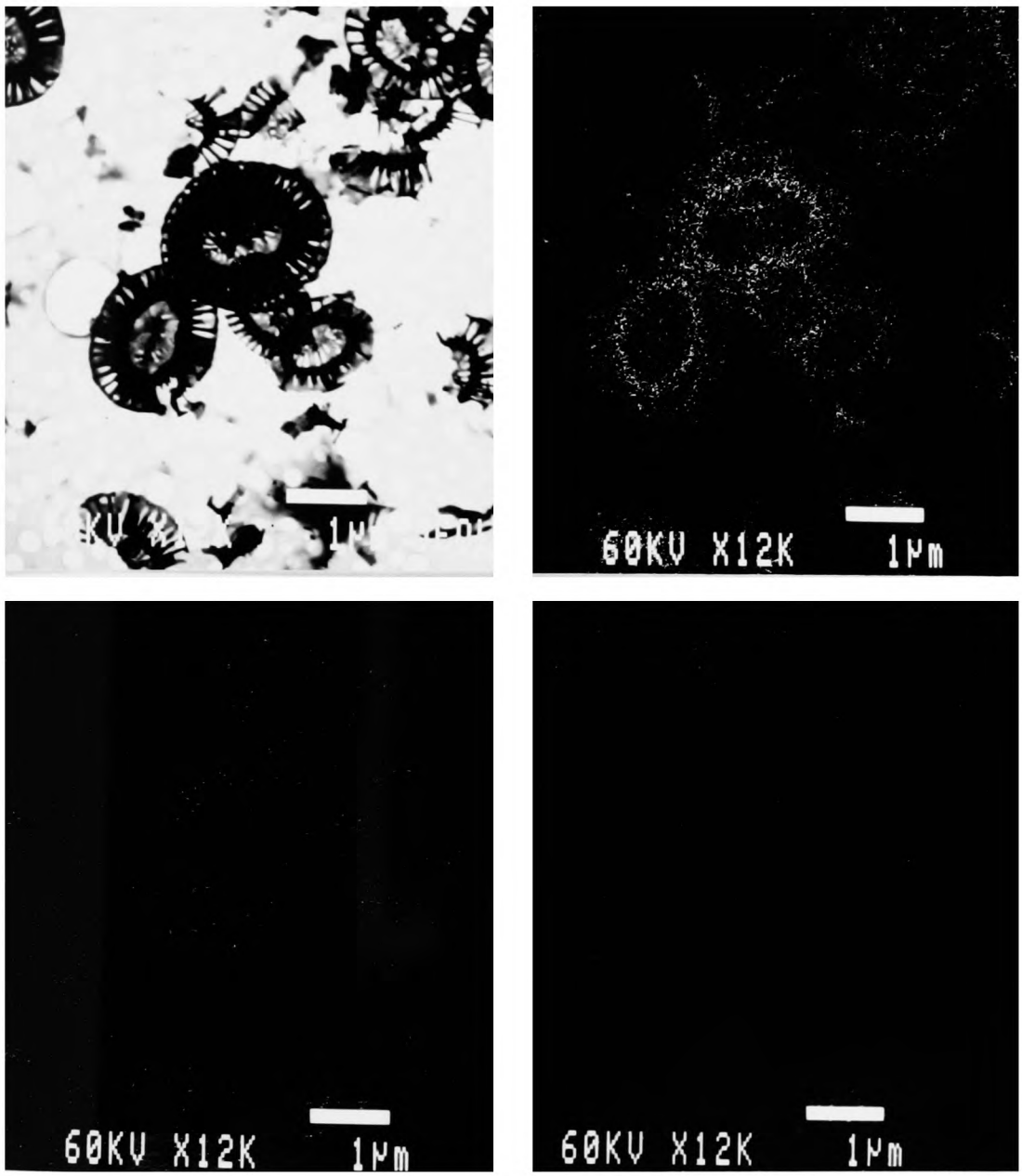

Figure 4.9

a) TEM and elemental analysis maps for b) Ca, c) P and d) S of coccolith sample. Magnification given by scale bars.

typical example is shown in Figure 4.10, along with the computer prediction of the pattern, showing it to be due to a [421] zone. the lattice image of the sample is shown in Figure 4.11. It is a single crystal, extending throughout the sample and Figure 4.12 shows that in regions of optimum defocus (the sample undulates slightly), a two-dimensional lattice image was obtained; to my knowledge, this is the first time that such an image has been observed in a biological specimen. The lattice image, with a d-spacing of 3.85 Å, arises from four of the six central reflections in the diffraction pattern, the $0\bar{1}2$, $01\bar{2}$, $\bar{1}12$ and $1\bar{1}\bar{2}$, which are the most intense in the pattern. Figure 4.12b shows the prediction for the lattice image arising from a [421] zone, with the hexagonal pattern apparent. The angle between the rows of spots in the prediction and the micrograph is slightly different this arises from the tilting of the specimen in the electron beam, which alters the perspective of the image. The thinness of the sample led to degradation by the electron beam and the quality of the image reduced to the extent that the diffraction pattern taken after the imaging process no longer showed the [421] zone, but one of higher index. As a consequence of this observation, only those lattice images obtained quickly, which do not show signs of degradation were considered in the analysis of the results.

The study of the upper elements revealed quite a different arrangement. As mentioned above, no diffraction patterns were obtainable from the samples, but lattice images were seen. Figure 4.13 shows a typical lattice image from an upper element. It was obtained from the end which is attached to the central element of the coccolith and clearly consists of several micro-crystals packed together with no apparent orientation. This is

Figure 4.10

Electron diffraction pattern obtained from the basal plate of the coccolith sample shown in Figure 4.11. This is [421] zone.

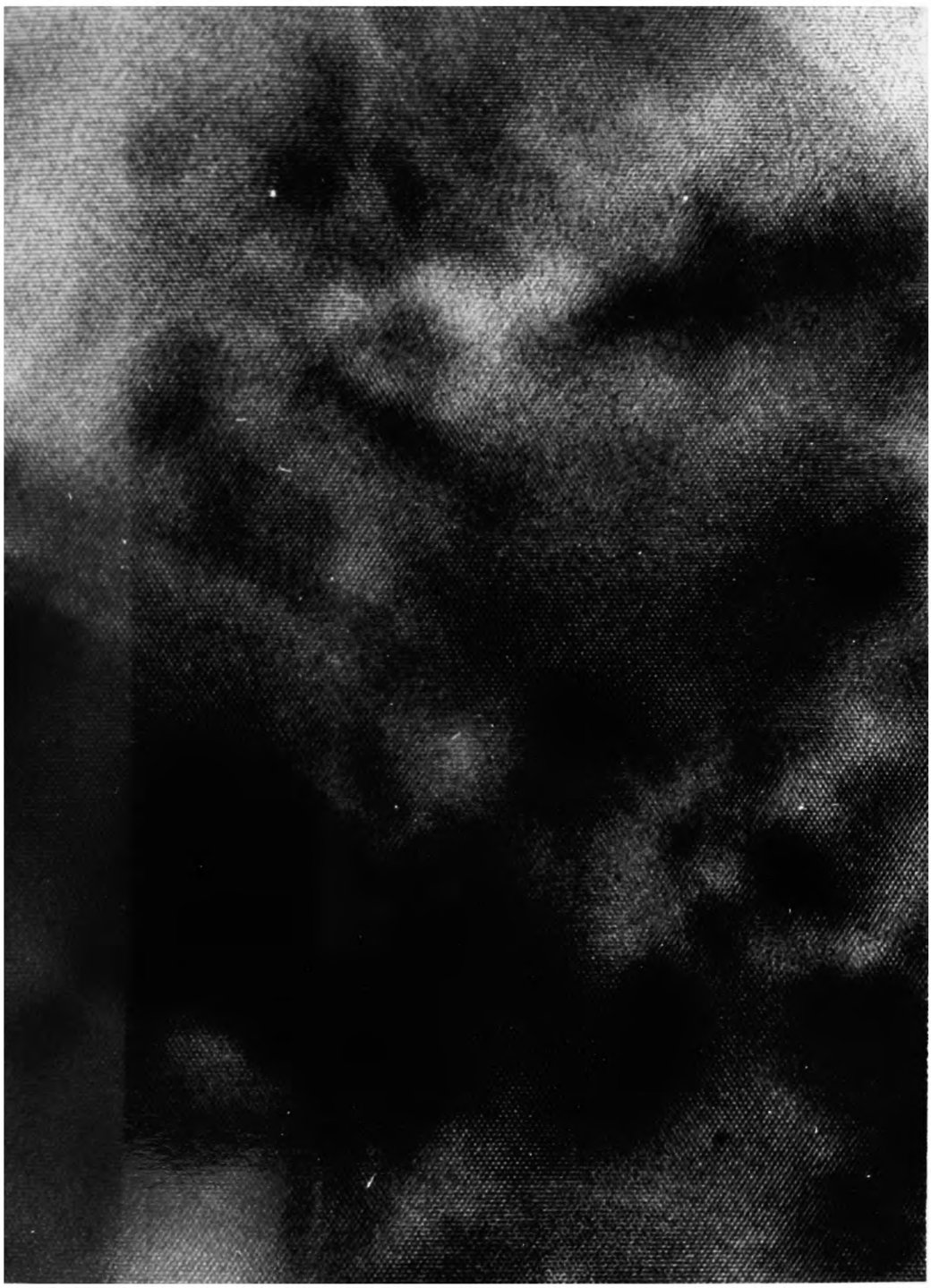

Figure 4.11

Ultra-high resolution electron micrograph from the basal plate of coccoliths from *E. huxleyi* (Lohmann) Hay and Mohler showing a two-dimensional lattice.

Magnification = x1 950 000

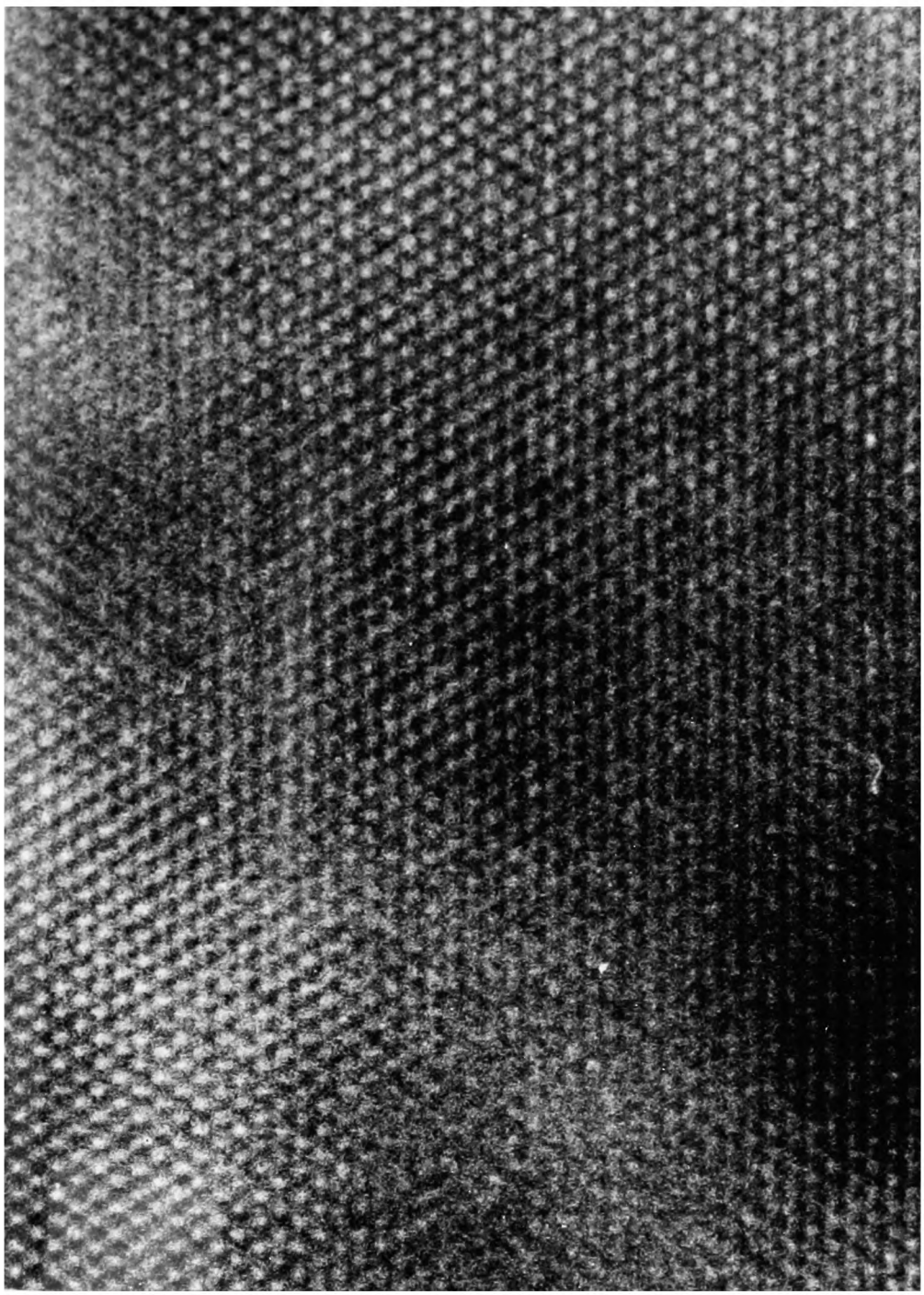

Figure 4.12a

HRTEM of the basal element of a coccolith from *E. huxleyi* (Lohmann) Hay and Mohler showing the two-dimensional lattice image.

Magnification = x9 090 000

Figure 4.12b

Theoretical lattice image for a [421] zone of calcite, showing the hexagonal pattern seen in the basal plate of the coccolith.

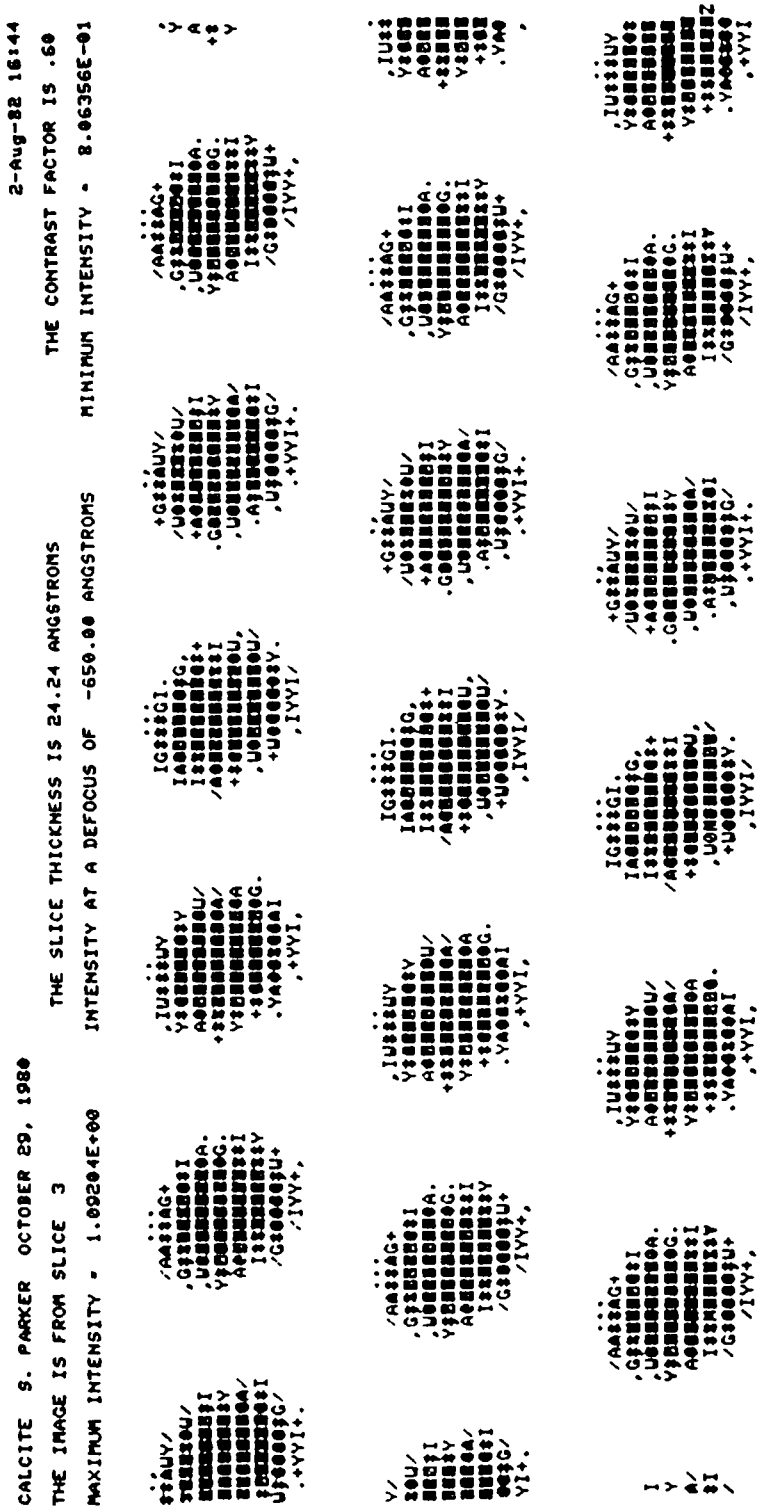

Figure 4.13

Lattice image of an upper element from coccoliths of *E. hurleyi* (Lohmann) Hay and Mohler. This is comprised of microcrystals packed together to form the overall morphology. Magnification = x1 700 000

in contrast to the results obtained by Watabe (10) and no simple explanation can be offered for this difference. The microcrystals are surrounded by quantities of amorphous material which could not be identified. One further observation of interest is the upper elements in the presence of lattice fringes arranged in a triangular pattern. This is illustrated in Figure 4.14. All fringes in the upper elements are one-dimensional due to the thicker nature of the sample and these triangular fringes have the appearance of emanating from a single point. The implications of this observation will be discussed below. Triangular fringes are also present in the T-shaped head of the upper elements. One such sample is illustrated in Figure 4.15. These heads have been one of the causes to doubt the single-crystal theory of Watabe, and the observation of microcrystals with these triangular fringes leads to a better understanding of the formation of the T-junctions.

Figure 4.16 illustrates the lattice image from an upper element at the point where it joins the central element. This shows an increase in the crystalline nature at the tip; although the central element itself was not imaged, this micrograph shows that its nature is likely to be more crystalline than the actual upper elements.

4.4 Discussion

4.4.1 The Ultrastructure of Coccoliths

The observation made at ultra-high resolution in this work give a picture of the ultrastructure of the coccoliths from *E. huxleyi* (Lohmann) Hay and Mohler that is in contrast to that reported by Watabe (11). The use of electron diffraction to elucidate ultrastructure is not a good technique if used alone,

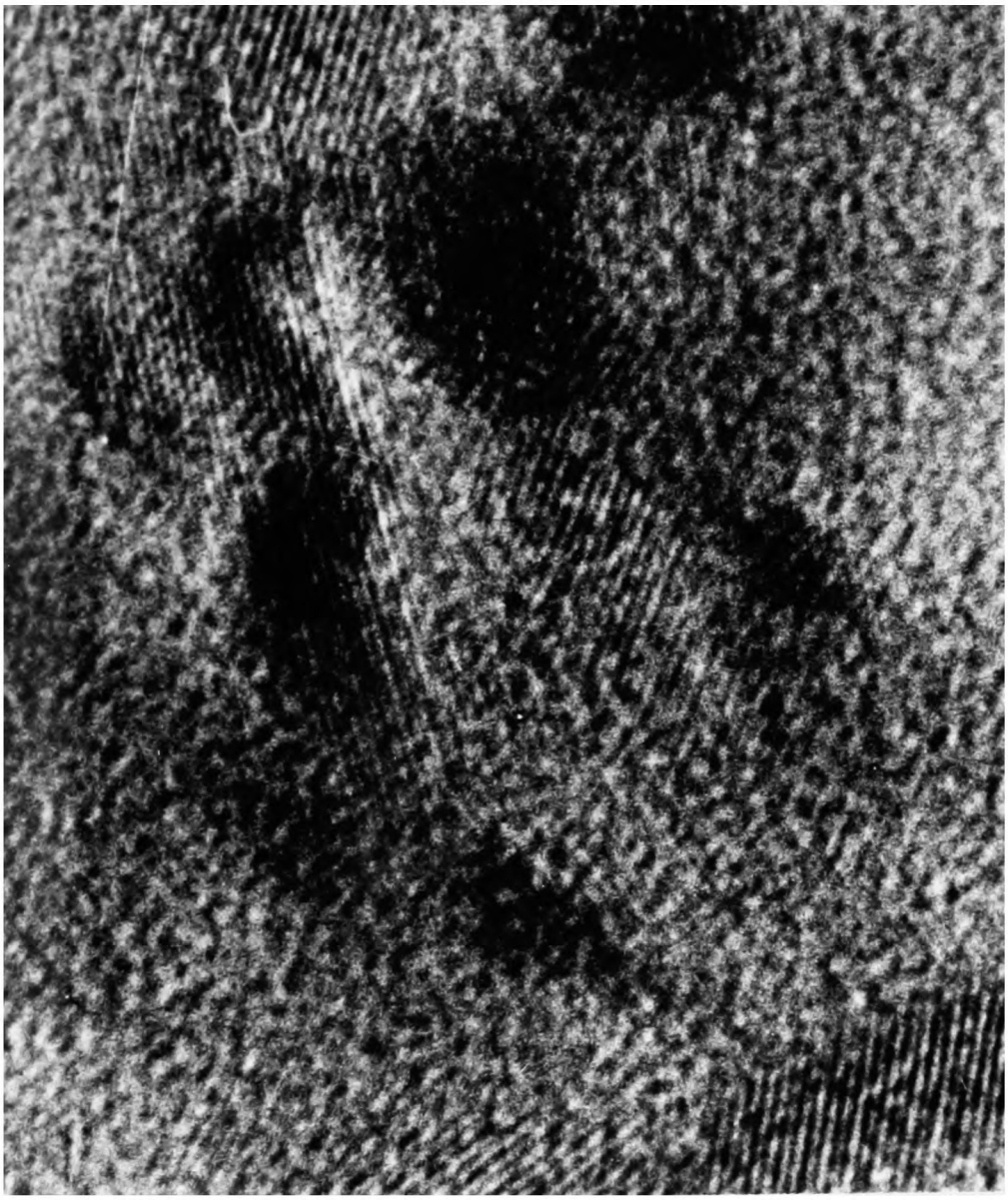

Figure 4.14

Enlargement of an area in FIgure 4.13 showing an area of triangular lattice fringes possibly forming a multiple nucleation centre in the upper element.

Magnification = x6 600 000

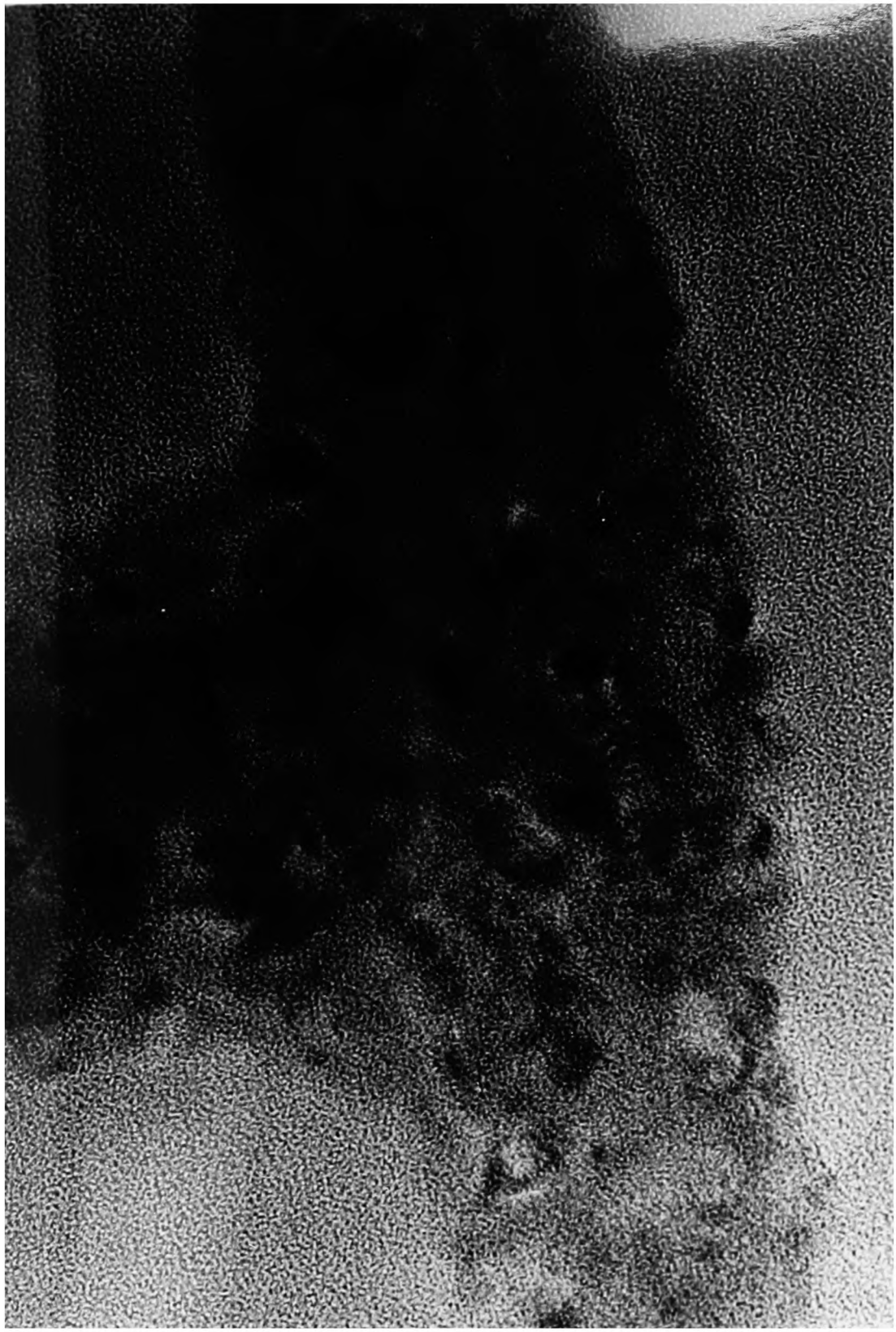

Figure 4.15

High resolution micrograph of a T-shaped head from an upper element of a coccolith. This again shows the packed micro-crystal structure and triangular nucleation points of the upper elements. Nucleation points are concentrated in the area of the junction. Magnification = x1 720 000

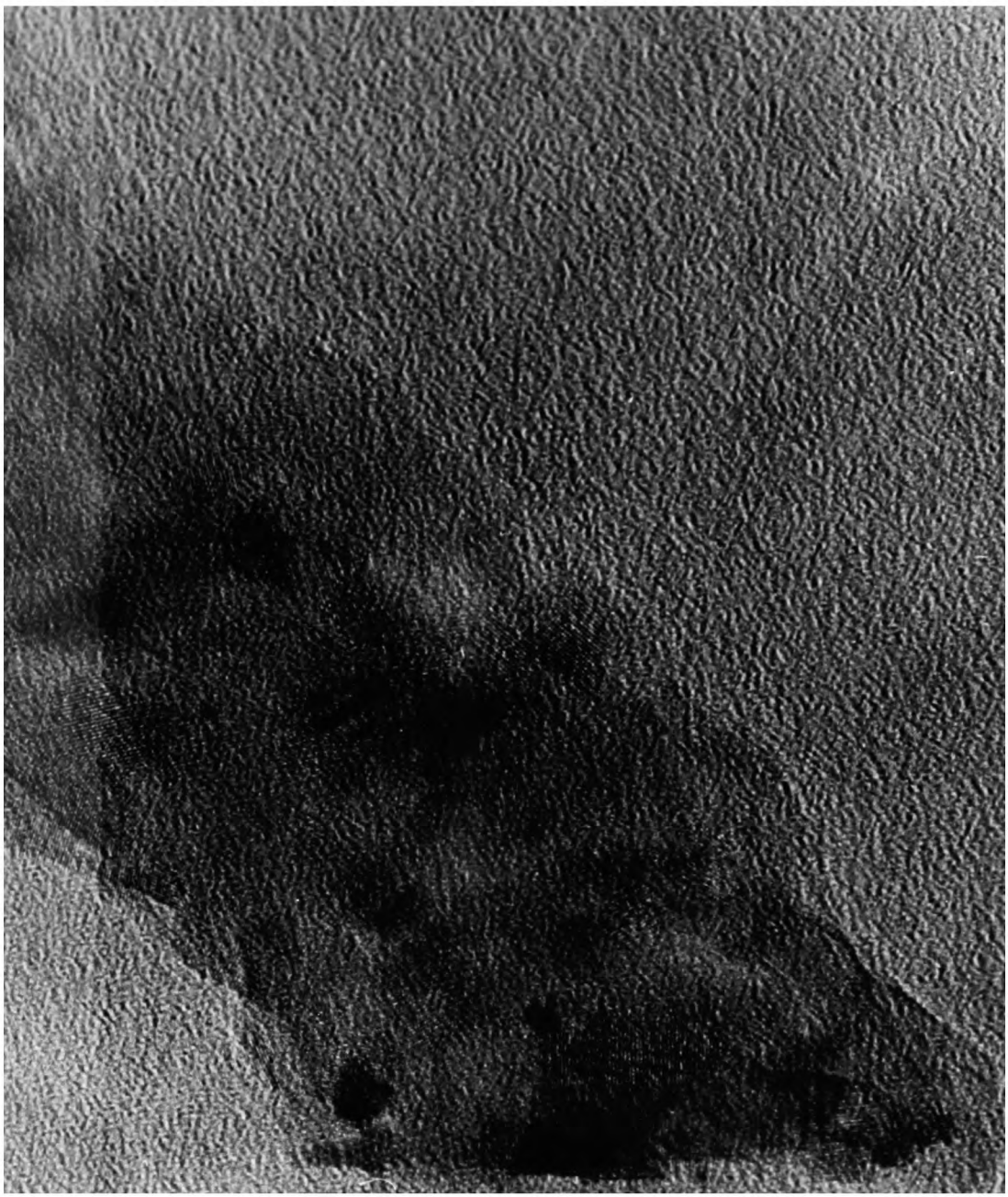

Figure 4.16

Lattice image of an upper element of a coccolith at the point where the upper element is joined to the central element, and showing an increase in crystallinity.

Magnification = x2 000 000

and Watabe refers to the observation of smears in the diffraction patterns obtained from the upper elements in his study. This would indicate that the structure was not, in fact, a single crystal as claimed, although the crystallites should be reasonably aligned to produce a pattern approaching that of a single crystal. Our observations indicate that the formation of a coccolith is not a simple process involving the formation of radially arranged single crystals, or even the formation of radially aligned components which, each being single crystalline, give the impression of radially aligned crystals (11). The crystal structure in the electron microscope shows unambiguously that the formation consists of two discrete mechanisms, producing an upper element comprised of crystallites with an apparent volume of some fifty unit cells, which is approaching the limit of stability of a crystal and a basal plate which, although occasional stacking faults may be observed, is a single crystal. At the resolution of this study, either composite crystallites, as defined above, or microdomains within the calcium carbonate structure would be apparent, leaving no doubt about the precise crystalline nature.

4.4.2 Observations on Coccolith Formation

The ultrastructural study was undertaken as part of a collaboration with Drs. Peter Westbroek and Elisabeth de Jong of the Department of Biochemistry, University of Leiden, Holland. The work carried out in Leiden concentrated on the cellular aspects of the algae and the coccolith vesicle in particular. Two observations were made by staining techniques; the first was the discovery of an entirely organic plate at the base of the coccolith vesicle which had the shape and segmented character of

the calcite basal element of the coccolith itself. This was visualised by palladium and carbon shadowing and an example of this plate is shown in Figure 4.17. The other observation was made after staining the cell for polysaccharide before the onset of coccolith formation, but after the coccolith vesicle had taken its shape. Sections through the vesicle revealed the presence of polysaccharide in the region of the vesicle where the upper elements later formed. This polysaccharide had the appearance of fronds hanging down from the top of the vesicle. The components of the vesicle before the onset of coccogenesis are depicted diagrammatically in Figure 4.18. The combination of observations made in Leiden and in Oxford led to the formulation of a new hypothesis for coccolith formation.

4.4.3 A New Hypothesis Concerning Coccolith Formation

Coccoliths are formed within a 'coccolith vesicle' within the cell of an alga. The process by which the nucleation and subsequent crystal growth occurs (as opposed to the biochemical pathways by which it occurs) can be sub-divided into two distinct stages. This process will be followed from its beginnings.

At the beginning of the calcification process, the coccolith vesicle is formed from the Golgi apparatus. The vesicle is joined to a complex system of tubes which form the Reticular Body. The entire arrangement is known as the CV-RB complex. We assume that the polysaccharide molecules are bound in some way to the membranes of the CV-RB complex prior to and at the earliest stages of calcification and extend into the lumen of the complex. This binding is probably through a non-covalent linkage to the positively charged proteins contained in the membrane. The polysaccharide is evenly distributed around both the RB and the CV before calcification commences and acts as an

the calcite basal element of the coccolith itself. This was visualised by palladium and carbon shadowing and an example of this plate is shown in Figure 4.17. The other observation was made after staining the cell for polysaccharide before the onset of coccolith formation, but after the coccolith vesicle had taken its shape. Sections through the vesicle revealed the presence of polysaccharide in the region of the vesicle where the upper elements later formed. This polysaccharide had the appearance of fronds hanging down from the top of the vesicle. The components of the vesicle before the onset of coccogenesis are depicted diagrammatically in Figure 4.18. The combination of observations made in Leiden and in Oxford led to the formulation of a new hypothesis for coccolith formation.

4.4.3 A New Hypothesis Concerning Coccolith Formation

Coccoliths are formed within a 'coccolith vesicle' within the cell of an alga. The process by which the nucleation and subsequent crystal growth occurs (as opposed to the biochemical pathways by which it occurs) can be sub-divided into two distinct stages. This process will be followed from its beginnings.

At the beginning of the calcification process, the coccolith vesicle is formed from the Golgi apparatus. The vesicle is joined to a complex system of tubes which form the Reticular Body. The entire arrangement is known as the CV-RB complex. We assume that the polysaccharide molecules are bound in some way to the membranes of the CV-RB complex prior to and at the earliest stages of calcification and extend into the lumen of the complex. This binding is probably through a non-covalent linkage to the positively charged proteins contained in the membrane. The polysaccharide is evenly distributed around both the RB and the CV before calcification commences and acts as an

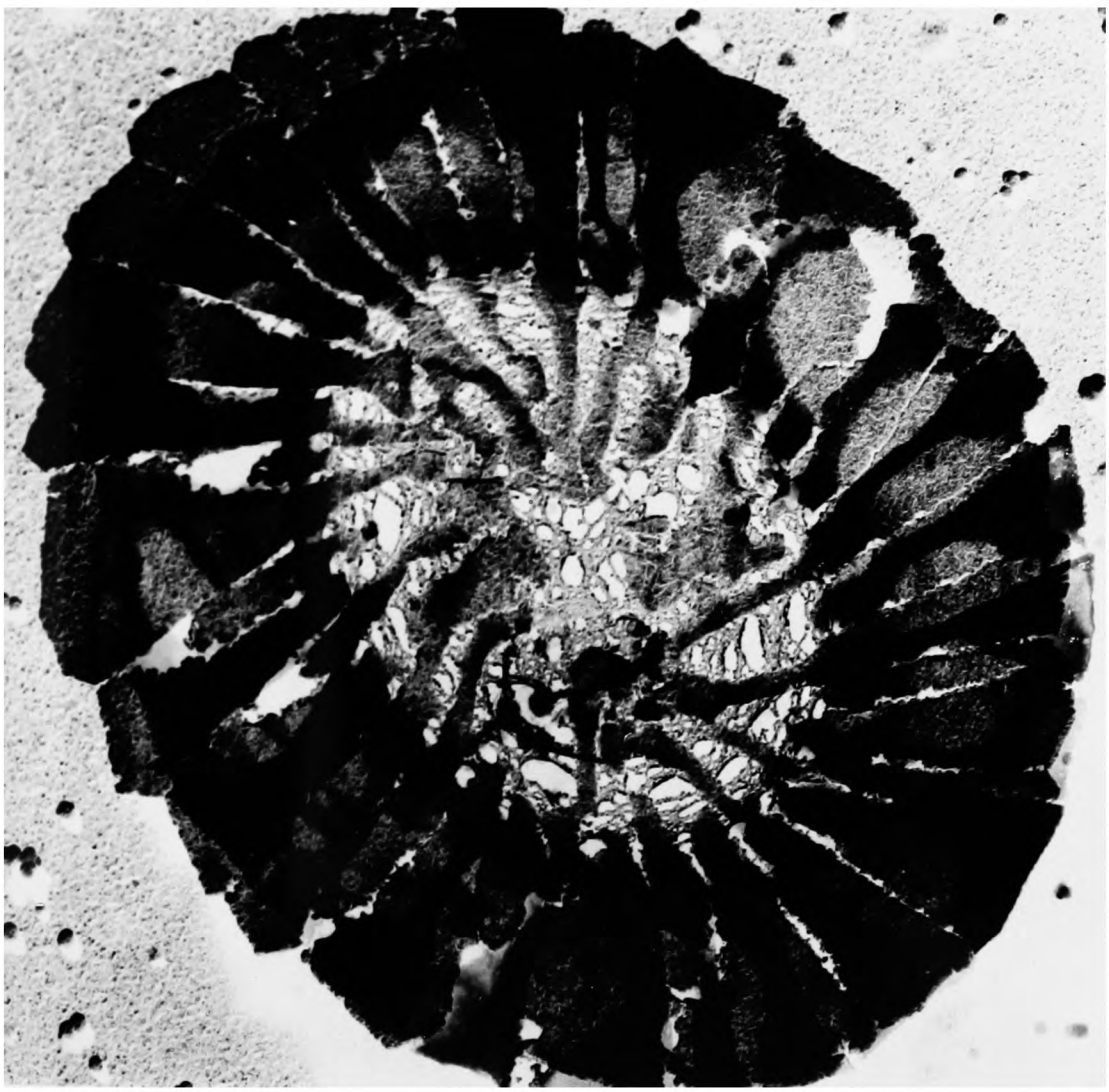

Figure 4.17

TEM of partially-decalcified coccolith, showing the organic base-plate beneath the lower elements. The sample is Pd/C shadowed. Magnification = x 55 000

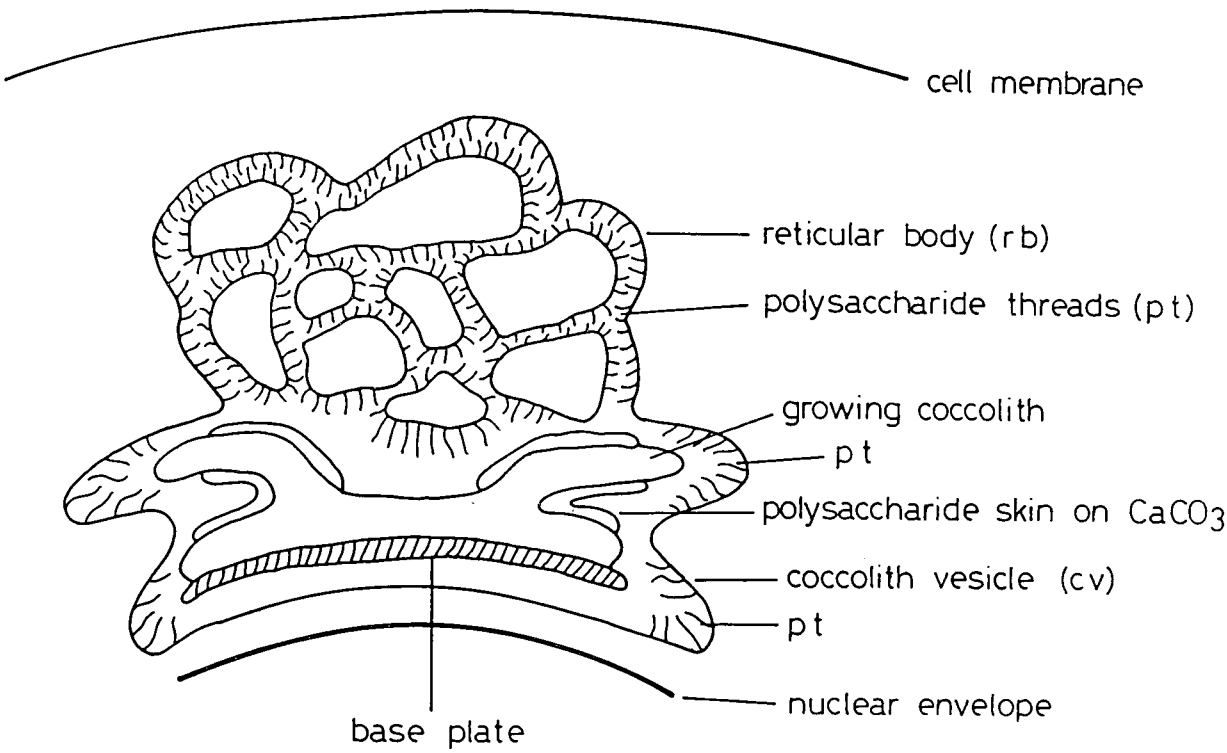

Figure 4.18

Cross section through an intracellular, growing coccolith showing the relationship between the reticular body and the coccolith vesicle

inhibitor of calcite formation, even if the lumen contains a solution which is supersaturated with respect to calcium carbonate (Figure 4.19a). When the shape of the CV is altered by the pull exerted by the cytoskeleton to resemble that of the final coccolith, a space is created which contains no polysaccharide and a calcium carbonate crystal may nucleate. This nucleation may be induced, controlled or accelerated by the same anchored polysaccharide, providing that a conformational change has occured during the dilation of the vesicle. The area of the CV without attached polysaccharide develops the organic base plate and the first crystals develop around the rim. Growth then extends over this base plate towards the centre and also, as the plate grows, radially outwards. The plate controls the crystal growth in an epitaxial manner, resulting in a very thin layer of single crystals each forming a segment of the plate.

Further growth of the coccolith is controlled by the pulling of the cytoskeleton on the CV which generates a dilation of the vesicle in certain well defined directions; the first being the radial direction described above, and the second being in a disto-radial direction and leads to the formation of the upper elements. Crystal growth here is less well controlled because there is no fixed template, but the polysaccharide bound to the vesicle in this region causes the formation of microcrystals which become bound together to form the final morphology of the elements. When growth is complete in the upper elements, the polysaccharide binds around the calcium carbonate and inhibits further growth (possibly becoming detached from the CV as it does so).

The formation and function of the reticular body is not well-understood, but it is believed to arise from parts of the

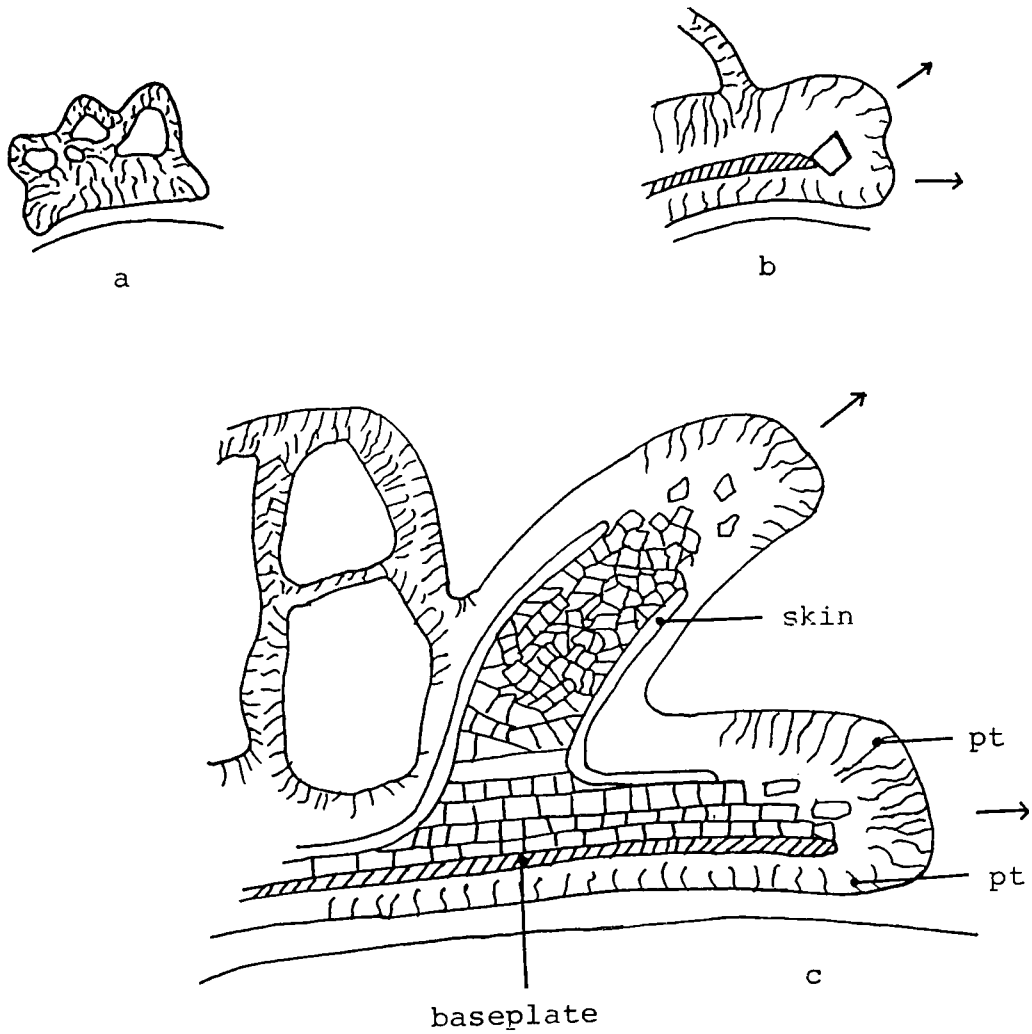

Figure 4.19

A new model for coccolith synthesis based upon the observations in Oxford and Leiden.

Golgi apparatus which are pinched off on the opposite side to the CV are added to the RB. The reticular body provides the CV with membranous material, polysaccharide and probably acts as a source of extra calcium ions.

The observations made in this work, together with the hypothesis described above is of significance to the general understanding of biomineralisation. The formation of coccoliths within a single cellular alga has been seen to occur within a single vesicle by two discrete and quite different mechanisms, confirming a hypothesis of Lowenstam (personal communication). Such an event has not hitherto been observed in biomineralising systems and gives a good illustration of the control exerted on crystal formation by the organic component.

4.5 References

1. Lowenstam, H.A. *Science* 211, 1126-1131, (1981)
2. de Jong, E.W., van der Wal, P., Borman, A.H., de Vrind, J.P.M., van Emberg, P., Westbroek, P. and Rosch, L. in *"Biomineralisation and Biological Metal Accumulation"* eds. P. Westbroek and E.W. de Jong, 291-301, (1983) pub. D. Reidel, Holland.
3. Sorby, H.C. *Ann. Mag. Nat. Hist.* 8, 193-200, (1861)
4. Huxley, T.H. Quart, J. *Micr. Sci.* 8, 203-212, (1868)
5. Klavaness, D. and Paasche, E. in *"Biochemistry and Physiology of Protozoa"* 191-213, (1979)
6. Black, M. *Endeavour* 25, 131-137, (1965)
7. Okada, H. and McIntire, A. *Micropaleontology* 23, 1-55, (1977)
8. Braarud, T. and Nordli, E. *Nature, Lond.* 170, 361-362, (1952)
9. Braarud, T., Gaarder, K.R., Markali, J. and Nordli, E. *Nytt Mag. Bot.* 1, 129-134, (1953)
10. Wilbur, K.M. and Watabe, N. *Ann. N.Y. Acad. Sci.* 109, 82-112 (1963)
11. Watabe, N. *Calc. Tiss. Res.* 1, 114-121, (1967)
12. Outka, D.E. and Williams, D.C. *J. Protozool.* 18, 285-297, (1971)
13. Isenberg, H.D., Lavine, L.S., Mandwell, C. and Weissfellner, H. *Nature, Lond.* 206, 1151-1152, (1965)
14. Westbroek, P., de Jong, E.W., Dam, W. and Bosch, L. *Calc. Tiss. Res.* 12, 227-238, (1973)
15. de Jong, E.W., Bosch, L. and Westbroek, P. *Eur. J. Biochem.* 70, 611-621, (1976)
16. Fichtinger-Schepman, A.M.J. *PhD Thesis*, State University of Leiden, Holland (1980)

17. Fichtinger-Schepman, A.M.J., Kamerling, J.P., Vliegenthart, J.F.G., de Jong, E.W., Bosch, L. and Westbroek, P. *Carbohydr. Res.* 69, 181-189, (1979)

18. Fichtinger-Schepman, A.M.J., Kamerling, J.P., Versluis, C. and Vliegenthart, J.F.G. *Carbohydr. Res.* 86, 215-225, (1980)

19. Fichtinger-Schepman, A.M.J., Kamerling, J.P., Versluis, C. and Vliegenthart, J.F.G. *Carbohydr. Res.* 93, 105-123, (1981)

20. Borman, A.H., de Jong, E.W., Huizinga, M., Kok, D.J., Westbroek, P. and Bosch, L. *Eur. J. Biochem.* 129, 179-183, (1982)

21. Watabe, N. *J. Ultrastruc. Res.* 12, 351-370, (1965)

22. Wheeler, A.P., George, J.W. and Evans, C.A. *Science (Wash. D.C.)* 212, 1397-1398, (1981)

23. de Jong, E.W., Borman, A.H., de Vrind, J.P.M., Kok, D., Parker, S.B. and Westbroek, P. *Proc. R. Soc. Lond. B* (1983) in press

24. Crenshaw, M.A. Unpublished results

25. Kamptner, E. *Arch. Protistenkde* 101, 171-201, (1956)

26. Klaveness, D. *Protistologica* 8, 335-346, (1972)

27. de Jong, E.W., van Rens, L., Westbroek, P. and Bosch, L. *Eur. J. Biochem.* 99, 559-567, (1979) ·

28. Steemann Nielsen, E. *Physiol. Plant* 19, 232-240, (1966)

29. de Jong, E.W., Dam, W., Westbroek, P. and Crenshaw, M.A. in *"The Mechanisms of Mineralisation in the Invertebrates and Plants"*. N. Watabe and K.M. Wilbur, eds. pub Univ. of South Carolina Press. 135-153, (1976)

Chapter 5

Preliminary Investigation of Organic Components of Biominerals

5.1 Introduction

The organic matrix of biominerals has been widely studied over many years. Systems studied include brachiopods (1), gastropods (2) and fish otoliths (3). All studies have traditionally used the following general procedure: dissolution of the mineral; separate proteinaceous material from the small ions; carry out amino acid analysis and, finally, carry out calcium carbonate crystallisation experiments. In addition, some workers[1] used gel electrophoresis to determine the purity of the protein sample. Recent work in both biomineralisation and also more general biochemistry has shown that the procedure is simplistic and that the final experiments have little relevance to the *in vivo* situation. The assumption that the procedure leaves a single protein component, even when gel electrophoresis has been carried out, is liable to error. This is because the staining method for visualising the proteins routinely used is Coomassie Brilliant Blue stain (4) which acts by binding to NH_3^+ groups and non-polar regions in the protein. The mineralisation proteins are known to be very acidic and the stain is very insensitive for them (5). As a consequence it is common to see no bands stained at all, and very rarely more than one component in the gel. This means that the amino acid analysis that has been carried out has not been performed on amino acids from single proteins, but from many polypeptide chains extracted from the minerals. Thus the only reasonable conclusion that can be drawn from the results is that the proteins involved in the mineralisation

process are highly acidic; no conclusions on the composition, far less the amino acid sequence can be drawn. Recent work by Weiner (6-9) has shown that each area of a gastropod shell contains at least twenty and possibly as many as thirty polypeptides. Thus the recent techniques of High Performance Liquid Chromatography (HPLC) or Fast Protein Liquid Chromatography (FPLC) need to be used to separate the fractions, the former being the more successful since it is not limited to aqueous solvents.

The problem with matrix-mediated crystallisation experimen became apparent with the discovery that the organic matrix layer was, in fact a sandwich of soluble and insoluble components (10). This is shown schematically in Figure 5.1. The centre is a chitinous layer which is coated with an insoluble matrix, which Weiner and Traub (11) found to be laid down in an antiparallel β-sheet. This layer is insoluble due to extensive cross-linking and a fairly high aromatic content. The soluble matrix is laid down over this layer and is also assumed to follow a β-sheet configuration (11). Thus, as shown diagrammatically in Figure 5.2, in order to bind to the insoluble layer and show an ordered array of carboxylic acid groups to the calcium ions in solution, t soluble matrix must have acidic groups on one side and hydrophobic or at least non-polar groups on the other. Solubilisation of this layer inevitably brings about a gross conformational change which leaves the acid groups facing the solvent, but loosely tucks the non-polar groups away into the body of the structure. Any experiment carried out with this structure reveals chemical properties relating to the solubilised complex, but nothing at all about the behaviour of the matrix when it is immobilised against the insoluble matrix *in vivo*.

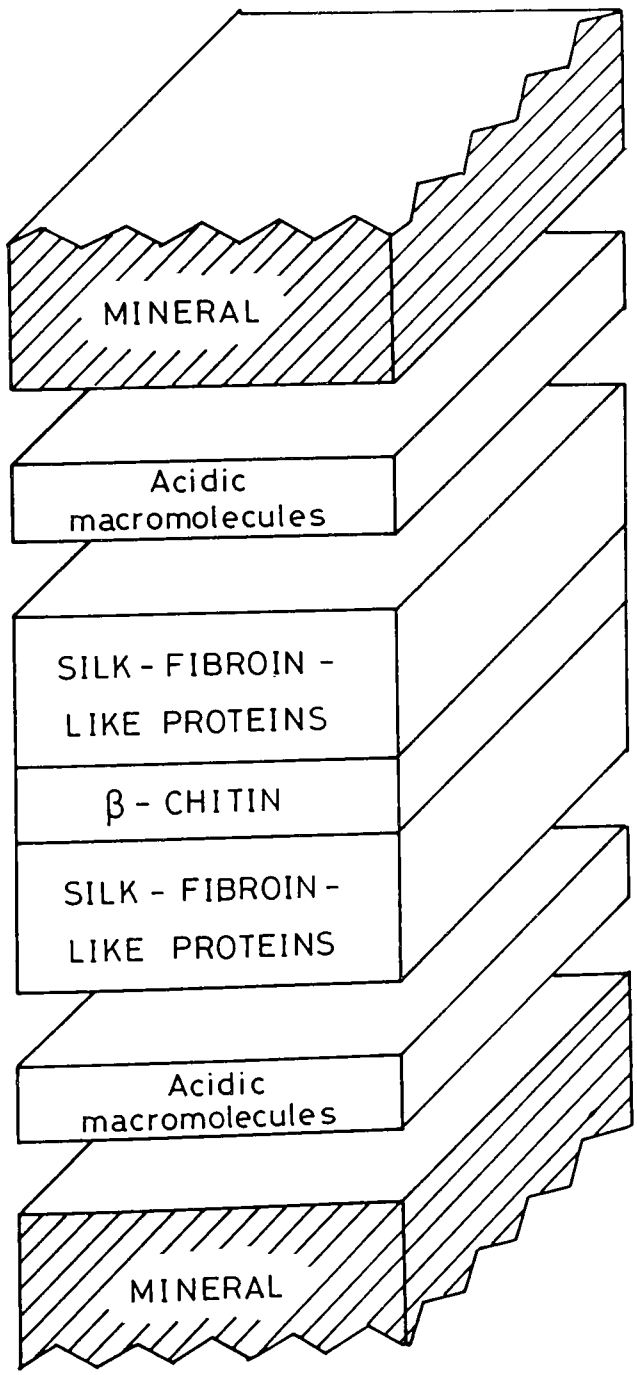

Figure 5.1

Representation of the layers which make up the organic component of a biomineral. Reproduced from (10).

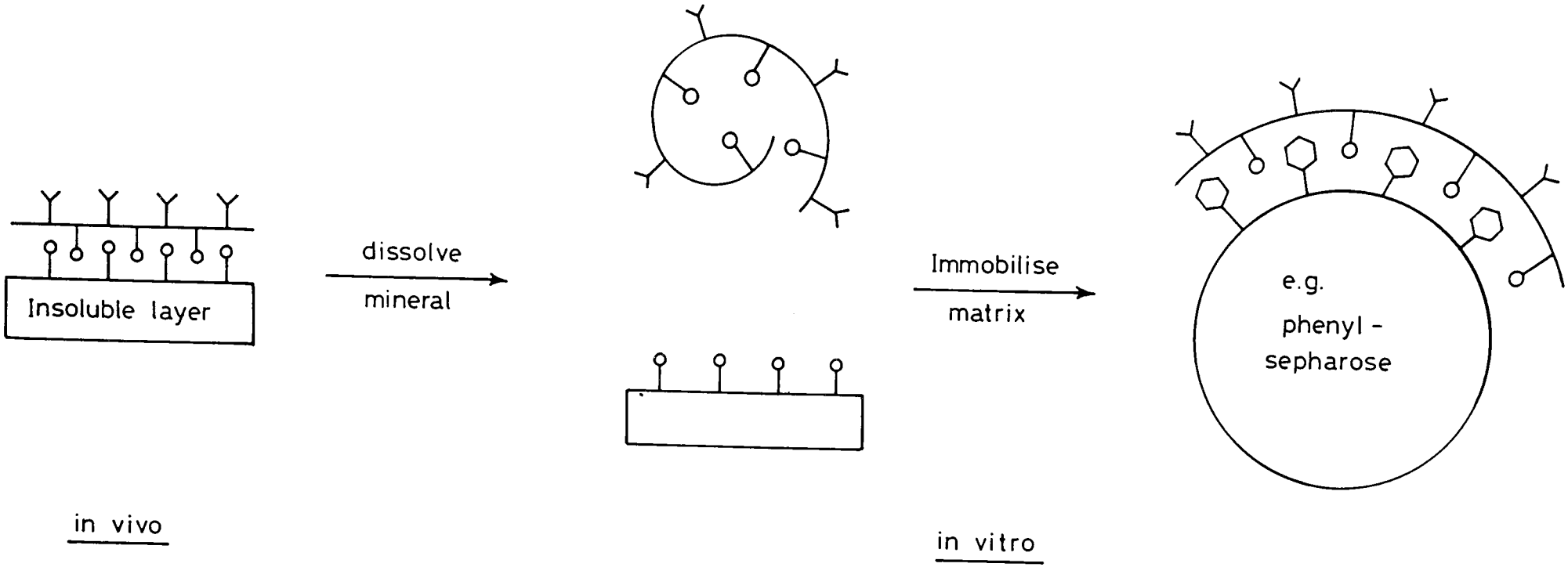

Figure 5.2

Diagram to illustrate the conformational changes arising from extracting the soluble acidic component from a biomineral

It was not possible in my work, as it had been hoped, to carry out the extensive experimental programme which is necessary to make definite conclusions about the exact relationship of the organic matrix to the inorganic matrix, or the way in which the protein composition and structure is controlled (genetically) to obtain the required polymorph and growth pattern. Experiments on the extraction and partial purification of these proteins were carried out, however, and an experiment to observe the effect of the soluble matrix on calcium carbonate crystallisation in a manner approximately to the *in vivo* condition was designed. The soluble matrices obtained were also studied by ^{1}H-NMR in order to attempt to observe common features of the proteins and also to attempt to ellucidate any structure which might be present in the solution. This is essentially a 'fingerprinting' technique, but titrations on the matrix proteins could lead to useful structural information.

5.2 Extraction of Proteins from Biominerals

The techniques described below were learnt and first used in the Nuffield Department of Clinical Biochemistry, Radcliffe Infirmary, Oxford under the supervision of Dr. M. Peter Esnouf. Samples of *Atrina vexillum* were kindly provided from Saudi Arabia by Mrs Doreen Sharabati; those of *Mytillus edulis* from the Marine Research Establishment, Aberdeen and samples of otoliths from various species of fish from Dr. Reg Blacker and colleagues, Fisheries Research Laboratory, Ministry of Agriculture, Fisheries and Food, Lowestoft, Suffolk. A general pattern of isolation and purification of the proteins was followed for each biomineral. This involved crushing the mineral into pieces and then pulverising into a fine powder. The powdering was carried out at liquid nitrogen temperature in an electromagnetic bone crusher, kindly

lent by Dr. R. Triffitt, Nuffield Orthopaedic Hospital, Oxford. The calcium carbonate powder was then suspended in either 10% Ethylenediamine tetra-acetic acid (EDTA), pH = 8 - 8.5, or 10% Formic Acid in order to dissolve away the mineral. If the former procedure was used, the powder was placed in a dialysi sack with a small volume of EDTA solution and then placed into a larger beaker containing the same solution. The advantage of this method is that the calcium is complexed by the EDTA and removed from the system; however, the powder tends to mass at the bottom of the sack, making it a very slow process. The acid dissolution is much faster but, because of the liberation of CO_2 by the reaction, it is necessary to add a small quantity of octan-2-ol to the reaction vessel to prevent frothing. Thus the alcohol must be removed in a later step. There is also a problem of the volume obtained from the reaction, since the protein will be dissolved in the acid,along with free calcium. I is then necessary to reduce the volume by a method which will preserve the protein and preferably without gross changes in pH. It was not possible to concentrate the protein by precipitating with Ammonium Sulphate ($(NH_4)_2SO_4$) since the free calcium precipitates as $CaSO_4$. The final method selected was to use the formic acid dissolution, followed by extensive dialysis against distilled water and then precipitating out the protein with 60% and then 80% $(NH_4)_2SO_4$. In the case of the protein from *A. vexilum*, this led to two different components, one highly coloured and one only slightly coloured. The concentrated protein was then lyophilised or dialysed against 50 mM Tris(hydroxymethyl)-methylamine (Tris) buffer, pH = 8.20 in preparation for ion-exchange chromatography.

Ion-exchange chromatography was carried out by a slightly modified form of the method of Weiner (16). Either Whatman DE 52 gel or DEAE Sephadex A50 gel (Pharmacia AC) was loaded into a Pharmacia column adjusted to have a volume of about 50 cm^3. The procedure was attempted both by stepping the quantity of NaCl passing through the column and by running a gradient between 0 and 1.0 M NaCl. It was found, and later confirmed by Weiner (personal communication),that the separation was better by a stepwise method. The separation was carried out using a LKB Ultrorac 7000 fraction collector and the solution was monitored at 280 nm (206 nm, which is more sensitive to proteins, could not be used due to the Tris absorbance in the region) with an LKB Uvicord S uv monitor. Fractions which showed absorption at 280 nm were checked at 280, 260, and 230 nm on a Pye Unican SP8-200 uv spectrophotometer, pooled, dialysed against distilled water and lyophilised.

5.3. Analytical Methods

5.3.1 Polyacrylamide Gel Electrophoresis

Polyacrylamide gel electrophoresis (PAGE) was used to determine the purity of the extracted protein samples. The system used was that of Watterson et al (12) using slab gels and a discontinuous system. The gel contained 10% (w/v) acrylamide in Tris buffer, pH = 8.8 in the lower phase and pH = 6.8 in the upper, or stacking,gel. This stacking gel was prepared from 2.7% acrylamide and was used to ensure that all samples entered the main gel at the solvent front. Samples were prepared for PAGE by being dissolved in 10 mM Tris containing 10% Sucrose to make the solution dense and 0.002% Bromophenol Blue to act as a tracking dye. If reducing conditions were required, 0.1%

Sodium Dodecyl Sulphate (Lauryl Sulphate, SDS) was added to both gels and SDS and also 2-mercapoethanol were added to the sample solution. In this case the samples were boiled for ten minutes in a water bath to ensure complete reduction. Electrophoresis was carried out using a constant voltage of 150 V applied by a Shandon Southern SAE 2761 power supply until the tracking dye was within 1 cm of the bottom of the gel. The gel was then stained by a silver-staining method as described below.

5.3.2 Silver Staining for Visualising Proteins

Silver staining gels for proteins was first described by Switzer et al (13) in 1979. This method was complex, but could detect protein concentrations of two orders of magnitude less than the standard Coomassie brilliant blue stain. The original method has been modified several times in order to further increase sensitivity and also to reduce the quantity of silver used (14-16). The method generally used in this work was that of Wray et al (15) which was considerably simpler than the original technique and is given below.

Step 1 Soak the gel in 50% methanol for at least 1 hour

Step 2 Prepare staining solution (C) as follows:

Solution A: Dissolve 0.8 g $AgNO_3$ in 4 mls distilled water

Solution B: Mix 21 mls of 0.=36% NaOH and 1.4 mls of 14.8 M NH_4OH.

Solution C: Add solution A dropwise into solution B with constant stirring and then dilute to 100 mls. This must be used within 5 minutes.

Step 3 Stain gel in solution C for 15 minutes with constant gentle agitation

Step 4 Wash the gel in deionised water with gentle agitation for 5 minutes

Step 5 Prepare the developer, solution D as follows:

Solution D: Mix 2.5 ml of 1% Citric Acid and 0.25 ml of 38% formaldehyde. Dilute to 500 ml. This solution must be fresh.

Step 6 Soak gel in solution D until bands appear (normally in less than 10 minutes and seldom longer than 15 minutes).

Step 7 Wash gel in water and place in 50% methanol or 45% methanol/10% ethanoic acid to stop development.

The action of the silver stain is believed to arise from binding to the carboxyl groups in the proteins when the procedure is carried out in an acid environment and to the amino groups in an alkaline environment; complexation also occurs with cysteine and methionine sulphur (15). The mineralisation proteins give good results with either procedure, but the alkaline system, as detailed above is commonly used as being applicable to all proteins.

5.3.3 Iso-Electric Focussing

Iso-electric focussing (17) was also used as an analytical method for the protein samples, although a restricted pH range was available (pH 3.5 - 9.5) since commercially prepared LKB Ampholine 'Pagplates' were used. The samples were applied to the gels,along with a sample of lysed blood cells which acted as a standard, and the proteins were allowed to focus for about two hours on an LKB Multiphor flat-bed electrofocusing apparatus which was cooled by a Grant circulating water bath. Power was applied at 400 W by an LKB 2103 power supply, which delivered a potential of 2 kV to the gel. The proteins were focused to a very thin line and consequently 0.5% Coomassie Brilliant Blue R-250 could be used for staining after the ampholines had been

removed in 3.5% sulphosalicyclic acid. 11.5% trichloroacetic acid (TCA) was also used to precipitate the proteins into place in the gel.

5.3.4 Fast Protein Liquid Chromatography

This is a technique developed by Pharmacia AC similar in style to High Performance Liquid Chromotography (HPLC). The equipment used belonged to Dr. H.A.O. Hill, Inorganic Chemistry Laboratory, University of Oxford. This technique was used following the report of Weiner (7) that HPLC separated protein fractions from *Nautilus repartis* which had been thought homogeneous by ion-exchange chromatography into many different fractions, some of which were, in fact, homogeneous. Proteins from gastropod shells were found to cause problems due to the coloured cross-linking agents which penetrated the gel beads in the column and bound irreversibly. Thus samples from otoliths were studied by this method.

Amino-acid analysis was not carried out since it was reasoned that analyses of proteins which were not homogeneous (7) would be ambiguous and could give no information about the epitaxial properties of the matrix.

5.4 Observations On the Organic Matrix

5.4.1 Isolation of the Proteins

Proteins from gastropods which were extracted from the shells (*A. vexillum* and *M. edulis*) were found to be coloured. This was due to quinone cross-linkage between the polypeptide chains, a phenomenon which is common in structural proteins (18). The colour was found to be tightly bound to one component and less concentrated in the other, of the two separated by an

Figure 5.3

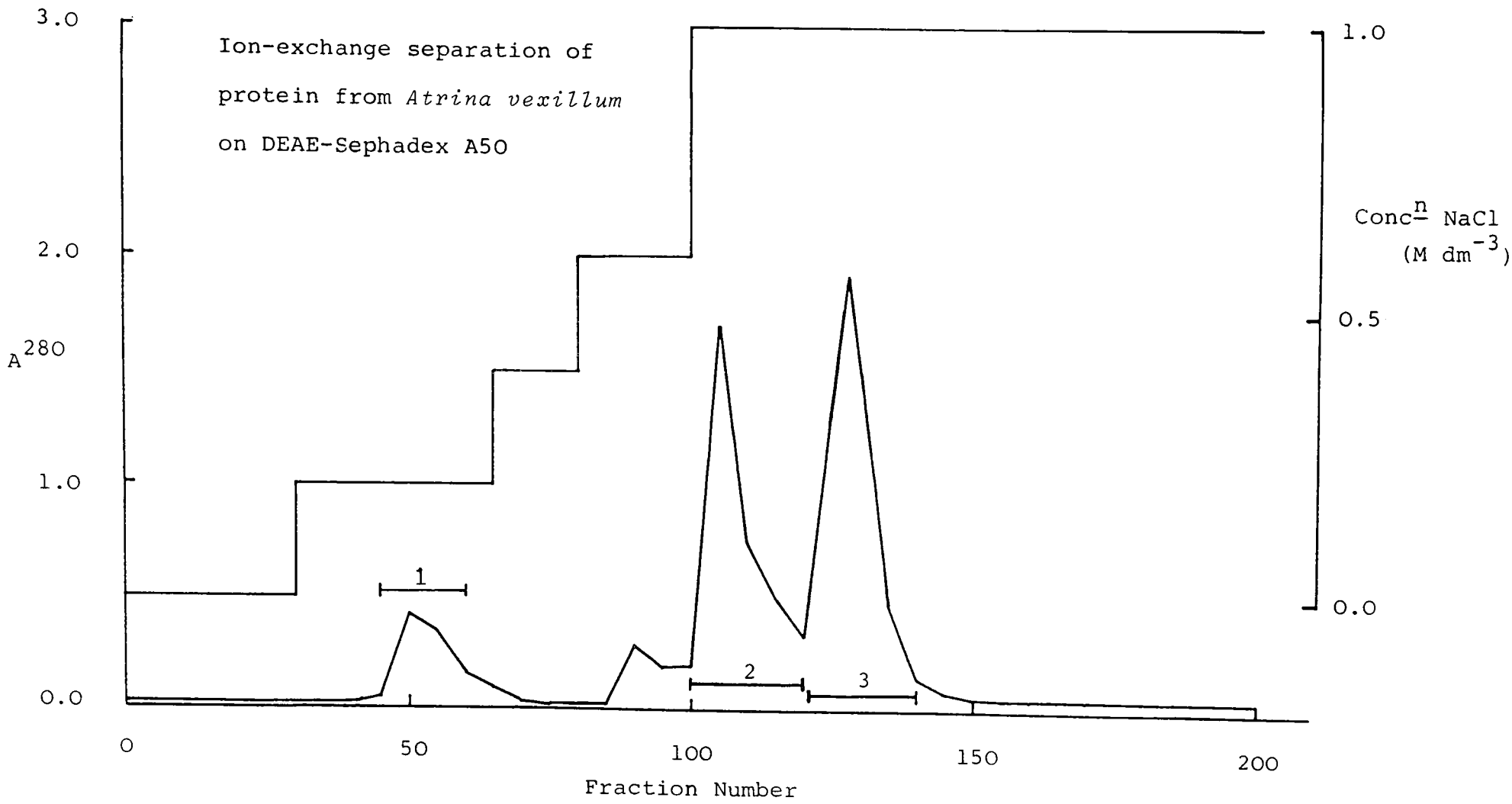
Ion-exchange separation of
protein from *Atrina vexillum*
on DEAE-Sephadex A50
3.0
2.0
1.0
0.0
A^{280}
1.0
0.5
0.0
Conc^{n} NaCl
(M dm^{-3})
1
2
3
0
50
100
150
200
Fraction Number

Figure 5.4

Gel filtration of peak 2 in the ion exchange separation on Sephacryl S-200

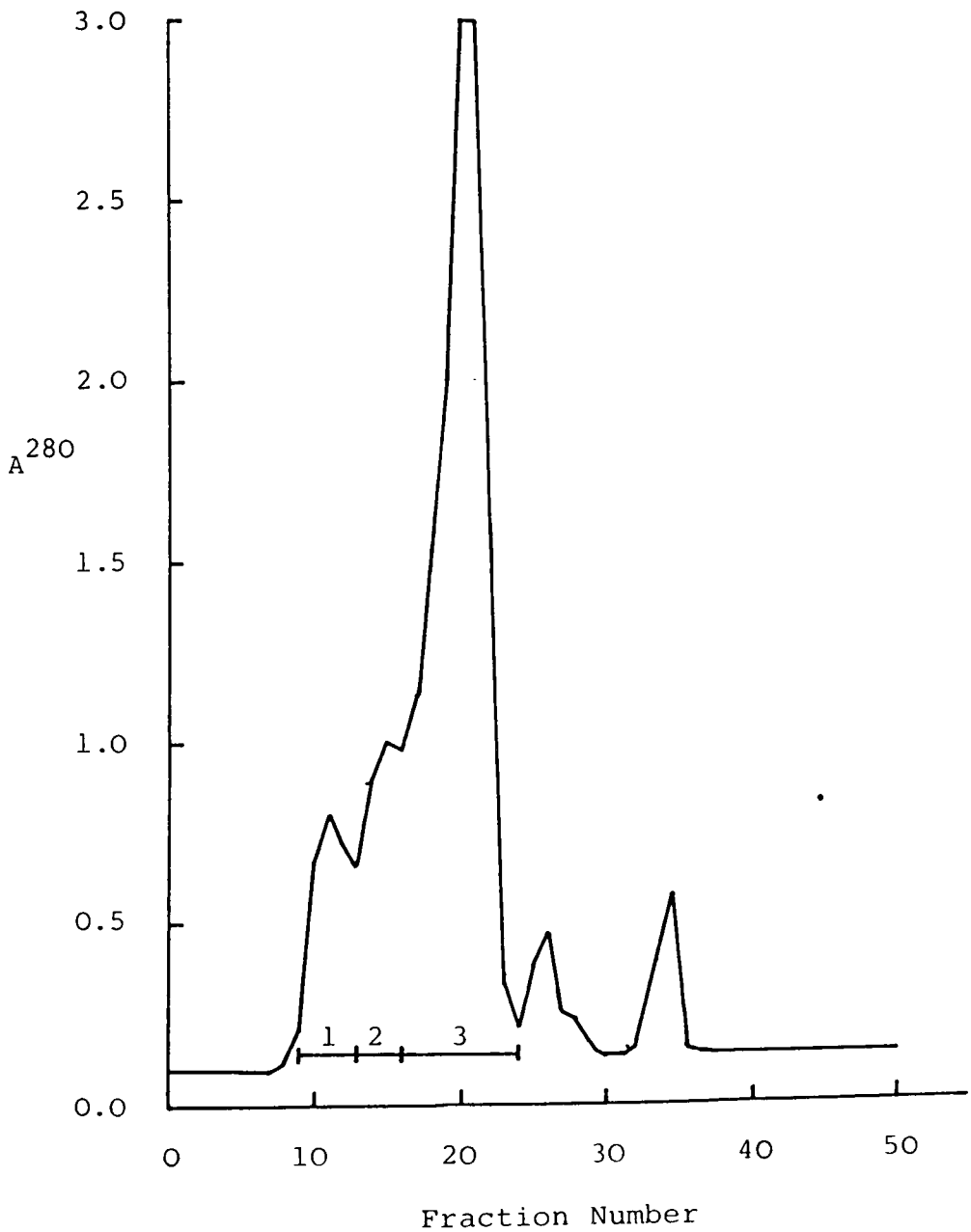

Figure 5.5

FPLC separation of peak 3 in the gel filtration separation using a weak cationic support

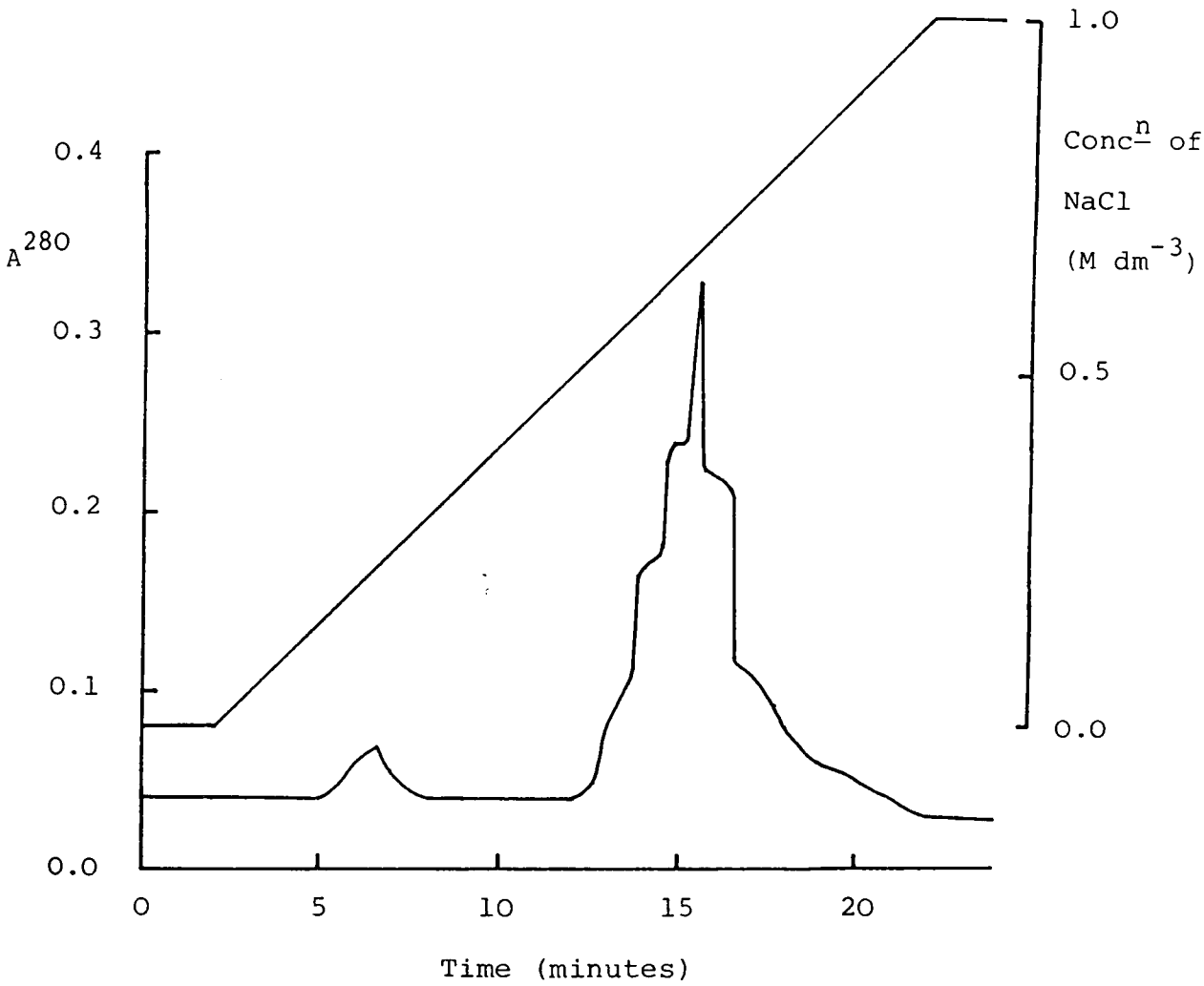

ammonium sulphate cut. The extracted organic matrix was partially purified by ion-exchange chromatography, as described above. Figure 5.3 shows the result of the elution with step-wise increments of NaCl solution. Three components could be observed by this procedure which were collected for further study. The second peak was further purified by gel filtration on Sephacryl S-200 (Pharmacia AC), the result being shown in Figure 5.4. This reveals that the ion-exchange-isolated peak contains one major component and five or more other proteins as separated by molecular mass. It is interesting to note that this major component can be further separated by FPLC into several components (Figure 5.5), although the separation is not good enough to isolate any homogeneous proteins.

Similar results were obtained for *M. edulis* and the brachipod *Terebratulina sp.* although neither were isolated by such a rigorous procedure. The separation of components from *Terebratulina* is of interest in comparison with the results of Jope (19) who found only two protein fractions in the shell by SDS electrophoresis; this could be accounted for by the use of Coomassie blue stain, as discussed above. An estimation of the molecular weight of the major component running just behind the solvent front of a Sephadex G-75 gel would be between 50 000 and 55 000 daltons. This is in good agreement with the values for the two components isolated by Jope of 53 000 and 49 000 and it is possible that the resolution of the gel was not sufficient to separate the two bands.

Figure 5.7 illustrates the separation of components from the organic matrix of Plaice otoliths. This protein is not coloured but still consists of many components, possibly as

Figure 5.6

Gel filtration of protein extracted from the brachiopod *Terebratulina* on Sephadex G-75

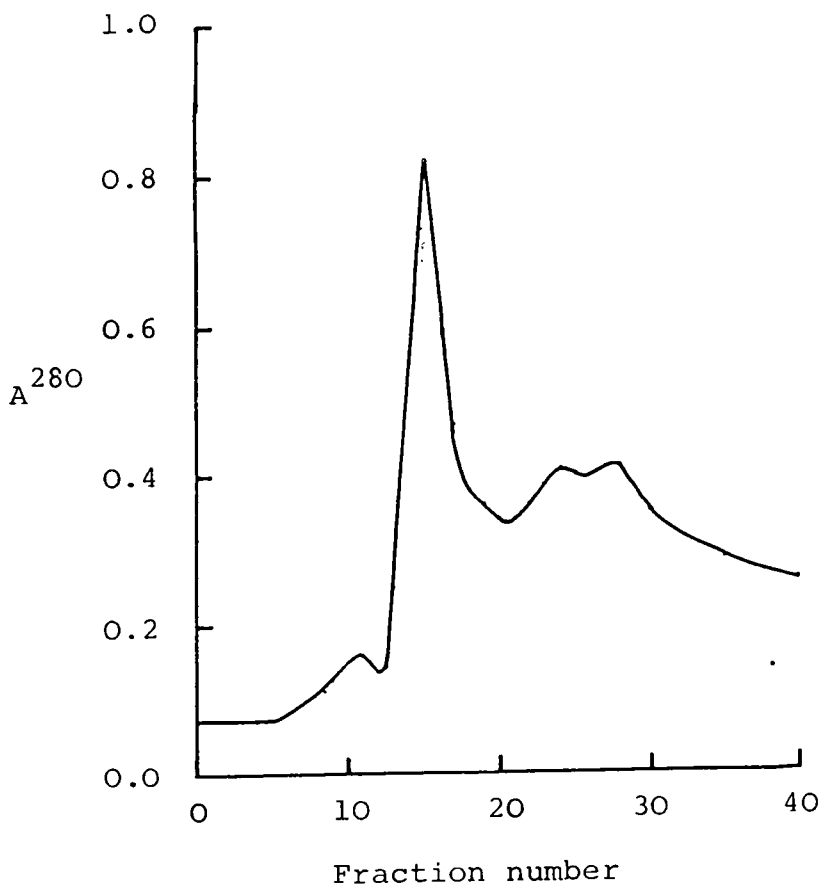

Figure 5.7

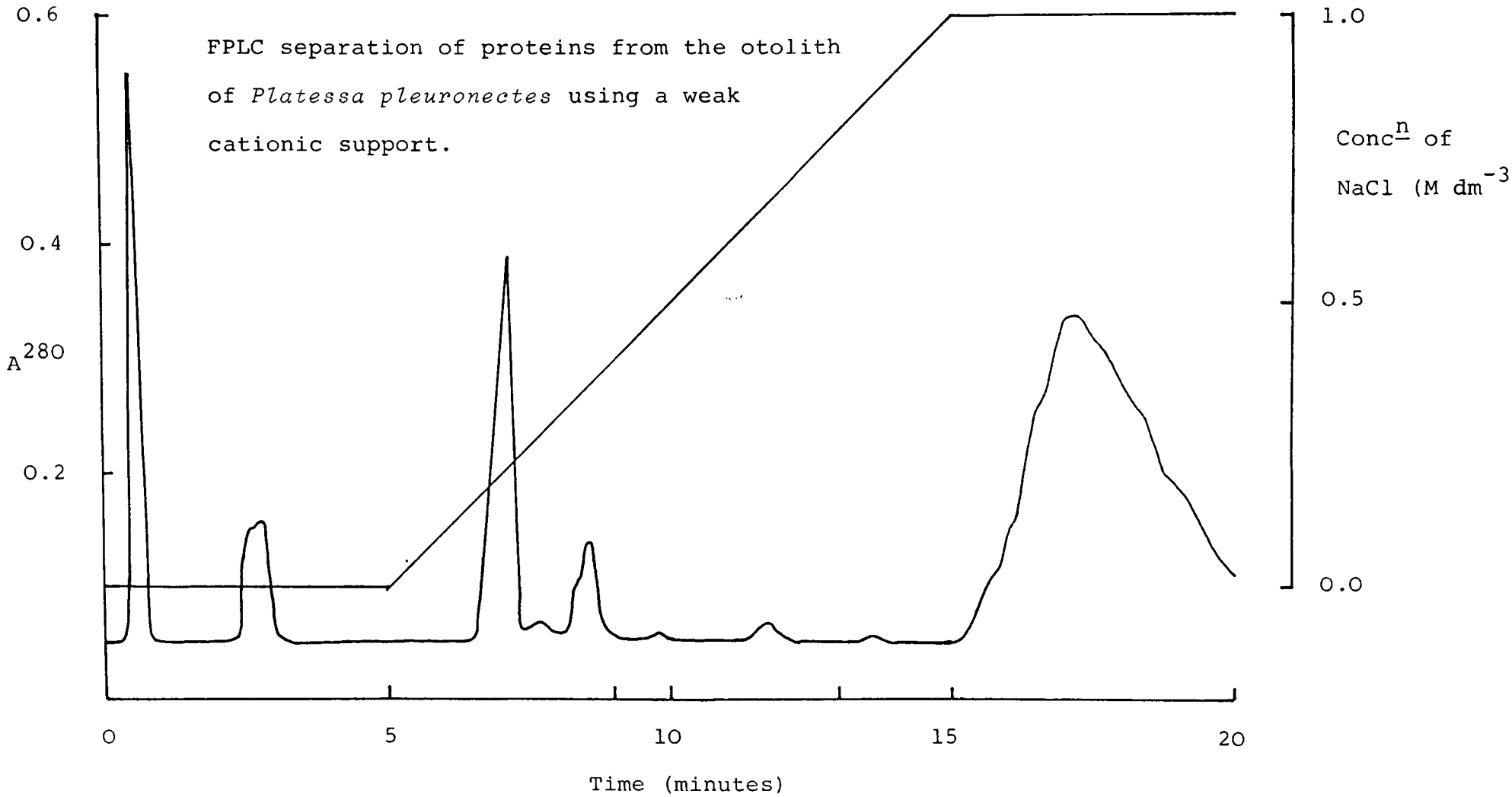
FPLC separation of proteins from the otolith of *Platessa pleuronectes* using a weak cationic support.
0.6
0.4
0.2
A^{280}
1.0
0.5
0.0
Conc^{n} of NaCl (M dm^{-3}
0
5
10
15
20
Time (minutes)

many as twenty. A better separation is probably only possible with the use of organic solvents and HPLC.

The broad conclusion as to the character of the organic components is that they are all aggregates of polypeptide chains with varying degrees of acidity. This has been shown by the use of IEF which separates the proteins into several components many of which were too acidic to focus on a plate extending to pH 3.5. No peaks focussed above 3.8. As a consequence, the isoelectric points (pI) of the proteins remain unclear beyond this general observation.

5.4.2 Calcium Carbonate Crystallisation Experiments

The effect of soluble organic matrix on *in vitro* precipitation has been noted for proteins from gastropods (20) and the acidic polysaccharide from coccoliths (21,22) (see above). Essentially, the matrix inhibits crystallisation in very low concentrations (Wheeler et al (20) estimate that inhibition occurs at concentrations as low as 10 nM) and will prevent further crystal growth if added to the solution after crystallisation has commenced. A series of experiments were carried out using the organic matrices extracted during this project. These experiments were in two stages; a confirmation that these proteins have similar properties to those reported in previous observations and an attempt to carry out crystallisation with the matrix having undergone a conformational change of the type described above and depicted in Figure 5.2.

Figures 5.8 and 5.9 show the pattern of crystallisation followed by the drop in pH resulting from the following reaction having taken place:

$$Ca^{2+} + HCO_3^- \longrightarrow CaCO_3 + H^+ \qquad (5.1)$$

Figure 5.8

Crystallisation of calcium carbonate in the presence of polypeptides

a : control experiment $Ca^{2+} + HCO_3^- \longrightarrow CaCO_3 + H^+$

b : the same reaction in the presence of met-Hb

c : the same reaction in the presence of the organic matrix extracted from *Atrina vexillum*

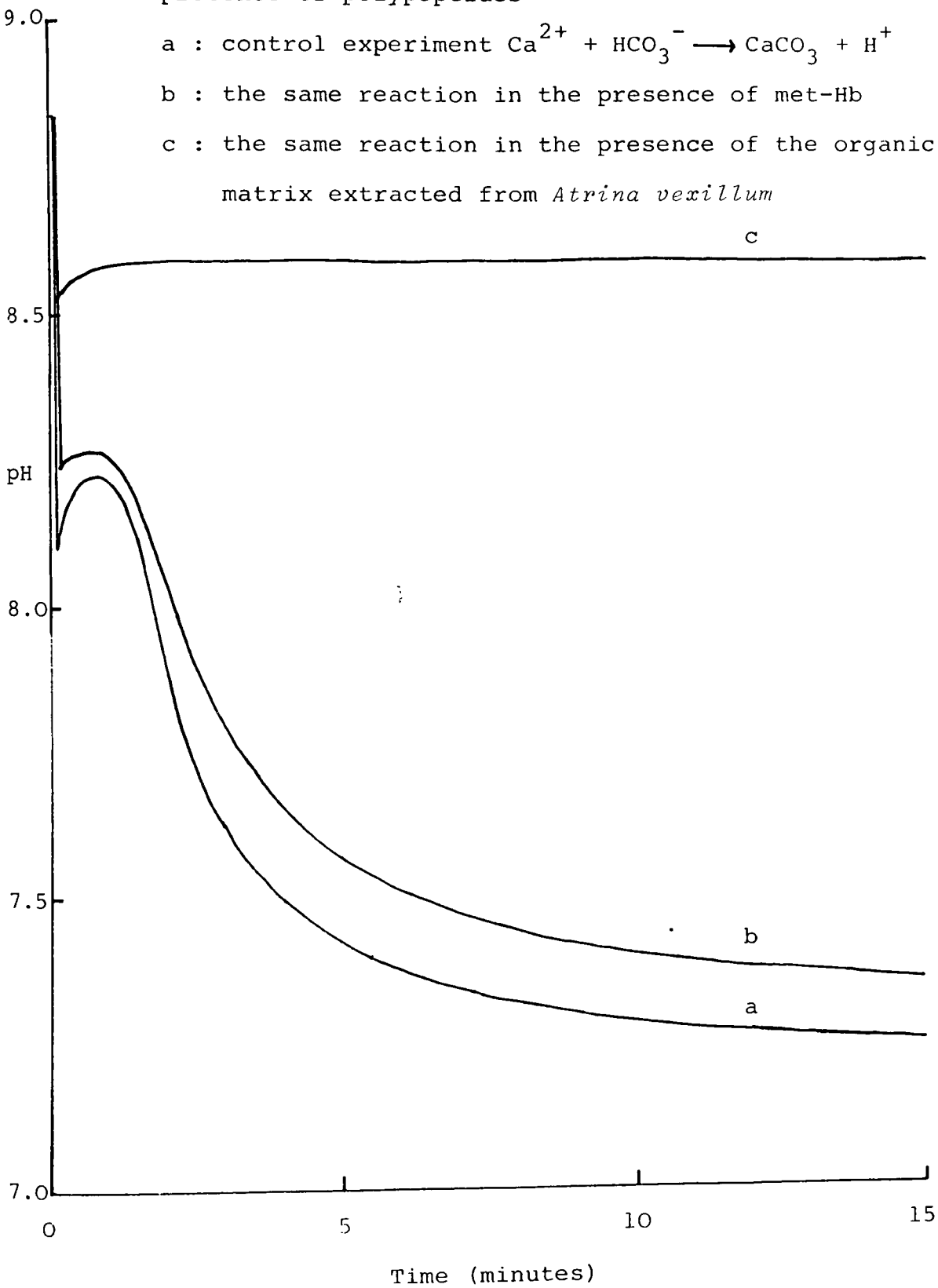

Figure 5.9

The influence of the organic matrix from *Atrina vexillum* on the crystallisation of Calcium Carbonate *in vitro*

a : control experiment with no addition

b : the same reaction with the matrix protein added after 2.5 minutes

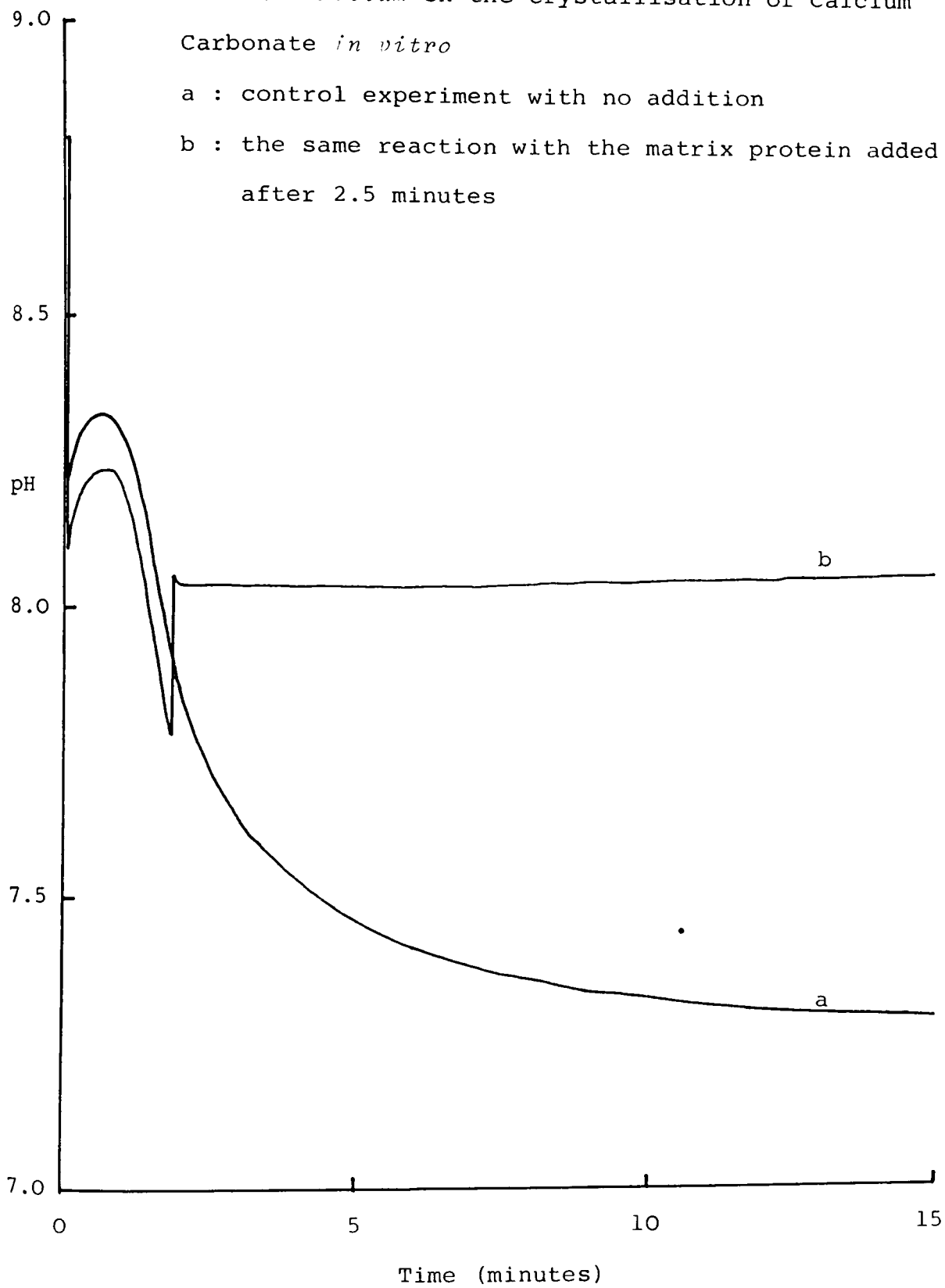

The reaction was observed by the addition of 3 mls of 20 mM $CaCl_2$ to 3 mls of 20 mM $NaHCO_3$ with constant stirring. The addition was made in 0.3 ml aliquots, with 0.3 mls of water being added as a blank when no other additions were made. Protein concentrations added were approximately 0.05 mM stock, giving a concentration in the reaction vessel of about 5 µM. The reaction was followed with an Orion pH electrode attached to a Radiometer pHM 83 pH meter linked to a Goerz Servoscribe Y-T chart recorder. The sensitivity of the pH meter was increased to give a full scale deflection in the range pH 7 to 9 on the recorder by coupling a Time Electronics DC voltage potentiometer, model 2003N in series to them.

Figure 5.8 shows that the inhibition of $CaCO_3$ formation is a specific property of matrix proteins; met haemoglobin (met-Hb) was used as a protein standard (trace b) and caused very little change to the reaction. In contrast, the addition of matrix protein from *Atrina vexillum* brings about complete inhibition (trace c). This inhibition property was again shown when the matrix was added to the reaction vessel after crystals had begun to form. Trace b shows that this formation is immediately halted and a stable pH level attained on addition of the matrix. The crystals already formed do not redissolve and can be observed as a weak suspension in the stirred reaction vessel. This type of reaction was repeated with matrix from *Terebratulina* (Figure 5.11) and fish otolith (Figure 5.12). It is interesting to observe that the capacity of the *Terebratulina* matrix to inhibit crystallisation is substantially less than the gastropod or otolith protein, despite the fact that the experiment was repeated with a 1 mM protein concentration (Figure 5.11, trace b). In order to demonstrate that the coloured cross-link of the

Figure 5.10

Inhibition of crystallisation of calcium carbonate with colourless soluble matrix from *Atrina vexillum*.

a : control experiment with no addition

b : the same reaction with "Atrina 2" added

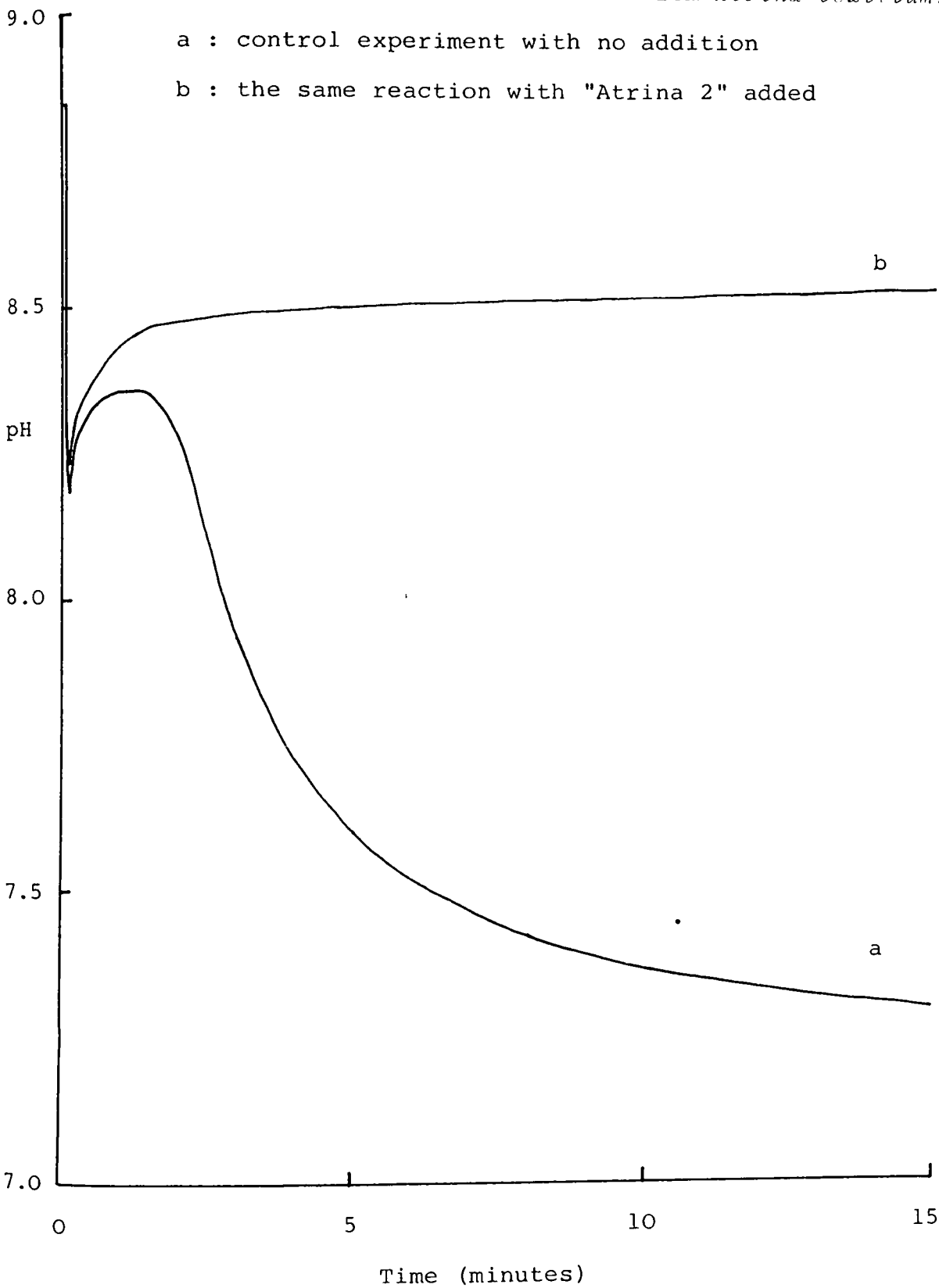

Figure 5.11

Inhibition of crystallisation of calcium carbonate with soluble matrix from *Terebratulina*.

a : control experiment with no addition

b : the same reaction with the addition of *Terebratulina* matrix.

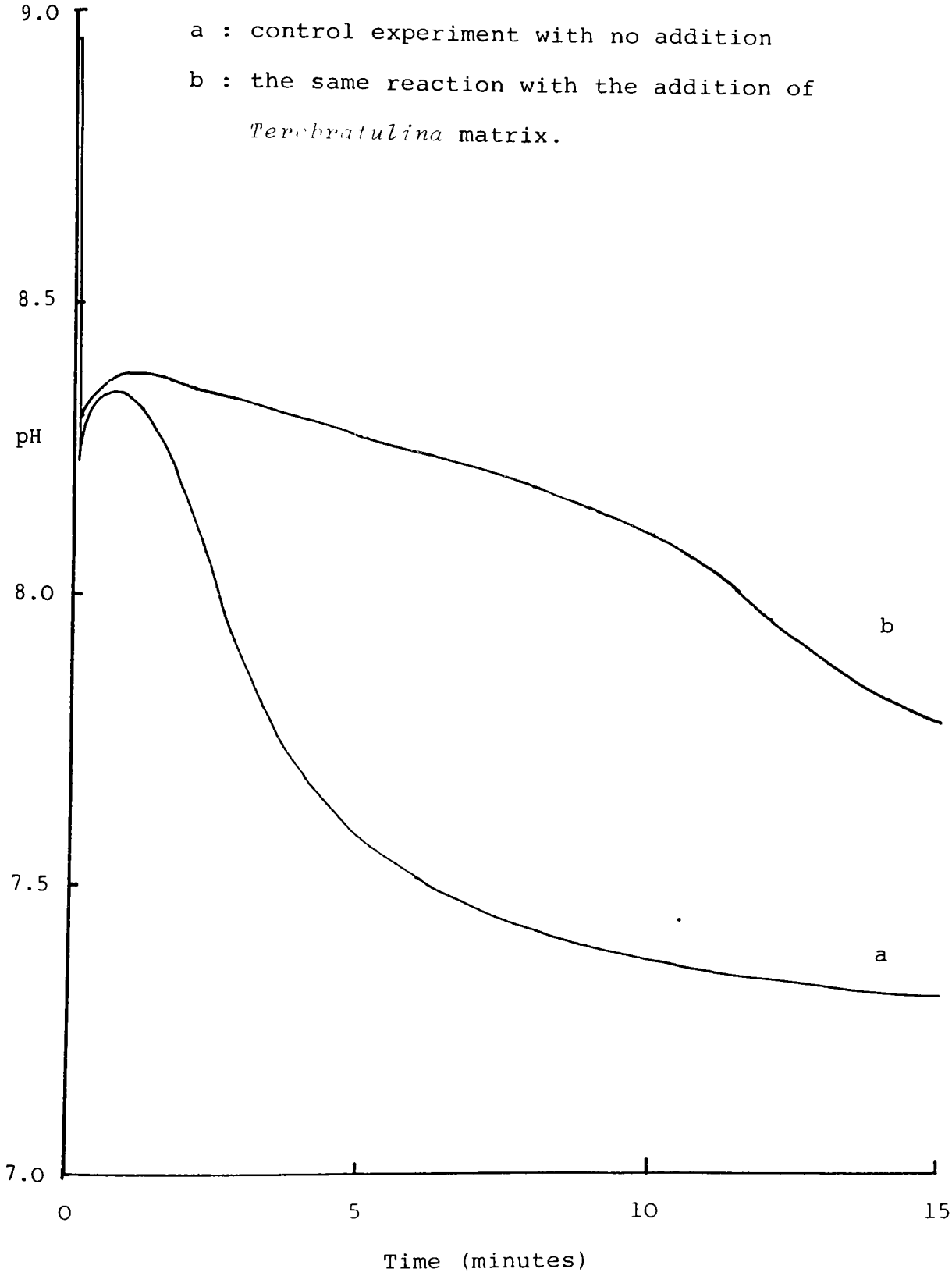

Figure 5.12

The effect on calcium carbonate crystallisation of soluble matrix from otoliths from *Pleuronectes platessa*.

a : control experiment with no addition

b : the same experiment with the addition of matrix protein

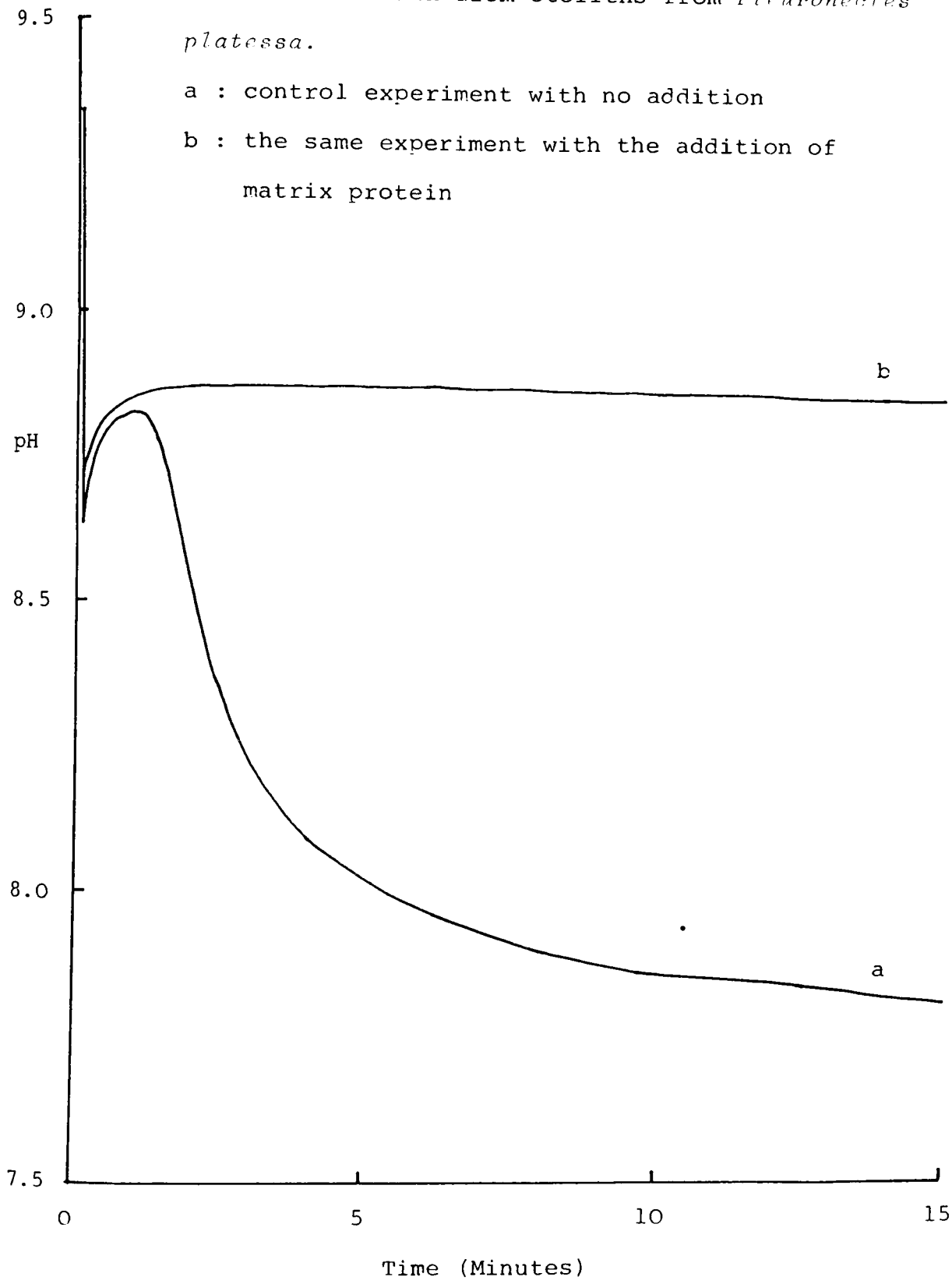

Atrina vexillum protein was not causing the inhibition, the fraction of *Atrina* separated by the $(NH_4)_2SO_4$ cut during extraction was used (Figure 5.10). This fraction was virtually colourless and showed the same property as the coloured fraction.

The second phase of the experiments was carried out exclusively on the *Atrina vexillum* proteins due to the quantities available. These experiments aimed to perturb the normal solution conformation in some manner and note the effect on crystallisation. The first experiment followed a report from work carried out on coccolith SIF (21,22), involving the addition of ethanol to the reaction vessel, which should interact with the non-polar regions of the matrix and open the structure slightly. Figure 5.13 illustrates the observations on this system. The blank experiment (trace b), in which crystallisation was carried out in the presence of about 5% ethanol showed a marked increase in the rate and extent of calcification. Addition of ethanol to the same concentration after the onset of crystallisation (arrow 1, trace c) produced a marked increase in the rate of crystal formation. The final experiment involved the addition (arrow 2, trace d) of "Atrina 1" protein to the reaction vessel after crystallisation had commenced in the presence of about 8% ethanol. The protein stopped calcium carbonate formation instantaneously despite being present in a far lower concentration than the ethanol.

Two attempts were made to immobilise the matrix onto a rigid support. The first used the principles of hydrophobic interaction chromatography; the second, affinity chromotography. The former route was preferred since one common mode of binding to affinity gel supports is via carboxyl groups. Hydrophobic binding was achieved by coupling the non-polar areas of the

Figure 5.13

The influence of ethanol on calcium carbonate crystallisation *in vitro*

a : control experiment with no addition

b : the same reaction with ethanol added

c : the same reaction with ethanol added after 1.5 minutes (arrow 1)

d : reaction b with *Atrina vexillum* protein added after 1 minute (arrow 2)

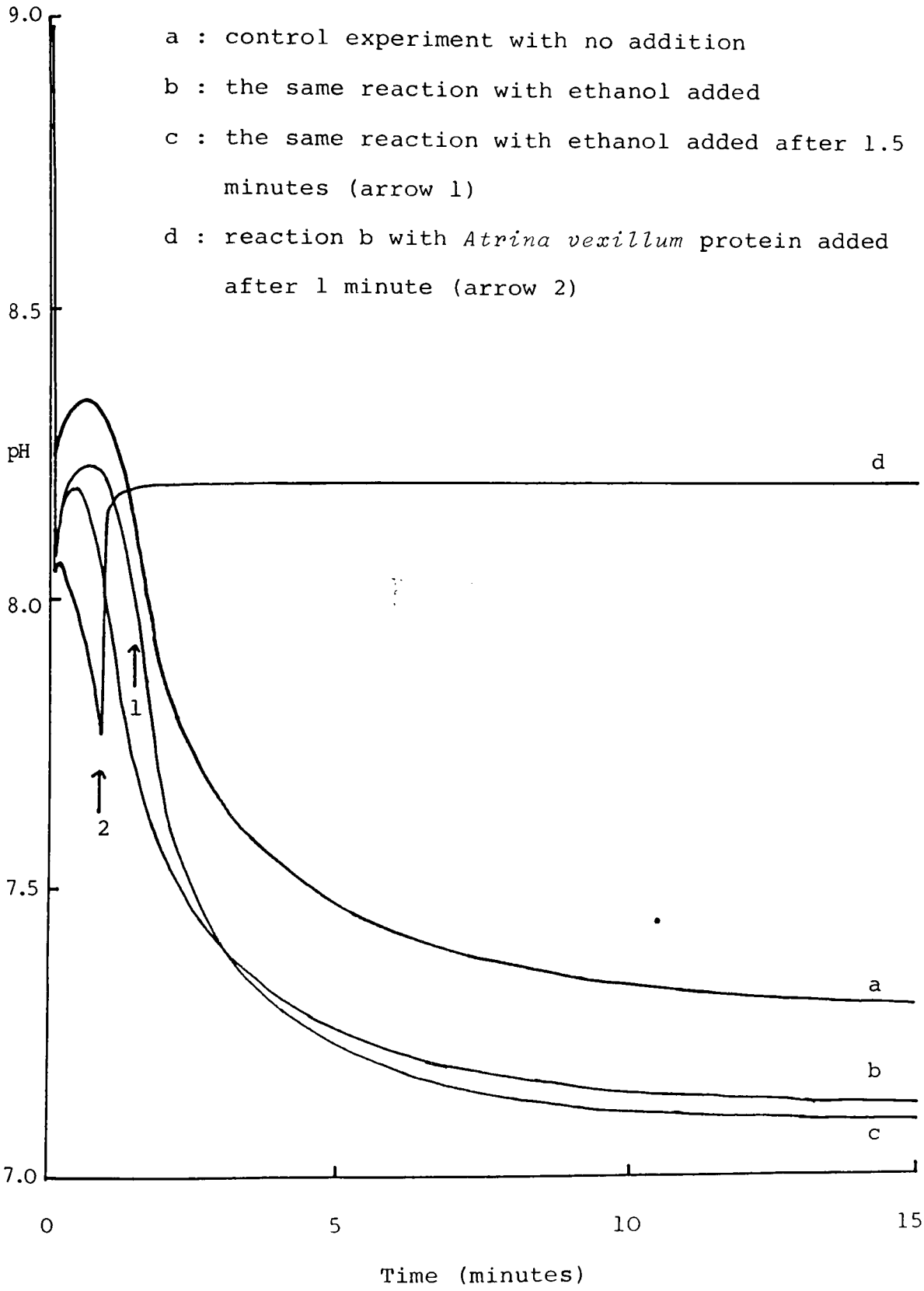

protein to octyl- or phenyl-sepharose (Pharmacia AC) under conditions of high salt (0.5 M NaCl). The unbound protein was washed away and the complex added to the crystallisation experiment Binding to an affinity gel is more complex and was carried out by following the suggested procedure, below:

1. 0.5 g AH-Sepharose 4B was swollen and washed in 0.5 M NaCl.
2. The protein to be coupled was dissolved in water and the pH adjusted to 4.5.
3. Carbodiimide was dissolved in water and adjusted to pH 4.5.
4. The two solutions were gently mixed with the gel suspension overnight at room temperature.
5. The coupled gel was washed to remove excess protein, urea derivative and unreacted carbodiimide.

The reaction which occurs during coupling is a two-stage peptide linkage by acid catalysed removal of water. The carbodiimide forms isourea upon hydration:

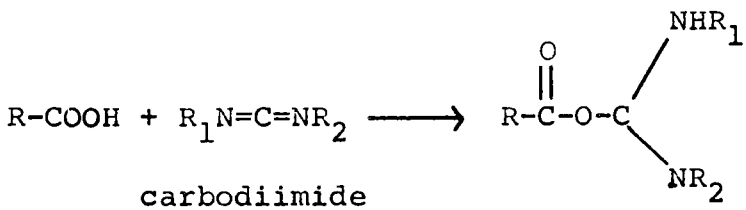

carbodiimide (5.2)

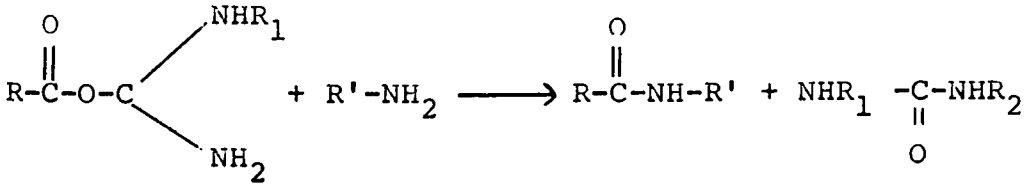

isourea (5.3)

The coupled protein was thoroughly washed and added to the crystallisation cell. The results of the two experiments are shown in Figures 5.14 and 5.15. The effect of immobilising the

Figure 5.14

Effect of immobilising soluble matrix from *Atrina vexillum* on calcium carbonate formation : 1

a : control experiment with no addition

b : the same experiment with the addition of uncoupled AH-Sepharose 4B

c : the same experiment with the addition of *Atrina vexillum* protein coupled to AH-Sepharose 4B

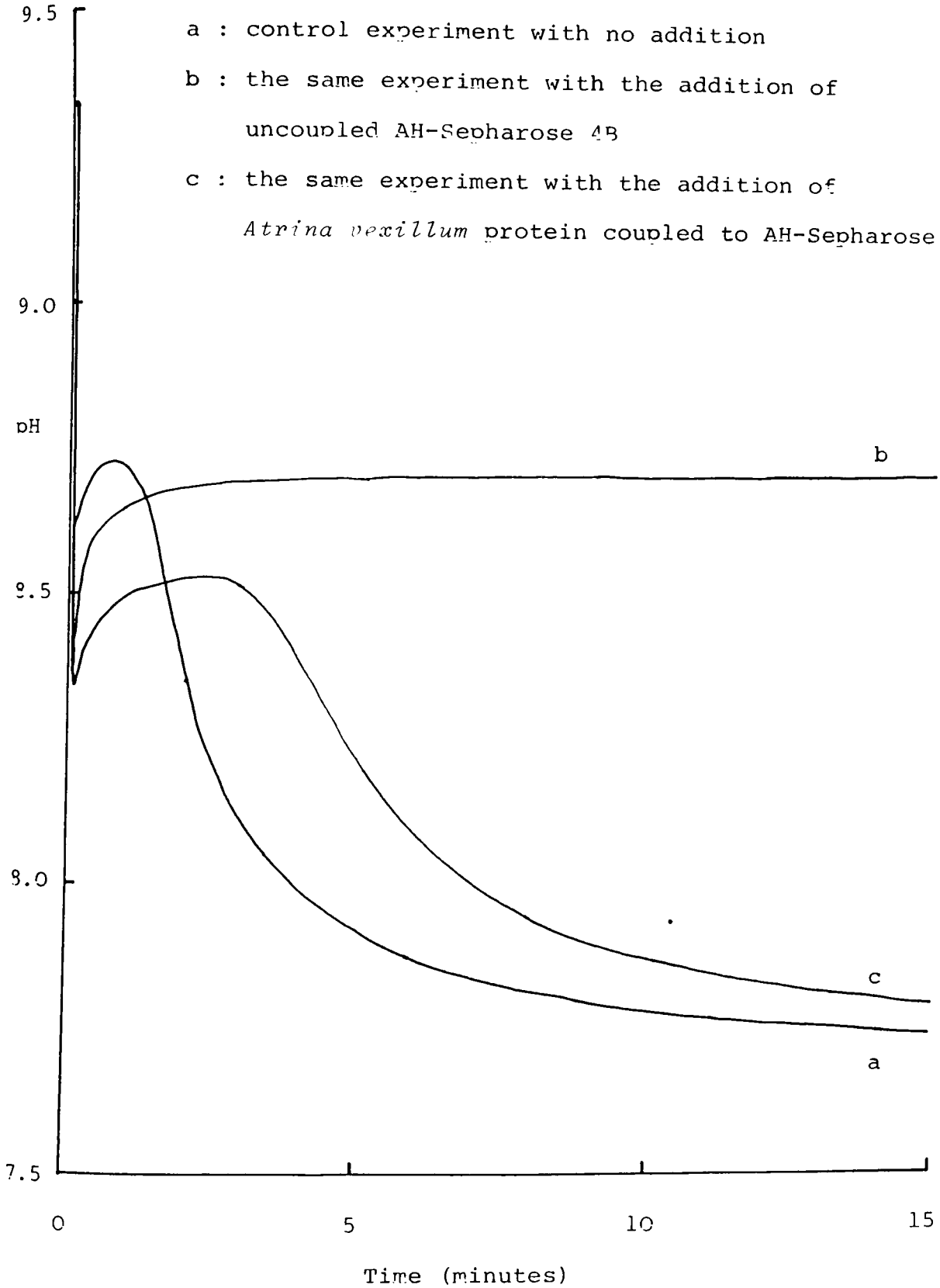

Figure 5.15

Effect of immobilising soluble matrix from *Atrina vexillum* on calcium carbonate fromation : 2

a : control experiment in the presence of uncoupled phenyl-sepharose

b : the same experiment in the presence of *Atrina vexillum* protein coupled to phenyl-sepharose

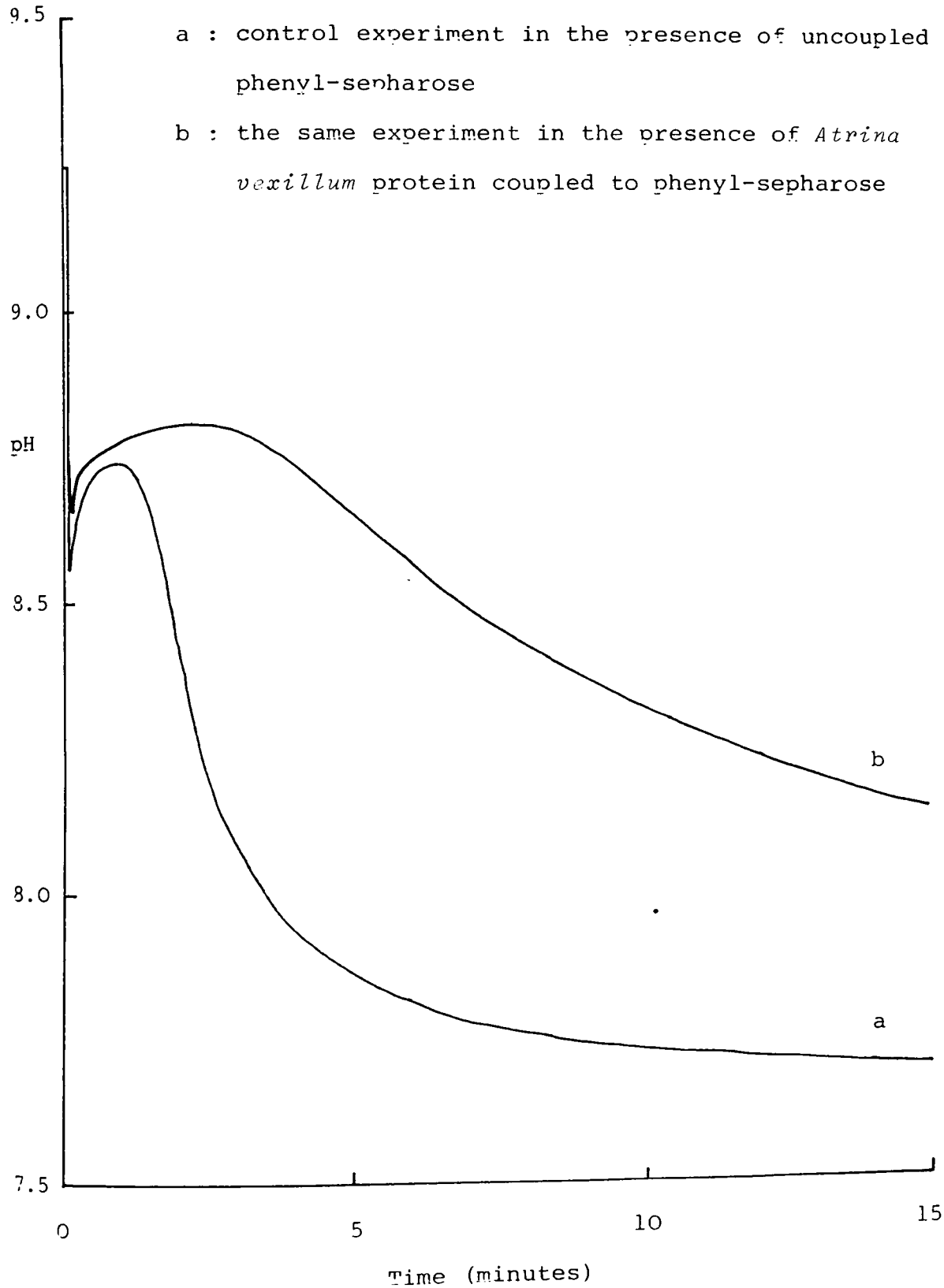

Atrina protein to AH-Sepharose-4B is shown on Figure 5.14. This is of interest in that the support itself inhibits crystal formatio but immobilising the protein leads to control of crystal formation. The rate of formation is less than the control (trace a), but shows the effect of changing the conformation of the protein in these experiments. One reason for the slow rate of crystallisation may be that the immobilisation process uses a proportion of the carboxyl groups, rendering them unavailable for binding calcium. It is of interest that the nature of the precipitate was quite different from that observed in all other cases in that large, floccular growths were seen around the sepharose beads (which gave a slight brown colouration to the crystals), clearly indicating that the immobilised protein was playing a positive role in nucleating the crystals, and not just blocking the inhibitor on the beads.

Immobilisation of *Atrina* protein onto phenyl-sepharose was successfully carried out. It was found, however, that the binding was only effective under conditions of high salt and thus the effect observed in the crystallisation experiment was not as marked as one would predict. The results are shown in Figure 5.15. Phenyl sepharose was found to have no effect upon crystallisation of calcium carbonate and the protein-bound system did not accelerate growth above the blank value. It was shown, however, that immobilising the protein again brought about a change in the properties. The protein no longer completely inhibited crystal growth; indeed, growth was observed to occur at the surface of the gel beads. It will be seen below that the protein from *Atrina vexillum* is particularly acidic, and it is possible that one could actually obtain an acceleration in

crystal growth by using a soluble matrix from *Mytillus edulis* immobilised onto octyl-sepharose, which is rather more hydrophobic than phenyl-sepharose and thus affords a tight binding at lower salt concentrations.

5.4.3 ^{1}H-NMR Studies of Matrix Proteins

The matrix proteins were studied by ^{1}H-NMR spectroscopy in order to determine any common component or structural patterns. Figures 5.16 and 5.17 show the aromatic and aliphatic regions respectively of the brachiopod *Lingula*. This is unique amongst the matrices studied in that it arises from a phosphatic shell (23). The amino acid composition of the matrix is known to differ in many respects from the other, carbonate, brachiopods, but chiefly in that chitin is associated with the matrix and also that the composition contains hydroxyproline, which is commonly found in collagen in bone. The major peak, at about 1.4 ppm is due to the β-CH_3 of Alanine, the most common of the amino acids in the protein. The aromatic region is the most interesting of the proteins studied in that -NH resonances are clearly visible downfield of 8.0 ppm. This is a clear indication that the protein contains regions which are inaccesible to solvent. This is normally interpreted as a property of a tertiary structure. The aromatics themselves consist of phenylalanines (phe) and tyrosines (tyr) with a peak at 8.1 ppm possibly due to a histidine (his) which is in the protein at a concentration of 0.8%. The aromatic region of *Mytillus edulis* matrix (Figure 5.18) shows no obvious -NH resonances and just phes and tyrs in the aromatic region itself. The aliphatic region (Figure 5.19), like that of *Lingula*, contains a large peak at 0.8 ppm, in this case split. This indicates that a large proportion of the protein is non-polar, since the peak must be due to valine (val), isoleucine (ile) or

Figure 5.16

Soluble matrix from the brachiopod *Lingula*. Aromatic region. (a) Normal spectrum. (b) Gaussian spectrum. (c) CPA spectrum.

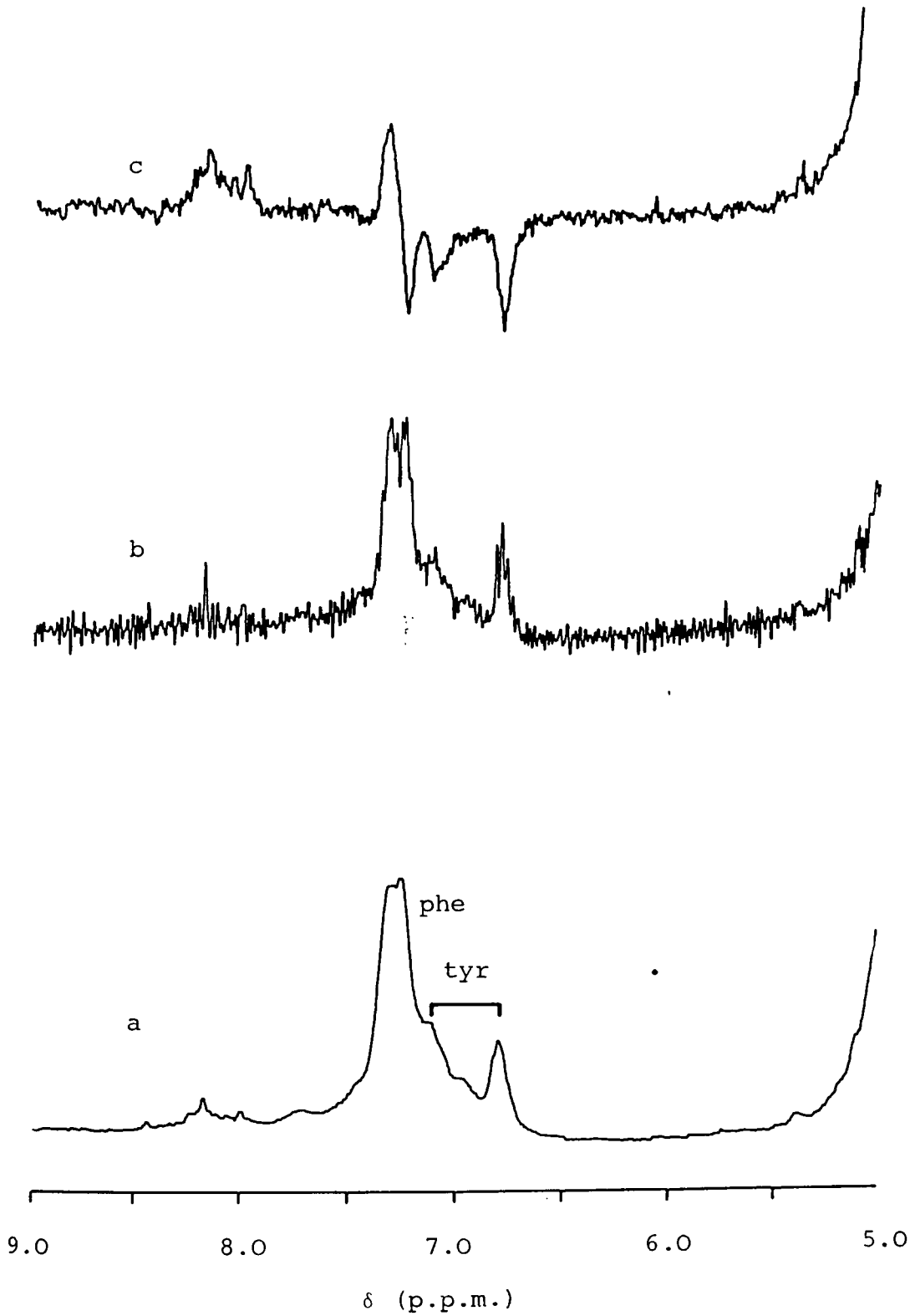

Figure 5.17

Soluble matrix from the brachiopod *Lingula*. Aliphatic region

(a) Normal spectrum. (b) CPA spectrum

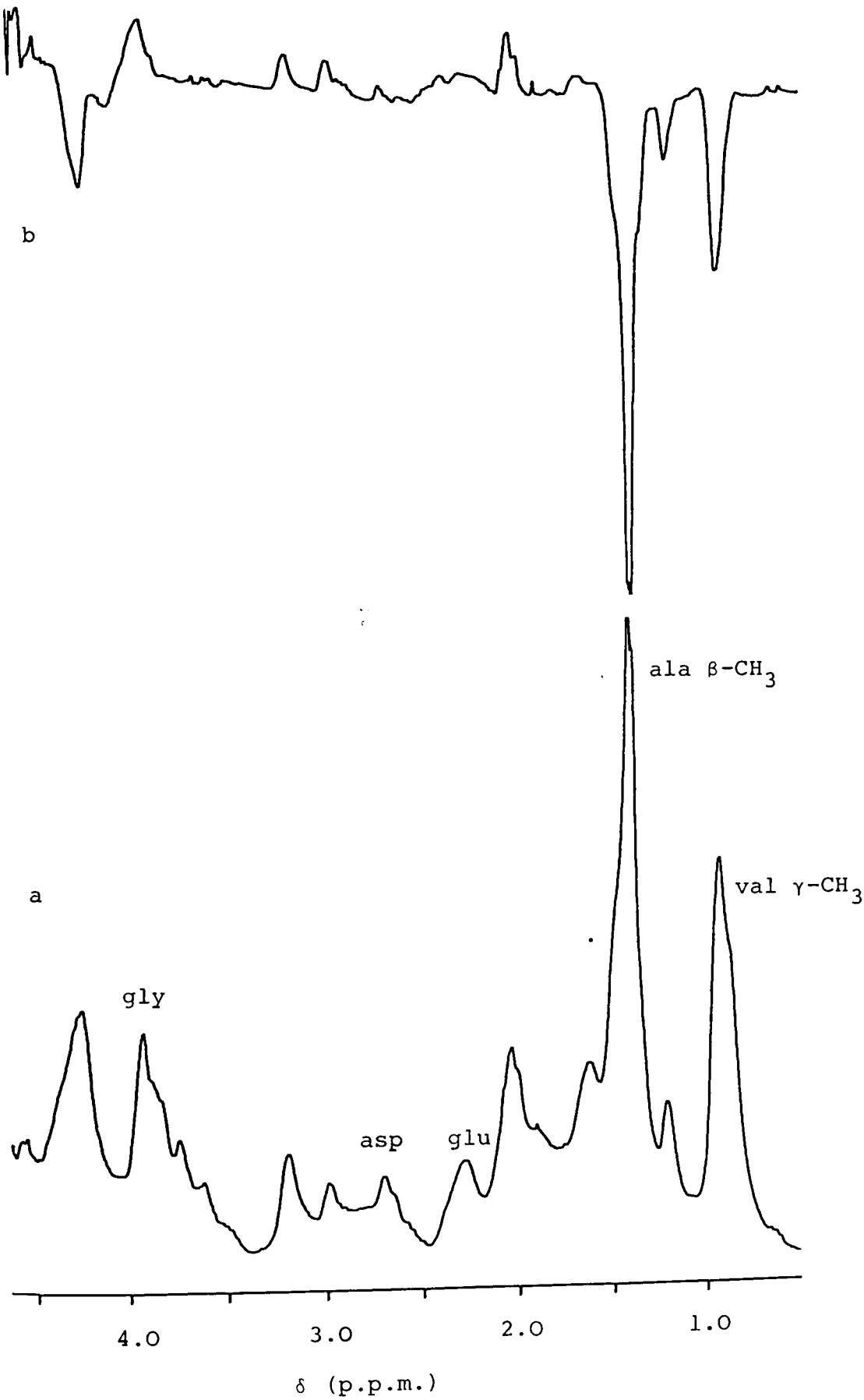

Figure 5.18

Soluble matrix from *Mytillus edulis*.Aromatic region.

(a) Normal spectrum

(b) Resolution enhanced (Gaussian) Spectrum

(c) CPA spectrum

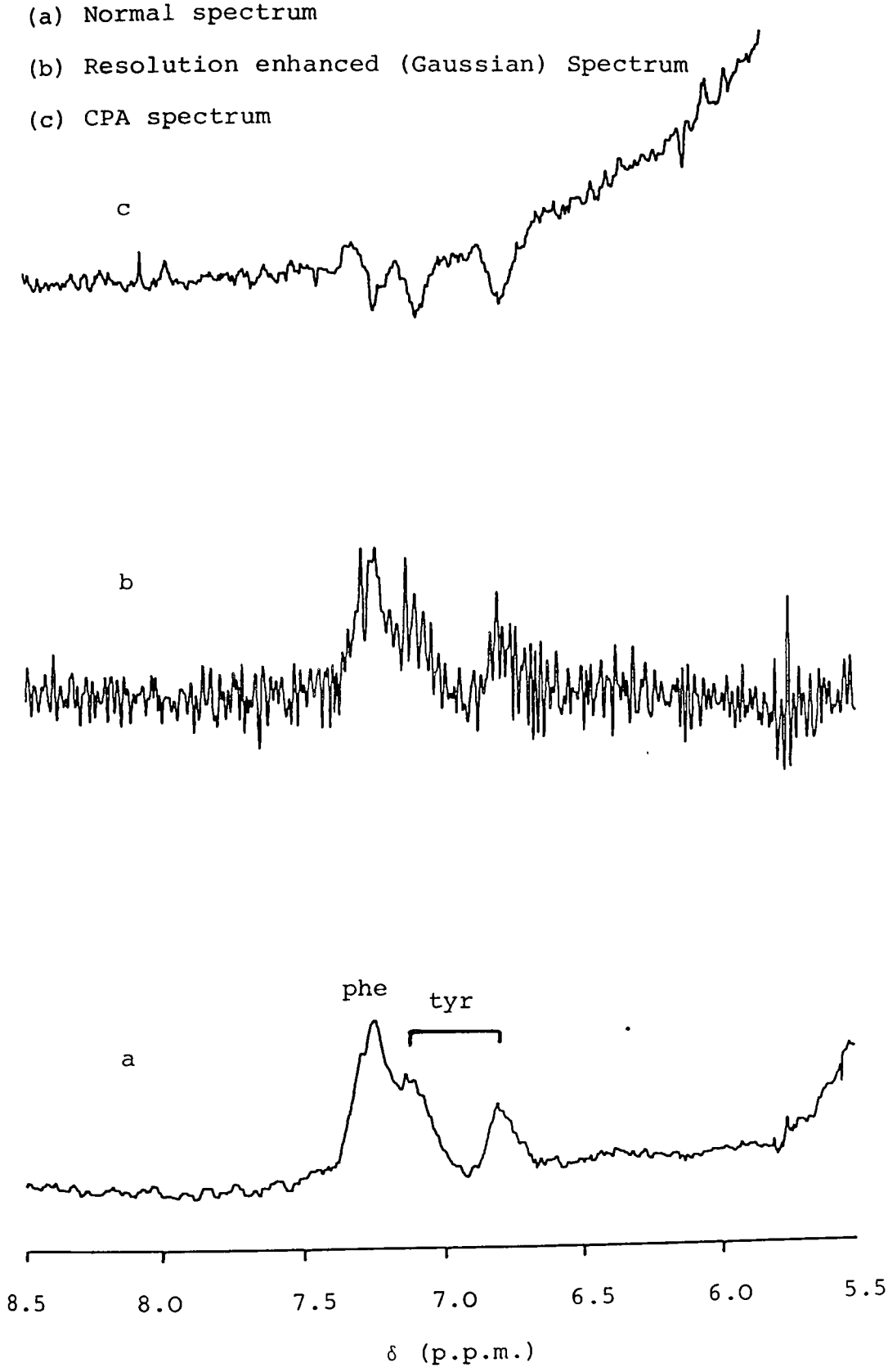

Figure 5.19

Soluble matrix from *Mytillus edulis*. Aliphatic region.

(a) Normal spectrum. (b) CPA spectrum

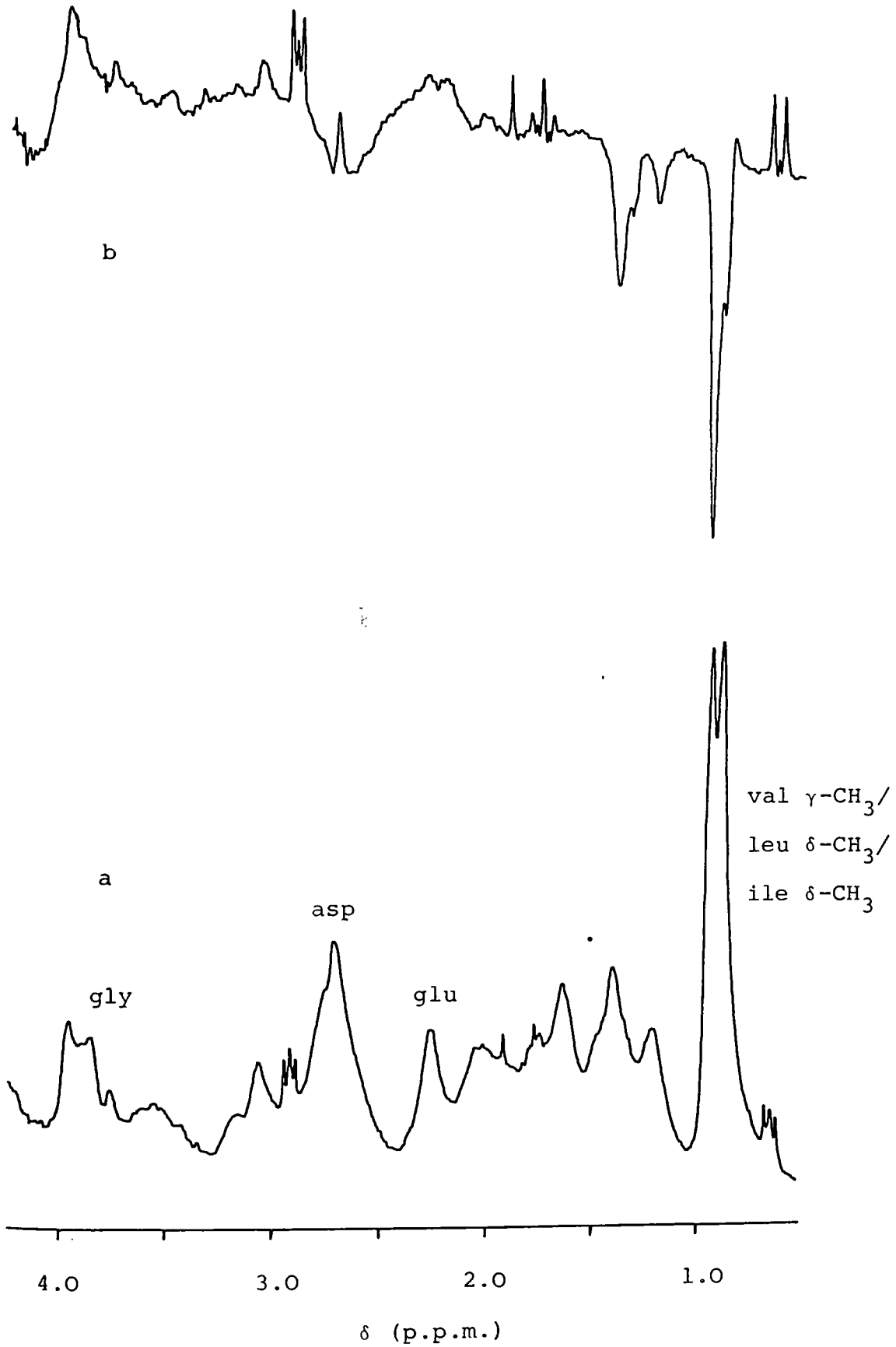

leucine (leu) itself. The major acid component is aspartic acid (asp) with a resonance in the region of 2.8 ppm. In complete contrast, the aliphatic region of *Atrina vexillum* protein (Figure 5.20) is very acid indeed. This is true of the highly coloured fraction, labelled "Atrina 1" and also of the less coloured component, labelled "Atrina 2". The protein contains a small amount of non-polar amino acids, but substantially less than the other matrices studied. The aromatic region (Figure 5.21) is chiefly of interest for the bands in the upfield region. The actual aromatics are in very low concentration and the major peak is probably due to the cross-linking quinone. Small peaks in the Atrina 1 spectrum indicate that histidine might be present and a few -NHs suggest the presence of tertiary structure; this is not certain since the aliphatic peaks closely resemble the random-coil distribution of resonances.

The addition of calcium to *Atrina* protein brings about several changes to the spectrum which may be interpreted as a conformational change to the protein. The main asp peak is split into two, being calcium bound and unbound and there are changes to the upfield aromatic region. This would indicate (24) that there is some formation of β-sheet in the structure on binding calcium. This is shown in Figures 5.22 and 5.23 for the aromatic and aliphatic regions respectively.

5.5 Conclusions on the Organic Matrix

The soluble organic matrix from calcium carbonate-forming systems has been shown in this, and other, work to be a highly complex system of polypeptides linked together in ways which are not completely understood; the coloured proteins have aromatic

Figure 5.20

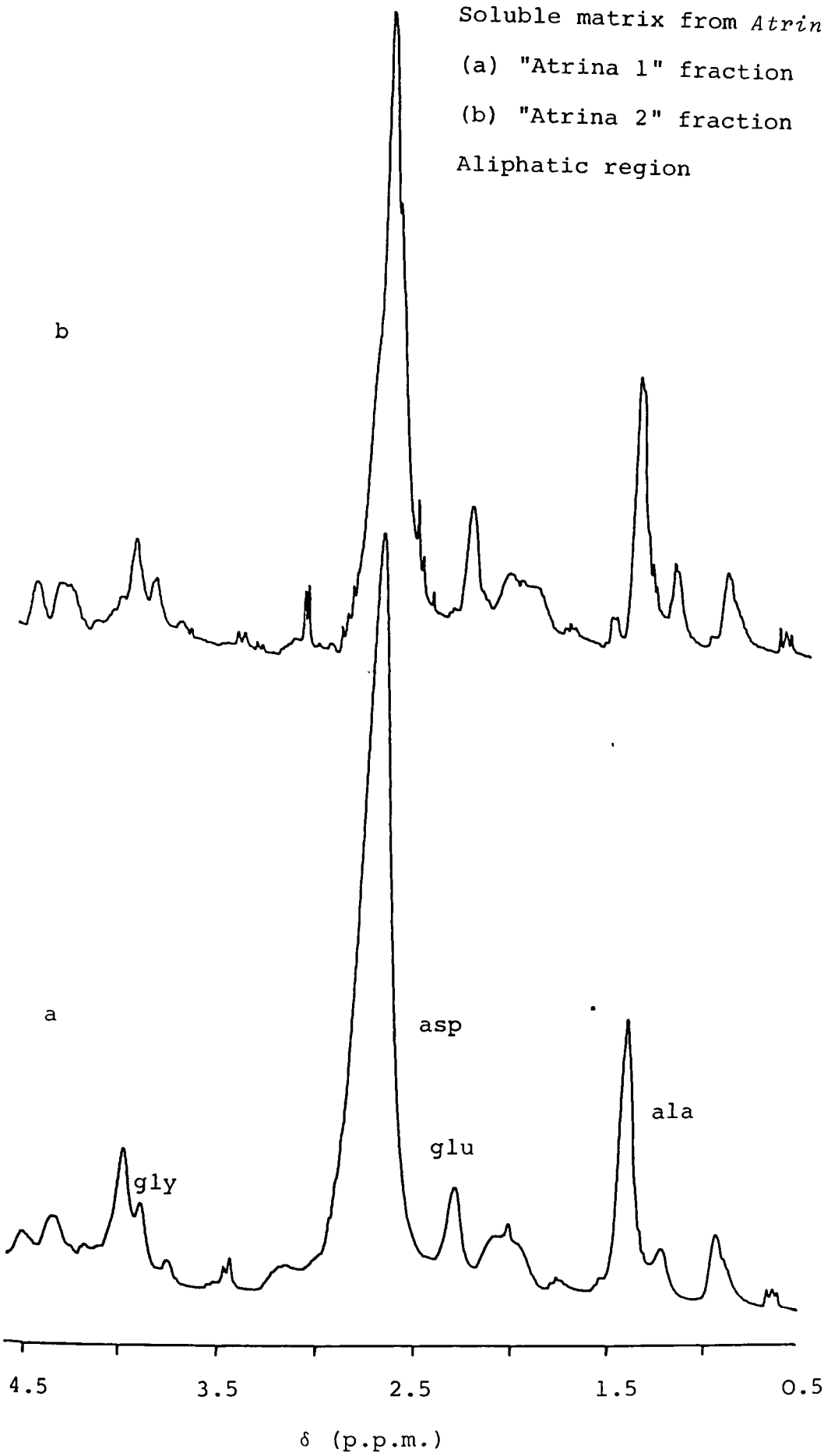
Soluble matrix from *Atrina vexillum*.
(a) "Atrina 1" fraction
(b) "Atrina 2" fraction
Aliphatic region
b
a
asp
ala
glu
gly
4.5
3.5
2.5
1.5
0.5
δ (p.p.m.)

Figure 5.21

Soluble matrix from *Atrina vexillum*. Aromatic region.

(a) "Atrina 1" fraction

(b) "Atrina 2" fraction

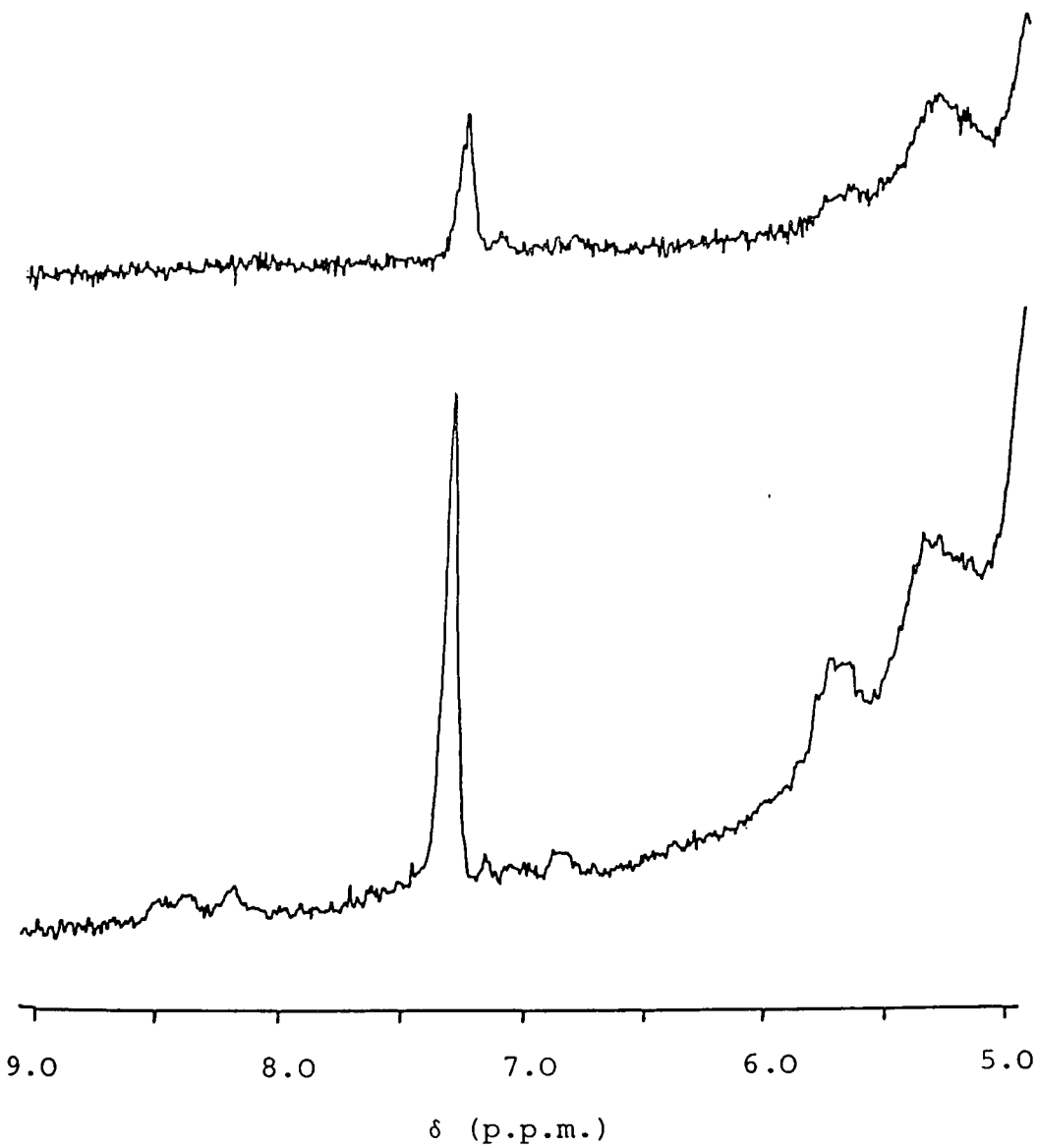

Figure 5.22

Addition of calcium to soluble matrix from *Atrina vexillum* at pH = 4.5. Note the collapse of the aromatic resonances and the increase of resonances in the upfield shifted α-CH region

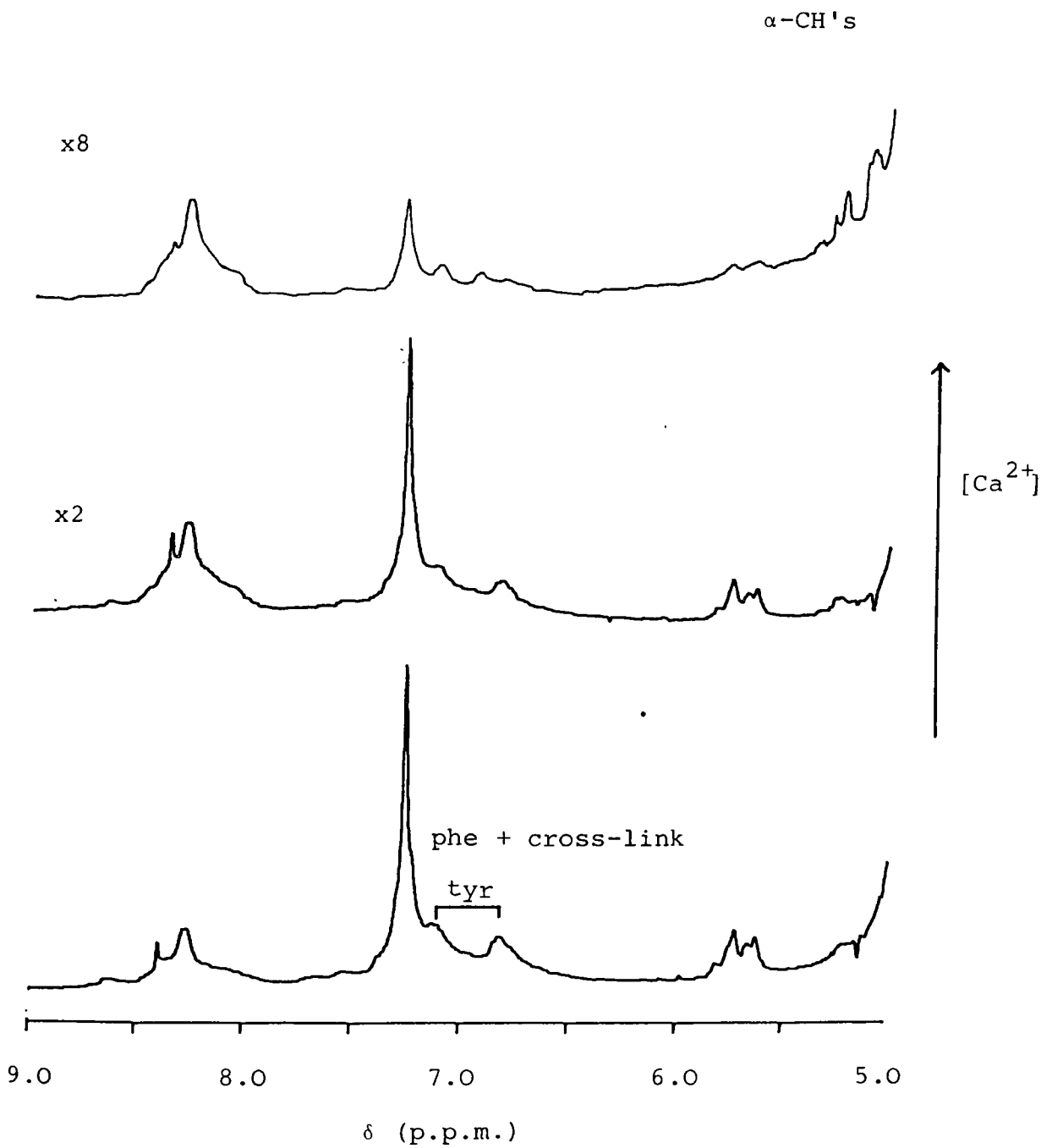

Figure 5.23

Addition of calcium to soluble matrix from *Atrina vexillum* at pH = 4.5. Aliphatic region. The asp peak is split in the apo- state since it is close to its pK_a. Note the movement of the α-CH's

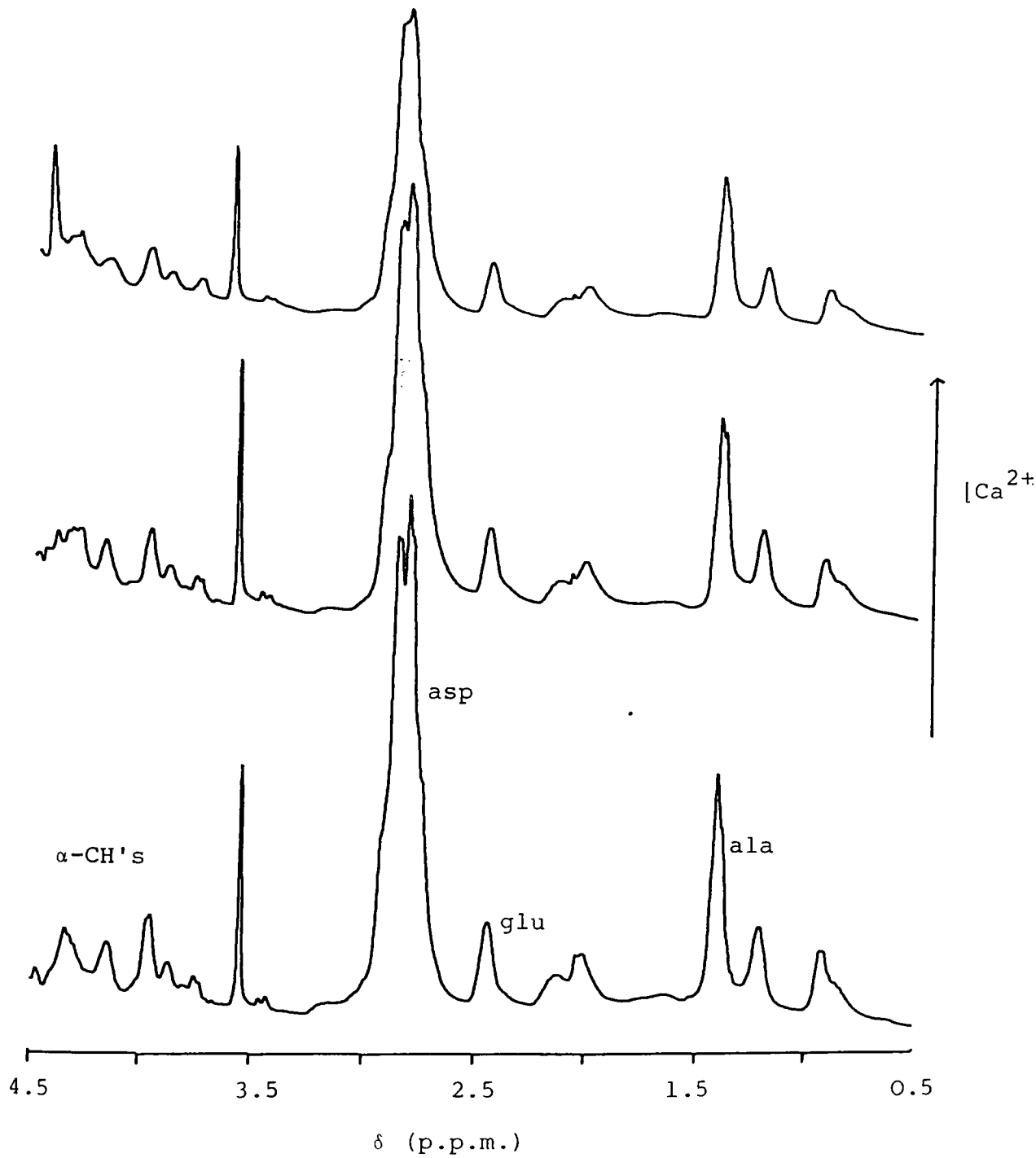

cross-links which have been studied in some systems (18), but the colourless matrix proteins are also linked in some way. The nature of the organic matrix, with soluble layers linked to insoluble layers leads to great difficulty in mimicking the process occurring *in vivo*. This work has demonstrated that one way of modelling the *in vivo* condition is to immobilise the acidic matrix in some way and then follow the pattern of calcification. This work has only been able to proceed a small way into the problem, but future study should provide many insights into the role of the soluble matrix in biological calcium carbonate growth.

5.6 References

1. Jope, M. in *'Comprehensive Biochemistry'* 26C, ed. M. Florkin and E.H. Stoltz, pp 749-784, (1971). Pub. Elsevier, Amsterdam.
2. Degens, E.T. and Spencer, D.W. Unpublished manuscript
3. Degens, E.T., Deuser, W.G. and Haedrich, R.L. *Marine Biol.* 2, 105-113, (1969)
4. Andrews, A.T. *"Electrophoresis: Theory, Techniques and Biochemical and Clinical Applications"* Chapter 2. Pub. Clarendon Press, Oxford. (1981).
5. Veis, A. and Sabsay, B. in *"Biomineralisation and Biological Metal Accumulation"* eds. P. Westbroek and E.W. de Jong. 273-284, (1983)
6. Weiner, S. *Calcif. Tissue Int.* 29, 163-167, (1979)
7. Weiner, S. *J. Chromatogr.* 245, 148-154, (1982)
8. Weiner, S. *Biochemistry* (1983) in press
9. Weiner, S. *Proc. R. Soc. London. B.* (1983) in press
10. Bevelander, G. and Nakahara, H. in *"The Mechanisms of Biomineralisation in Animals and Plants"* eds. M. Omori and N. Watabe. 19-27. Pub. Tokai University Press, Tokyo, (1980)
11. Weiner, S. and Traub, W. *FEBS Letters*, 111, 311-316, (1980)
12. Watterson, D.M., Harrerson, W.G., Keller, P.M., Sharief, F. and Vanaman, T.C. *J. Biol. Chem.* 251, 4501-4513, (1976)
13. Switzer, R.C., III, Merril, C.R. and Shifrin, S. *Anal. Biochem.* 98, 231-237, (1979)
14. Oakley, B.R., Kirsch, D.R. and Morris, N.R. *Anal. Biochem.* 105, 361-363, (1980)

15. Wray, W., Boulikas, T., Wray, V.P. and Hancock, R. *Anal. Biochem.* 118, 197-203, (1981)

16. Porro, M., Viti, S., Antoni, G. and Saletti, M. *Anal. Biochem.* 127, 316-321, (1982)

17. Andrews, A.T. *"Electrophoresis: Theory, Techniques and Biochemical and Clinical Applications".* Chapter 6, Pub. Clarendon Press, Oxford. (1981).

18. Pau, R.N., Brunet, P.C.J. and Williams, M.J. *Proc. Roy. Soc. Lond. B.* 177, 565-579, (1971)

19. Jope, M. *Comp. Biochem. Physiol.* 63B, 163-173, (1979)

20. Wheeler, A.P., George, J.W. and Evans, C.A. *Science,N.Y.,* 212, 1397-1398, (1981)

21. Borman, A.H., de Jong, E.W., Kok, D.J., Westbroek, P. and Bosch, L. *Eur. J. Biochem.* 129, 179-183, (1982)

22. de Jong, E.W., Borman, A.H., de Vrind, J.P.M., Kok, D.J., Parker, S.B. and Westbroek, P. *Proc. Roy. Soc. Lond. B.* (1983). In press

23. Jope, M. *Comp. Biochem. Physiol.* 20, 593-600, (1967)

24. Dalgarno, D.C., Levine, B.A. and Williams, R.J.P. *Bioscience Reports,* 3, 443-452, (1983)

Chapter 6

The Control of Precipitation with Bilayer Vesicles

6.1 Introduction

Vesicles are aggregates of lipids arranged so as to leave a central cavity. They are often spherical and may comprise a single layer or two layers of lipids arranged so that the hydrophobic chains of each layer interact and both the outer and inner layers are comprised of the hydrophilic head groups (1). The most common lipids used in these structures are the phospholipids such as phosphatidylcholine (lecithin) and phosphatidylserine. The bilayers are of greater interest as they model the bilayer membrane used in cells. A bilayer vesicle can contain aqueous solutions and this property has been used as a means of delivering drugs to the required sites (2). Multi-lamellar vesicles are known in biology; these are "liposomes" and are of limited interest in this study. The vesicles form semi-permeable membranes and the size can be controlled by osmotic effects. It is thus necessary to balance the ionic strengths inside and outside the structures. Permeabilit to ions is dependent on the charge density of the species; singly-charged anions will pass through the membrane whereas higher charged species will normally not do so. Various experiment have been carried out on ways of facilitating this transport and a series of ionophores are used. These are of two types, channel formers and complex formers. Valinomycin was found to be specific for sodium and potassium (1) and favoured the transport of potassium over sodium. This functions by complexing the ion; a typical channel former is Gramicidin A (3).

6.1.1 ^{1}H-NMR Studies of Vesicles

Bilayer vesicle systems, chiefly those composed of phosphatidylcholine (PC), have been studied by ^{1}H, ^{13}C and ^{31}P nmr (4-9). The proton spectrum was first assigned by Hauser et al (6) and Figure 6.1 shows a typical PC bilayer vesicle nmr spectrum labelled with their assignments. It is interesting to note that many of the resonances have an assymetrical lineshape; this is due to an inequality of population in the inner and outer layers of the vesicle. Hauser et al studied the site of cation binding to PC by spin-lattice relaxation time (T_1) measurements. They concluded that binding of lanthanides occured at the phosphate head-group only. This was confirmed by ^{31}P spectroscopy. Later work (7) showed that the conformation of the head-group remained unchanged during this binding and also anion binding.

NMR has been used to follow the passage of ions through the bilayer vesicle. This is commonly facilitated with an ionophore. Degani (10) used Lasalocid A to follow the transport of manganese II ions across the PC vesicle. The process was followed by observing the broadening of the internal $N(CH_3)_3$ resonance.

6.1.2 Interaction of Calcium Ions with Bilayer Vesicles

The binding of Ca^{2+} by the head-group of phosphatidylcholine was first observed by Bangham and Dawson in 1959 (11) although subsequent work has not been in complete agreement. One reason for this apparent contradiction is that the effects of the interaction are very small at low concentrations of calcium (12,13) and were not detected by the techniques available at the time. Hauser et al (6) found by surface potential measurement

Figure 6.1

Normal spectrum of phosphatidylcholine bilayer vesicles in D_2O. Assignments from (6).

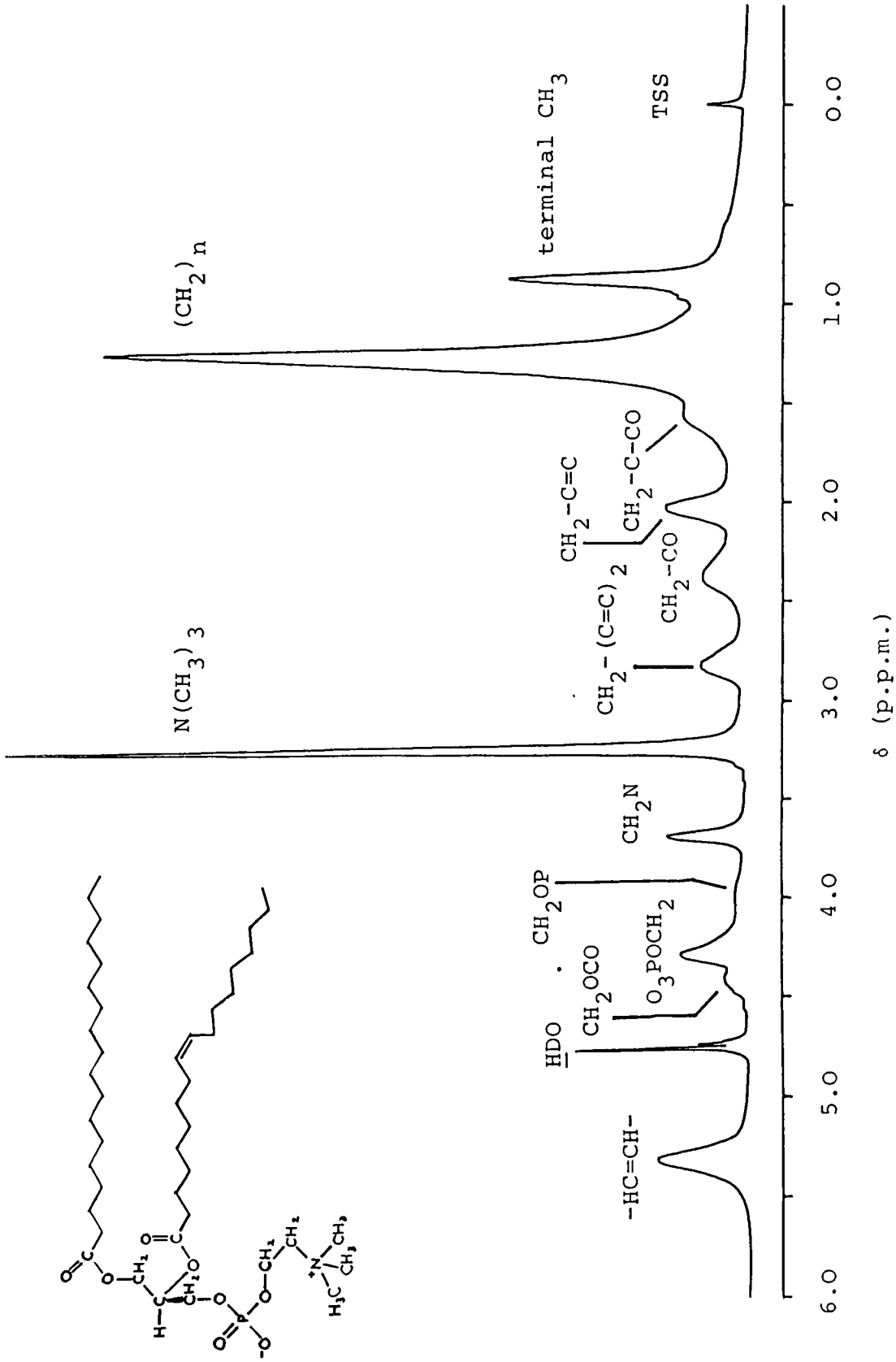

of PC monolayers that calcium has no observable effect at concentrations below 10^{-5} M; binding studies by radio-isotope counting of ^{45}Ca found that the count rate became significant at 10^{-4} M, a concentration also found to be significant in electrophoretic mobility measurements. It is interesting to compare the concentration required for the onset of turbidity in a vesicle sample, which was found to be 1 mM, with the rate of precipitation rising rapidly above 100 mM Ca^{2+}.

The question of the effect of calcium and other alkaline earth ions on binding to phospholipids in bilayer vesicles has aroused great interest in recent years. This is because membranes *in vivo* are known to fuse controllably (14,15) and vesicle systems have been used as a model system for studying this phenomenon. Duzgunes and Ohki (16) found that PC and mixed phosphatidylcholine/phosphatidylserine (PC/PS) vesicles will interact with phospholipid membranes in a reaction which is vesicle and calcium concentration dependent. Papahadjopoulos et al (17) and Day et al (18) followed the fusion of PS vesicles with the addition of calcium. Both studies showed that addition of calcium causes cochleate cylinders to form from sonicated bilayer vesicle dispersions; on addition of EDTA, these cylinders reformed as large monolayer vesicles. Day et al (18) kept the calcium concentration below the threshold for precipitation and found that the process could be followed by both dynamic light scattering and turbidity measurements, but the formation of unilamellar vesicles was not apparent in the latter technique, making certain observations ambiguous. Liao and Prestegard (19) found that fusion of PC/phosphatidic acid mixed vesicles was controlled by ionic radius as well as cation concentration. They found that Ca^{2+} and Cd^{2+} were the most effective at fusing vesicles, whilst Mg^{2+}, Ba^{2+} and Eu^{3+} caused less effect. They concluded that the ionic radius of Ca^{2+} and

and Cd^{2+} is ideal for an intermediate formed during vesicle fusion. They suggested that this intermediate must be stabilised by the phosphatidic acid to bring about minimum leakage of the vesicle contents. This is in contrast to the cochleate cylinders discussed above, which spill the solution contained within the vesicle. Zimmerberg et al (20) determined that calcium is effective in causing lipid fusion at micromolar concentrations (about 10 μM) and that this rate of fusion is not affected by the presence of Mg^{2+} in millimolar concentrations. This specificity for calcium over magnesium was further investigated by Wilschut et al (21). Calcium was found to induce fusion of PS vesicles, with complete spillage of the internal contents. They further found that at concentrations of calcium close to the threshold for fusion, the presence of magnesium cooperates to bring it about; at higher calcium concentrations, the magnesium has an inhibitory effect.

The mechanism by which the fusion proceeds was investigated by Tokutomi et al (22) using PS, PC and phosphatidyl-ethanolamine. They described the changes as an induced phase separation in the membrane. This separation was calcium induced and occured at a calcium concentration of 1.4×10^{-7} M for the PS/PE vesicles and at 1.2×10^{-6} M for the PS/PC system. These are the lowest concentrations of calcium recorded for phase changes to phospholipid systems. Studies of PS vesicles (23-29) have further demonstrated the capacity of calcium to bring about phase and conformational chagnes in the vesicles and, ultimately, to cause "crystallisation" of the bilayers. Hauser and Shipley

(23) showed that Li^+ is also capable of "crystallising" the lipids into hexagonal arrays in a gel state. A recent study from the same authors (29) showed that the different alkaline earth ions behave in different ways with PS bilayer vesicles. Calcium brings about a gel to liquid crystal bilayer transition at 39°C with a further transition occurring at about 155°C, immediately followed by PS decomposition. They suggest from X-ray data at 20°C that Ca^{2+}-PS complexes exhibit bilayer structures and that each hydrocarbon chain is "crystallised" on calcium binding.

6.1.3 The Formation of Solid Phases Within Bilayer Vesicles

Various examples of membrane-limited granules of solids have been identified in biological systems (30-32); these are normally associated with the isolation of unwanted elements in the internal organs. It is possible to cause precipitation of a solid phase inside a bilayer vesicle by entrapping one of the components of the final mineral and then allowing the other, or others, to diffuse through the membrane causing precipitation as the two components mix. It is interesting to determine if the form that the precipitate takes is identical to, or different from, the form of a similar precipitate under test-tube conditions. Previous studies have succeeded in precipitating $Co(OH)_2$ (33), Ag_2O (34,35), Fe_3O_4 (36), CoS, $CoSiO_3$ and Ag_2SiO_3(37). The silver oxide system has been shown to be crystalline in an identical form to the test-tube product, but $Co(OH)_2$ was an amorphous solid when precipitated within vesicles. Mann et al (38,39) have discussed the varying factors controlling ion transport across membranes and nucleation points within vesicles.

6.1.4 Vesicles In Biological Calcification

Biology has evolved a mechanism for utilising phospholipid vesicles in mineralisation. The use of "Membrane Limited Mineralisation" occurs mainly in those systems which construct solid structures from amorphous silica (40) but crystalline magnetite (41) and certain calcium carbonate structures are also formed within a vesicle. The best example of this is the coccolith which have been discussed in chapter 4 but corals (42), the cestode corpuscle (43) and the mid-gut of insects (44) all have intracellular vesicles which contain calcium carbonate. In the case of the last three, this calcification is a concentrically layered structure which also contains magnesium and phosphate in large quantities. The delicate structuring of the coccoliths is unique in calcium carbonate mineralisation, closely resembling the amorphous silica diatoms in their morphologies (45).

Extracellular vesicles are commonly observed in calcium phosphate forming species but have not been observed in invertebrates. These matrix vesicles may play a role in the mineralisation of cartilage and skin (46), but current theories of bone and teeth formation do not favour vesicle action (47).

The mechanism by which biology utilises these vesicles is not understood, even for the simplest cases, but the problems found with ion binding and consequent disruption to the vesicle are obviously dealt with. This could be done by using sophisticated ion pumps, similar to those found in mitochondia or thylakoid membranes, or by restricting the number of ions in the vicinity of the vesicle.

6.1.5 Gold in Vesicles: A Chemical Approach to Chrysotherapy

The use of gold drugs has been known for many centuries, but current understanding of the biochemistry of gold is still limited (48). The major application of gold drugs is currently in the treatment of rheumatoid arthritis (chrysotherapy) (49), but there is also much interest in the accumulation of the metal in other organs of the body, where it appears to bring about a wide range of deliterious effects (50). It has been observed that a rheumatoid arthritis (RA) patient undergoing chrysotherapy develops membrane-enclosed particles of gold-containing material in the synovial tissue at the site of the disease. The drugs normally administered are complexes of Au^{+} with an organic thiol, such as Au-Thiomalate ("Myocrisin"), Au-β-D-Thioglucose ("Solganol-B-Oleosum") or simple $Na_3Au(S_2O_3)_2$ ("aurothion") (51). At first, it was thought that the gold vesicles, or "Aurosomes" were small particles of pure Au(0), the product of a reduction of the drug which could not be repeated by chemical means (52) but use of electron X-ray microprobe analysis (53) has demonstrated the presence of sulphur and phosphorus as well as gold in the structures. It is now believed (54) that the aurosome is formed as the result of disulphide linkages forming and causing the drug molecules to precipitate. Recent work (55) has shown that Au(0) itself will interact with amino acids, in particular the thiol containing acids to give solutions of gold complexes. This might be one mechanism by which gold is absorbed through the skin.

The chemistry of the reduction of gold salts has mainly been studied by colloid chemists. Frens (56) found that the formation of colloidal gold by reduction of Au^{3+} as $HAuCl_4$ with citrate was controlled by the concentration of citrate used;

thus controlled particle sizes ranging from 16 nm to 150 nm could be obtained by decreasing the citrate added to the solution. These experiments were carried out at 100°C. More recent work (57-59) has studied the particles formed by evaporating gold onto NaCl crystals at 300°C under vacuum by ultra-high resolution electron microscopy. They found that a variety of multiply-twinned particles were formed in decahedral, icosahedral and "poly-icosahedral" morphologies.

6.1.6 The Aim of This Study

It was hoped to continue the work described above by precipitating calcium carbonate within a vesicle system and thence adding varying organic and inorganic components, including the soluble matrix proteins described above, in order to control the formation of the mineral. In addition, the reduction of gold within bilayer vesicles by chemical reduction at room temperature was studied. The reactions were followed by light scattering measurements, ^{1}H-nmr spectroscopy and electron microscopy, including ultra-high resolution electron microscopy for the gold system. Part of the study of precipitates in vesicles was carried out with Professor Grover W. Everett Jr., during his sabbatical from the Department of Chemistry, University of Kansas, U.S.A.

6.2 The Preparation of Vesicles

The specific constituents of each vesicle system are described below, but a general preparative method was followed for each type of vesicles.

Phosphatidylcholine (Grade 1) from egg yolk was obtained as a solution in chloroform/methanol (4:1) under nitrogen from Lipid Products. This was diluted with the same solvent to form a stock solution of 25 mg cm^{-3}. This solution was kept at $4^{o}C$ to prevent oxidisation of the lipid. Vesicles were prepared by evaporating the solvent from 2 cm^3 of the stock solution using a rotary evaporator with a liquid nitrogen trap. In order to completely remove the methanol, the sample was heated to about $45^{o}C$ in a water bath. Evaporation was complete within 20 minutes. The lipid was removed from the wall of the flask by swirling 4 cm^3 water, or the solution to be entrapped within the vesicle, aided by a few glass balls. This produced a milky suspension of gross liposomes and micelles which was sonicated in an MSE probe sonicator at about 9 μm peak-to-peak for 5 to 10 minutes until the solution had become opalescent. The sonication process produced vesicles with a diameter of about 30 nm (4) giving an internal volume of about 10^{-17} cm^3. The final concentration of vesicles obtained was 17mM. The theoretical yield was calculated and shown in Table 6.I.

When ions were to be encapsulated within the vesicles, they were removed from the bulk solution by passing the sonicated solution down a Pharmacia PD-10 disposable column which is packed with Sephadex G25 medium and accepts volumes up to 3 cm^3 and will separate large molecular weight moities from small ions with a dilution of only 30%. The column was equilibrated before use

Table 6.I

Vesicle Dimensions

Assume outer vesicle radius = 200 Å

inner vesicle radius = 160 Å

Thus the lipid layer is 40 Å thick

Volume of lipid in vesicle = $4/3\pi(r_o^3 - r_i^3)$

$= 4/3\pi(8 \times 10^6 - 4.096 \times 10^6)$

$= 1.64 \times 10^7$ Å^3

$= 1.64 \times 10^{-17}$ cm^3

Assume a density of 1.0 g cm^{-3}

Thus one vesicle contains 1.64×10^{-17} g lipid.

The RMM of phosphatidylcholine = 787 g mol^{-1}

Thus one vesicle contains $\frac{1.64 \times 10^{-17}}{787}$

$= 2.08 \times 10^{20}$ moles of lecithin

$= 2.08 \times 10^{20} \times 6.02 \times 10^{23}$

= 12 545 molecules

Ratio of outer : inner surface areas is given by

$$\frac{A_o}{A_i} = \frac{4\pi r_o^2}{4\pi r_i^2} = \frac{r_o^2}{r_i^2} = 1.56$$

Thus $\frac{1.00}{2.56}$ = 0.39 of the molecules will be in the inside layer of the vesicle as follows:-

$$4\ 893_{in} + 7\ 652_{out} = 12\ 545_{total}$$

Table 6.I continued

Relative nmr peak areas, in/out = 4893/7652 = 0.64

The effective RMM of a vesicle = 787 x 12 545

$= 9.9 \times 10^{6}$ daltons

Inside aqueous volume = $4.3\pi(160)^{3}$

$= 1.72 \times 10^{7}$ Å^{3}

$= 1.72 \times 10^{-17}$ cm^{3}

Thus capacity of vesicle is 9.53×10^{-19} moles of water which is 573 706 molecules H_2O.

A 50 mg sample of phosphatidylcholine will prepare 3.05×10^{15} vesicles of the stated dimensions.

with water or NaCl solution in order to prevent osmotic effects on the vesicles; all solutions used were in D_2O when the sample was being prepared for study by ^1H-nmr.

6.2.1 Preparation of Calcium Carbonate in Vesicles

Calcium will not cross a lipid bilayer unassisted and thus the first method of preparation attempted involved encapsulating the cations within the vesicle. It was found that these vesicles were not stable, as shown by light scattering, particularl at high calcium concentrations when sonicating did not produce an opalescent solution which was an indication that the vesicles had not formed. Carbonate ions will not cross a lipid bilayer, and thus hydrogen carbonate was used, together with an increase in pH to move the hydrogen carbonate : carbonate equilibrium to the right. The pH change was probably not detected inside the vesicle, since there is a lag in the equilibration (38) across the membrane.

When Professor Everett arrived in Oxford, work began on aspects of the ionophore antibiotic Lasalocid A (X537-A) which was incorporated into the vesicles as a vehicle for transporting calcium across the membrane. Vesicles prepared for this form of experiment involved the encapsulation of carbonate ions within the vesicles and then calcium was added outside them and transported across the membrane. The advantages of this method were that the quantity of calcium to interact with the lipid could be carefully regulated and that the pH was at a level to bring about fast precipitation (see below) without adjustments being required.

6.3 Results

6.3.1 ^{1}-NMR Studies of Vesicles

The assigned PC vesicle spectrum at 300 MHz is shown in Figure 6.1. Many of the resonances have an asymmetrical character due to the inequality of molecules on the outside and inside layers. Peaks which are affected by the presence of ions arise from the hydrophilic components of the lipid. Thus the O_3POCH_2 resonance, at δ = 4.28 ppm, the CH_2N peak, at 3.69 ppm and the $N(CH_3)_3$ peak at 3.25 ppm will be affected by the addition of ions. Figure 6.2 shows the effect of adding Co^{2+} to a vesicle sample. The major peak affected is at 4.28 ppm, the outside component of which is broadened. If the same experiment is carried out in the presence of lasalocid (Figure 6.2c) the $N(CH_3)_3$ peak develops a side band as the internal signal is affected more than the outside signal due to the sequestering of the metal ion into the vesicle. The effect of metal ions on bilayer vesicles is demonstrated even more strikingly in Figures 6.3 and 6.4. Figure 6.3 shows the effect of adding 10 μM Pr^{3+}, a lanthanide which acts as a shift probe. The $N(CH_3)_3$ signal is split as only the outer signal is perturbed. Also affected is the CH_2N signal, but those arising from the protons adjoining the phosphate group are not particularly affected. In contrast, Figure 6.4 shows the effect caused by adding the same concentration of Pr^{3+} to a vesicle sample containing lasalocid. This spectrum was recorded immediately after the addition, and it is apparent that the lanthanide has accumulated inside the vesicles as well as the outside, causing both $N(CH_3)_3$ peaks to shift downfield. Also affected are the CH_2N peaks. In this spectrum no signal is observed from the O_3POCH_2 group. This could be due to the

Figure 6.2

(a) Phosphatidylcholine bilayer vesicles

(b) The same sample with the addition of 10 mM Co^{2+}

(c) The same experiment in the presence of Lasalocid

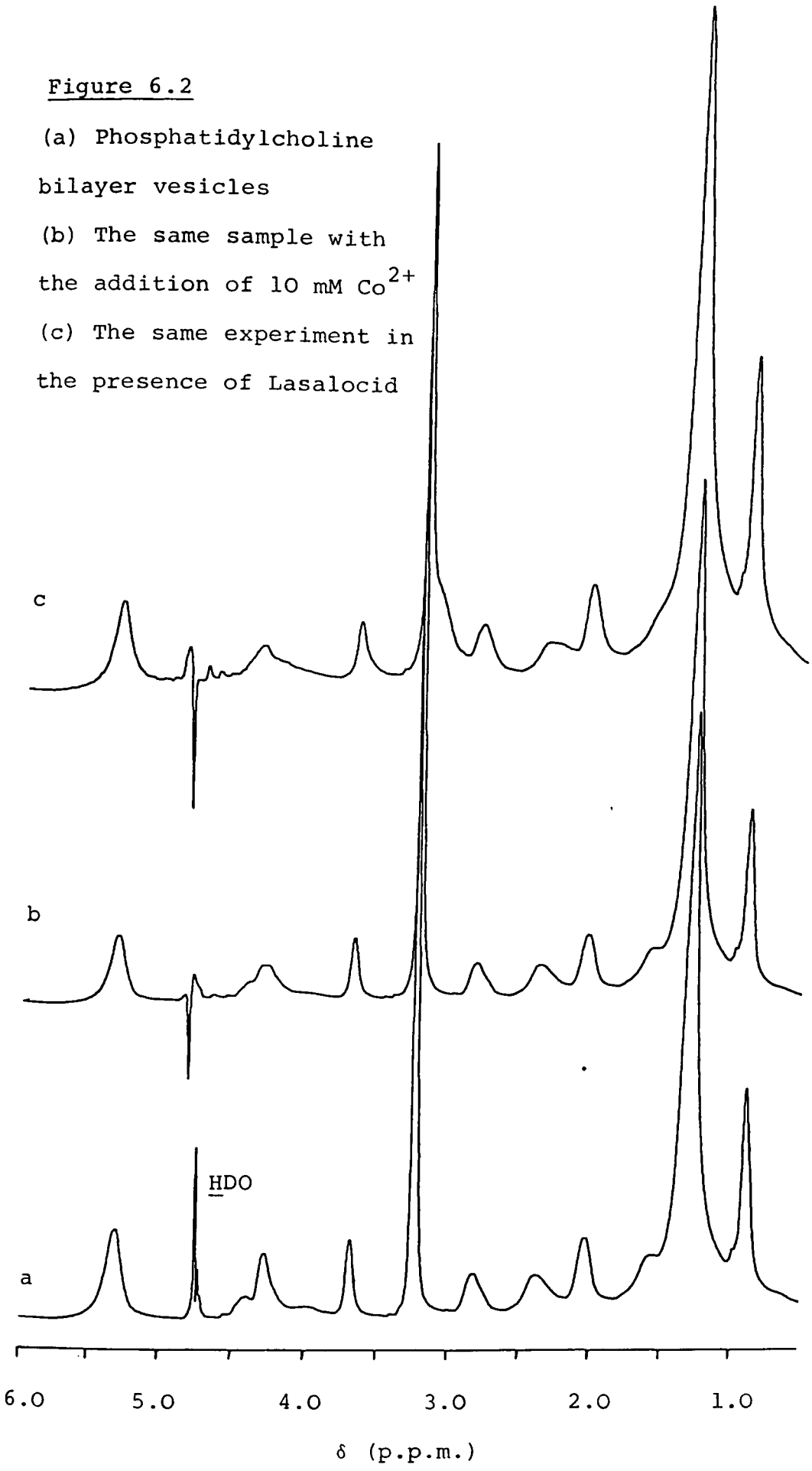

Figure 6.3

(a) Phosphatidylcholine vesicles (17 mM)

(b) The same sample with the addition of 10 μM Pr^{3+}

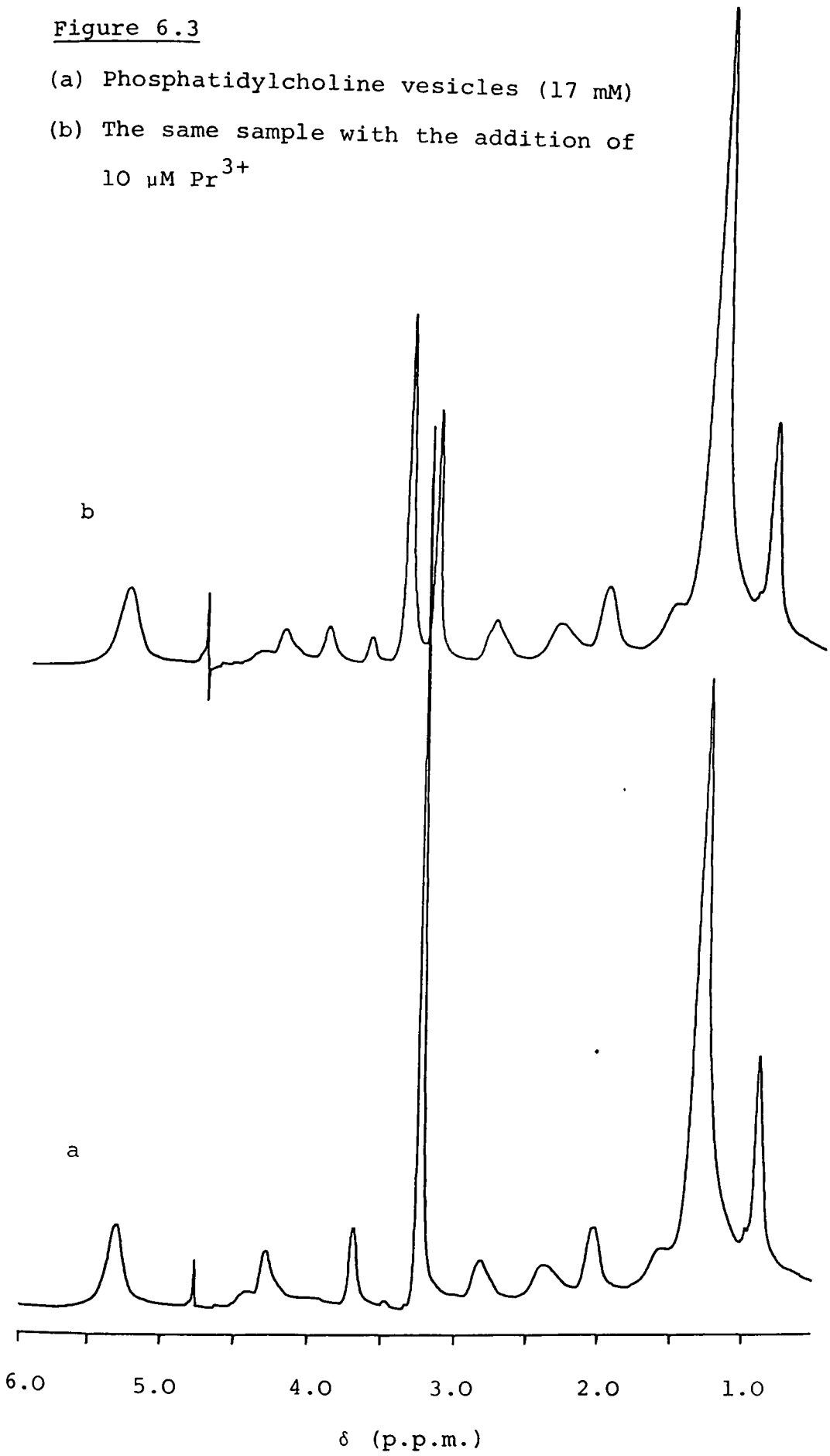

Figure 6.4

(a) Phosphatidylcholine vesicles with 1 mM Lasalocid

(b) The same sample with the addition of 10 μM Pr^{3+}

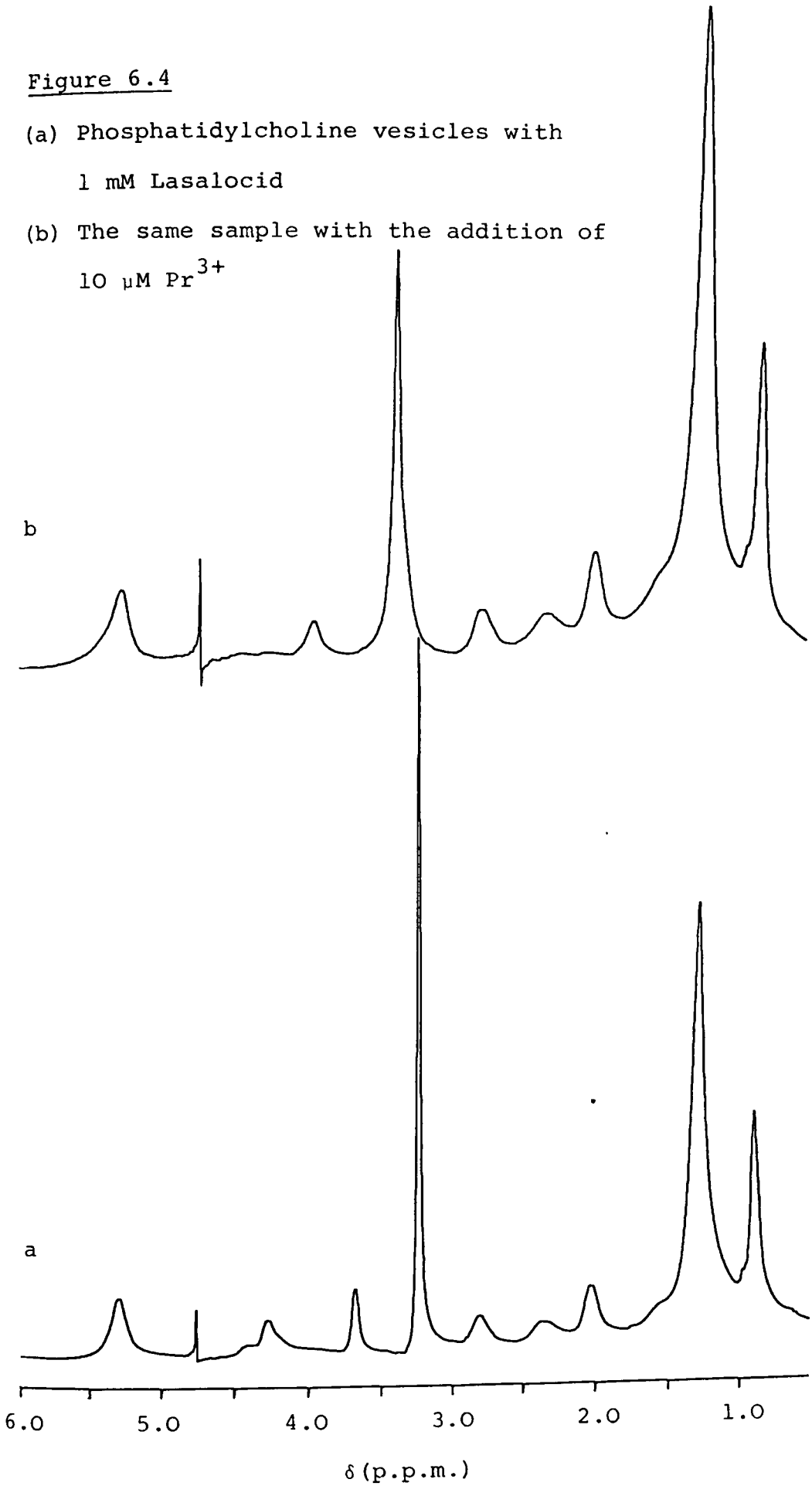

downfield shift being large enough to carry it into the area affected by the solvent suppression irradiation.

It was hoped to follow the progress of mineral formation by the change in peak shape as the metal ions were removed from the membrane into the bulk of the vesicle, but this proved to be insensitive given the problems encountered with the stability of the vesicles.

6.3.2 Calcium Carbonate in Vesicles

The successful preparation of calcium carbonate in vesicles proved to be very difficult due to the problems encountered with calcium binding to the lipid although a great deal of effort was made to obtain a stable system. The experiments attempted are described in detail below, but generally involved stabilising the system by creating isotonic conditions, complexing the calcium present or limiting the concentrations of the ions to calculated theoretical optima. This phenomenon is now well understood (see section 6.1.2 above) but the problem proved to be insurmountable for vesicles prepared without an ionophore. Precipitates were obtained, but they either had no lipid associated with them, or the precipitate occurred on sheets of lipid. This is shown in Figure 6.5. Electron microscopy was used to determine the nature of the precipitates obtained and X-ray microprobe analysis determined whether the calcium carbonate was associated with phospholipid, or not.

Samples prepared with lasalocid-A in the lipid enabled a much closer control to be kept upon the system. The theoretical concentrations of calcium and carbonate required to bring about precipitation within the vesicular space were determined (see

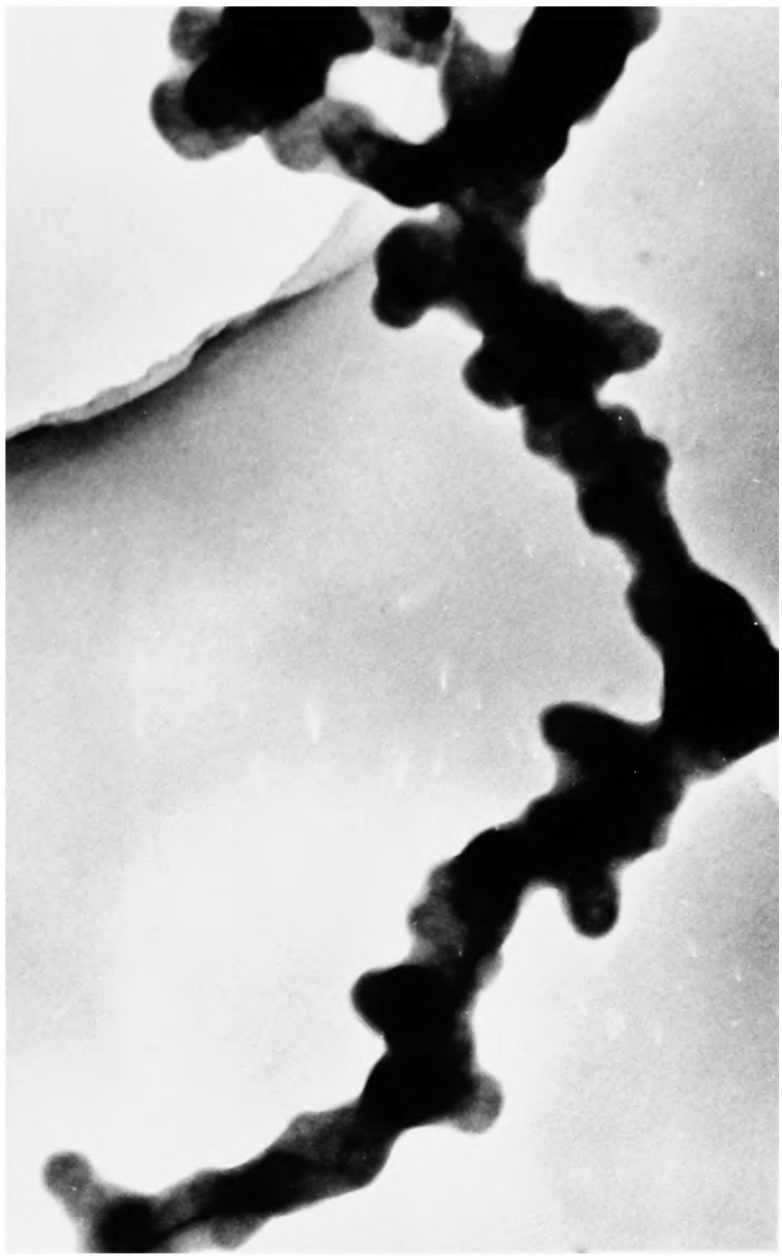

Figure 6.5

TEM of calcium carbonate precipitated in conjunction with the phospholipid from the vesicle solution. The lipid can be seen as a dark line, about which the mineral has formed.

Magnification = x120 000

Table 6.II

Calculation of Carbonate Concentration Within Vesicles

i) Outside Vesicles - Cations

From Haynes and Pressman (63) the following complexation constants for membrane-bound lasalocid are given:

$$L^-_{membrane} + Ca^{2+}_{aq} \rightleftharpoons L\text{-}Ca^+_{membrane} \qquad K_{Ca} = 10^{3.2}$$

$$L^-_{membrane} + Na^+_{aq} \rightleftharpoons L\text{-}Na_{membrane} \qquad K_{Na} = 10^{1.9}$$

$$L^-_{membrane} + H^+_{aq} \rightleftharpoons L\text{-}H_{membrane} \qquad K_{H} = 10^{6.8}$$

H^+ will compete with Ca^{2+} for lasalocid binding unless the $Ca^{2+}/\ H^+$ ratio is high:

$$K_{Ca} = \frac{[L\text{-}Ca^+_{mem}]}{[L^-_{mem}]\,[Ca^{2+}_{aq}]}$$

$$K_{H} = \frac{[L\text{-}H_{mem}]}{[L^-_{mem}]\,[H^+_{aq}]}$$

Then:

$$\frac{[L\text{-}Ca^+_{mem}]}{[L\text{-}H_{mem}]} = \frac{K_{Ca}\ [Ca^{2+}_{aq}]}{K_H\ [H^+_{aq}]} = 10^{-3.6}\ \frac{[Ca^{2+}_{aq}]}{[H^+_{aq}]}$$

Thus at pH = 7, $[Ca^{2+}_{aq}]$ must be greater than 10^{-3} in order to compete with H^+. At higher pH, this value decreases.

ii) Inside vesicles - carbonate

$$CO_3^{2-} + H^+ \rightleftharpoons HCO_3^- \qquad K = 10^{10.2}$$

$$CO_3^{2-} + Ca^{2+} \rightleftharpoons CaCO_3 \qquad K = 10^{-8.1}$$

$$\frac{[HCO_3^-]}{[CO_3^{2-}]} = 10^{10.2}\,[H^+]$$

Thus a 1:1 ratio is obtained at pH = 10

Assume inner radius of vesicle = 160 Å

$$= 1.6 \times 10^{-7} \text{ dm}$$

Then, inner vesicle volume, V $= 4/3\pi r^3$

$$= 1.72 \times 10^{7} \text{ Å}^3$$

$$= 1.72 \times 10^{-20} \text{ l}$$

Using a 100 mM Na_2CO_3 solution at pH = 10,

$$[CO_3^{2-}] = 50 \text{ mM}$$

$$= 0.05 \text{ mol } l^{-1}$$

Thus, carbonate concentration in one vesicle is given by

$$0.05 \times 1.72 \times 10^{-20} = 8.6 \times 10^{-22} \text{ moles}$$

$$= 6.0 \times {}^{23} \times 8.6 \times 10^{-22}$$

$$= 516 \text{ ions}$$

If $CO_3^{2-} = 5.0 \times 10^{-2}$, to initiate a precipitate of $CaCO_3$, we need

$$[Ca^{2+}][CO_3^{2-}] = 10^{-8.1}$$

$$[Ca^{2+}] = \frac{10^{-8.1}}{5.0 \times 10^{-2}}$$

$$= 1.59 \times 10^{-7} \text{ mol } l^{-1}$$

Thus, calcium concentration, for precipitation, in one vesicle

$$= 1.59 \times 10^{-7} \times 1.72 \times 10^{-20}$$

$$= 2.74 \times 10^{-27} \text{ moles}$$

$$= 6.0 \times 10^{23} \cdot 2.74 \times 10^{-27}$$

$$= 1.64 \times 10^{-3} \text{ ions}$$

Thus the solubility product will not allow $[Ca^{2+}]$ inside the vesicle to exceed 1.6×10^{-7} mol l^{-1} if pH = 10 (or higher)

Consider the competition between H^+ and Ca^{2+} for lasalocid:

$$\frac{[L\text{-}Ca^{+}_{mem}]}{[L\text{-}H_{mem}]} = 10^{-3.6} \frac{[Ca^{2+}_{aq}]}{[H^{+}_{aq}]} = \frac{10^{-3.6}(1.6 \times 10^{-7})}{(10^{-10})}$$

$$= 0.4$$

Consider the competition between Na^+ and Ca^{2+} for lasalocid:

$$\frac{[L\text{-}Ca^{+}_{mem}]}{[L\text{-}Na_{mem}]} = \frac{K_{Ca}\ [Ca^{2+}_{aq}]}{K_{Na}\ [Na^{+}_{aq}]} = 10^{1.3} \frac{[Ca^{2+}_{aq}]}{[Na^{+}_{aq}]}$$

$$= \frac{10^{1.3}(1.6 \times 10^{-7})}{2 \times 10^{-1}}$$

$$= 3.2 \times 10^{-5}$$

Thus sodium should be exported from the vesicle.

Tables 3.II and 3.III) and used in preparations. Under a close regime, it was possible to obtain calcium carbonate precipitation within vesicles, but the system remained unstable and there was a tendency for the lipids to fuse after precipitation had occurred. Figure 6.6 shows a typical preparation of this sort. A few isolated vesicles are present (arrows), but the majority of the sample has coagulated and the precipitate can be observed massed together within a large coating of lipid.

This sample was also studied at ultra-high resolution with Dr. S. Mann. Great difficulty was experienced in successfully imaging the precipitate as calcium carbonate is not very electron dense and also because it tends to form a hollow "shell" precipitate within a vesicle. Examples of high resolution images are shown in Figure 6.7. Analysis of powder electron diffraction patterns at 100 keV obtained from the sample revealed that the polymorph of calcium carbonate formed was calcite (Figure 6.8). The sample was not stable under the electron beam and consequently it was not possible to obtain diffraction patterns and images from the same sample. The difficulty in imaging at 200 keV led to most work being carried out on an analytical electron microscope. The vesicle samples were shown to contain calcium carbonate by X-ray microprobe analysis. Signal-to-noise levels were not good due to the very small size of the sample, but a typical spectrum is shown in Figure 6.9.

These results were not obtained consistently and one part of the study involved trying to optimise the conditions for vesicle stability.

Table 6.III

Calculation of Volume of Calcium Carbonate Crystallising Within a Bilayer PC Vesicle

Assume outer vesicle radius = 200 Å

inner vesicle radius = 160 Å

$CaCO_3$ forms a ring 20 Å wide

Thus lipid layer is 40 Å wide

Inner vesicle volume $= 4/3\pi r_i^3$

$= 1.72 \times 10^7$ Å^3

$= 1.72 \times 10^{-20}$ dm^3

Let Na_2CO_3 be 0.5 M.

Then concentration of CO_3^{2-} inside vesicle

$= 0.5 \times 1.72 \times 10^{-20}$

$= 8.58 \times 10^{-21}$ moles

$= 5164$ ions

Volume of $CaCO_3$ formed is $(r_i^2 - r_{ii}^2)t$ where t is the thickness of the layer in centimetres

$V = (160 \times 10^{-8})^2 - (140 \times 10^{-8})^2 t$

$= 1.88 \times -12\ t$ (cm^2)

Density of $CaCO_3$ (calcite) $= 2.71$ g cm^{-3}

RMM $CaCO_3 = 100$

Number of moles of $CaCO_3 = \dfrac{2.71 \times 1.88 \times 10^{-12} t}{100}$

$= 5.11 \times 10^{-14} t$

Number of formula units of $CaCO_3 = 5.11 \times 10^{-14} t \times N$

$= 3.08 \times 10^{10}$

In order to account for 5164 CO_3^{2-} ions:

$3.08 \times 10^{10}\ t = 5164$

$t = 1.68 \times 10^{-7}$ cm

Thus

$= 16.8$ Å

If this $CaCO_3$ were spread evenly around the inner vesicle surface, the thickness would be about 1 Å:

$$\text{Volume of } CaCO_3 = \frac{8.58 \times 10^{-21} \times 100}{2.71} = 3.17 \times 10^{-19} \text{ cm}^3$$

$$= 317\,000 \text{ Å}^3$$

This volume would be contained in a cubic crystal of side length 68.2 Å.

But, using $V = 4/3\pi(160)^3 - r_{ii}^3 = 317\,000$

$r_{ii} = 159$ Å and the thickness of the $CaCO_3$ layer = 160 Å - 159 Å = 1 Å

Thus in order to image a crystal, it must not form as an even shell inside the vesicle.

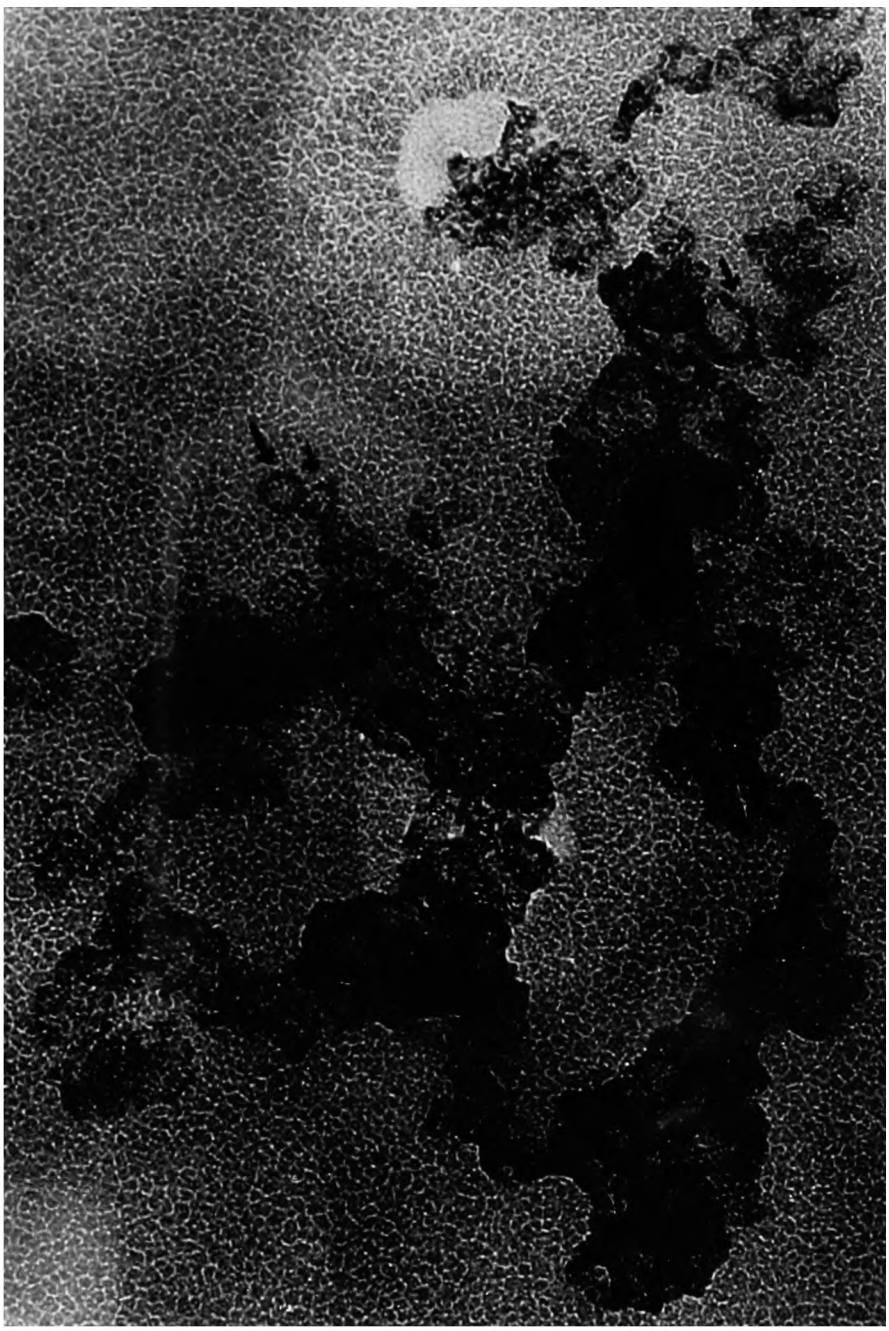

Figure 6.6

Electron micrograph of $CaCO_3$ formation in bilayer vesicles. The mineral is laid down in a hollow coat within the vesicle. Arrows show the few isolated vesicles; others have fused as the carbonate is precipitated. Magnification = x294 000

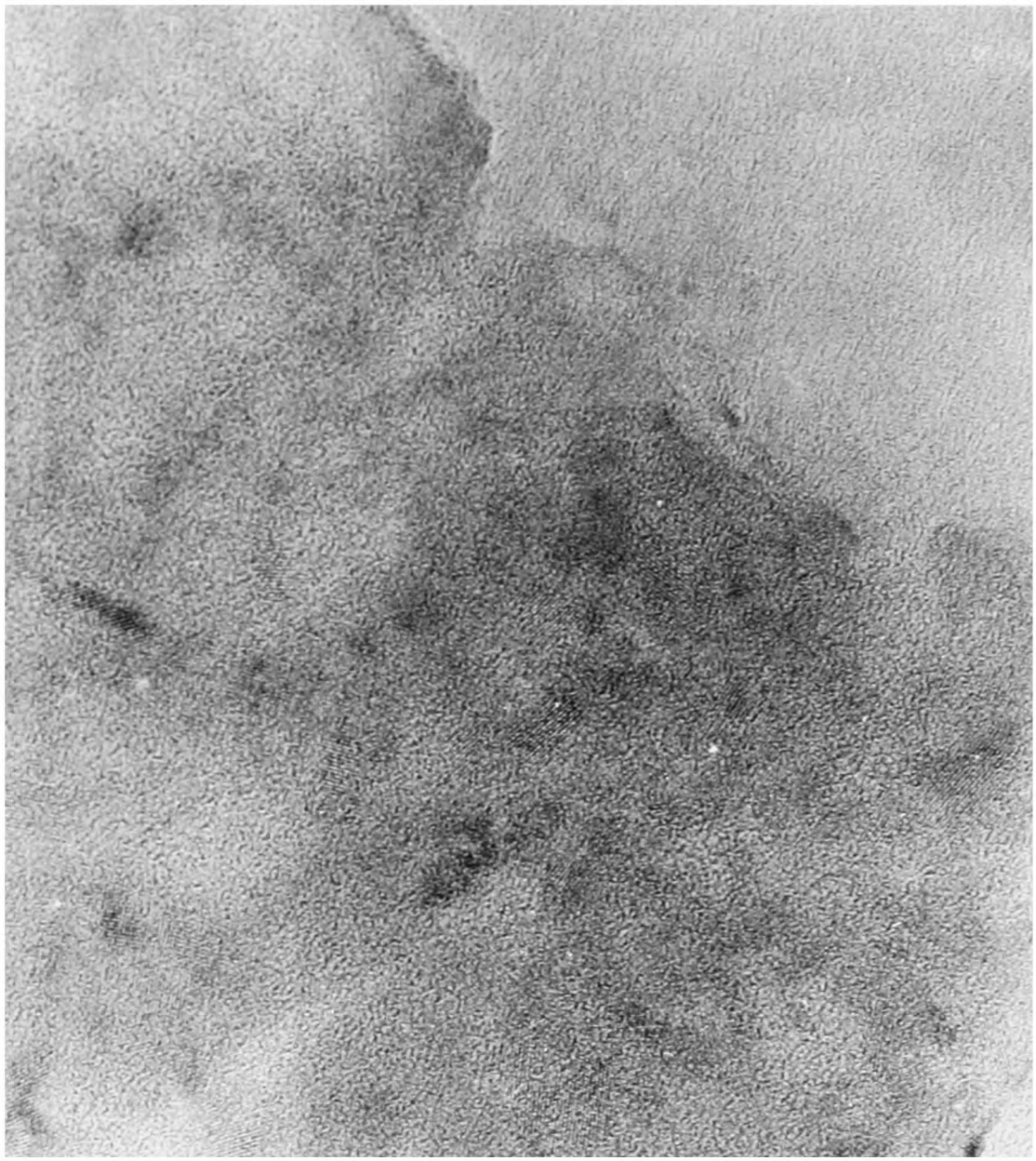

Figure 6.7

High resolution micrograph of a sample of calcium carbonate in bilayer vesicles. Lattice fringes may just be made out, suggesting that there are several points of nucleation within the vesicale.

Magnification = x2 000 000

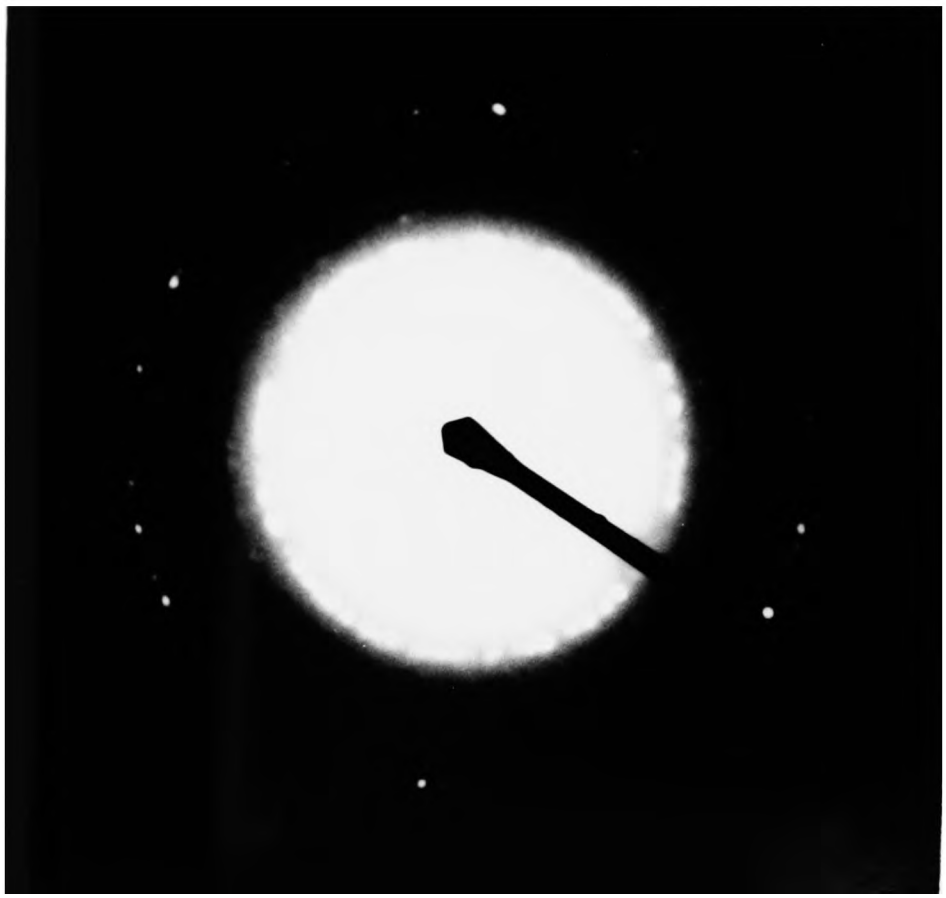

Figure 6.8

Powder electron diffraction pattern from the sample shown in Figure 6.7. The pattern is of calcite, and the strong reflections are due to the (104), (110) and (116) faces, moving out from the centre.

Figure 6.9

X-ray microanalysis of calcium carbonate precipitated in bilayer vesicles

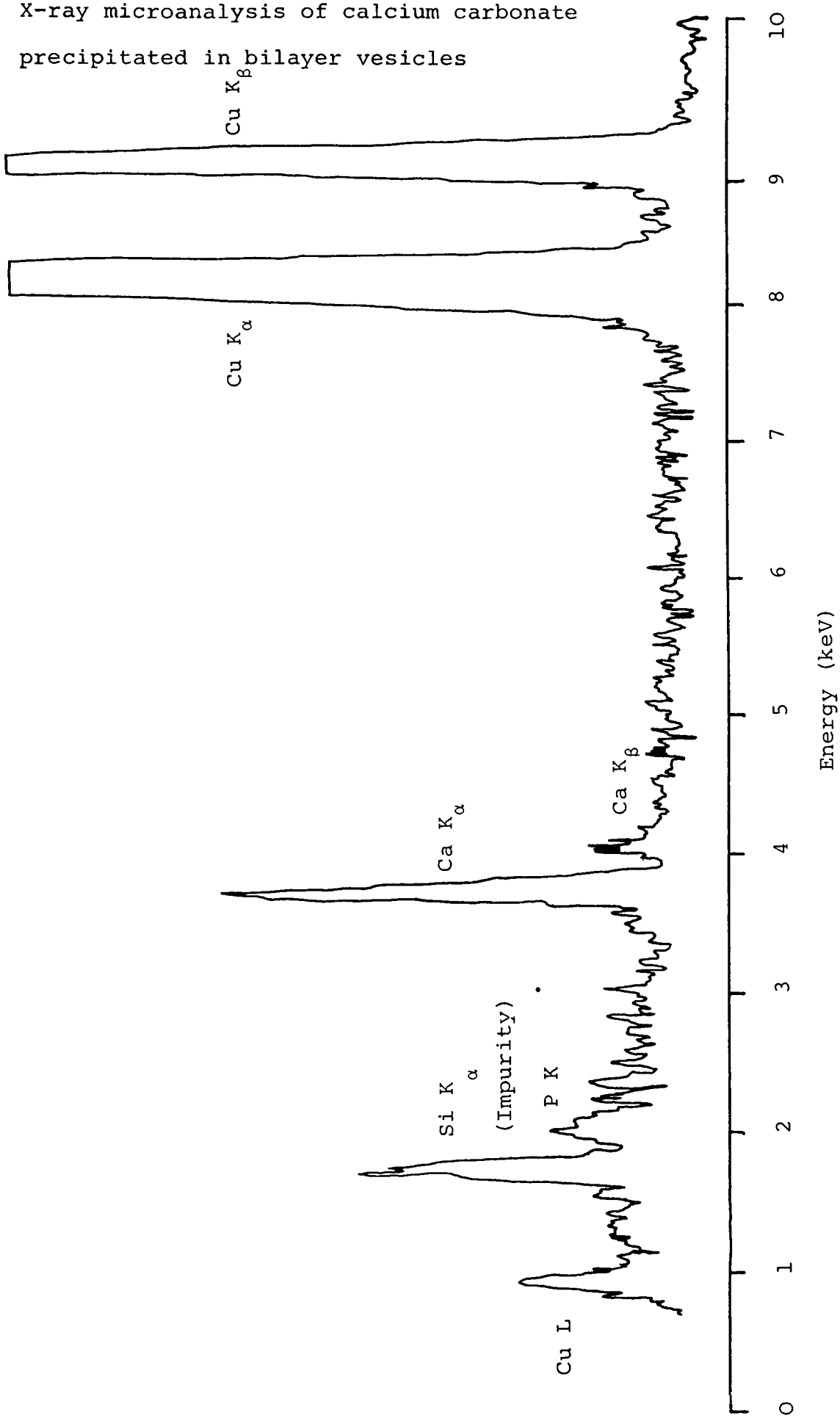

6.3.3 The Stability of Vesicles in Solution

The stability investigations were carried out on vesicles with and without lasalocid-A. In the first experiment, vesicles were prepared containing 0.5 M Na_2CO_3 and 0.5 M NaCl outside. Light scattering experiments on a Cary 17 spectrophotometer at 600 nm indicated that the system was stable for 15 minutes, after which time, 50 µl of 1M $Ca(NO_3)_2$ was added. Over a period of 1.5 hours, the absorbance rose by only 0.03, which is not a significant change. The experiment was repeated with the same result. A further experiment, which balanced the ionic charge on either side of the lipid by putting the vesicles in 0.75 M NaCl, again gave no significant precipitation results, but indicated that the vesicles themselves were stable throughout the experiment under isotonic conditions. These conditions were used for all subsequent experiments.

One explanation to account for the poor results obtained was that the vesicles were separated from the carbonate ions in the bulk solution, which had a pH of 11, into an NaCl solution with a pH of about 7. It was reasoned that there would be a movement of protons across the membrane to equilibrate the pH leading to the export of Na^+ ions. The incoming protons would cause a very rapid drop in pH within the vesicle, causing the CO_3^{2-} to be lost across the membrane as CO_2. As a consequence, no reaction had previously been observed since there was little or no carbonate inside the vesicle. This hypothesis was tested by equilibrating vesicles which contained lasalocid, in order to facilitate easy ion transport, with a 0.75 M solution of NaCl at pH = 12. Addition of calcium ions into the bulk solution brought about a rapid increase of absorbance, which continued to rise

over a 2 hour period, a total rise of 0.42. Similar results were obtained, however, when a blank experiment which did not use lasalocid was run. Electron microscopy showed that these vesicles tended to break up with the addition of calcium, although precipitate was observed associated with sheet-like structures of lipid.

In order to determine the efficiency of the passage of ions across the membranes, pH titrations were carried out on two vesicle samples, with and without lasalocid. The vesicles contained 0.5 M $NaHCO_3$ and were in 0.5 M NaCl. Blank experiments were run on the NaCl solution and water. The results of the experiments are shown in Figure 6.10. The theoretical curve was obtained as shown in Table IV. It was determined that the passage of ions across the membrane was sufficiently rapid for vesicles without the ionophore to reduce the pH from its expected level; the passage of protons out of the vesicles is enhanced markedly in the presence of the lasalocid, however. The final solution was tested for carbonate; the negative result of this test led us to conclude that the suppression of the pH was due entirely to the export of protons from the vesicles (with the corresponding import of Na^+).

The passage of calcium in a vesicle system was followed by the use of the complexing indicator murexide. At pH = 12 the murexide anion, which is blue-violet, complexes calcium at concentrations of 10^{-5} M (pCa = 5) with a concommitant colour change to red. A 10 mM solution of ammonium murexide was prepared at pH = 11.85 and was tested by adding 10 μmoles of calcium to an aliquot. The violet colour became red and was not reversed by the addition of 10 μmoles Na_2CO_3 to the solution. When a 10-fold excess of Na_2CO_3 was added, the colour became a darker

Figure 6.10

pH titration of HCO_3^{2-}-containing PC vesicles

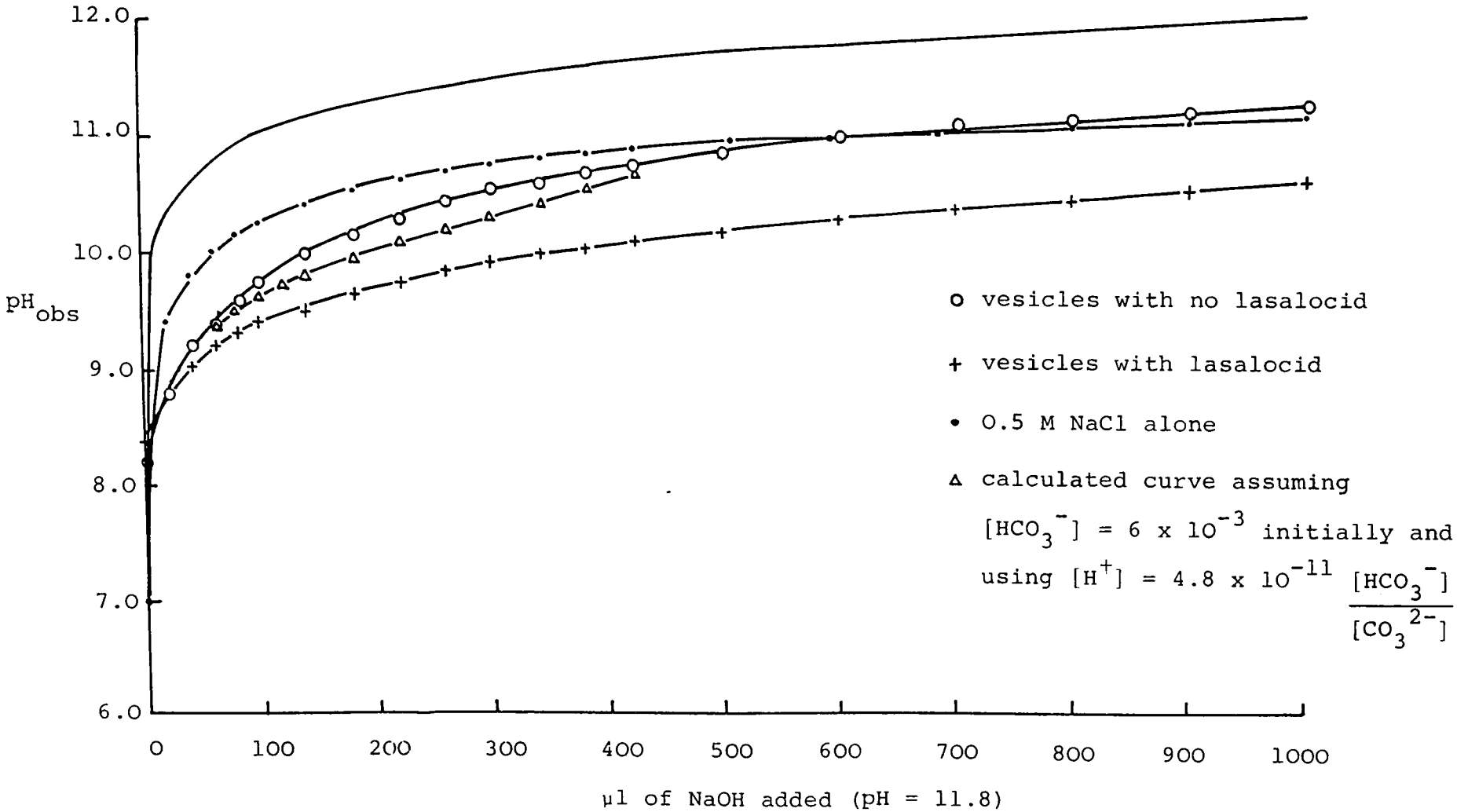

Table 6.1V

Determination of Theoretical Curve for Vesicle pH Titration

Assume outer vesicle radius = 200 Å

Assume inner vesicle radius = 160 Å

Thus vesicle volume = 1.72×10^{-20} l

Assume 3×10^{15} vesicles per 50 mg preparation.

But one titration uses only one quarter of the preparation.

Thus, the total internal volume of all vesicles in the titration is

$$(0.75 \times 10^{15}) \times (1.72 \times 10^{-20})$$

$$= 1.3 \times 10^{-5} \text{ l}$$

$$= 1.3 \times 10^{-2} \text{cm}^3$$

Thus total number of moles of HCO_3^- is

$$(1.3 \times 10^{-2}) \times 0.5 = 0.65 \times 10^{-2} \text{ moles}$$

Thus 0.6×10^{-2} = ml NaOH $\times 10^{-2}$ M

Thus ml NaOH = 0.65

Then 650 ul is required to titrate all HCO_3^- to CO_3^{2-}.

(The pH will be about 11 at this point)

Assuming no buffering,

$$1 \text{ ml} \times 10^{-4} \text{ NaOH} = \text{ml NaOH} \times 10^{-2} \text{ M}$$

$$\text{ml NaOH} = 10^{-2}$$

Thus 10 µl are needed to reach pH = 10,

100 µl are needed to reach pH = 11, and

1 ml is needed to reach pH = 12

red but did not revert to its original purple. Murexide also complexed calcium in direct competition to carbonate ions when the latter was in a 10-fold excess of the other two ions.

A sample of vesicles was prepared containing 10 mM murexide at pH = 9.8 in water at the same pH. Murexide was cleared from the outside of the vesicles by being passed through a desalting column twice, resulting in a pale violet solution. An absorption spectrum was run, which showed a maximum at 520 nm, and 10 µmoles of calcium was added. The absorption maximum approximately doubled in intensity and shifted to 500 nm, which is consistent with the formation of the calcium complex (59). It was concluded that the calcium had disrupted the vesicles in order to complex with the murexide as the sample had no ionophore in it. An attempt to repeat the experiment under isotonic conditions caused the murexide to precipitate.

6.3.4 The Formation of Gold in Vesicles

Gold was precipitated within vesicles by trapping the reducing anion, originally sulphite, but also citrate, in the intra-vesicular space. The anion was cleared from the outside of the vesicles by desalting on a PD-10 disposable column and 0.1 mls of a 10 mM solution of $HAuCl_4$ added to the resulting vesicle solution. This gold complex had been prepared in the laboratory by dissolving about 350 mg of gold foil in aqua regia. The resulting solution was evaporated nearly to a solid and then redissolved in concentrated HCl. This process was repeated several times until a dark red hygroscopic solution was obtained which analysed as $HAuCl_4.4H_2O$. Vesicles were also prepared which contained 2.7 mg lasalocid in the lipid. The presence of the ionophore caused an increase in the rate of precipitation, as

Figure 6.11

Light scattering experiment of change of absorbance at 600 nm with the addition of $AuCl_4^-$ to SO_3^- - containing vesicles

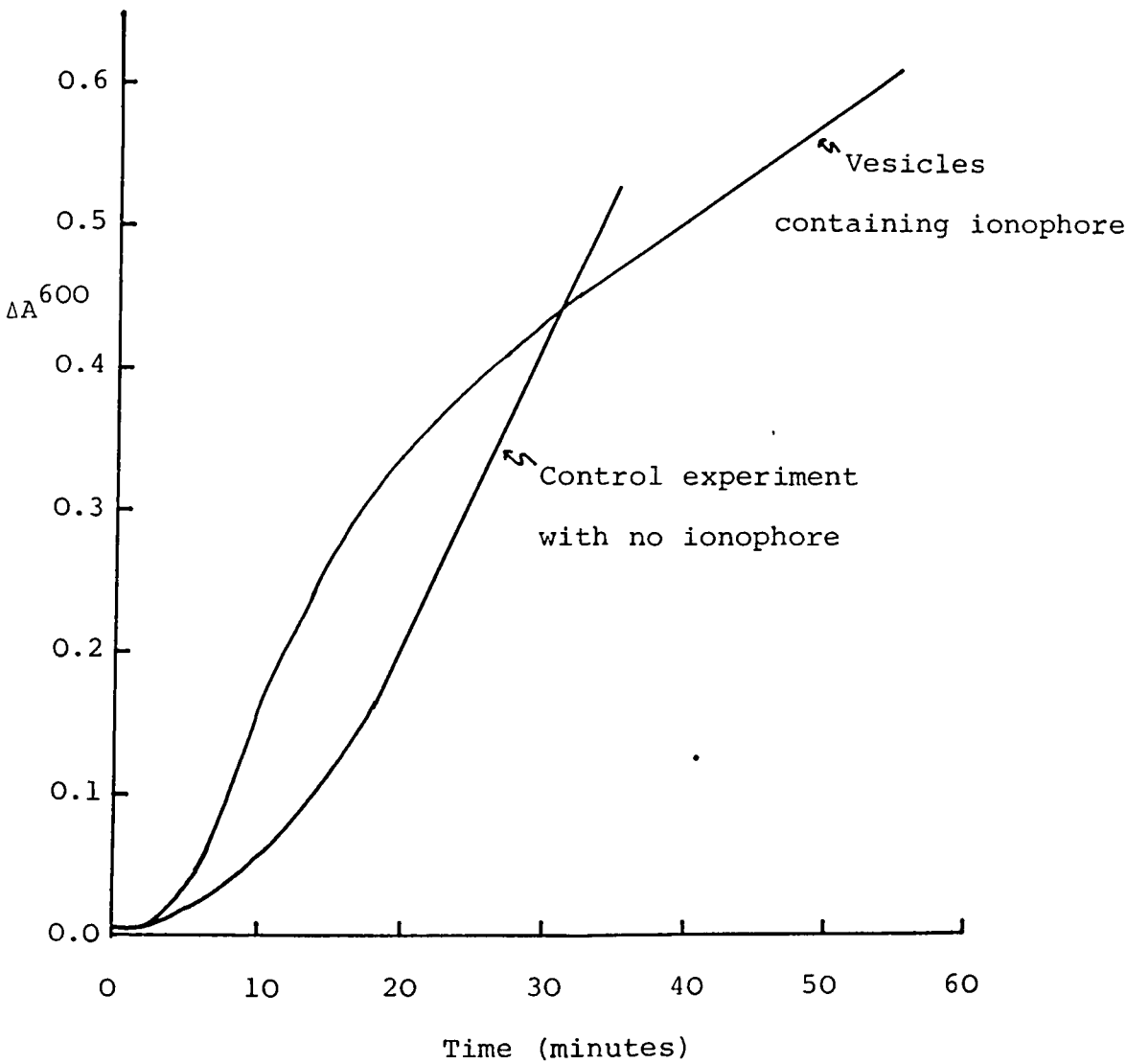

measured by light scattering (Figure 6.11). The reason for this change was thought to be that the lasalocid exported sodium ions as the gold complex passed through the membrane. The complex itself may have become a neutral species, $AuCl_3$, before crossing the vesicle wall, but this is uncertain. The visible absorption spectrum (Figure 6.12) shows a maximum at 530 nm, which makes the average particle size in the precipitate between 300 Å and 350 Å (56). Statistical analysis (Figure 6.13) of the particles seen in the electron microscope found that they had diameters between about 200 Å and 350 Å, although a very few particles outside this range were observed; the most common diameter lying between about 250 Å and 300 Å. Electron microscopy revealed that the particles are a variety of morphologies, but normally with curved sides. Figure 6.14 shows some particles under the analytical electron microscope which clearly show the gold precipitate surrounded by a less electron dense coating which appears to be the vesicle. X-ray microanalysis on the sample (Figure 6.15) shows gold peaks and phosphorus present as a side peak on the Au M with which it coincides. Photographs taken at ultra-high resolution (Figures 6.16-6.18) reveal that the particles exhibit twinning and also have clearly defined faces. This observation is in agreement with the results of Smith and Marks (57-59); their observations, however are from sputtered samples at low pressure and high temperatures.

The d-spacings visible on the gold particles are all of the (110) face and were measured as 2.7 Å (gold is a cubic symmetry crystal and hence zones are synonomous with faces and need no conversion factor). The actual d-spacing for a (110)

Figure 6.12

Visible spectrum of ionophore-containing vesicles 1 hour after the addition of $AuCl_4^-$ solution

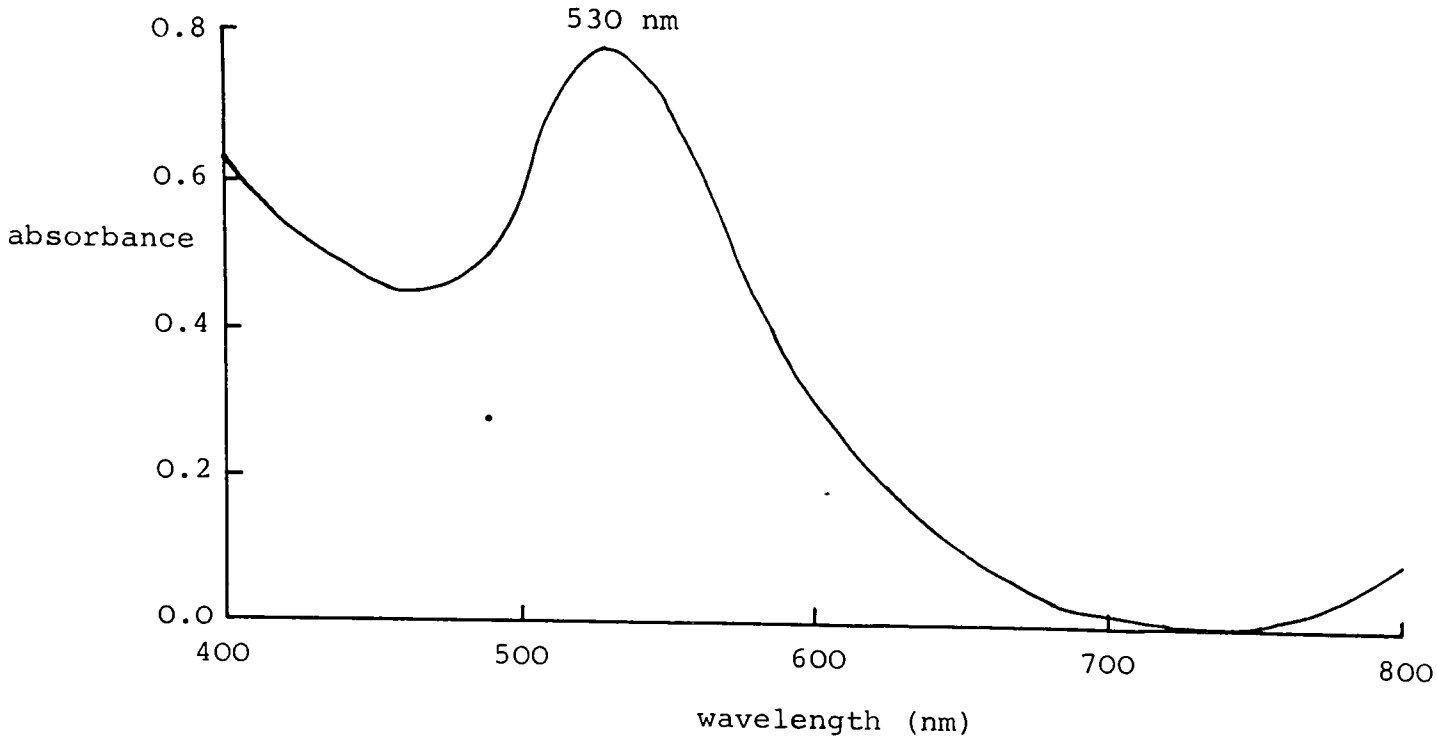

Figure 6.13

Distribution of sizes of gold particles precipitated within PC vesicles

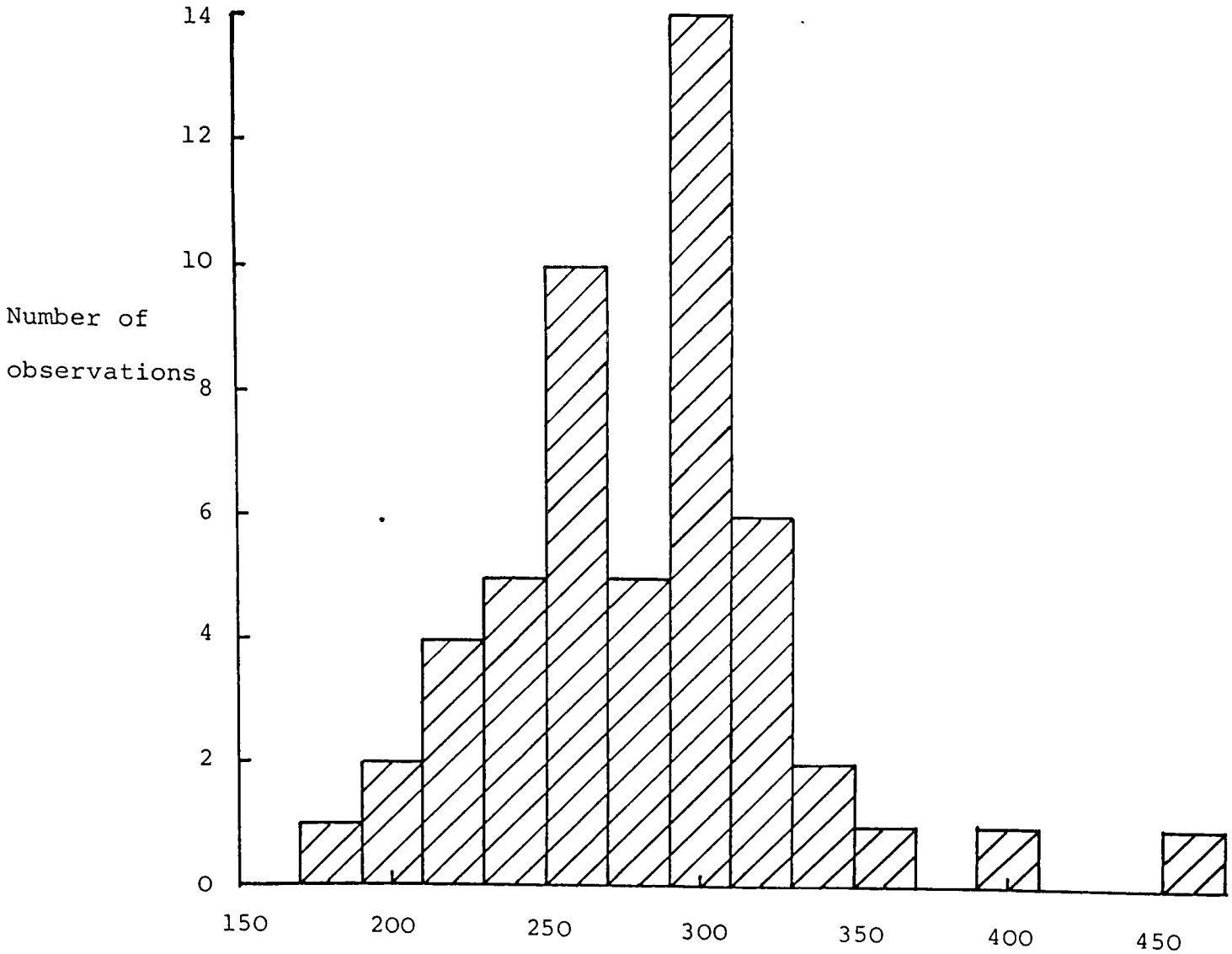

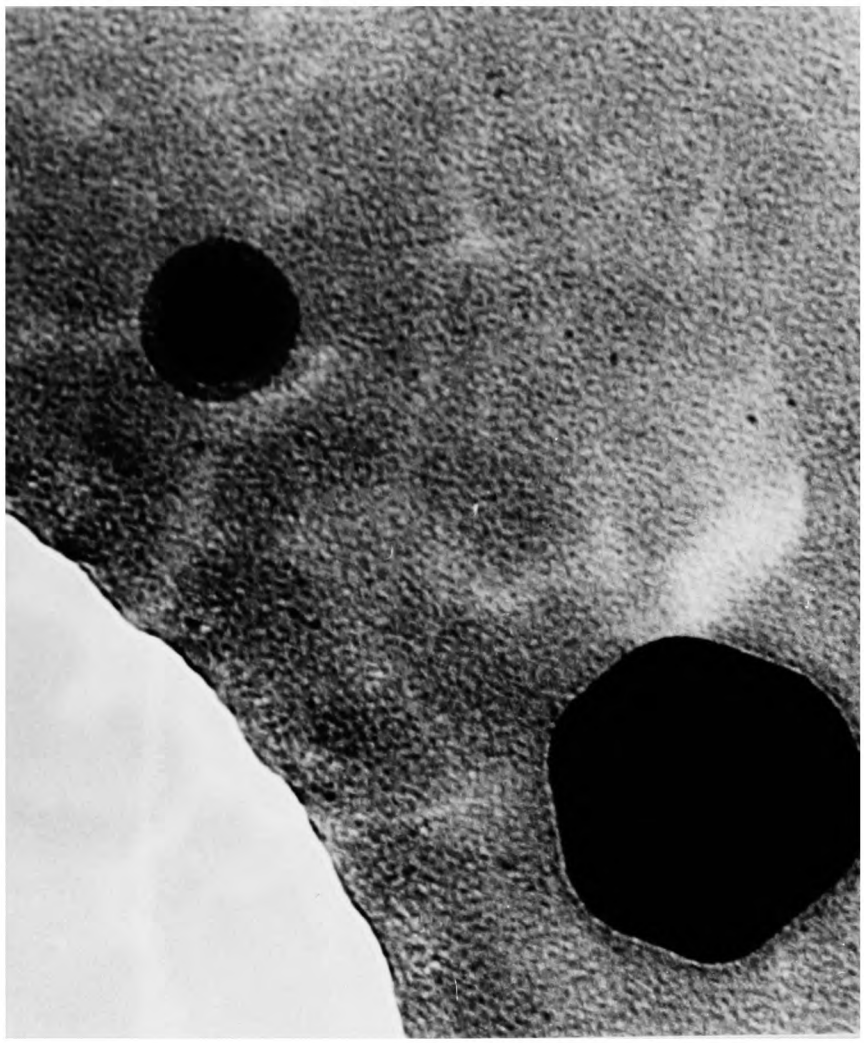

Figure 6.14

TEMs of gold precipitated within bilayer vesicles clearly showing the organic lipid around the precipitate. This is presumably due to heavy metal binding to the lipid head-groups.

Magnification = x480 000

Figure 6.15

X-ray microanalysis of gold in vesicles

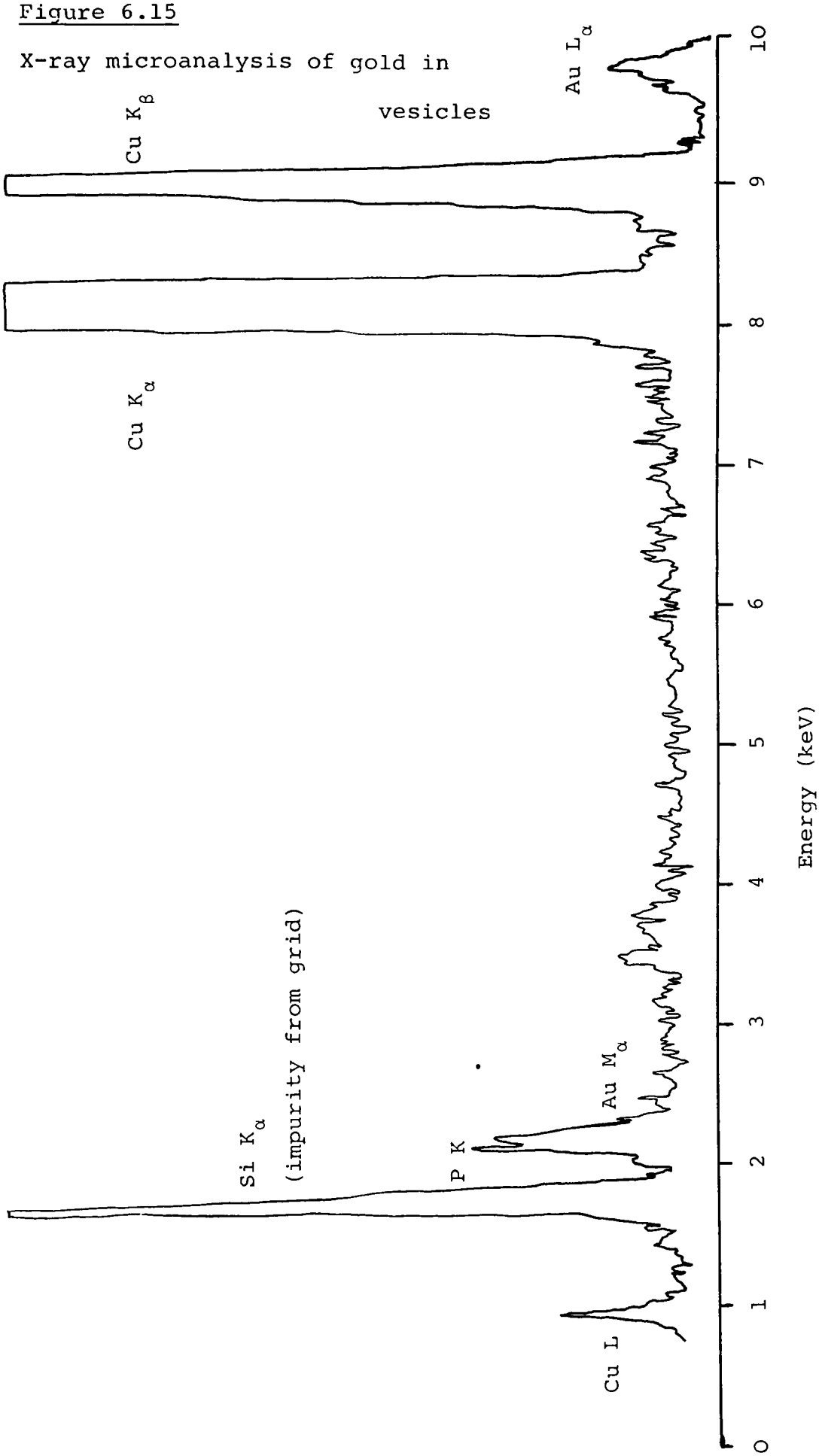

face is 2.88 Å, but without a diffraction pattern to give a precise alignment of the face under study, this error was not unexpected.

The same reaction was attempted with citrate as the reducing agent, but this caused the vesicles to break and the particles to clump together as shown in Figure 6.19. Sulphite acted as a controlled reducing agent and consequently was selected for repeating this reaction under different concentrations of reducing agent,rather than follow the experimental method of Frens (56). It was determined that, for the most part, the vesicles act as the limit to crystallisation, although some larger crystals were found due to the lysing of the vesicles.

6.4 Discussion

6.4.1 Problems in Forming Calcium Carbonate in Vesicles

The use of phospholipids as a control mechanism in biomineralisation is known to occur in several species. Using vesicles as a chemical model of this process, however, can give rise to several problems of stability. The use of calcium brings about conformational changes, and, often, disruption of the membrane. In this work, it was found to be possible to prepare calcium carbonate in vesicles, but despite a great deal of work, it was not possible to stabilise PC vesicles to enable a preparation to be carried out as a routine matter. This problem arises for almost all of the common phospholipids, either singly, or in mixtures.

Recent work has shown that it is possible to form calcium phosphate in a multilamellar liposome (Eanes, personal communication This uses a 7:2:1 mixture of phosphatidylcholine, dicetyl phophate

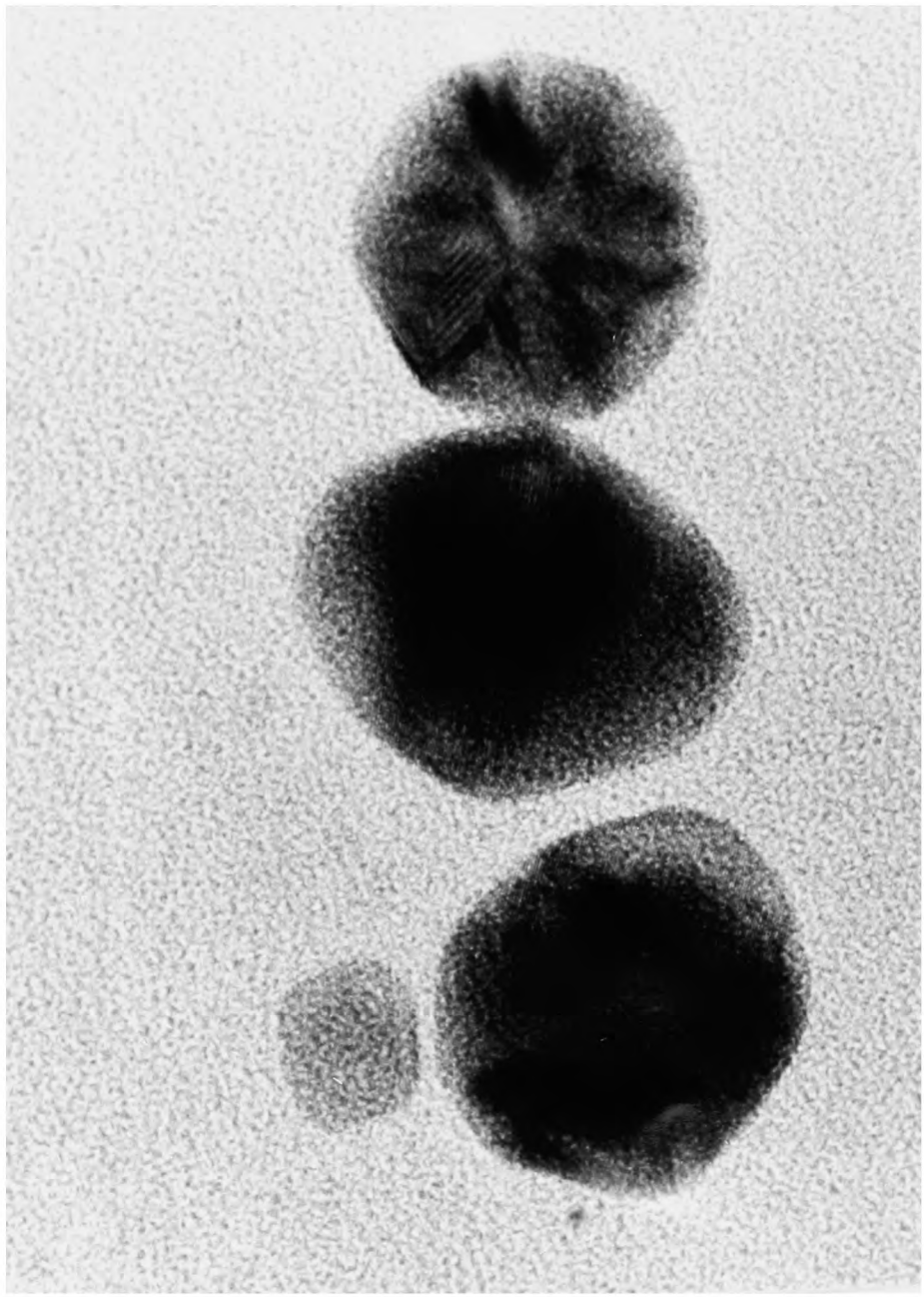

Figure 6.16

HRTEM of gold precipated within bilayer vesicles.

Each example shows a different morphology.

Magnification = x2 210 000

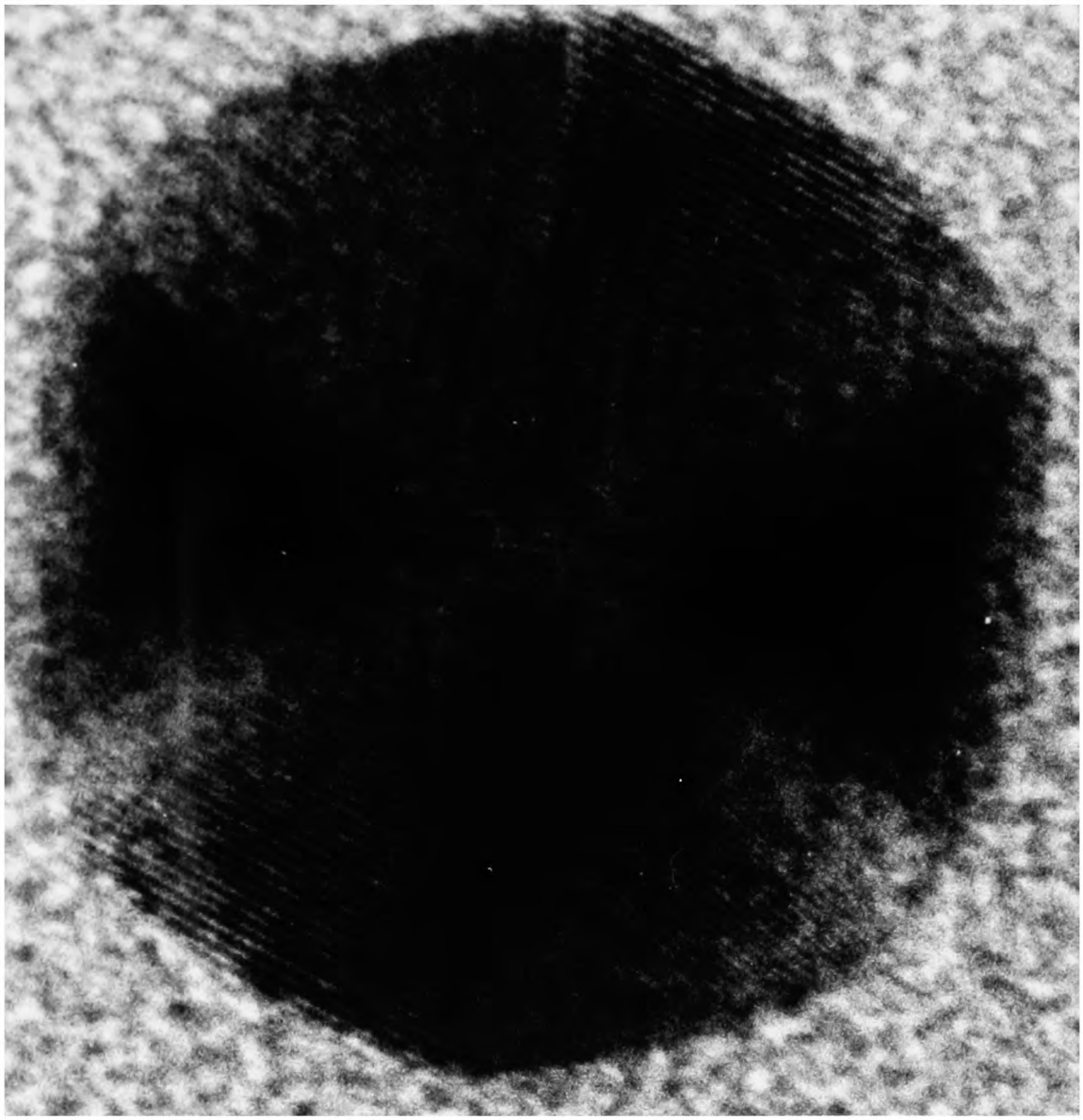

Figure 6.17

Ultra-high resolution micrograph of gold precipitated within bilayer vesicles. This is a single crystal in an octahedral structure, viewed down the apex.

Magnification = x7 000 000

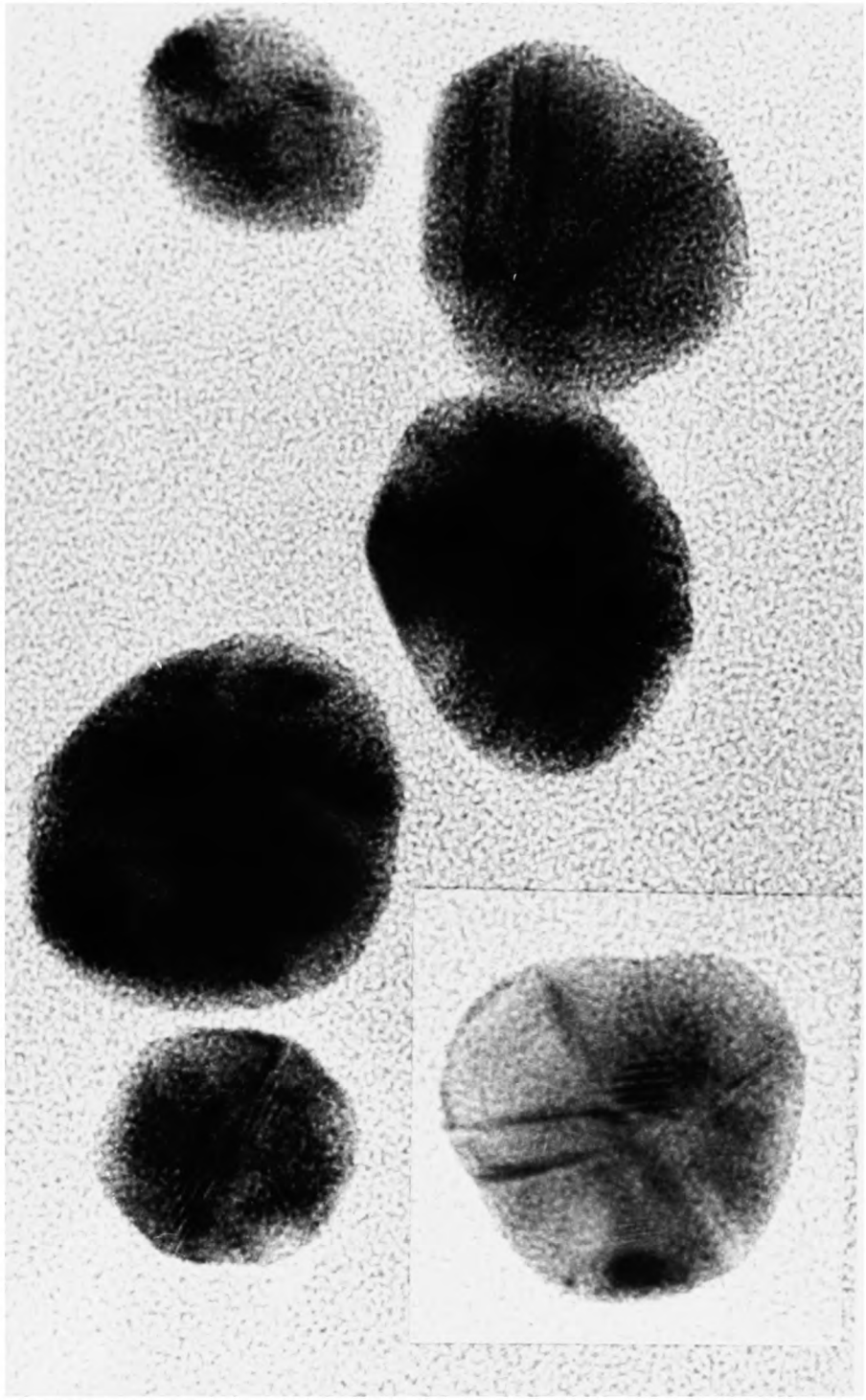

Figure 6.18

High resolution images of gold particles precipitated within bilayer vesicles, showing several different morphologies, including examples of twinning.

Magnification = x2 200 000

Figure 6.19

Gold precipitated by citrate ions break the bilayer vesicles and fuse to form large particles. Here, the process has just begun. Magnification = x250 000

and cholesterol (61,62). The calcium is transported across the membranes by the use of lasalocid. Tests have shown that this vesicle system is stable in the presence of extra-vesicular calcium and although the addition of the ionophore disturbs the lipids slightly, there is no gross breakage of the vesicles. It is possible that the stabilising factor is the dicetyl phosphate and it is not known whether the system is applicable to calcium carbonate formation as well as calcium phosphate.

It is apparent that the conditions of stability of PC bilayer vesicles require that they are strictly isotonic. Even in the absence of calcium, it was observed that isotonic vesicles (i.e. those which were left in the original solution) retained their opalescent condition for at least 24 hours, whereas those which were passed through the desalting column so that the extra-vesicular medium was water lost opalescence in about two hours. Equally, those vesicles eluted against salt solution became increasingly stable, with a peak at isotonic conditions. This indicates that great care must be exercised in the accumulation of ions in vesicles, both *in vitro* and *in vivo*, particularly when there is an ionophore present to facilitate the movement of ions across the membrane.

The relevance of vesicle-limited mineralisation to biological systems which utilise crystalline minerals is not fully understood, but it has been shown that the precipitation of calcium carbonate inside bilayer vesicles is a feasible operation.

6.4.2 Gold in Vesicles

The reduction of Au^{3+} ions to metallic gold inside vesicles is an interesting observation, but cannot be applied to models of aurosomes. As discussed above, aurosomes are not believed to be formed by a reduction of the gold present in the drug, but by a cross-linking of the thiol groups to give an insoluble mass. The accumulation of the structure in a vesicle is due to phagocytosis of the drug-target complex. I am most grateful to Dr. Peter Sadler, Birkbeck College, University of London for helpful discussion arising out of this work and suggestions on applying this research to the complexing of the drugs used.

6.5 References

1. Bangham, A.D., Hill, M.W. and Miller, N.G.A. *Meth. Membrane Biol.* 1, 1-68, (1974)
2. Papahadjopoulos, D., Mayhew, E., Poste, G., Smith, S. and Vail, W.J. *Nature, Lond.* 252, 163-166, (1974)
3. Rondelez, F. and Litster, J.D. *Biophys. J.* 27, 455-460, (1979)
4. Finer, E.G., Flook, A.G. and Hauser, H. *Biochim. Biophys. Acta* 260, 49-69, (1972)
5. Penkett, S.A., Flook, A.G. and Chapman, D. *Chem. Phys. Lipids,* 2, 273-290, (1968)
6. Hauser, H., Phillips, M.C., Levine, B.A. and Williams, R.J.P. *Eur. J. Biochem.* 58, 133-144, (1975)
7. Hauser, H., Phillips, M.C., Levine, B.A. and Williams, R.J.P. *Nature, Lond.* 261, 390-394, (1976)
8. Hauser, H., Hinkley, C.C., Krebs, J., Levine, B.A., Phillips, M.C. and Williams, R.J.P. *Biochim. Biophys. Acta* 468, 364-377, (1977)
9. Levine, B.A., Sackett, J. and Williams, R.J.P. *Biochim Biophys. Acta* 550, 201-211, (1979)
10. Degani, H. *Biochim. Biophys. Acta* 508, 364-369, (1978)
11. Bangham, A.D. and Dawson, R.M.C. *Biochem. J.* 72, 486-492, (1959)
12. Hauser, H. and Dawson, R.M.C. *Eur. J. Biochem.* 1, 61-69, (1967)
13. Santis, M. and Rojas, E. *Biochim. Biophys. Acta* 193, 319-332, (1969)
14. Papahadjopoulos, D., Poste, G. and Schaeffer, B.E. *Biochim. Biophys. Acta* 323, 23-42, (1973)

15. Lucy, J.A. *Nature Lond.* 227, 815-817, (1970)

16. Duzgunes, N. and Ohki, S. *Biochim. Biophys. Acta* 467, 301-308, (1977)

17. Papahadajopoulos, D., Vail, W.J., Jacobson, K. and Poste, G. *Biochim. Biophys. Acta* 448, 265-283, (1975)

18. Day, E.P., Ho, J.T., Kunze, R.K., Jr. and Sun, S.T. *Biochim. Biophys. Acta* 470, 503-508, (1977)

19. Liao, M-J. and Prestegard, J.N. *Biochim. Biophys. Acta.* 601, 453-461, (1980)

20. Zimmerberg, J., Cohen, F.S. and Finkelstein, A. *Science, N.Y.* 210, 906-908, (1980)

21. Wilschut, J., Duzgunes, N. and Paphadjopoulos, D. *Biochemistry* 20, 2126-2133, (1981)

22. Tokutomi, S., Lew, R. and Ohnishi, S-I. *Biochim. Biophys. Acta* 643, 276-282, (1981)

23. Hauser, H. and Shipley, G.G. *J. Biol. Chem.* 256, 11377-11380, (1981)

24. Lin, K-C., Weis, R.M. and McConnell *Nature, Lond.* 296, 164-165, (1982)

25. Rehfield, S.J., Hansen, L.D., Lewis, E.A. and Eatough, D.J. *Biochim. Biophys. Acta* 691, 1-12, (1982)

26. Ohki, S., Duzgunes, N. and Leonards, K. *Biochemistry* 21, 2127-2133, (1982)

27. Hauser, H., Paltauf, F. and Shipley, G.G. *Biochemistry* 21, 1061-1067, (1982)

28. Hauser, H. and Shipley, G.G. *Biochemistry*, 22, 2171-2178, (1983)

29. Hauser, H. and Shipley, G.G. *Biochemistry* (1983) in press

30. Simkiss, K. *Calcif. Tiss. Res.* 24, 199-200, (1977)

31. George, S.G., Coombs, T.L. and Pirie, B.J.S. *Biochim. Biophys. Acta* 716, 61-71, (1982)

32. Simkiss, K. in *"Biomineralisation and Biological Metal Accumulation"* eds. P. Westbroek and E.W. de Jong, 363-371. Pub. D. Reidel, Holland. (1983)

33. Skarnulis, A.J., Strong, P.J. and Williams, R.J.P. *J.C.S. Chem. Comm.* 1030-1031, (1978)

34. Hutchison, J.L., Mann, S., Skarnulis, A.J. and Williams, R.J.P. *J.C.S. Chem. Comm.* 634-635, (1980)

35. Mann, S. and Williams, R.J.P. *J. Chem. Soc. Dalton Trans.* 311-316, (1983)

36. Mann, S., Skarnulis, A.J. and Williams, R.J.P. *J.C.S. Chem. Comm.* 1067-1068, (1979)

37. Mann, S. *D. Phil. Thesis* (1982)

38. Mann, S. Kime, M.J., Ratcliffe, R.G. and Williams, R.J.P. *J. Chem. Soc. Dalton Trans.* 771-774, (1983)

39. Mann, S. *Structure and Bonding* 54, 125-174, (1983)

40. Mann, S., Parker, S.B., Perry, C.C., Ross, M.D., Skarnulis, A.J. and Williams, R.J.P. in *"Biomineralisation and Biological Metal Accumulation"* P. Westbroek and E.W. de Jong (eds) 171-183, (1983). Pub. D. Reidel, Dordrecht, Holland.

41. Blakemore, R.P. and Frenkel, R.B. *Scientific American* 245(6), 42-49, (1981)

42. Kawaguti, S. and Kamishmia, Y. *Publs. Seto Mar. Biol. Lab.* 20, 785-794 , (1975)

43. Nieland, M.L. and von Brand, T. *Exptl. Parasit.* 24, 279-289, (1969)

44. Gouranton, J. *J. Cell. Biol.* 37, 316-328, (1968)

45. See,for example, *"Silicon and Siliceous Structures in Biological Systems"*. T.L. Simpson and B.E. Volcani

(eds). Pub. Springer-Verlag, New York. (1981)

46. Anderson, H.C. *J. Cell. Biol.* 41, 59-72, (1969)

47. Glimcher, M.J. *Proc. Roy. Soc. Lond. B.* (1983) in press

48. Shaw, C.F., III *Inorganic Perspectives in Biology and Medicine* 2, 287-355, (1979)

49. Lorber, A. and Simon, T.M. *Gold. Bull.* 12, 149-158, (1979)

50. Davis, P. *J. Rheumatol. (suppl. 5)* 6, 18-24, (1979)

51. Sadler, P.J. *Structure and Bonding* 29, 171-219, (1976)

52. Sadler, P.J. *Gold Bull.* 5, 110-118, (1976)

53. Ghadially, F.N. *J. Rheumatol (suppl. 5)* 6, 25-30,(1979)

54. Ghadially, F.N. *J. Rheumatol (suppl. 5)* 6, 45-50, (1979)

55. Brown, D.H., Smith, W.E., Fox, P. and Sturrock, R.D. *Inorg. Chim. Acta* 67, 27-30, (1982)

56. Frens, G. *Nature Physical Science* 241, 20-22, (1973)

57. Marks, L.D., Howie, A. and Smith, D.J. *Inst. Phys. Conf. Ser. No. 52. Chapter 9: Electron Microscopy and Analysis* 1979, 397-400, (1980)

58. Marks, L.D. and Smith, D.J. *J. Crystal Growth*, 54, 425-432, (1981)

59. Smith, D.J. and Marks, L.D. *J. Crystal Growth* 54, 433-438, (1981)

60. Schwarzenbach, G. and Flaschka, H. *Complexometric Titrations".* Translated by H.M.N.H. Irving. Pub. Methuen & Co. Ltd. p83ff (1969)

61. Weissmann, G., Collins, T., Evers, A. and Dunham, P. *Proc. Nat. Acad. Sci. USA* 73, 510-514, (1976)

62. Schieren, H., Rudolph, S., Finkelstein, M., Coleman, P. and Weissmann, G. *Biochim. Biophys. Acta* 542, 137-153, (1978)

63. Hayes,D. and Pressman,B. *J. Membrane Biol.* 16, 195-205 (1974)

Chapter 7

^{1}H-NMR Study of Metal-Ion Complexes of Lasalocid-A

7.1 Introduction

Lasalocid-A (formally known as X537-A) is a member of a series of polyether antibiotics, mainly produced by the *Streptomyce* genus (1). It contains two of the cyclic ether groups common to all the members of the series, but is unusual in that it contains a charged group and an aromatic ring. The molecule is shown in Figure 7.1, with the numbering based upon that of Westley (2). Lasalocid-A has the unusual property of complexing divalent and trivalent metal ions and also biogenic amine cations in addition to the more usual 'hard' monovalent cations commonly transported by ionophores. The family of polyether antibiotics have been extensively reviewed from both biological and chemical aspects in a recent publication (3,4).

7.1.1 Structures of Lasalocid-A

Lasalocid-A (LAS) has been studied by several physico-chemical techniques which give some information about its solution and crystal structure. These include X-ray crystallography, ^{1}H- and ^{13}C-NMR and mass spectrometry. Antenuis has found (5) that the uncomplexed molecule in solution is restricted by hydrogen bonds between one oxygen of the carboxy group and 4-OH and the other carboxyl oxygen and 11-OH. This can be seen in Figure 7.2 a and b, which show the normal structure of the molecule; part b having protons added for use in the nmr work.

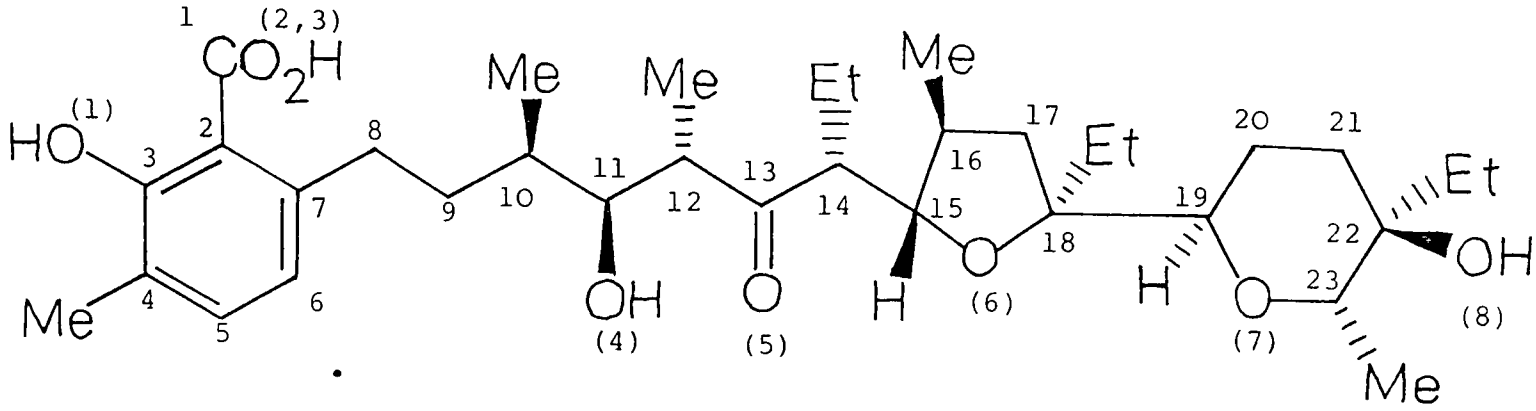

Figure 7.1

The structure of the free acid form of Lasalocid-A with numbering system adapted from that of Westley (2)

Figure 7.2a

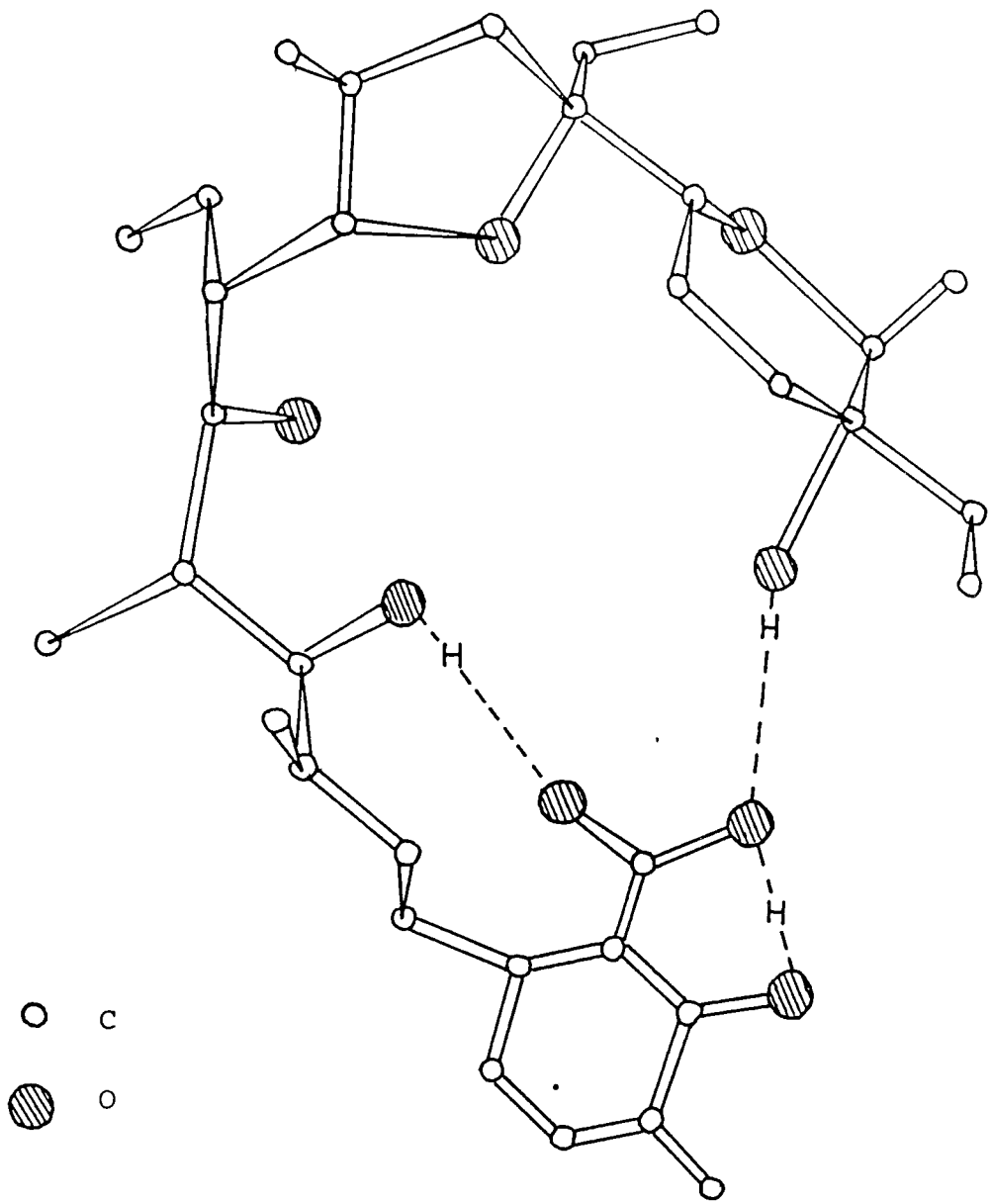

X-ray crystal structure of a single lasalocid molecule showing intramolecular hydrogen bonding. Adapted from (7).

Figure 7.2b

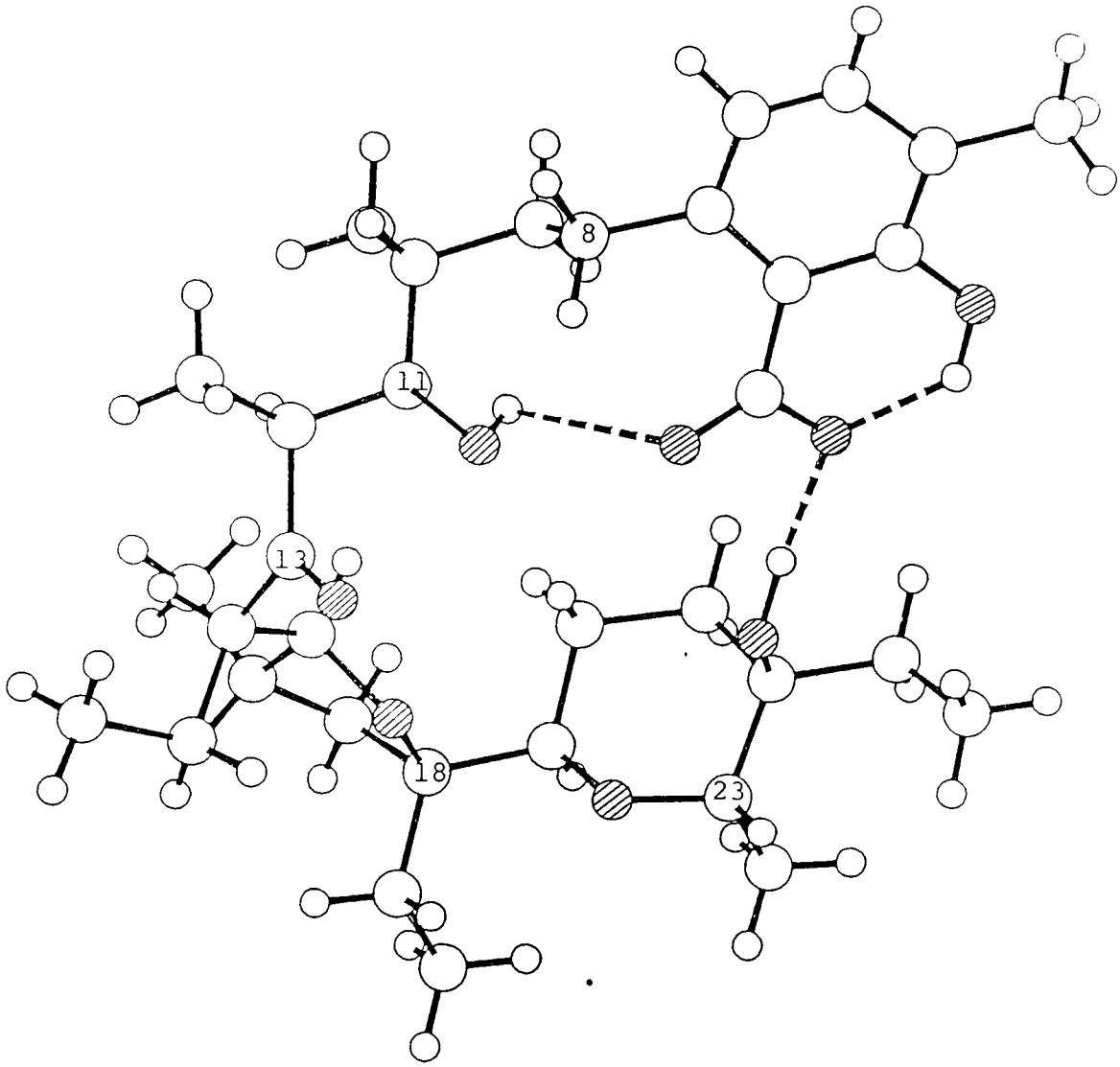

Natural structure of lasalocid showing the intramolecular hydrogen bonds. Protons were added to the crystal data of Johnson et al (7) by use of the graphics program MODEL.

X-ray crystallography has been carried out on AgLAS (6) and $Ba(LAS)_2$ (7). The barium complex is of greater interest in that it will resemble the calcium and cadmium complexes studied in this work. The structure of the barium complex in various forms and at different planes of view is shown in Figure 7.3. Johnson et al found that the two lasalocid molecules do not coordinate the barium in an identical manner, with O(3), O(4), O(6), O(7) and O(8) complexing from one molecule and only O(3)' and O(8)' from the other. The final point of coordination to the metal is the solvent. In addition, intra-molecular hydrogen bonds exist between O(3) and O(4), O(8) and O(2) and O(1) and O(2), as marked in Figure 7.2. The structure is a tight cyclic conformation with the oxygen atoms pointing inwards, forming a hydrophilic pocket in which the cation resides. The crystal structure of AgLAS shows this to be a dimer with two cations sandwiched between the two lasalocid anions. The outside of these structures is hydrophobic, explaining their solubility in non-polar solvents and virtual insolubility in water. These structures do not, however, account for the solubility of the complexes in polar solvents such as methanol; indeed, Chiang and Paul (8) have suggested that NaLAS and the free acid crystalise as the monomer from a methanol solution. In order to discover if gross changes occur with increasing polarity of solvent, solution nmr techniques have been used.

Figure 7.3a

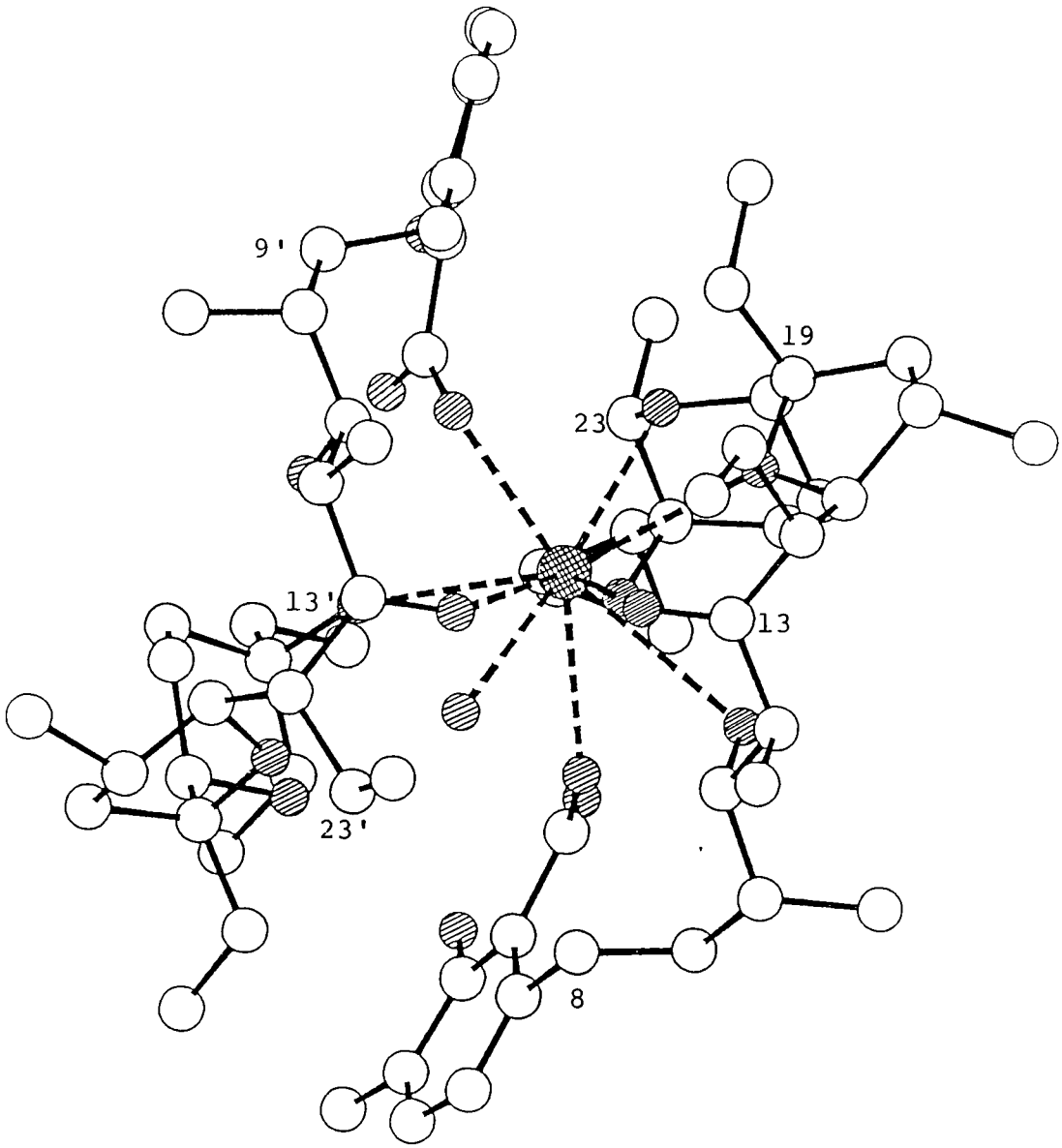

Computer model of the structure of the $Ba(LAS)_2$ complex. The oxygen atoms are shaded; the barium is cross-hatched. Original data taken from the crystal structure of Johnson et al (7).

Figure 7.3b

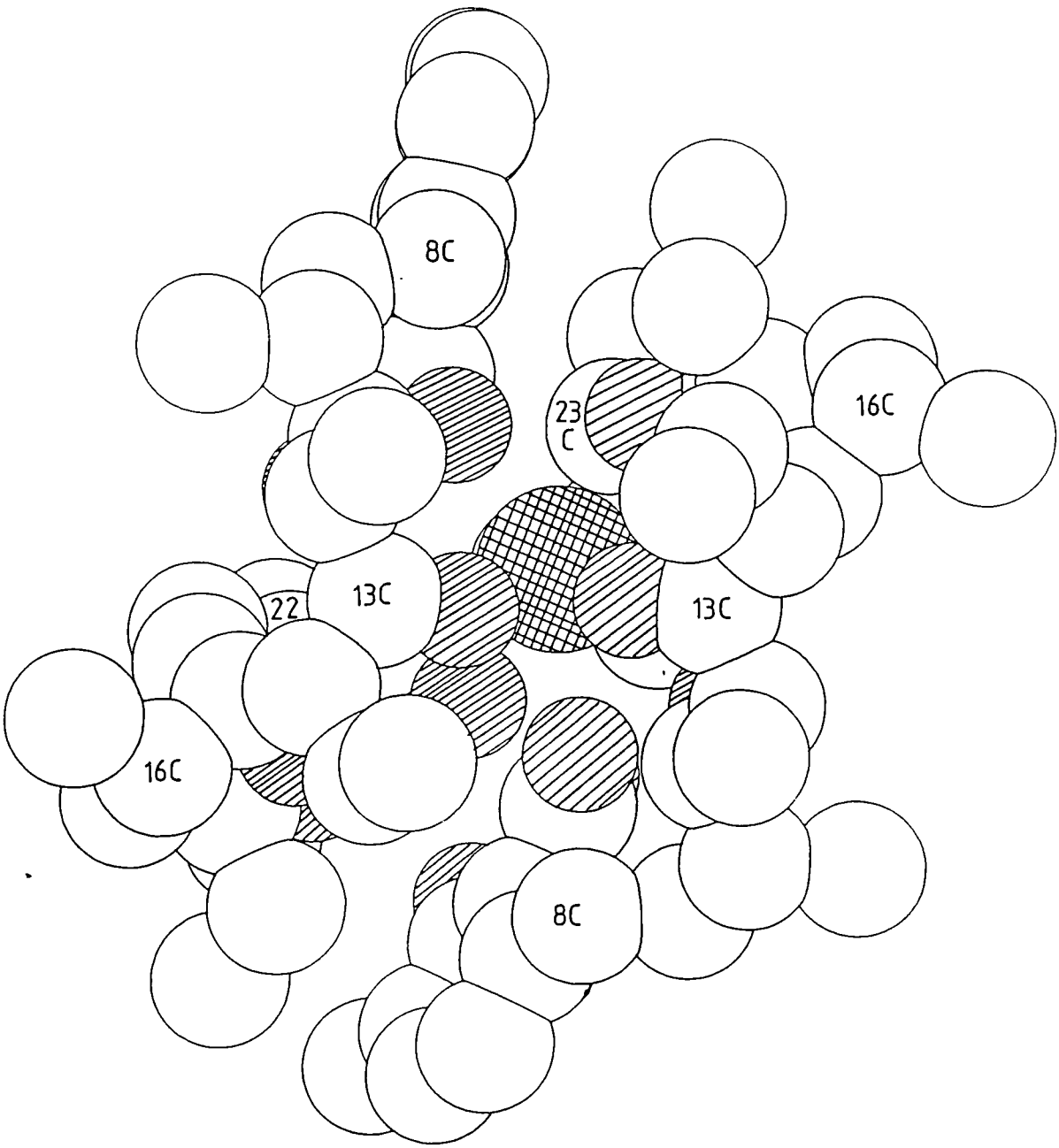

The same view of the $Ba(LAS)_2$ complex seen in a space-filling model (0.6 vdw radius) to illustrate the immediate surroundings of the Ba^{2+} ion.

Figure 7.3c

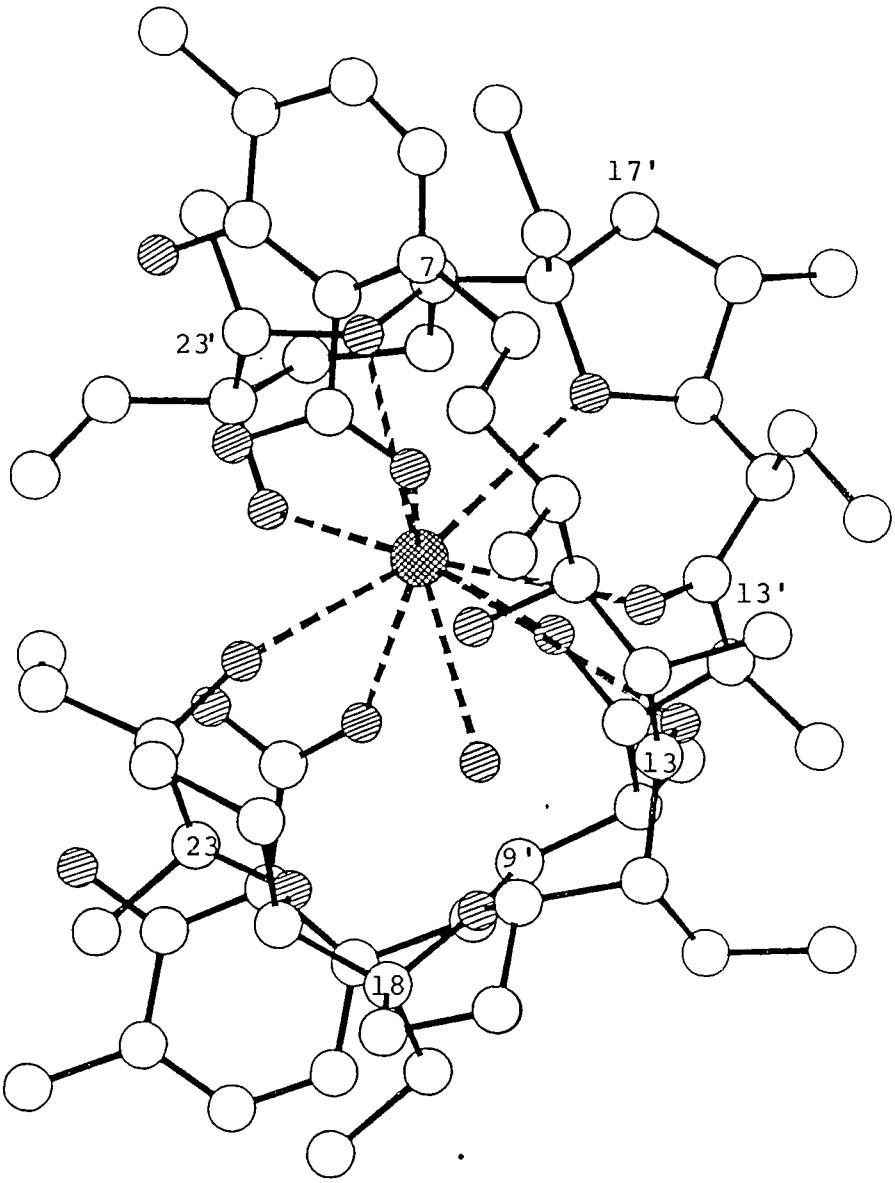

Computer model of $Ba(LAS)_2$ viewed normal to the structure in Figure 7.2a. This clearly shows the positions of the pyran and furan groups relative to the aromatic rings.

7.1.2 NMR Studies of Lasalocid Complexes

Both ^{1}H- (9) and ^{13}C-nmr (10) have been used to study metal ion-binding and complex conformation in lasalocid. Antenuis found that there is very little difference in the solution conformations of the free acid and the sodium salt (11), presumably due to the intramolecular hydrogen bonding discussed above. He assigned certain resonances in the sodium spectrum, listed in Table 7.I. These assignments were taken as a starting point for the current investigation and have been adopted as the standard nomenclature for this work; part of the discussion will reflect upon these assignments. A preliminary report of work carried out on the calcium salt has appeared (12),which concluded that coordination to the metal occurred through O(3), O(6) and O(7). This result is disputed by Hanna et al (13) who used ^{13}C-nmr to study the spin-lattice relaxation parameters of the $Mn(LAS)_2$ complex. They found that conformation was solvent-polarity dependent and that binding in non-polar solvents occurred at O(2), O(3), O(4), O(7) and O(8). Furthermore, this binding was thought to arise from the same oxygen atoms on each of the lasalocid ligands in the Mn^{2+} and the Gd^{3+} complexes. In chloroform, the binding via the carboxylate appeared to be of two conformations in fast exchange with each other, presumably either O(2) or O(3) at any instant. Chen and Springer (14) studied the interaction of LAS with Pr^{3+} in methanol and concluded that binding occurred with an open conformation at the carboxylate and phenol oxygens only (O(2), O(3) and O(1)). This result has been confirmed for the lanthanide complexes by T_1 measurement (13).

Table 7.I

NaLAS Assignments After Antenuis (11)

Residue	Assignment (ppm)	
4-CH_3	2.20	
5-H	6.95	
6-H	6.45	
8-H	2.23	3.98
9-H	1.30	1.79
10-H	1.60	
10-CH_3	0.99	
11-H	4.52	
12-H	2.82	
12-CH_3	0.82	
14-H	2.53	
14-CH_2-	1.93	1.30
14-CH_3	0.57	
15-H	3.70	
16-H	1.60	
17-H	1.40	1.15
18-CH_2-	--	
18-CH_3	0.76	
19-H	3.45	
20-H	1.19	2.24
21-H	1.43	
22-CH_2-	1.48	
22-CH_3	0.95	
23-H	3.98	
23-CH_3	1.07	

7.1.3 The Aim of This Study

The calcium complex of lasalocid is of biological importance for the understanding of several biochemical mechanisms, including biomineralisation. Little work has been carried out on this complex, however and the purpose of this work has been to increase the understanding binding of the ionophore to cations and to note conformational changes which occur as the cation changes, the ratio of cation to anion increases and as the polarity of the solvent increases. This work was commenced during Professor Grover Everett's sabbatical in Oxford and has been continued as a collaborative effort. The discussion uses some work carried out in Kansas as yet unpublished.

7.2 Preparation of the Complexes

Lasalocid was obtained in the sodium salt form from Aldrich Chemicals and used without further purification. Other complexes included the calcium, cadmium and lanthanum forms for study by ^{1}H-NMR and a variety of paramagnetic lanthanide and transition-metal forms to act as shift or broadening probes on the spectra; it was found that the transition metal complexes were not successful as probes because shift probes were non-axial and the other probes (notably the manganese complex) caused non-selective broadening.

These other complexes were all prepared by dissolving 1 g of NaLAS in 25 ml of $CHCl_3$ and then stirring this solution vigorously with an aqueous solution of, say, $Ca(NO_3)_2 \cdot 4H_2O$ (2 g in 30 ml) for 2 to 3 hours. The solution was allowed to separate into two layers and then the aqueous layer removed and

Table 7.II

Elemental Analysis of Various Lasalocid Complexes

NaLAS	Calculated:	C: 66.64%	H: 8.72%
	Found:	C: 66.41%	H: 9.03%
$Ca(LAS)_2 \cdot CHCl_3$	Calculated:	C: 61.89%	H: 8.05%
	Found:	C: 62.04%	H: ¾.01%
$Ca(LAS)_2 \cdot 2CHCl_3$	Calculated:	C: 57.65%	H: 7.46%
	Found:	C: 57.73%	H: 7.35%
$La(LAS)_3 \cdot CHCl_3$	Calculated:	C: 61.01%	H: 7.95%
	Found:	C: 60.86%	H. 8.28%
$La(LAS)_3 \cdot 2CHCl_3$	Calculated:	C: 58.18%	H: 7.56%
	Found	C: 58.70%	H: 7.46%

the process was repeated twice more. Finally, the chloroform solution was washed with water in the same way and then the two layers separated. The chloroform solution was then filtered and then the chloroform removed from the filtrate using a rotary evaporator cooled with liquid nitrogen.

Chemicals used were all of the 'AnalaR' grade, supplied by BDH Chemicals Ltd. with the exception of $La(NO_3)_3 \cdot 6H_2O$ which was an Alfa Ultrapure chemical.

7.3 Results

7.3.1 Determination of the Purity of the Complexes

The purity of the complexes was checked by thin layer chromatography (TLC) and when one spot was observed they were analysed with the results given in Table 2.II. Analysis was carried out on a Carlo Erba 1106 Elemental Analyser. The complexes were kept dry at room temperature until required.

7.3.2 ^{1}H-NMR Spectra of the Complexes

Lasalocid complexes of sodium, calcium, cadmium and lanthanum have been studied by nmr at 300 MHz. Figures 7.4 to 7.9 show the normal and CPA spectra, with the sodium complex assigned from the work of Antenuis. Certain resonances do not shift between complexes, or retain a characteristic line-shape. Thus, 5-H, 6-H, 11-H, 8-H, 23-H, 19-H, 12-H and 4-CH_3 can be tentatively assigned by inspection.

The structure of the lasalocid molecule allows certain predictions to be made, notably for the methyl groups. One would expect the spectrum to contain one methyl singlet (4-CH_3), four

Figure 7.4

Fully relaxed spectrum of NaLAS in $CDCl_3$

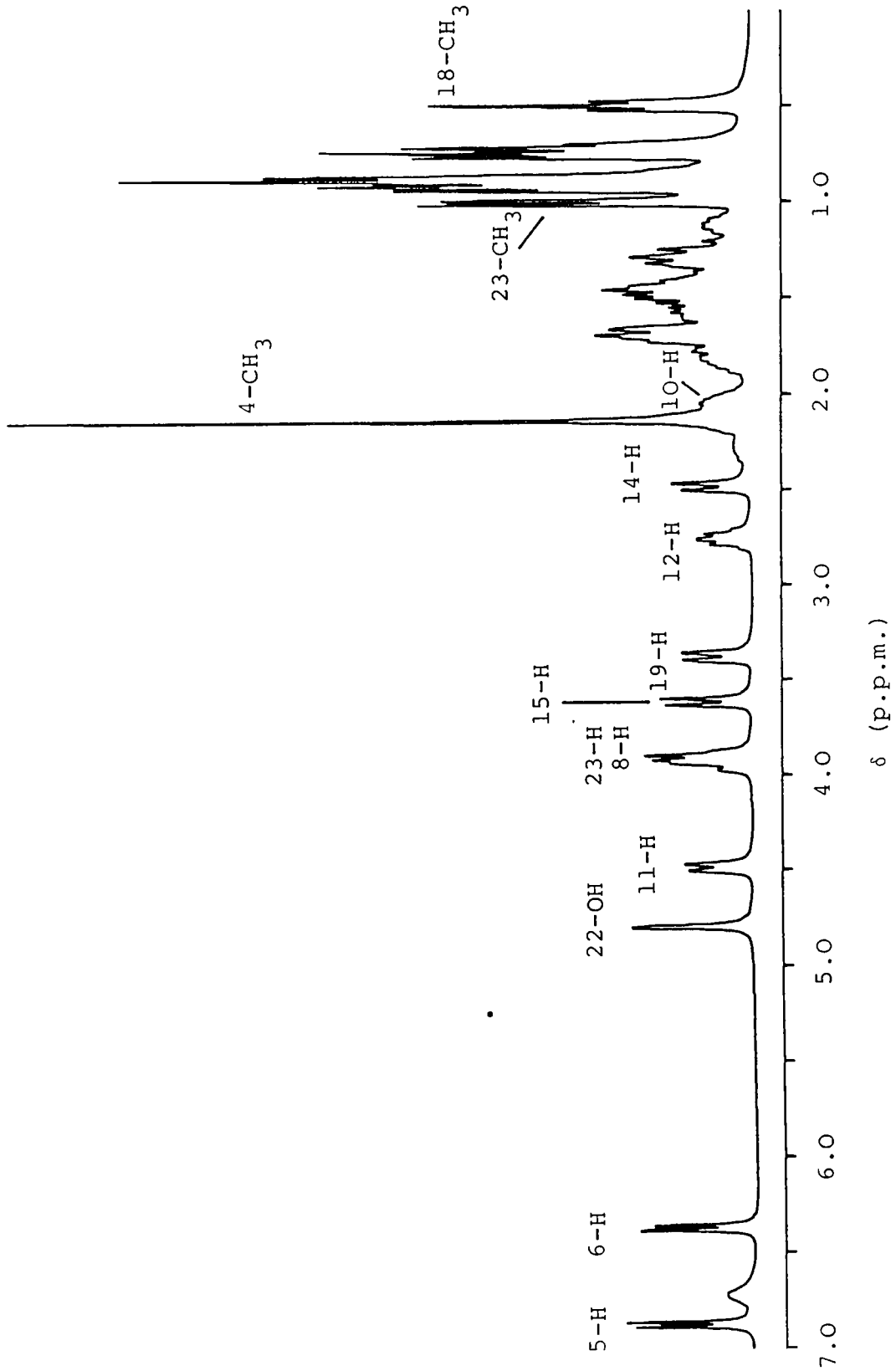

Figure 7.5

Fully relaxed spectrum of $Ca(LAS)_2$ in $CDCl_3$

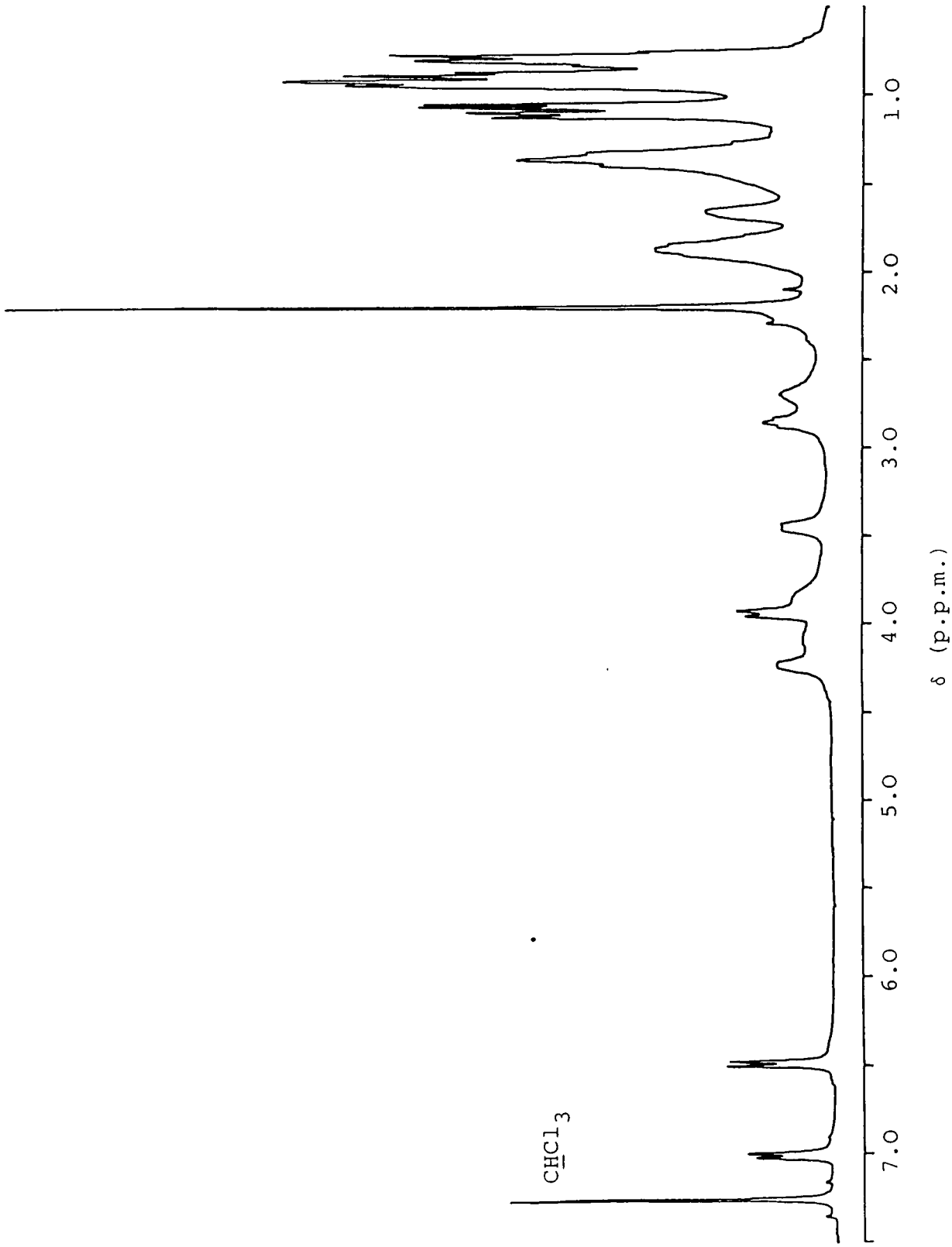

Figure 7.6

CPA spectrum of $Ca(LAS)_2$ in $CDCl_3$

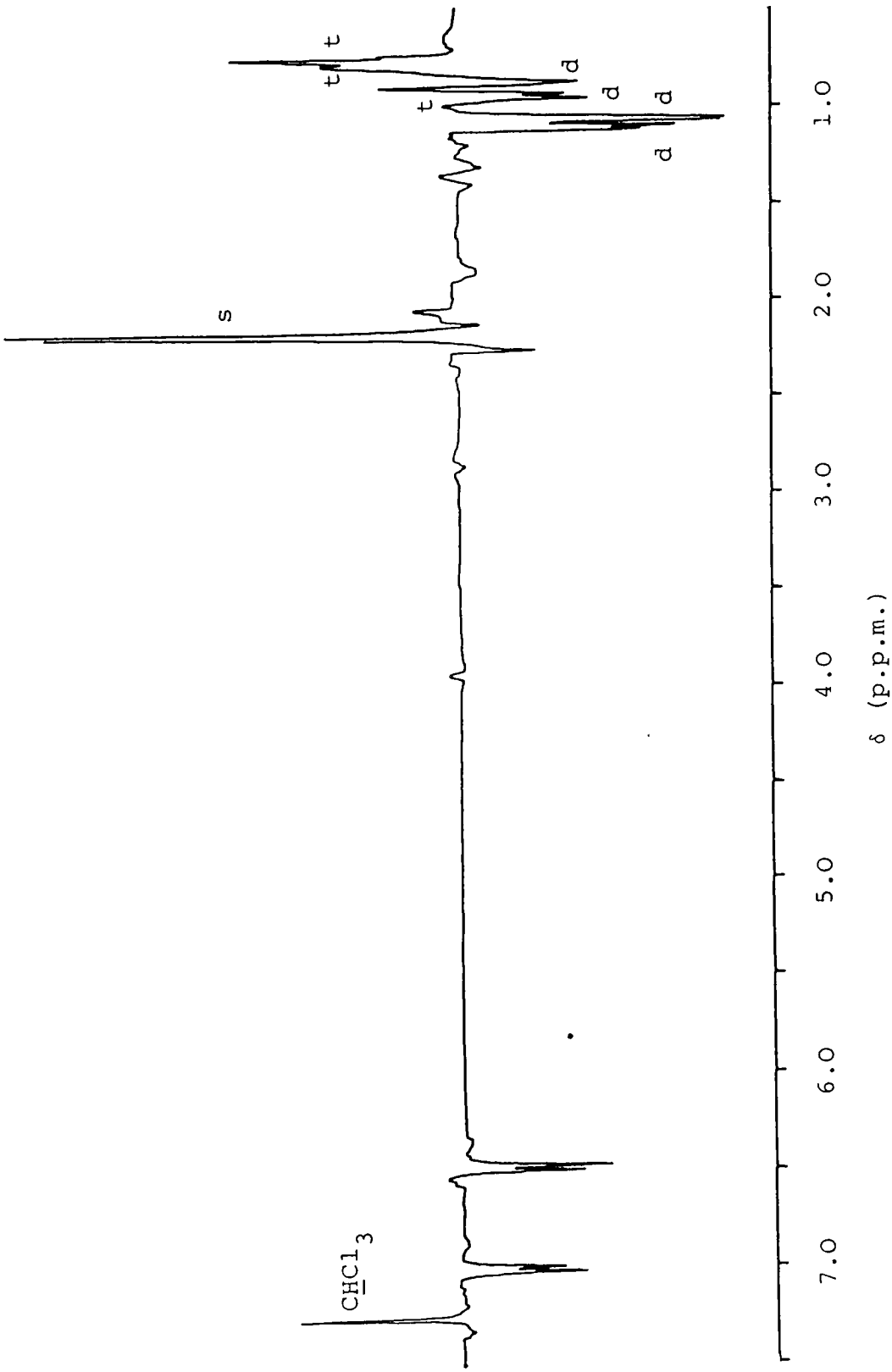

Figure 7.7

Fully relaxed spectrum of $Cd(LAS)_2$ in $CDCl_3$

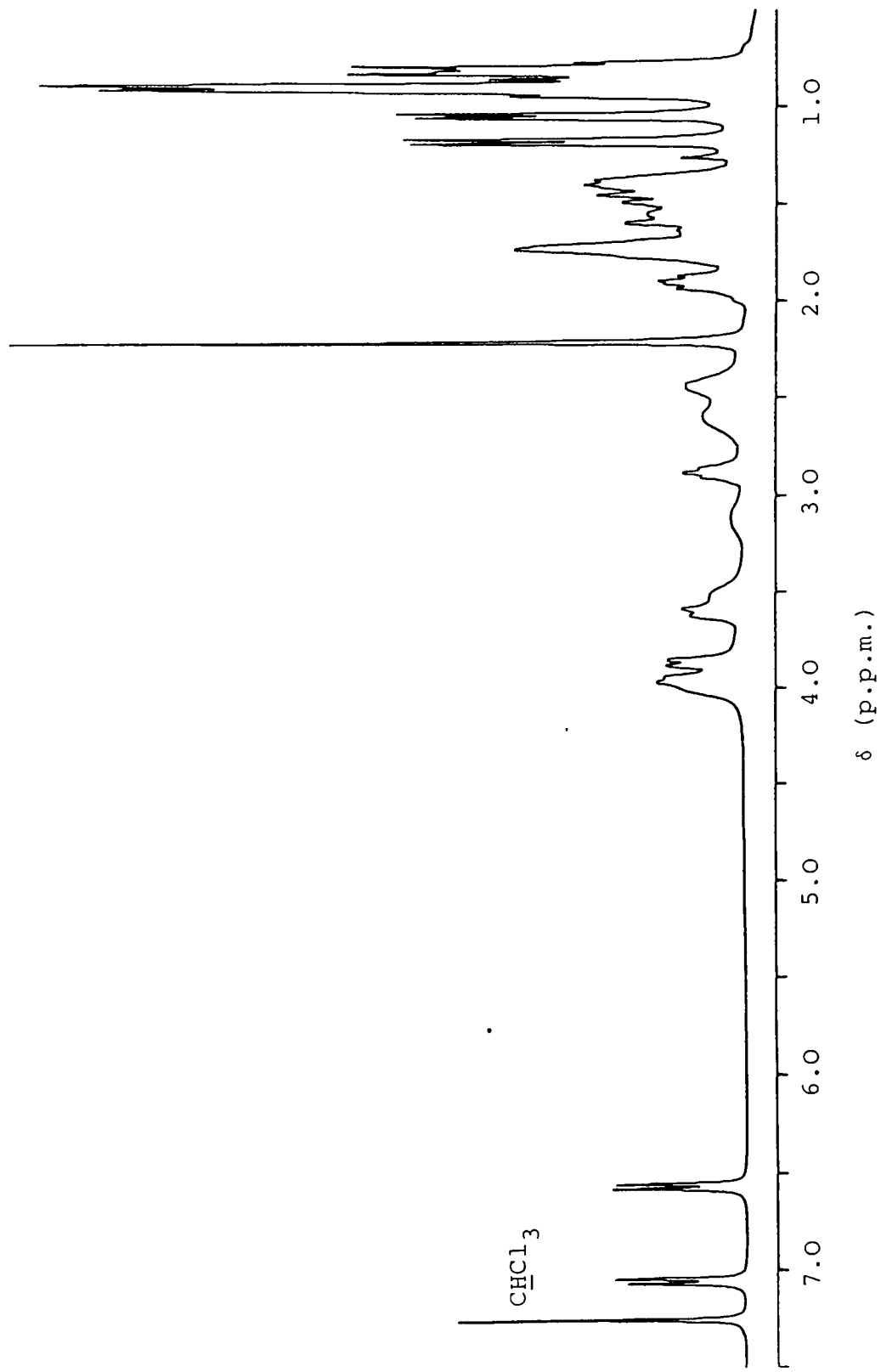

Figure 7.8

CPA spectrum of $Cd(LAS)_2$ in $CDCl_3$

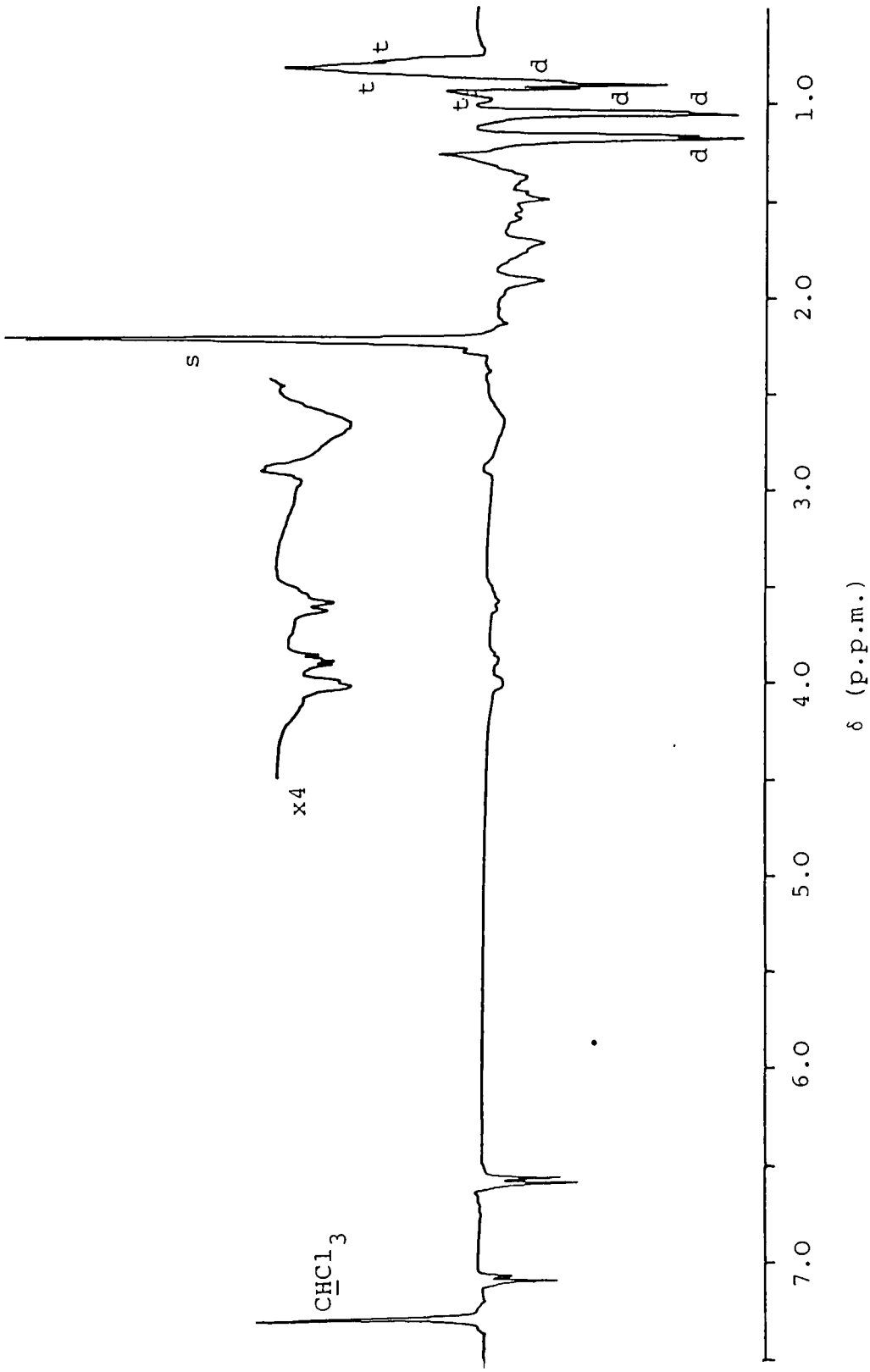

Figure 7.9

(a) normal and (b) resolution enhanced spectrum of $La(LAS)_3$ in $CDCl_3$

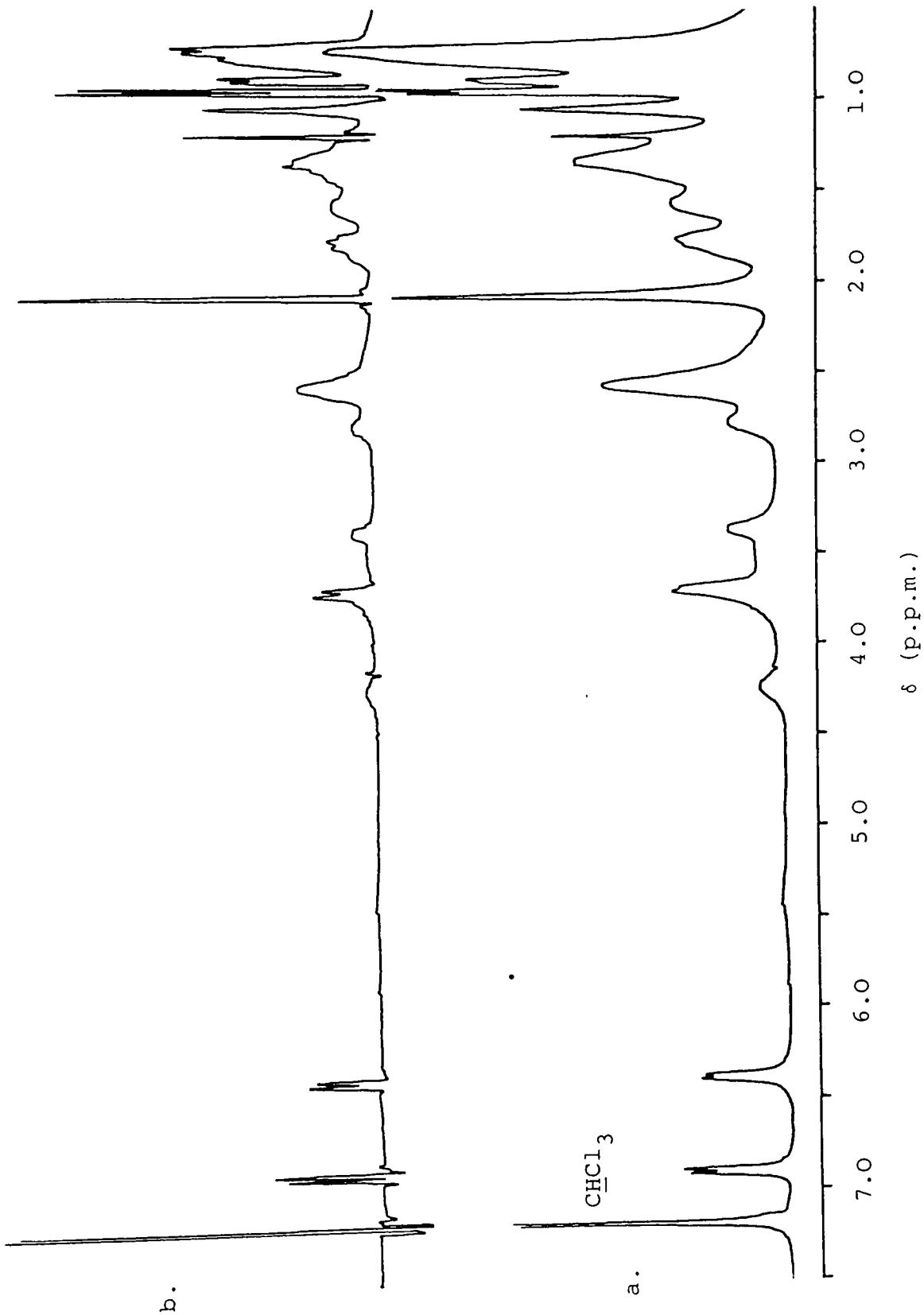

doublets (10-CH_3, 12-CH_3, 16-CH_3 and 23-CH_3) and three triplets (14-CH_3, 18-CH_3 and 22-H_3). These resonances can be located, although not assigned by inspecting the Carr-Purcell A spectra, in which singlets and triplets point upwards and the doublets are inverted. All of these resonances can be identified for the calcium and cadmium spectra and are marked on Figure 7.5 and 7.7 respectively.

Oxygen atoms cause the resonances from protons lying nearby to be shifted downfield of their predicted positions in the spectrum. Thus one might expect 23-CH_3 to lie furthest downfield, followed by 16-CH_3, 12-CH_3 and 10-CH_3. These cannot be assigned confidently by this process, however.

7.3.3 Calcium-Lasalocid Titration

It was possible to determine the fate of resonances observed in the sodium lasalocid spectrum but not easily identified in the calcium complex by titrating a sample of the calcium complex with carefully measured aliquots of NaLAS solution. The central portion of the spectrum is shown in Figure 7.10 and it can be seen that the resonances assigned by Antenuis to 14-H and 22-OH are broadened completely out of the spectrum. In addition, 15-H moves downfield to join the complex peak due to one 8-H proton and the 23-H proton. The extent of this movement has lead to some confusion over the final positions of these three resonances, but the chemical shifts can be determined by pulse methods. The other peak to move any distance is the 18-CH_3 triplet, which shifts into the body of the methyls. Pulse requirements reveal that it remains the resonance further upfield, however.

Figure 7.10

Titration of $Ca(LAS)_2$ with lasalocid.

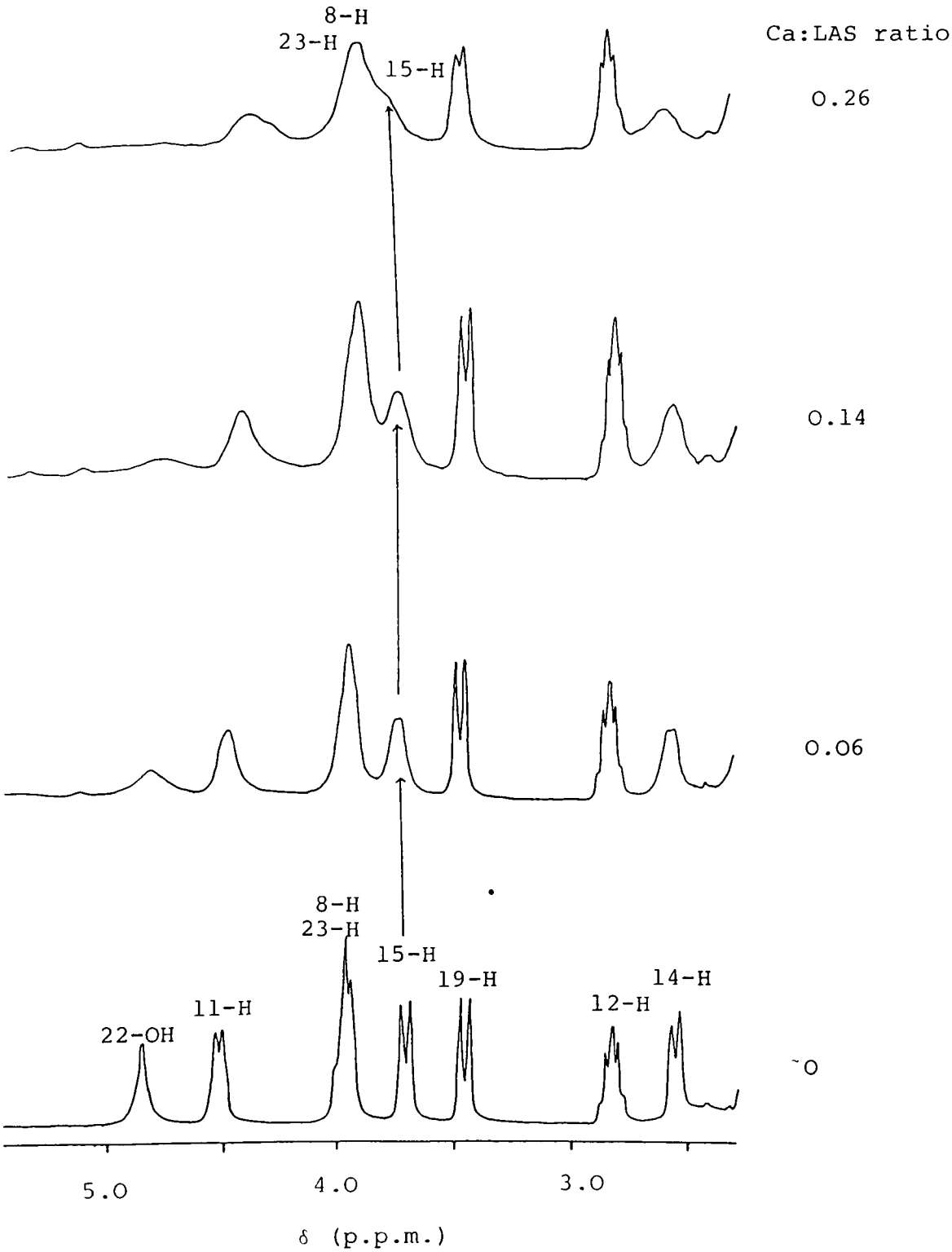

7.3.4 Pulse Experiments on $Ca(LAS)_2$

The major method of assignment of the complexes was to use spin (J-) decoupling. This takes advantage of the fact that many of the resonances show splittings due to spin-spin interactions The technique reveals those protons lying next to each other along the backbone of the molecule (and not in three-dimensional space). By making use of the known assignments, many additional assignments can be obtained, particularly the doublet methyls. Figure 7.11 lists the results of the J-decoupling experiments and the assignment obtained by this method are listed in Table 7.III. Those resonances contained within the three broad peaks which lie between 1.2 ppm and 2 ppm cannot be assigned with great accuracy in the calcium complex. These broad peaks complicate the interpretation of decoupled resonances when the original irradiation was in one of them since several resonances beneath the envelope are inevitably affected. It is, however, easier to interpret J-decoupling patterns than NOE effects under these conditions since the former is a short-range effect.

It can be seen from Table 7.III that the order of resonances, moving downfield is 15-H, 8-H, 23-H. This assignment was made because the peak designated 23-H produced a strong decoupling effect in a sharp methyl doublet at 1.098 ppm. This effect could not have been produced by 15-H since it is unlikely that the decoupling would be felt at a distance of four bonds; any effect would certainly not be large.

The effectiveness of spin decoupling in assigning the calcium complex is reduced due to the three gross peaks which contai several important methylene protons, particularly those arising

Figure 7.11

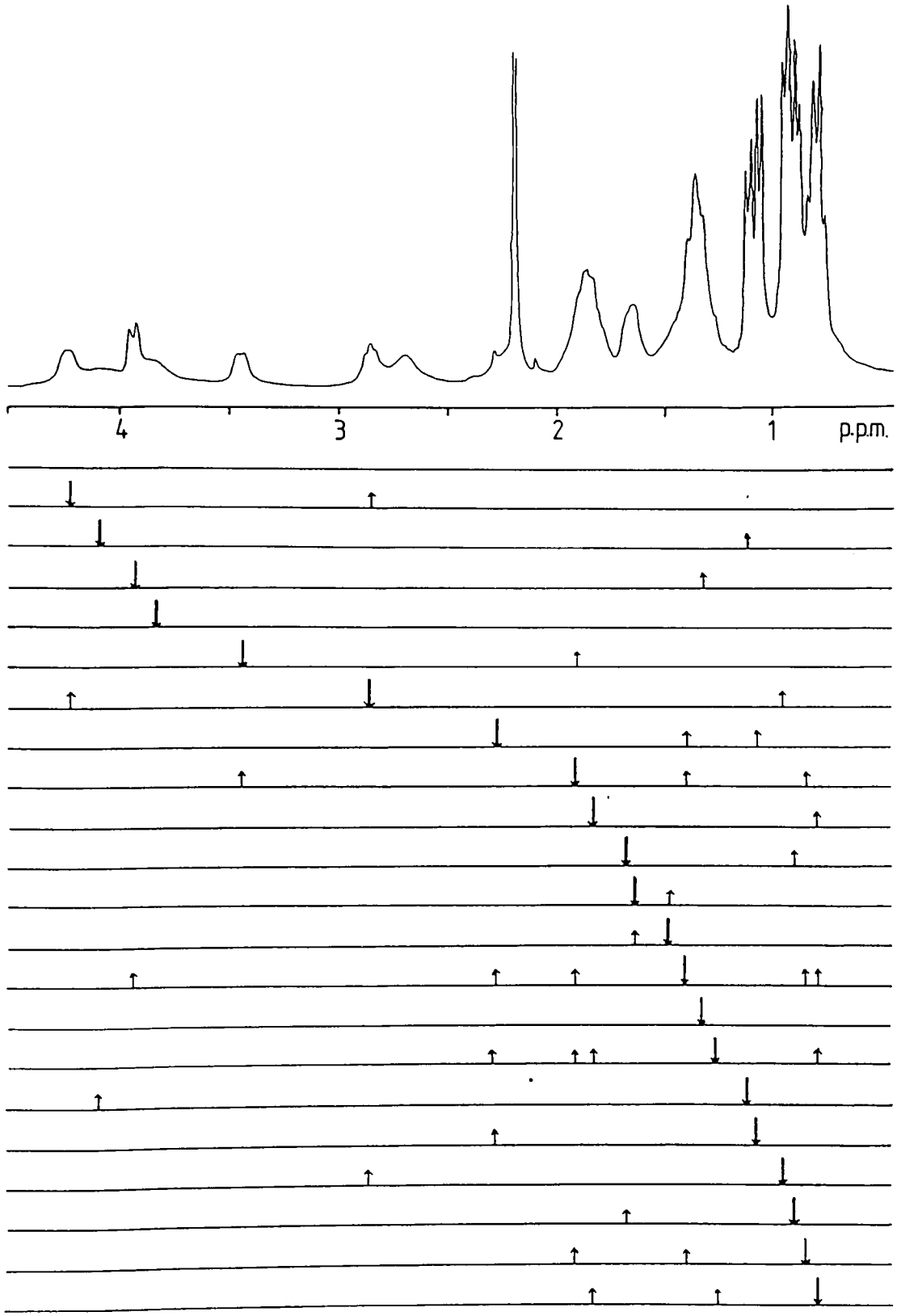

Results of the spin-decoupling experiments on $Ca(LAS)_2$. Irradiations in the 1.2 to 2.0 ppm region led to several effects simultaneously.

Table 7.III

Resonances Identified by J-decoupling of $Ca(LAS)_2$

Residue	Chemical shift (ppm)
10-H	c 2.45
10-CH_3	1.059
12-CH_3	0.936
15-H	3.819
16-H	c 1.70
16-CH_3	0.878
18-CH_2-	c 1.35
18-CH_3	0.785
23-H	4.103
23-CH_3	1.098

Resonances Possibly Identified by J-decoupling of Ca(LAS)

8-H'	c 1.35
9-H	c 1.35
9-H'	c 1.86
20-H	c 1.86

from the ethyl groups, and also due to the broad nature of several resonances. These broad peaks are a consequence of the exchange processes occuring in the complex and will be discussed at greater length below.

7.3.5 Temperature Dependence of the Spectrum of $Ca(LAS)_2$

The exchange process which leads to broad peaks in the normal spectrum of the calcium complex is also observed in the other complexes studied. The broadening becomes more marked as the number of anions in the complex increases. The exchange processes occuring are in the 'intermediate' timescale, which is identified by observing a single peak which is broader than the sharp single peak expected for a system in fast exchange in the nmr timescale, yet not two discrete resonances which is observed for a system in slow exchange. The definition is not absolute and depends on how many states are present in the sample during the time of an irradiation. Intermediate exchange is an unsatisfactory condition and experiments were carried out to try to move the exchange rate to one of the extreme conditions. These experiments included attempting to attain fast exchange by increasing the temperature at which the spectrum was obtained. This was not possible at 300 MHz due to the high field and the comparatively low boiling point of chloroform, the solvent used. A later experiment carried out by Professor Everett in Kansas achieved fast exchange on an 80 MHz instrument in an nmr tube sealed under argon at an elevated temperature of 82°C. Attempts to attain slow exchange were made by running the spectrum at 470 MHz and also by cooling the sample at 300 MHz. This experiment was partially successful for the calcium complex, the results of which are shown in Figure 7.12.

Figure 7.12

Effect of temperature change on $Ca(LAS)_2$ in $CDCl_3$. Peaks moving into slow exchange are marked.

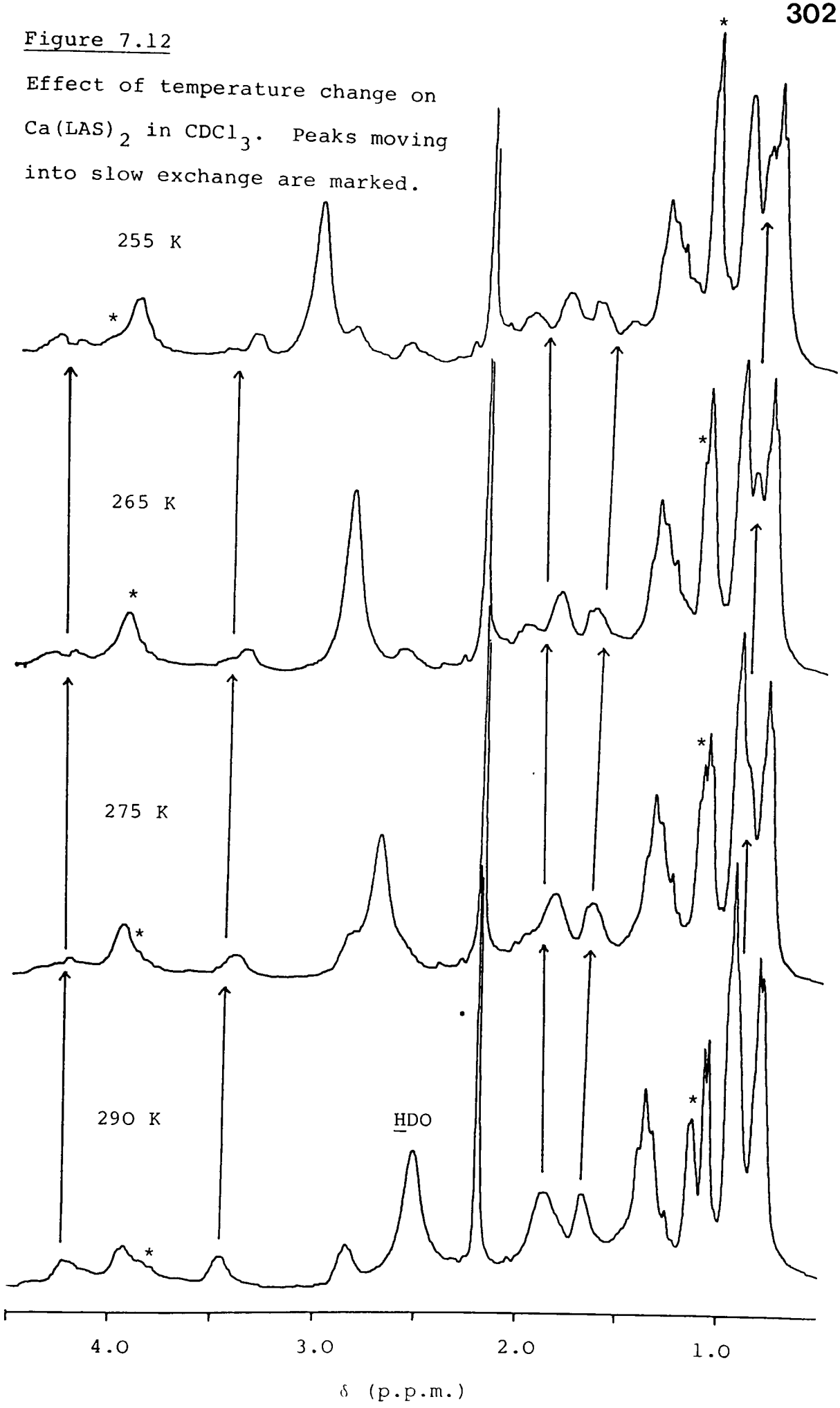

A slow exchange condition was attained for 5-H, 6-H, 11-H, 19-H, 16CH_3 and possibly 10-H. In addition, components of the large envelopes at about 1.7 ppm and 1.86 ppm move into slow exchange. The effect in the upfield envelope could be due to 16-H, which lies in that region. This would mean that both residues on the 16-C are affected by the temperature change. There are also two resonances that shift without changing their exchange states (in addition to HDO). These are 15-H and 10-CH_3. These movements are marked with asterisks on Figure 7.12. It is interesting to note that 6-H was affected at a higher temperature (290 K) than 5-H (not illustrated).

One further consequence of the intermediate exchange in the complex was noted in a T_1 measurement by the inversion-recovery method. The residues around the aromatic ring were of interest in that they all had a slower T_1 time than the aliphatic residues (the inversion-recovery spectra of the aromatic protons are illustrated in Figure 7.13). The measured T_1 times were 0.405 s for 4-CH_3 (not illustrated), 0.511 s for 6-H and 0.892 s for 5-H. Thus, either 5-H must be affected by an external contribution which is slowing the relaxation time, or 6-H has a contribution which is speeding it. It is possible that there is some interaction between one of the protons in the aromatic ring and part of the pyran ring of the other lasalocid molecule. In the barium complex, these regions are about 5 Å apart (see Figure 7.3), but they could move closer when complexing the smaller cation.

The structure of the complexes will be discussed at greater length below, but these results indicate that the solution structure is generally similar to the crystal structure of $Ba(LAS)_2$

Figure 7.13

Inversion-recovery (T_1) spectrum of $Ca(LAS)_2$

Aromatic protons.

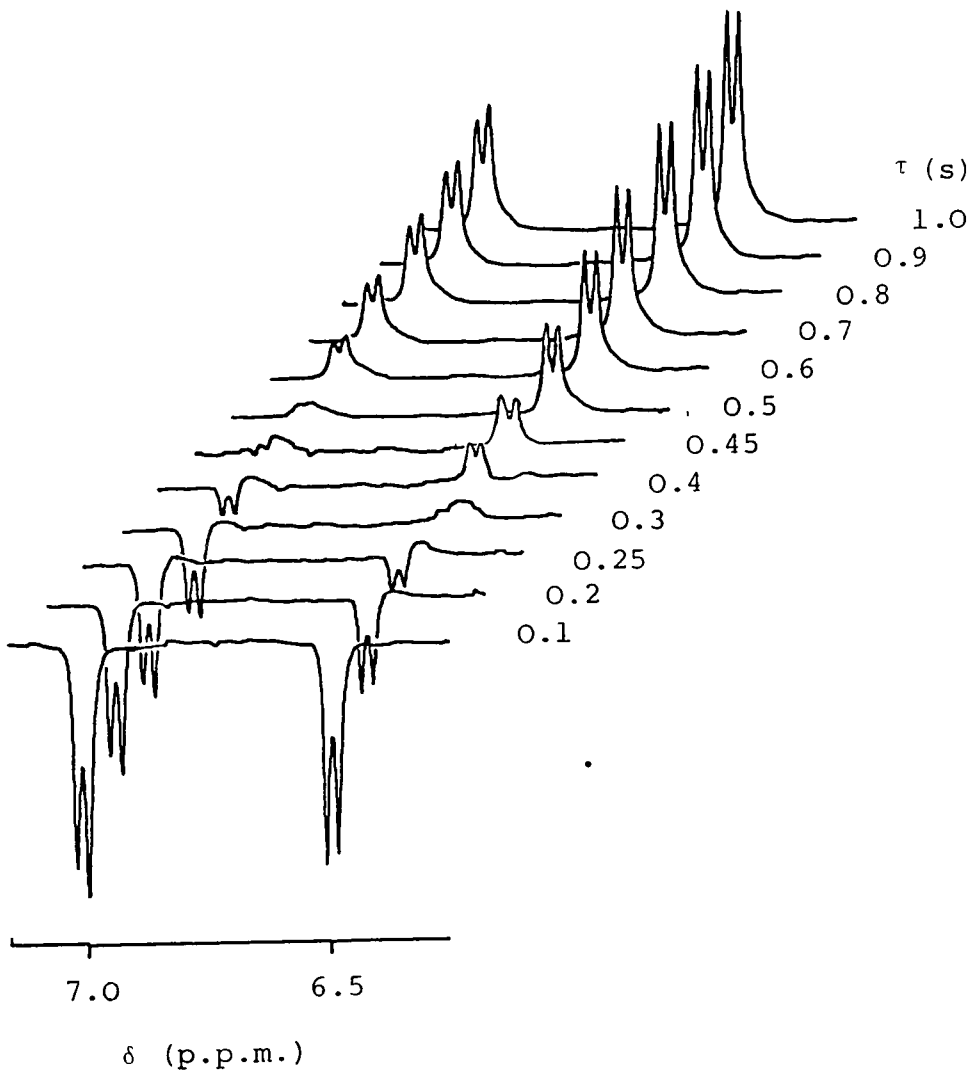

except that exchange processes lead to an increase in the overall symmetry of the complex; thus the crystal structure is one possible conformation, and others are continually forming with different oxygens taking turns to complex the cation.

7.3.6 Calcium : Cadmium Complex Titration

The nmr spectrum of the cadmium lasalocid complex shows many similarities to the calcium complex spectrum, which allows certain assignments to be made by inspection (Figure 7.14 to 7.16). The most interesting region of the spectrum lies between 2 and 4.5 ppm (Figure 7.15). Several changes can be followed in the spectra as the proportion of $Cd(LAS)_2$ is increased. 11-H moves upfield to coalesce with 23-H to produce the complex peak at 4 ppm. 8-H drifts slightly upfield and 15-H moves markedly upfield to form a complex peak with 19-H which moves downfield. The broad resonance which appears at about 3.15 ppm is possibly due to 14-H which was broadened out of the calcium spectrum but showed as a sharp doublet at 2.5 ppm in the sodium spectrum. 12-H is unchanged, but 10-H moves downfield to about 2.45 ppm. The majo point of interest in the upfield region is that the three broad envelopes seen in the calcium spectrum split into several component resonances; there is also more clarity in the methyl region, with 23-CH_3 moving downfield, 12-CH_3 moving upfield, as does the CH_3 triplet lying beneath 12-CH_3 and 16-CH_3 in the calcium spectrum. These changes are probably, in part, due to a 'breathing' of the ligands to accomodate a slightly smaller cation (the ionic radius of Cd^{2+} is 0.097 nm whilst that of Ca^{2+} is 0.099 nm. This will change the points of interaction of the two anions with each other, thus changing the spectrum slightly.

Figure 7.14

$Ca(LAS)_2$:$Cd(LAS)_2$ titration. I: Low field resonances

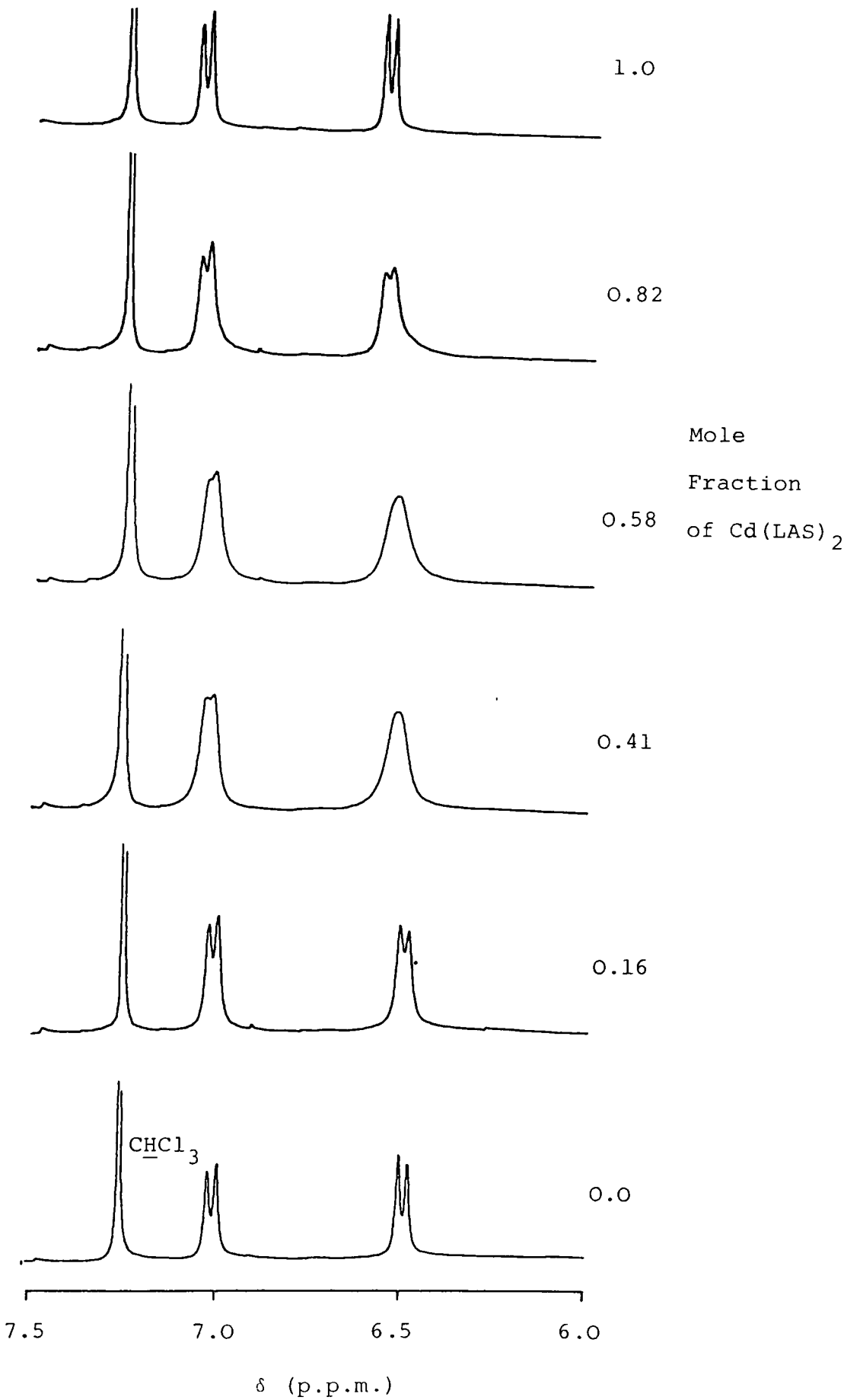

Figure 7.15

$Ca(LAS)_2$:$Cd(LAS)_2$ titration. II: Central region

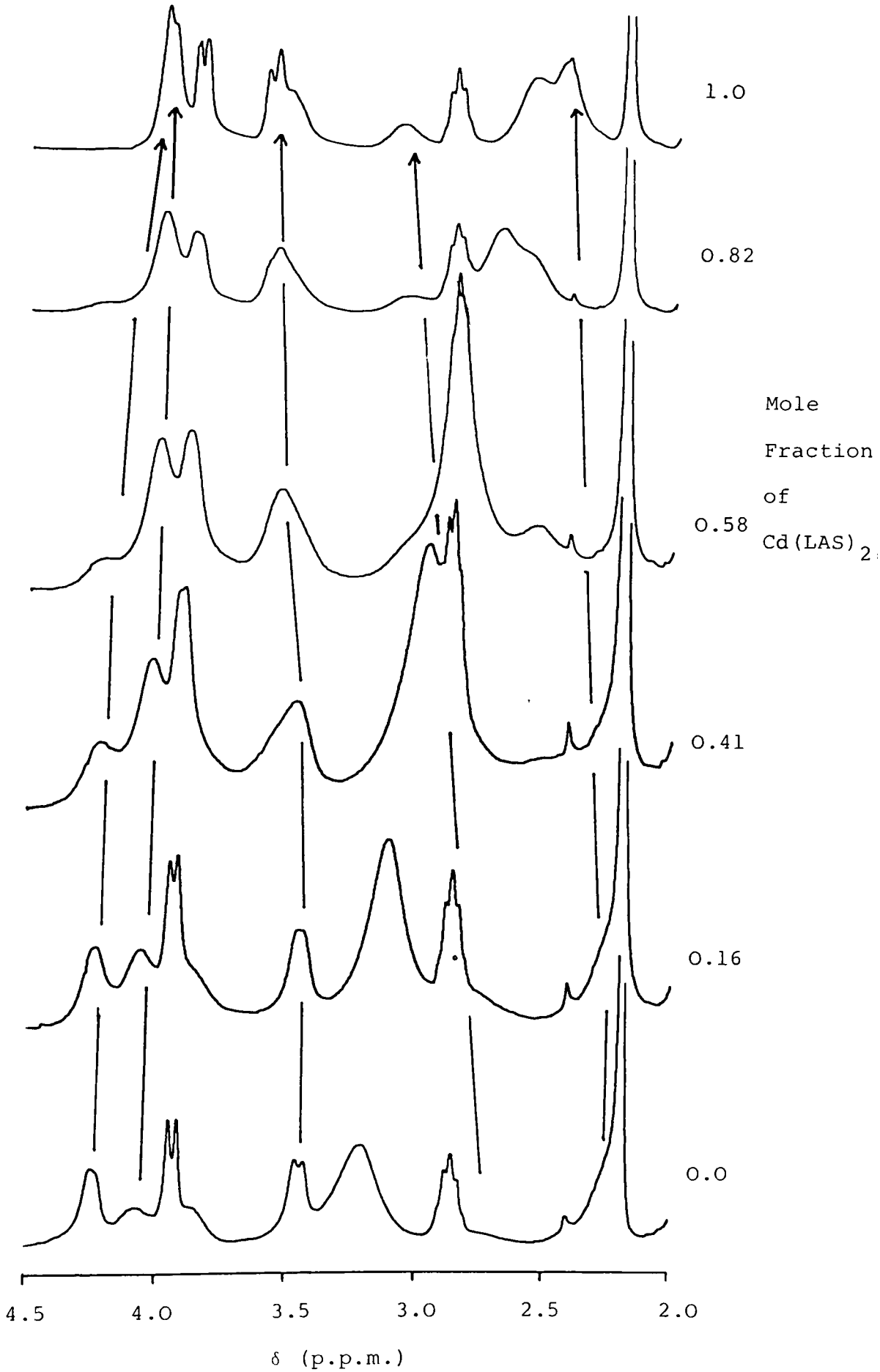

Figure 7.16

$Ca(LAS)_2$:$Cd(LAS)_2$ titration. III: upfield region

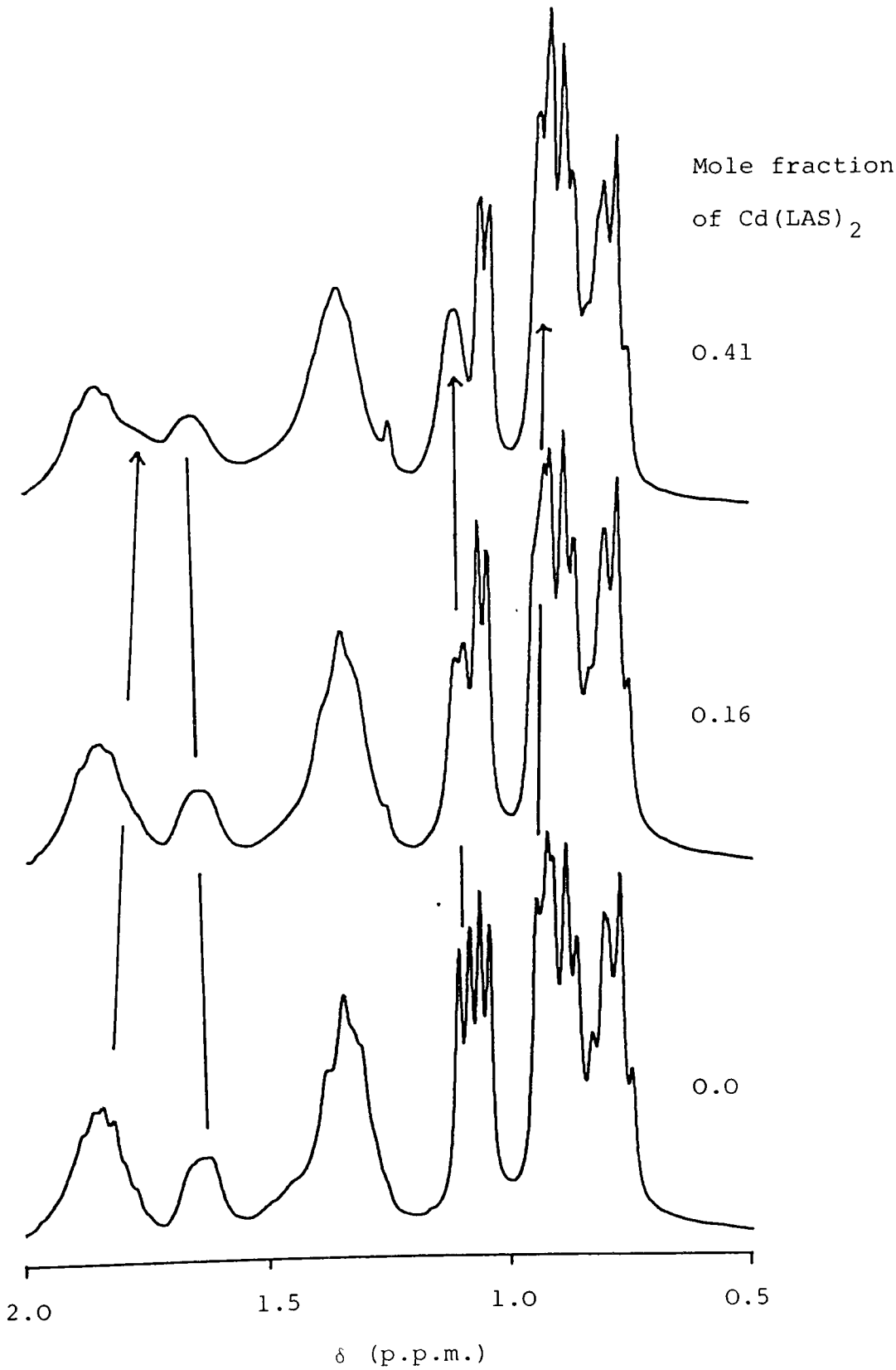

Figure 7.16

$Ca(LAS)_2$:$Cd(LAS)_2$ titration. III: Upfield region (cont^{d})

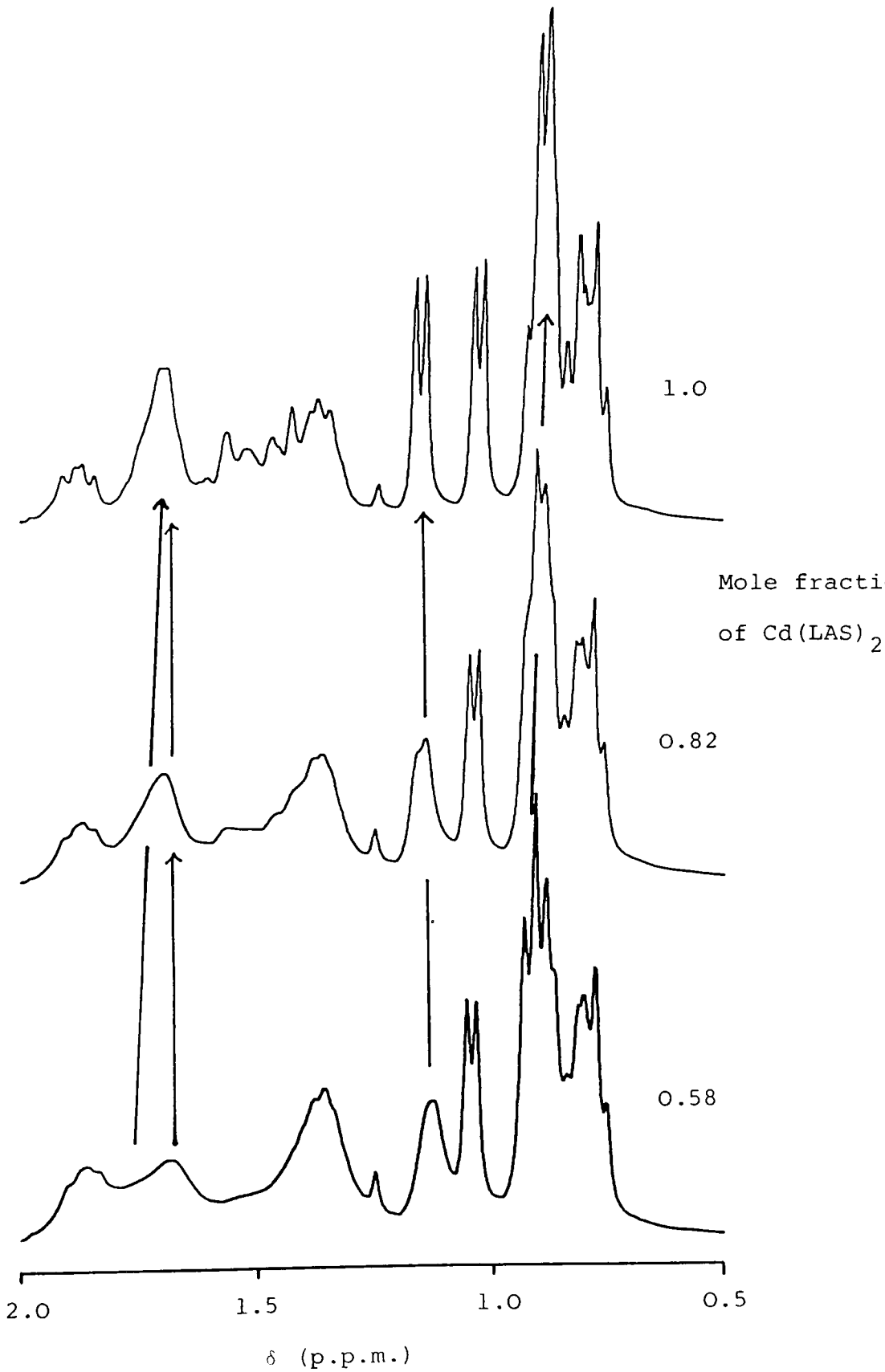

The phenomenon observed during the course of the transition from the calcium to cadmium complex is one of exchange broadening. This is illustrated perfectly in Figure 7.14 which shows the progress of the aromatic protons which broaden and then shift during the course of the titration. It is interesting to note that this broadening first appears at 6-H and later at 5-H, which again suggests that the exchange conditions that the two protons are under are not identical, in agreement with the T_1 data.

7.3.7 Pulse Experiments on $Cd(LAS)_2$

Although several resonances could be assigned in the cadmium complex spectrum by following the course of known resonance from the calcium spectrum, spin decoupling was also used to confirm the assignments and to probe into the upfield region of the spectrum. These experiments were not as satisfactory as the calcium complex ones in that several resonances which would be expected to decouple others in the upfield region of the spectrum failed to do so. Those results which were obtained are shown in Figure 7.17. The position of 23-H is confirmed at 4.0 ppm by the decoupling of its methyl, as is the position of 10-H. The complete list of resonances assigned in the cadmium complex is given in Table 7.IV. It was hoped that cadmium-proton coupling would be observed in the spectrum (both ^{111}Cd and ^{113}Cd are spin = 1/2 nuclei), but no large splittings are observed. Two peaks have hyperfine splittings which may be due to this effect. They are at 3.85 ppm and 1.4 ppm, but the splittings are so small that they would not provide important information on the mode of binding the cation even if they were genuine.

Figure 7.17

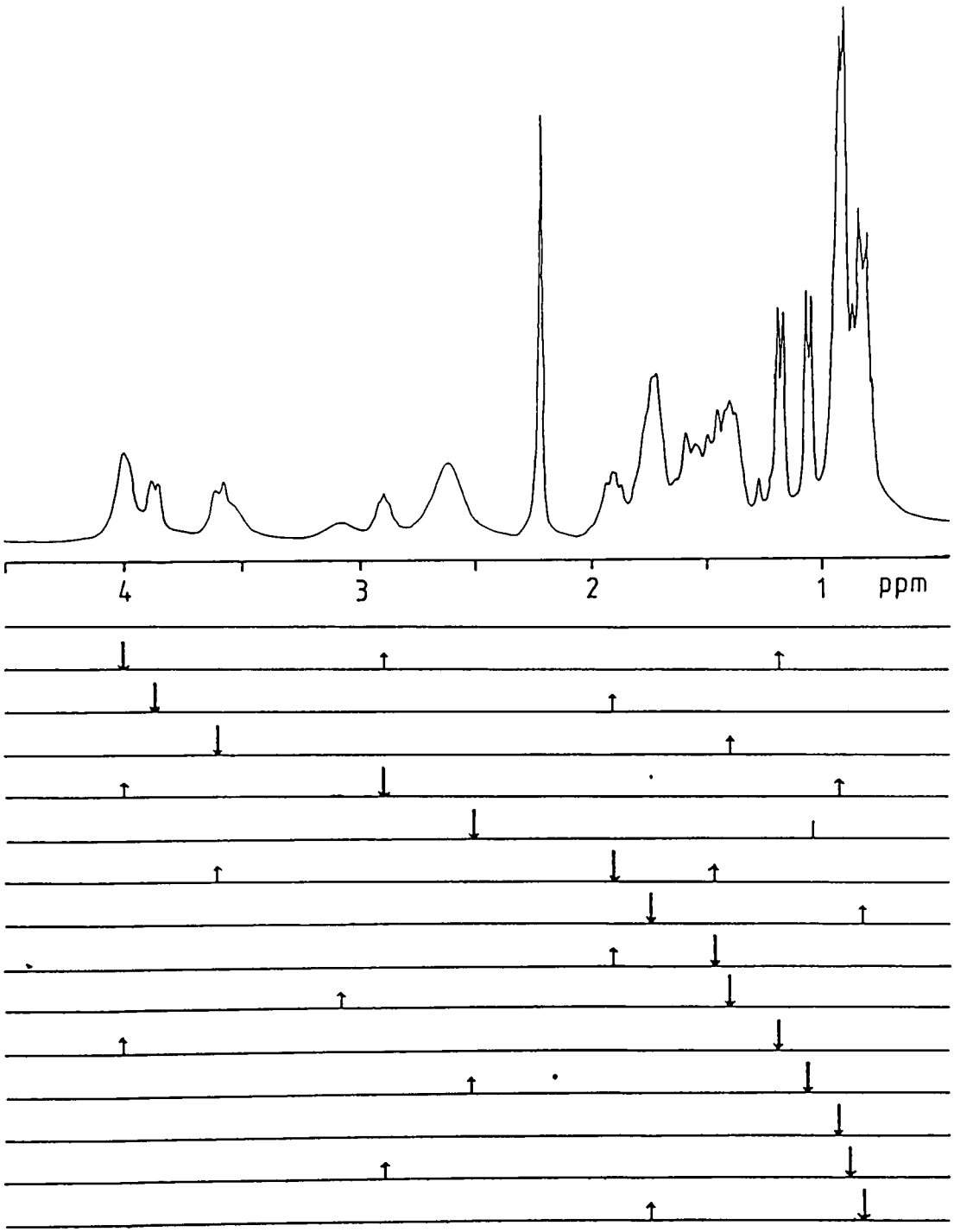

Results of the spin decoupling experiments on $Cd(LAS)_2$.

Table 7.IV

Resonances Assigned in the Spectrum of $Cd(LAS)_2$

Residue	Chemical shift (ppm)
5-H	7.020
6-H	6.485
11-H	3.983
23-H	6.983
8-H	3.848
19-H	3.576
12-H	2.891
10-H	2.143
4-CH_3	2.213
23-CH_3	1.154
10-CH_3	1.029
16-CH_3	0.892
12-CH_3	0.867
18-CH_3	0.770

Resonances Possibly Identified in the Spectrum of $Cd(LAS)_2$

Residue	Chemical shift (ppm)
15-H	3.576
14-H	3.065
20-H	1.861
18-CH_2-	1.354
14-CH_3	0.808

7.3.8 Experiments on the $La(LAS)_3$ Complex

The lanthanum complex of lasalocid is much broader than the divalent cation complexes and, as a consequence, it is not easy to identify resonances by inspection. 12-H retains its characteristic shape, as do 5-H, 6-H, 4-CH_3 and 23-CH_3. All other resonances which were known in the other complexes were assigned by titrating the lanthanum complex with lasalocid, which sharpened the peaks and shifted them back towards their sodium complex positions. The titration is shown in Figure 7.18 for the mid-spectrum region. It is interesting to note that the complex peak of 8-H and 23-H broadens out leaving 15-H as the major doublet. All three of these resonances lie at higher field in this complex than the calcium one. This is in contrast to the observations of the divalent complex spectra. The final order of resonances, from low to high field is 5-H, 6-H, 22-OH (which broadens out of the spectrum), 11-H, 15-H, 8-H/23-H, 19-H, 12-H and 14-H, which is strong in this complex. It is probable that 10-H also moves downfield out of the 4-CH_3 band, but this is obscured by the broad water peak.

Low temperature experiments were carried out for the $La(LAS)_3$ complex and it was found that the 6-H and 4-CH_3 resonances broadened considerably at 290 K,whilst at 275 K these and the 5-H signal moved into slow exchange, with the peaks splitting to form pairs with ratios of about 1:3 for each resonance.

Pulse experiments were carried out using both the NOE and J-decoupling techniques. These were not as successful as the divalent cation complexes, however since the spectrum was too broad to allow many peaks to show spin coupling. It

Figure 7.18

Lanthanum:lasalocid titration at 300 MHz

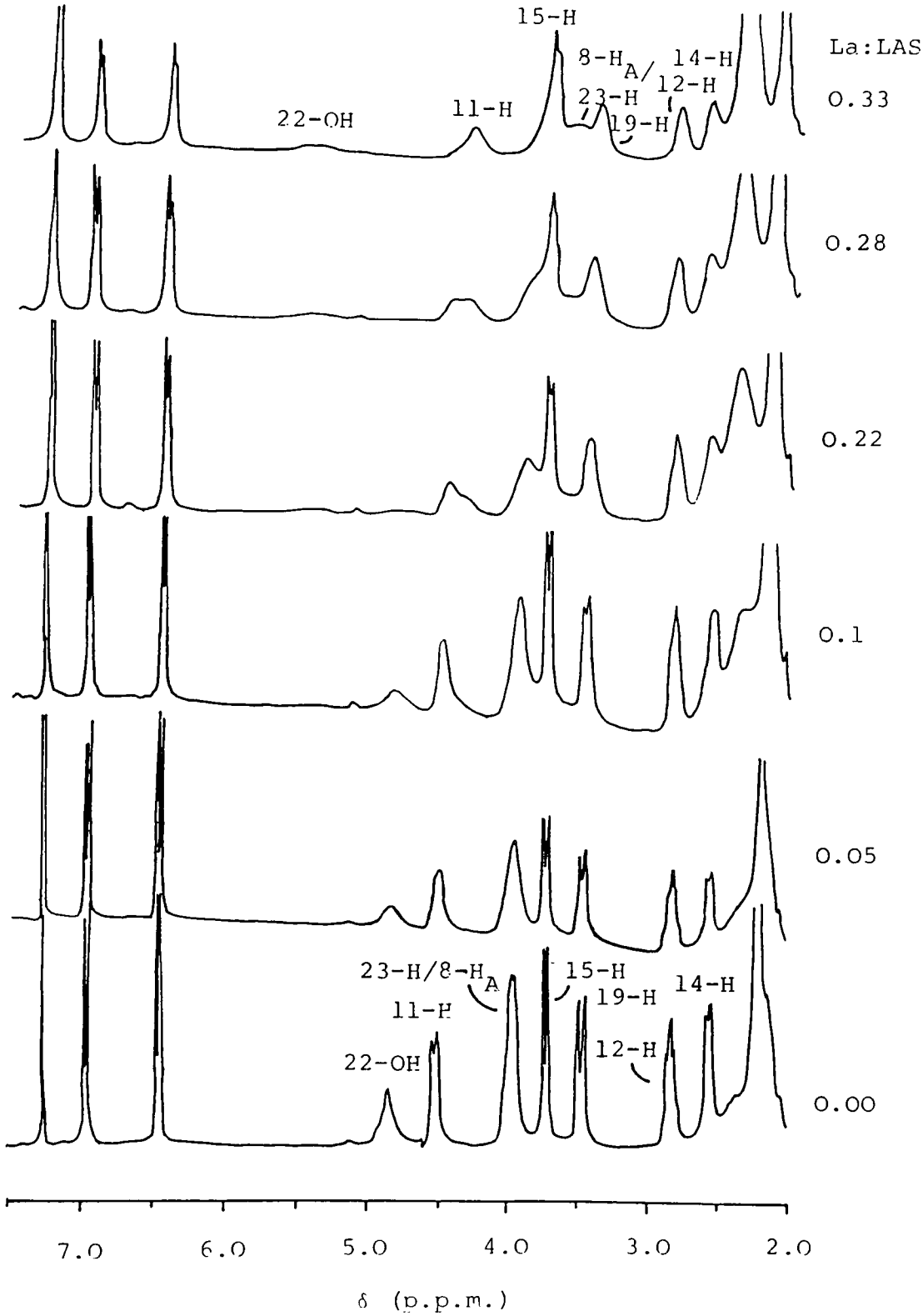

was possible to demonstrate, however, that 10-H does lie beneath the water peak and that the order of doublet methyl resonances remains 23-CH_3, 10-CH_3 and 16-CH_3 moving from low to high field. No identifiable resonances were observed in the broad region of the spectrum between 2.2 ppm and 1.3 ppm, which restricted the number of assignments obtainable from the spectrum. NOEs were used to attempt to overcome the broadness of the spectrum and the interesting observation was made that irradiating 4-CH_3 caused an NOE to 6-H but not to 5-H. T_1 measurements again showed 4-CH_3 and 6-H to have similar relaxation times, whilst the T_1 of 5-H was much longer. This is further evidence of some unusual interaction in the region, and will be discussed further below.

7.3.9 The Effect on the Conformation of $Cd(LAS)_2$ of Increasing the Solvent Polarity

Lasalocid complexes are very soluble in alcohols, and thus methanol was chosen as a good example of a polar solvent. The nmr spectrum of the complex is shown in Figure 7.19. It is apparent that the spectrum is much sharper and all exchange effects seem to have quickened to give a fast exchange system. The spectrum is shown in comparison to the spectrum of the complex in chloroform in Figures 7.20 and 7.21. The region between 4.5 and 2.5 ppm shows marked changes as the complex moves into fast exchange. Complex peaks are observed but these are due to the coincidence of two resonances. The shifts of the resonances are marked on Figure 7.20. Figure 7.21 also reflects the change of exchange conditions, leaving the seven methyl peaks visible.

The sharpening of the spectrum produced good J-decoupling effects which were used to confirm the assignments of the resonances. These are marked on Figures 7.20 and, as far as they could be identified, 7.21, but the mid-spectrum signals are, from low

Figure 7.19

Fully relaxed spectrum of $Cd(LAS)_2$ in d_4-methanol

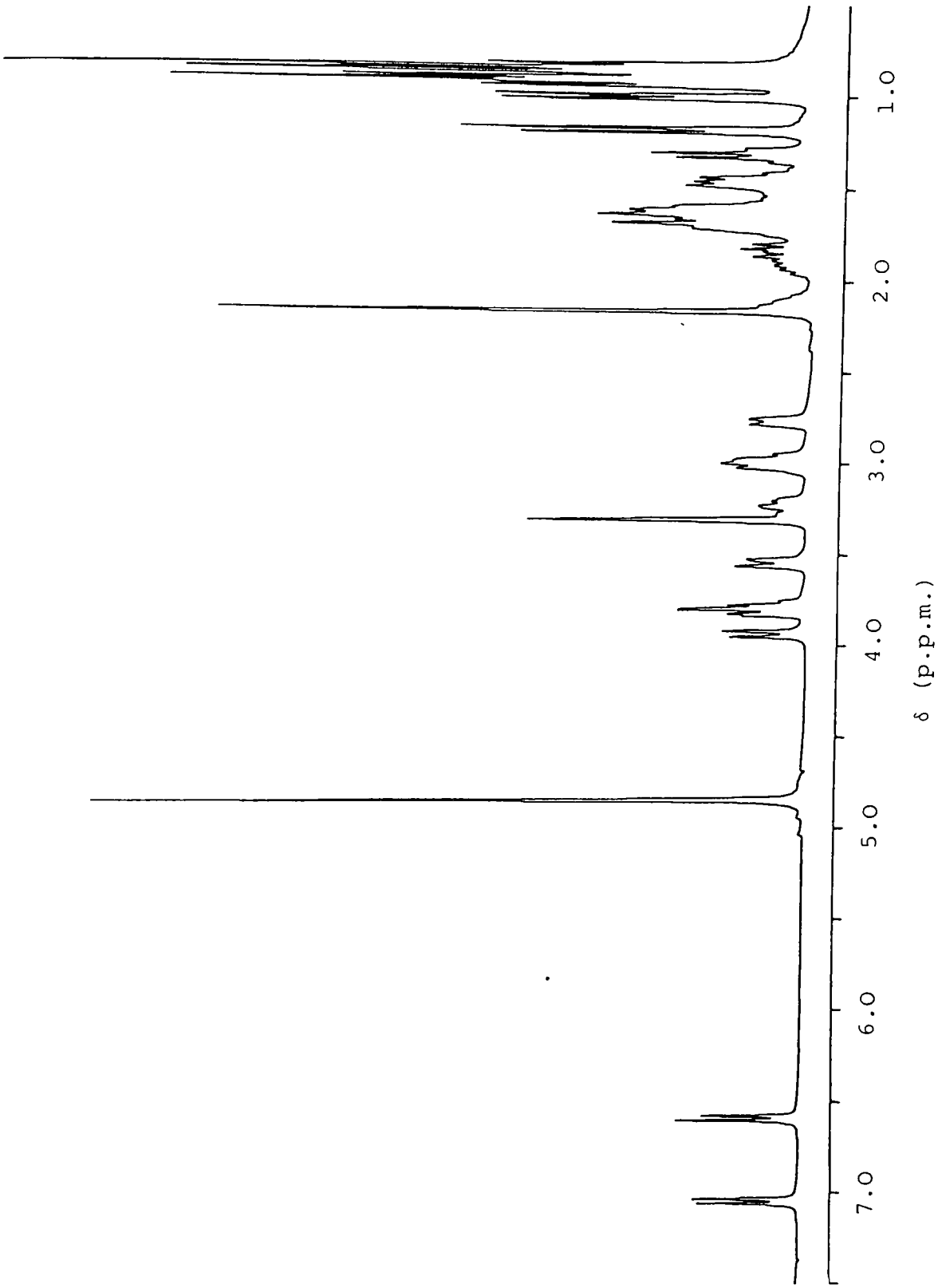

Figure 7.20

Fully relaxed spectrum of $Cd(LAS)_2$ in (a) $CDCl_3$ and (b) d_4-methanol

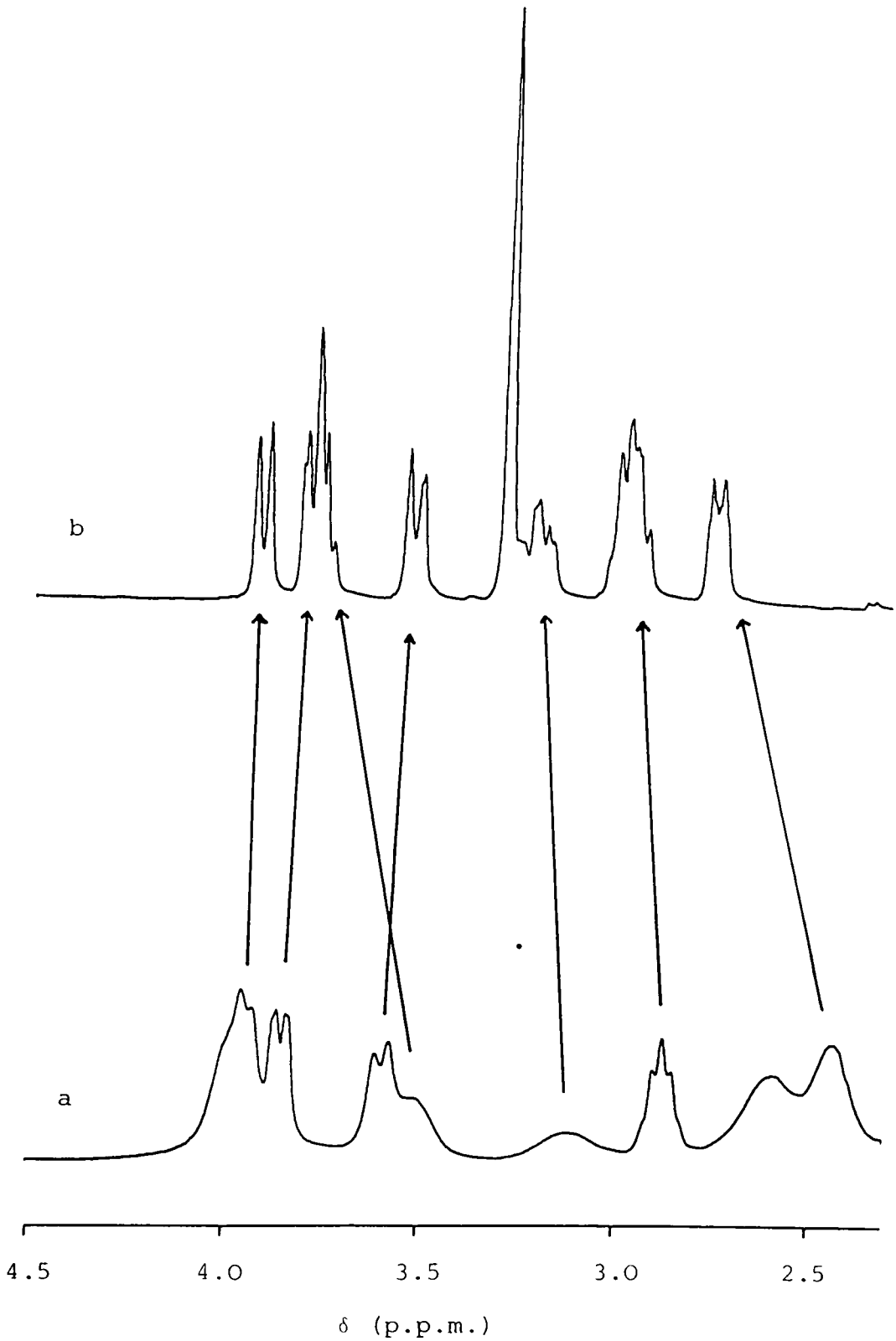

Figure 7.21

Fully relaxed spectrum of $Cd(LAS)_2$ in (a) $CDCl_3$ and (b) d_4-methanol

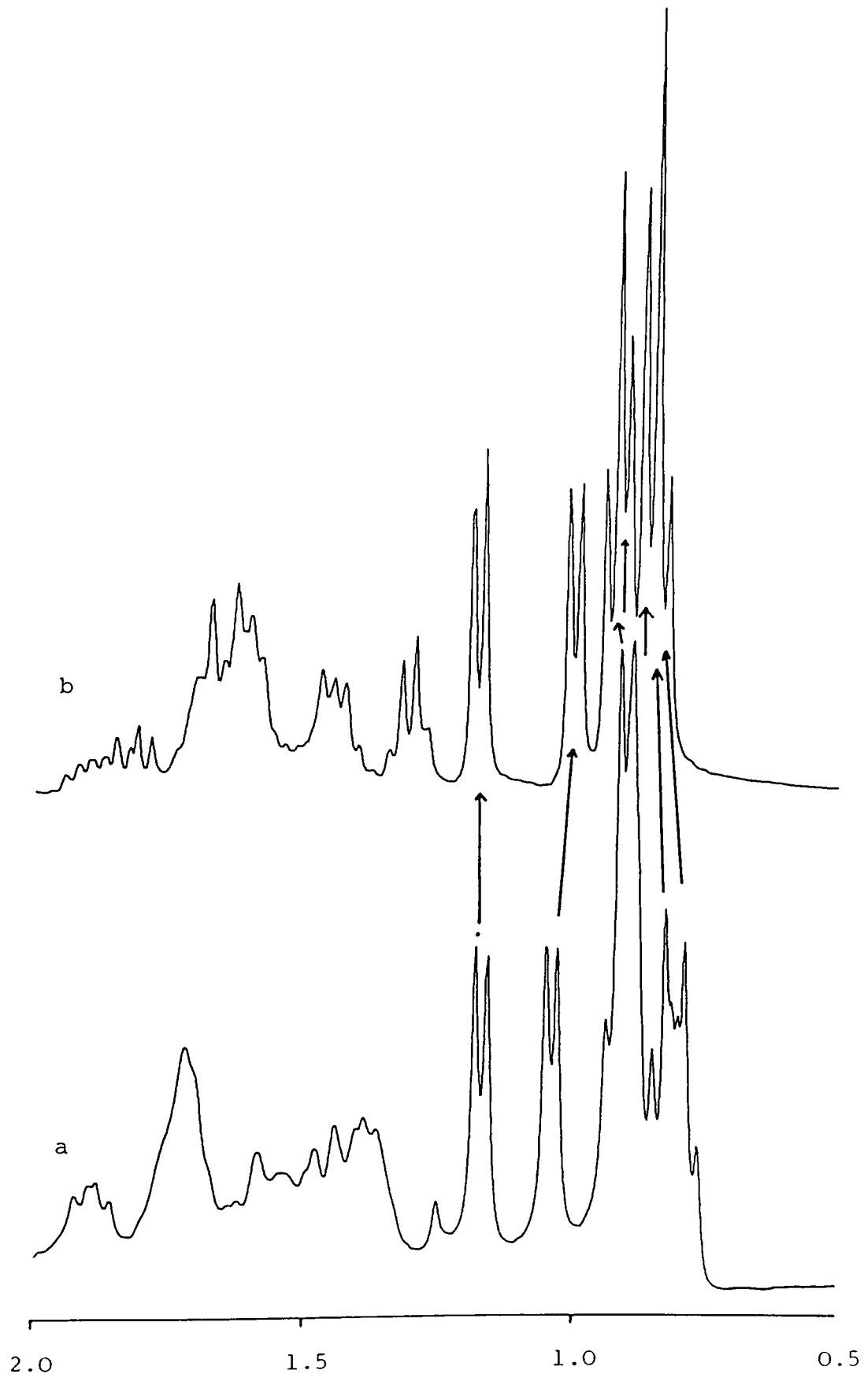

to high field, 11-H, 8-H/23-H, 19-H, 14-H, 12-H and 10-H. There is little movement of the methyl doublets, but two of the methyl triplets (14-CH_3 and 18-CH_3) coalesce to form a six proton peak at 0.9 ppm.

7.4 Discussion

7.4.1 The Accuracy of the Antenuis Assignments

Experiments on several different complexes of lasalocid have shown that the original assignments made by Antenuis on the sodium salt are self-consistent and provide a good basis for assigning other complexes. The assignment of the two aromatic protons, however, to 5-H and 6-H moving upfield, is not obviously supported by observations made in this work.

The interpretation of exchange phenomena to give information about spatial position is very difficult since the observations can be produced by many different factors. Thus the result of the inversion-recovery experiment on the calcium complex could have been brought about by an interaction of one of the protons with another group in the molecule which affected it T_1 time. In the same way, the difference in the extent of broadening in the two doublets in any titration or temperature dependence experiment could be due to the steric hindrance arising from such an interaction; it is clear,though, that the two protons are in different environments.

The data from NOE experiments give a strong indication that the assignments of Antenuis may be incorrect since irradiating 4-CH_3 should produce a strong NOE in 5-H but none (or a weak effect) in 6-H. The interpretation of the data on the basis of Antenuis' assignments would indicate that 4-CH_3 give a reversible strong NOE to 6-H but not to 5-H and 5-H gives a reversible

strong NOE to 6-H. This would indicate that the assignment of the aromatic protons should be reversed, which would make the T_1 data more consistent, in that 4-CH_3 and 5-H would have similar relaxation times and 6-H, which is closest to the sterically constrained 8-H_A is affected and thus the longer T_1.

7.4.2 Intra-molecular Exchange In the Complexes

The nmr spectrum of the lasalocid complexes show two different sorts of resonances; very sharp peaks with well-resolved multiplet structures and broader peaks in which the multiplet structure can only just be made out. This spectrum indicates that different regions of the molecule experience different constraints; comparison of those assigned, broadened resonances with the crystal structure of $Ba(LAS)_2$ show that they tend to arise from the region largely constricted by complexing oxygens. Thus, the central region of the spectrum contains broad peaks from 11-H, 8-H, 23-H, 15-H, 19-H, 12-H 14-H and 10-H and the complexing oxygens lie at carbons 1, 4, 11, 22 and 23. It is thus reasonable to assume that the broadening is brought about by metal binding (the free acid spectrum of Antenuis (11) is very sharp indeed). Those resonances not affected by the constraints are mainly the side-chains which point out of the complex and those resonances which lie at the opposite side of the aromatic ring to the complexing carboxyl group. The broad peaks can be followed by the titration experiments and also the temperature dependence work.

We have concluded that the broad nature of the peaks arise from intermediate exchange effects which are occuring in the molecule. In the lanthanum complex, these are inter-molecular effects due to the exchange between the three lasalocid

complexes. This arises from the large amount of steric hindrance which must arise when packing three anions around the metal; as a consequence, it is highly likely that one of the three is bound only by the carboxylate group and otherwise hanging free in the solution. This is a dynamic equilibrium which gives rise to the intermolecular effects. In addition, intramolecular effects can be seen, in the same way as the binary complexes, which are discussed below. The intermolecular effects are pronounced in 11-H, 22-OH and 23-H, with two peaks visible for each of these resonances during the titration experiments, indicating that the intermolecular binding is occuring at O(4), O(7) and O(8). These are the three resonances with the greatest chemical shift differences between the sodium and lanthanum salts. In the lanthanum complex, the peaks which become broadest are 22-OH, 23-H, 11-H, 12-H, 14-H and 19-H, which also supports the above conclusion.

The calcium and cadmium complexes show a similar behaviour except that there is evidence that the exchange in the system is intramolecular only, with varying combinations of the lasalocid oxygens taking turns to bind the metal, whilst keeping a constant coordination number for the cation. This conclusion arises from the fact that no extra peaks are observed in the calcium: lasalocid titration; thus the spectra represent averages of the spectrum, with certain signals broadened by intramolecular exchange. These are notably 11-H, 15-H, 19-H, 23-H and 22-OH, indicating binding at O(4), O(6), O(7) and O(8). The large chemical shift differences during the titration also support binding at O(4) and O(6). This result is in reasonable agreement with the crystal structure of $Ba(LAS)_2$, given that the crystal structure has frozen one particular conformation out of

the complex and observed that; there is no direct evidence to support assymmetic binding in non-polar solution. The other binding site is at the salycillate group which is in fast exchange. These results are consistent with those of Hanna et al (13) studying the manganese complex by ^{13}C-nmr. The cadmium complex is concluded to be in a similar intramolecular exchange only since no extra signals arise during the cadmium complex: calcium complex titration.

7.4.3 Conformational Changes Due to Solvent Polarity

The nmr spectrum of the $Cd(LAS)_2$ complex in d_4-methanol shows several changes to that in $CDCl_3$. These changes mainly involve the chemical shifts of the resonances and also the line width of several signals. Both these factors indicate that a conformational change has taken place with the change of solvent polarity. It is apparent that there has been a reduction in the number of secondary chemical shifts arising from the nature of the complex; those that remain are generally due to the conformation of each lasalocid anion. This indicates that the hydrogen-bonded structure shown in Figure 7.2 is not completely disrupted by the polar solvent.

The information about the conformation which arises from the linewidth of the signals is of great interest in that it indicates that the entire complex has moved into fast exchange and that binding is no longer taking place by the oxygens along the aliphatic chain or the furan and pyran rings. No direct evidence can be obtained for binding to the carboxylate (and, possibly, O(1)) by proton nmr, but this can be deduced from previous work by Hanna and Everett on the Gd^{3+} complex using ^{13}C-nmr (15). It is also of interest to note that the complex has either become symmetrical about the metal ion or free to move

in the fast exchange timescale.

7.4.4 General Conclusion

The metal-ion complexes of lasalocid are solvent-dependent for their conformation. Thus one may picture their passage through a membrane as a conformational change from the extended structure, with binding at the salicylate group only, in the aqueous phase, to the cage structure in the body of the membrane and out into the extended structure again as the complex passes into the organelle. It would be of great interest to determine whether the binding constants for the two solvents were significantly different, since it would be advantageous to the system to be able to release the calcium ion quickly once the correct site of, say, biomineralisation had been reached. This may be carried out by a competition reaction between the lasalocid complex and the precipitating counter ion. The proton work supports the idea of a conformational change between solvent systems and also explains the very assymetrical crystal structure (7) by identifying exchange processes occurring in the intermediate timescale in the complexes in non-polar solvent systems.

7.5 References

1. Berger, J., Rachlin, A.I., Scott, W.E., Sternbach, L.H. and Goldberg, M.W. *J. Amer. Chem. Soc.* 73, 5295-5298, (1951)
2. Westley, J.W. *J. Antibiotics* 29, 584-586, (1976)
3. Westley, J.W. (ed.) *"Polyether Antibiotics : Carboxylic Ionophores. Volume 1 : Biological Aspects."* Pub. Marcel Dekker, New York (1983)
4. Westley, J.W. (ed.) *"Polyether Antibiotics : Carboxylic Ionophores. Volume 2 : Chemical Aspects."* Pub. Marcel Dekker, New York (1983)
5. Antenuis M.J.O.
6. Maier, C.A. and Paul, I.C. *J. Chem. Soc. Chem. Comm.* 181-182, (1971)
7. Johnson, S.M., Herrin, J., Liu, S.J. and Paul, I.C. *J. Amer. Chem. Soc.* 92, 4423-4435,(1970)
8. Chiang, C.C. and Paul, I.C. *Science (N.Y.)* 196, 1441-1443, (1977)
9. Antenuis, M.J.O. in *"Polyether Antibiotics"* Ed. J.W. Westley, Vol. 2, 245-334. Pub. Marcel Dekker, New York (1983)
10. Seto, H. and Otake, N. in *"Polyether Antibiotics"* Ed. J.W. Westley, Vol. 2, 335-400, Pub. Marcel Dekker, New York (1983)
11. Antenuis, M.J.O. *Biorganic Chemistry* 5, 327-337, (1976)
12. Easwaran, K.RK. and Vishwanath, C.K. *Abstracts of the Xth International Conference on Magnetic Resonance in Biological Systems, Stanford, California.* p192, (1982)

13. Hanna, D.A. Yeh, C., Shaw, J. and Everett, G.W., Jr. *Biochemistry* (1983). In press.

14. Chen, S-T, and Springer, C.S., Jr. *Biorganic Chemistry*, 9, 101-122 (1978)

15. Hanna, D.A. and Everett, G.W., Jr. *J. Amer. Chem. Soc.* (1983) in Press

Chapter 8

A ^{1}H-NMR Study of a Glycopeptide Antifreeze from Fish Plasma

8.1 Introduction

The concept of biomineralisation by selective inhibition is one of the hypotheses proposed to explain the general phenomenon; it is not, however, widely accepted as a satisfactory explanation of the observed facts (1). There are certain macromolecules which do, however, have a clearly defined physiological role as inhibitors of mineral formation in biology. One is Statherin, a phosphoprotein found in saliva, which inhibits hydroxyapatite formation on the teeth (2); another is the gla-containing protein Osteocalcin (Bone-Gla-Protein) which is believed to inhibit unwanted bone-type growth in the body (3) and a third is a series of peptides and glycopeptides which have been found in the plasma of teleost fish which live in polar waters. There are believed to inhibit ice formation in a non-colligative manner. We have been able to obtain good samples of Osteocalcin and the glycopeptide and have started nmr investigations of them. The work on Osteocalcin will not be presented here, but the glycopeptide work is included as an example of the contribution that ^{1}H-nmr spectroscopy can make to the understanding of mineralisation processes.

8.1.1 The Requirement for Agents to Depress the Freezing Point of Water in Tissues of Polar Fish

The temperature of polar waters during the winter season is usually at the freezing point of sea water, -1.9^{o}C, which is below the freezing point of the plasma of typical marine fish (-0.8^{o}C) (4). Any freezing of the plasma in fish leads to inevitable death, even if the body has completely thawed again (5). The polar fish will not freeze until the temperature drops below -2.0^{o}C;

this results in death (6). Many fish, which have been found to contain the antifreeze agents, live out their lives in these freezing conditions and have been found to use the ice growths in the freezing water as protection against predators (7).

In most temperate marine fish, the main electrolyte in the plasma is NaCl, which is responsible for 85% of the colligative freezing point depression (8). The balance arises from trace quantities of K^+, Ca^{2+}, urea, glucost and the free amino acids (9). Fletcher has found (10,11)) that fish inhabiting freezing environments have elevated quantities of NaCl, but the colligative contribution to freezing point depression in these fish is only about 40% to 50%. In these fish, the freezing point depression necessary is achieved by the presence of the peptides and glycopeptides in the colloidal fraction of the blood. The former range between 3 200 and 14 000 daltons (12) whilst the glycopeptides are found in many sizes between 2 600 and 34 000 daltons (13). On a weight for weight basis, both forms of anti-freeze are as effective as NaCl in depressing the freezing point; by molarities, however, the antifreeze molecules are between 200 and 300 times more effective than the calculated colligative effect at depressing the freezing point (14). Melting of ice in the presence of the glycopeptides or peptides follows the expected colligative effect rather than a reveral of the non-colligative process by which the system freezes. The proteinaceous antifreezes are kinetic reagents which inhibit ice formation.

8.1.2 The Biochemistry of the Glycopeptides

The glycopeptides were first isolated from the blood of Antartic nototheniid fish by DeVries and Wohlschlag in 1969 (15). They are present in a concentration of approximately 3.5% (w/v) of most of the body fluids except the crytosol and the urine. As many as eight separate glycopeptides have been isolated in the body fluids, except the bile and intestinal fluid, which contain only two low molecular weight forms (2 400 to 3 400 daltons (16,17).

Glycopeptides 1 to 5 are composed of repeating units of alanine and threonine in a tripeptide, with a disaccharide, n-acetyl galactosamine-(1→ 3)-galactose linked to the -OH of the threonine. The sequence is shown in Figure 8.1. The amino acid sequence of the peptide is -ala-ala-thr-. Glycopeptides 6,7 and 8 differ from the others in that proline replaces alanine at residue 7 of the primary sequence, and appears at every third position thereafter (18,19); glycopeptide 8 is a heterogenous mixture of three identical sized glycopeptides with the proline successively at position 1, 2 and 3 of the tripeptide sequence. Glycopeptides have also been isolated from fish from arctic waters and are largely identical, except that the proline positions in glycopeptide 8 varies and that arginine is occasionally found (20, 21).

8.1.3 Physicochemical Properties of Glycopeptides

Both peptides and glycopeptides have been shown to be expanded molecules, the work on glycopeptides having involved X-ray scattering, circular dichroism and ^{13}C-NMR (22-25). There has been no detailed study and no crystal structure has been obtained; the peptides, in contrast, have been found to have a

Figure 8.1

The sequence of the repeating unit in the antifreeze glycopeptide

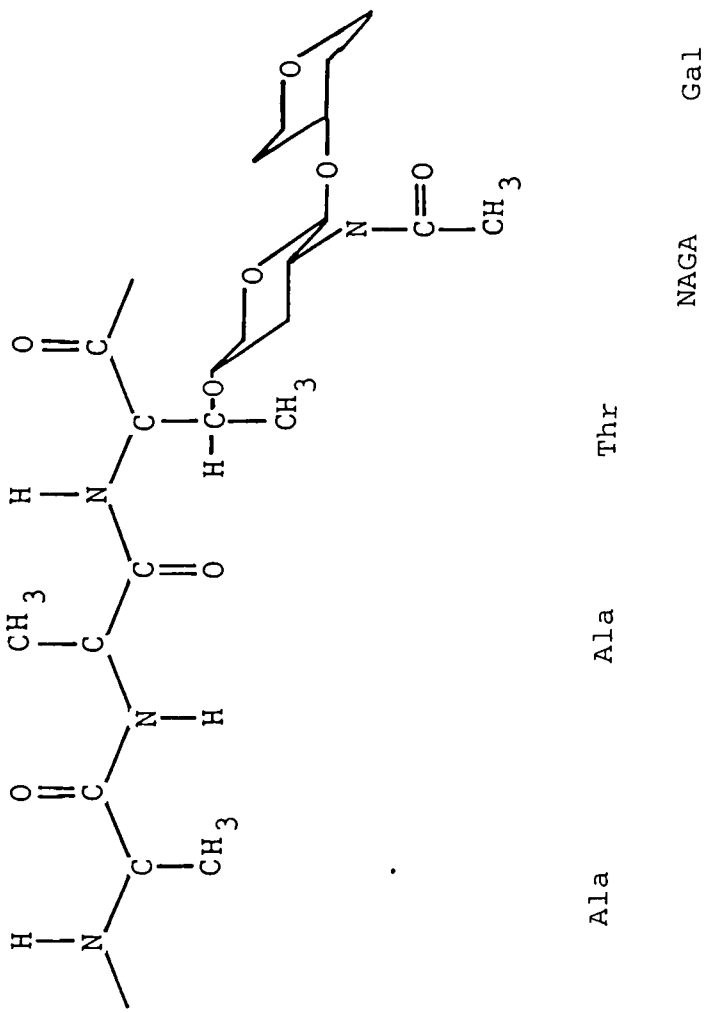

helical structure, with aspartate and threonine separated by two alanine residues, giving a separation of the polar 'head-groups' ($-COO^-$ in the aspartate and -OH in the threonine) of 4.5 Å in a regular repeat (26). This value is significant in that it is also the separation of the oxygens parallel to the a-axis in an ice crystal.

The freezing point of water which contains antifreeze glycopeptide is depresses far below the predicted colligative temperature. The system is entirely stable; in a 2% solution of the glycopeptide, a 100 μm diameter seed crystal will melt at about 0.02°C, but will not increase in size until the temperatur drops to -1.2°C. In between these temperatures, neither melting nor growth occurs, even over a period of several weeks (27). When the temperature drops below this value, the resulting growth is very fast, but occurs in long spicules along the unfavoured c-axis of ice (14) (Note that the normal pattern of ice growth is in hexagonal plates parallel to the a- and b-axes of the unit cell, and not along the c-axis). The effectiveness of the glycopeptides falls off rapidly below a certain molecular weight.

8.1.4 Hypotheses on the Inhibitory Action of Antifreeze Agents

Several hypotheses have been put forward as to the action of agents which act as antifreezes and many of these have been adapted to the specific case of the peptide and glycopeptide antifreezes. These include immobilation of water, inhibition of nucleation and adsorption-inhibition. The most recent hypothesis, put forward by DeVries (28) maintains that nucleation of ice crystals is an essential part of the inhibition process. Once the crystallites have grown to a diameter of about 100 μm the helical peptides, which have an overall length of about 100 Å,

adsorb onto the hexagonal growth areas of the a- and b-axis, breaking them up into several small areas (the non-polar residues will point out into the water, which will increase the free energy at those points). These small areas are much less stable for crystallisation, having a high energy and an increasing curvature as the slow growth occurs about a small point. The size of the antifreeze is critical for this process; if it is too small, the curves of growth could join up again to form a "cusp" around the antifreeze, which will stimulate growth again as it is unstable due to edge tension. This will eventually lead to a new edge for crystal growth to proceed. This is prevented by the adsorption of large molecules (27). Raymond (29) has shown that the spacing of the antifreeze molecules on the ice crystals is a function of their solution concentration and their size. If one assumes that there is a single surface density of antifreezes and a square array distribution of antifreeze molecules on the crystal face, then the freezing point depression is proportional to the square root of the concentration of the adsorbed molecules. This prediction has been shown to hold for the peptides and large glycopeptides (27).

8.1.5 The Aim of This Study

The conformation and mode of action of the glycopeptide antifreezes is not known. It was our intention to make use of ^{1}H-nmr to monitor the changes in the spectrum of the antifreeze as the temperature of the solution was lowered to the temperature of polar seawater. We also hoped to assign the spectrum by means of two-dimensional COSY spectroscopy and spin-spin decoupling. The experimental details of the COSY procedure will be found as

an appendix to this chapter.

8.2 Sample Preparation

The glycopeptide sample studied was provided by Dr. A.L. DeVries, Department of Physiology and Biophysics, University of Illinois. The sample contained three glycopeptides of Type 3, 4 and 5. They differed in their molecular weights, being 23 500, 17 500 and 10 500 daltons respectively. The sample was prepared for nmr as described in chapter 2, but was prepared to a concentration of 4% w/v in D_2O in the presence of NaCl in order to mimic the *in vivo* conditions. Spectra were run on the 300 MHz machine for low temperature and pulse work and on the 470 MHz machine for a two-dimensional COSY spectrum.

8.3 Results

8.3.1 Preliminary Assignment of the Glycopeptide

The nmr spectrum, shown in Figure 8.2, revealed that there is little or no tertiary structure in the glycopeptides. This is because the spectrum is composed of a limited number of resonances without particular broadening or shifts. This was surprising as the sample contained three different moities which each had many amino acid and saccharide components. One may thus conclude that the observed spectrum arises from each repeating unit, giving an apparent molecular weight of about 600 daltons. The peptide component may be recognised by the $-CH_3$ resonances from the three amino acids in the sequence. Each of the methyl groups is shifted slightly from its random-coil position (30) which is indicative of some interaction between the groups in the repeating unit. The data is shown in Table 8.I. The positions of the α-CHs of all three amino acids and the β-CH of the threonine are not immediately apparent, but the CPA spectrum in

Figure 8.2

Antifreeze glycopeptide from fish plasma

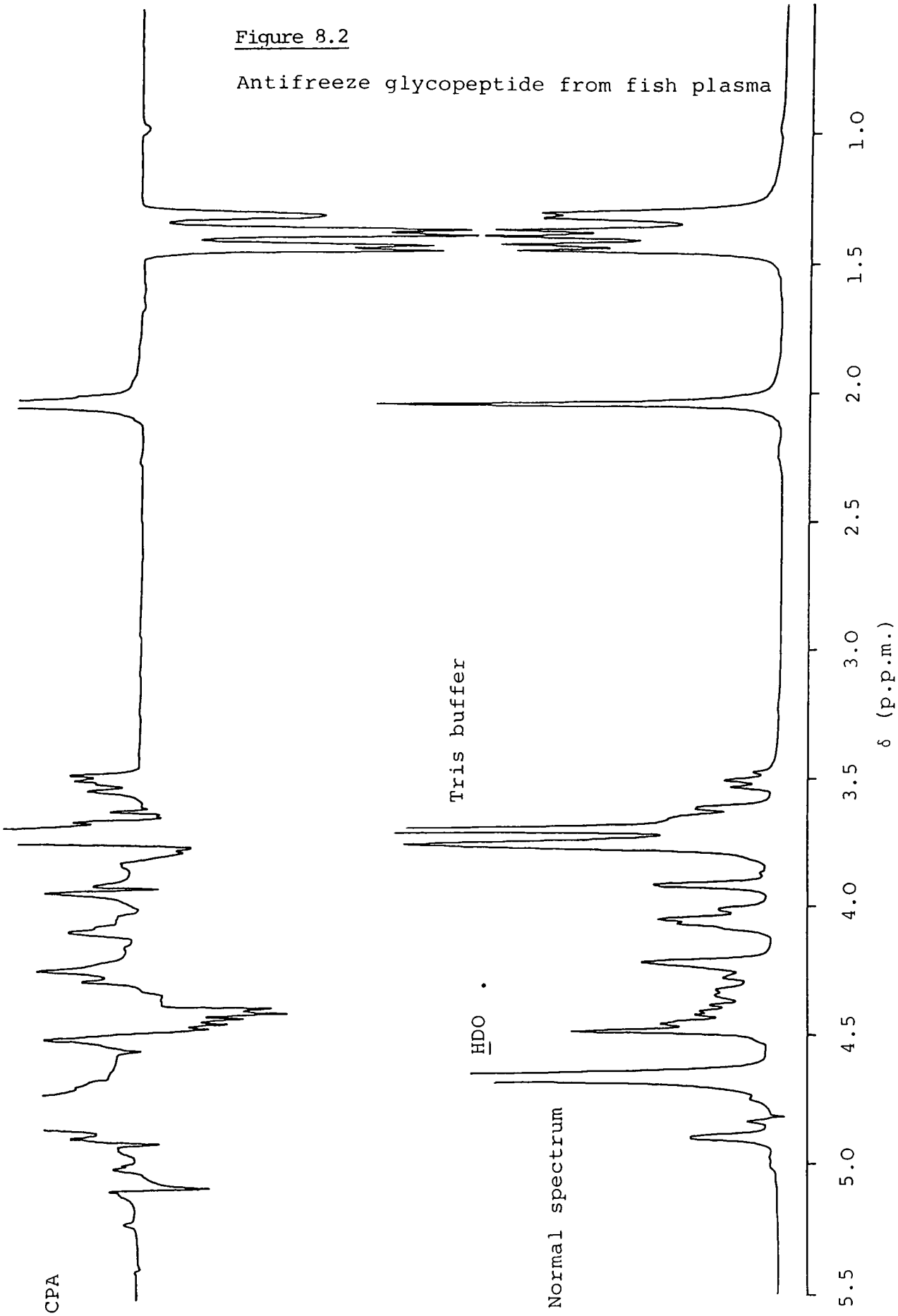

Table 8.I

Predicted and Observed Chemical Shifts of the Amino Acids in the Antifreeze Glycopeptides

Chemical shift values are given in parts per million. In the Difference column, a negative sign represents an upfield shift.

Residue		Random Coil	Observed	Difference
Ala	-CH	4.349	4.424	0.075
	$-CH_3$	1.395	1.436	0.041
Ala	-CH	4.349	4.384	0.035
	$-CH_3$	1.395	1.378	-0.017
Thr	-CH	4.346	4.440	0.094
	-CH	4.220	4.326	0.106
	$-CH_3$	1.232	1.314	0.082

Figure 8.2 shows several sharp doublets at 4.384,4.424 and 4.440 ppm, which are approximately correct for the α-CH resonances in a random peptide, but not in an α-helix or β-sheet, which again indicates little or no overall structure. The alanine resonances can be distinguished from the threonine resonances by the larger spin-spin coupling constant, 6.9 Hz for ala but only 6.3 Hz for thr. This confirms the assignments of the methyls, but cannot be used to distinguish between the α-CHs.

The glycopeptide resonances are more difficult to distinguish at first sight, but two signals may be assigned by inspection; the sharp singlet at 2.040 ppm is due to the N-acetyl methyl and the signal downfield of the water at 4.885 ppm arises from the proton at position 1 of the furan rings. This resonance was used as the starting point for assigning the spectrum using J-decoupling and two-dimensional COSY (COrrelated SpectroscopY).

8.3.2 Pulse Experiments on the Glycopeptide

The major assignment work of both components of theglycopeptide was carried out by COSY and J-decoupling the saccharide resonances. The results of the COSY experiment are shown in Figure 8.3. This shows the coupling of the methyls of the amino acids to their α-CHs and β-CH, in the case of threonine. The peptide signals are shown to lie at 4.326 ppm for the β-CH of the threonine, 4.384 ppm for the α-CH of alanine 1 and 4.424 ppm for the α-CH of alanine 2. The α-CH of the threonine is not apparent in the COSY spectrum due to the extension of the water peak and is not decoupled when irradiating the β-CH, but the CPA spectrum indicates that it lies with the other α-CHs.

The identification of the saccharide begins from the proton at position 1 and may be followed around the rings from

Figure 8.3

J-decoupling Results of antifreeze glycopeptide

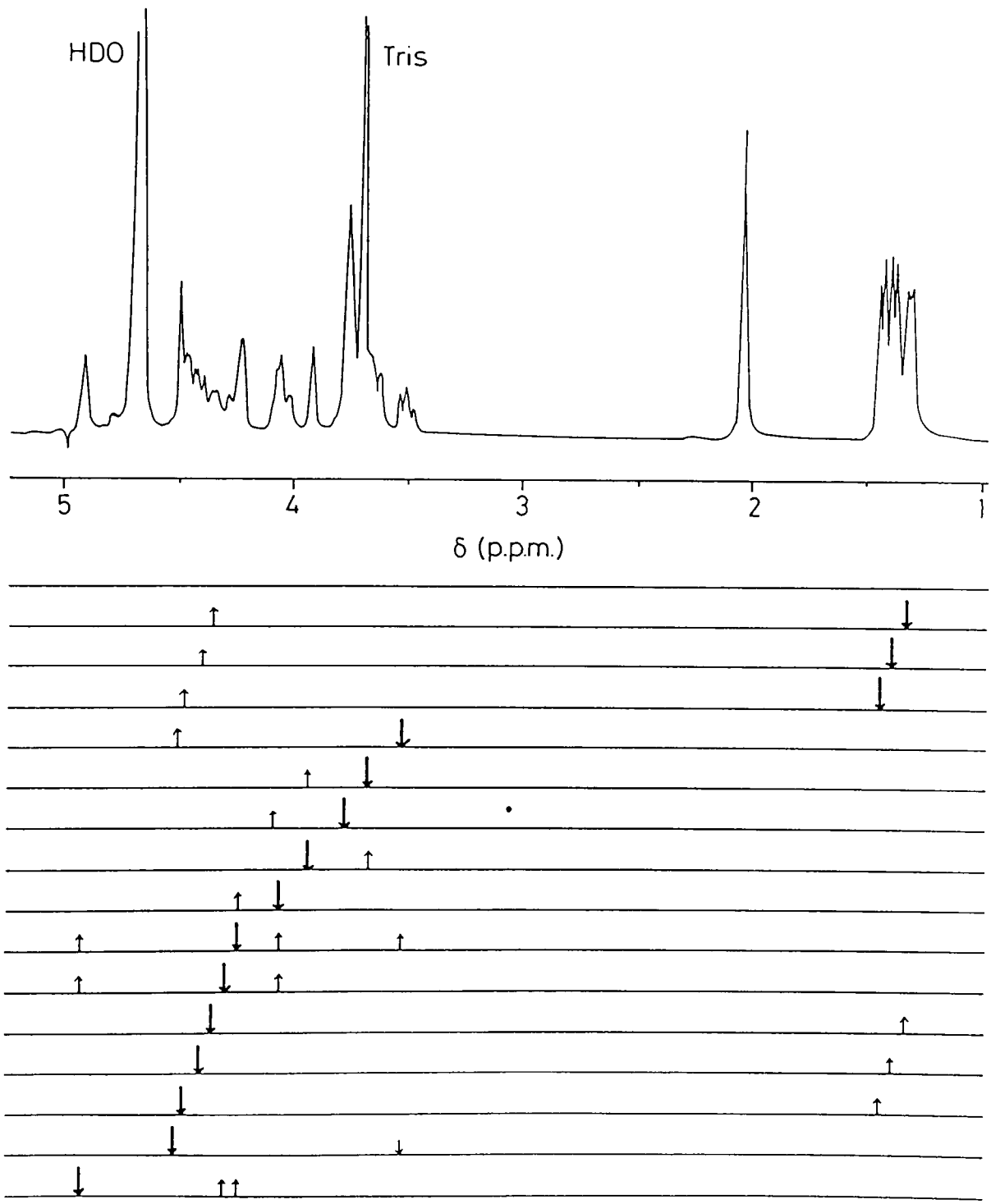

position 1 to 4 in each saccharide, by following the cross peaks from the 1-H of N-acetyl galactosamine (NAGA) at 4.9 ppm and the 3-H' of galactose (Gal) at 4.02 ppm, giving tentative assignments listed in Table 8.II. This Gal signal is upfield shifted due to the linkage to the NAGA, which runs from position 1 of the NAGA to position 3 of galactose; an equivalent shift is also observed in the ^{1}H-nmr spectrum of lactose, which consists of glucose-(1⟶ 4)-galactose. Resonances from the -OH protons of the sugars are never seen when running spectra in D_2O due to an isotope exchange effect. The protons in the 5 and 6 positions in each case are believed to be obscured by the Tris buffer and have small couplings so that the cross-peaks are not visible either. The COSY spectra are shown in Figures 8.4 and 8.5.

8.3.3 Temperature Dependence of the Glycopeptide

The sample of glycopeptide was prepared to be comparable to the *in vivo* condition and this sample was run at low temperature to try to monitor the action of inhibiting ice formation. The changes in the spectrum are shown in Figures 8.6 to 8.9. The first pair follow the methyls as the temperature is dropped from 300 K to 270 K (this is -3°C, but no ice formation was observed). It can be seen that the threonine -CH_3 is affected at once and broadens and eventually shifts downfield into Ala 2. The alanine methyls are affected to the extent of being slightly broadened, but they are still clearly doublets at 270 K. This indicates that the threonine is moving from fast into intermediate exchange, but that the alanines are essentially unaffected.

Figures 8.8 and 8.9 follow the downfield resonances over the same temperature drop. It is interesting to note that the first resonance to be affected is the β-CH of the Threonine

Figure 8.4

COSY spectrum of the antifreeze glycopeptide from fish. The entire spectrum, showing both peptide and saccharide cross-peaks.

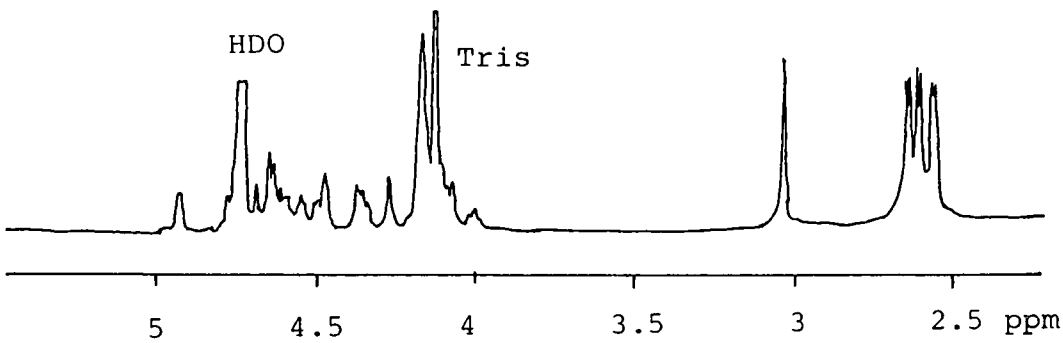

Figure 8.5

COSY spectrum of the antifreeze glycopeptide from fish. The region containing the resonances from the disaccharide. Tentative assignments are marked; numbers refer to the carbon position. Resonances from the galactose are marked with a prime.

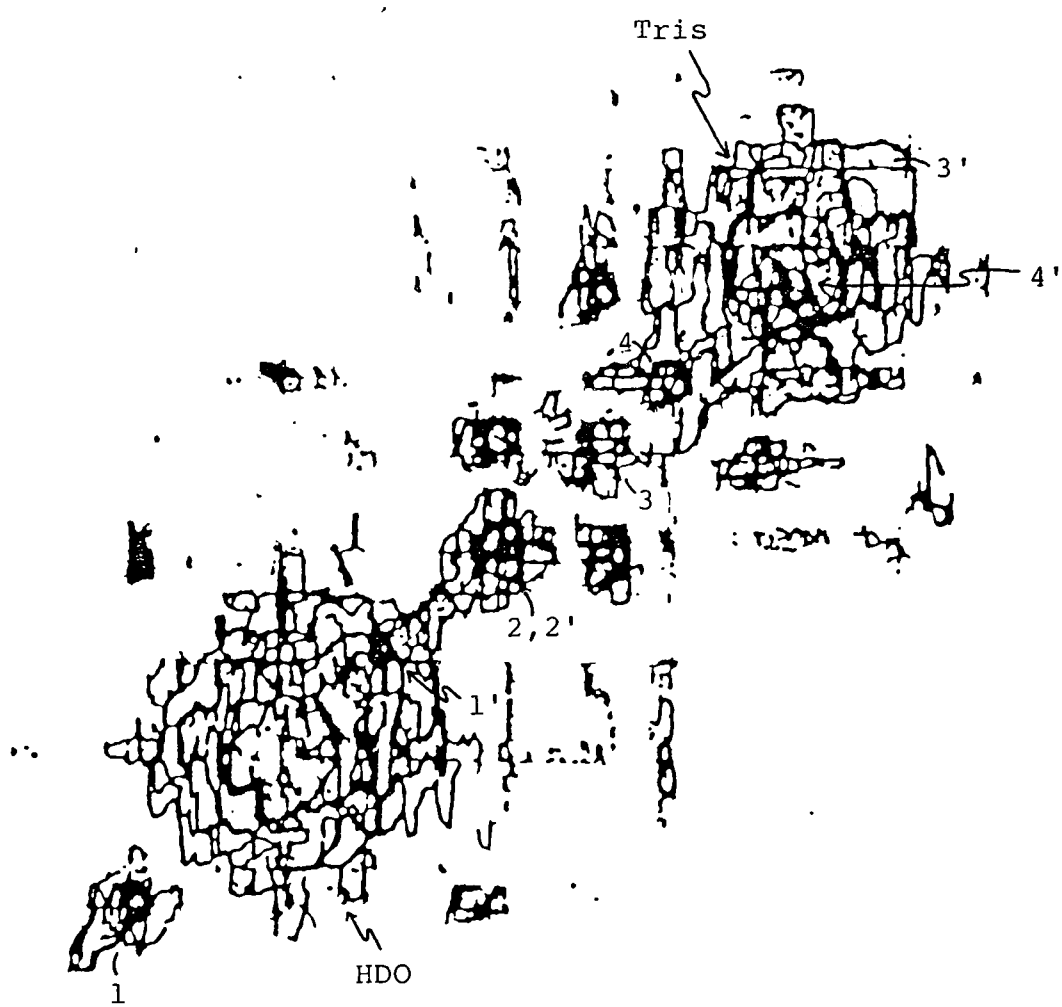

Figure 8.6

Temperature dependence of the antifreeze glycopeptide

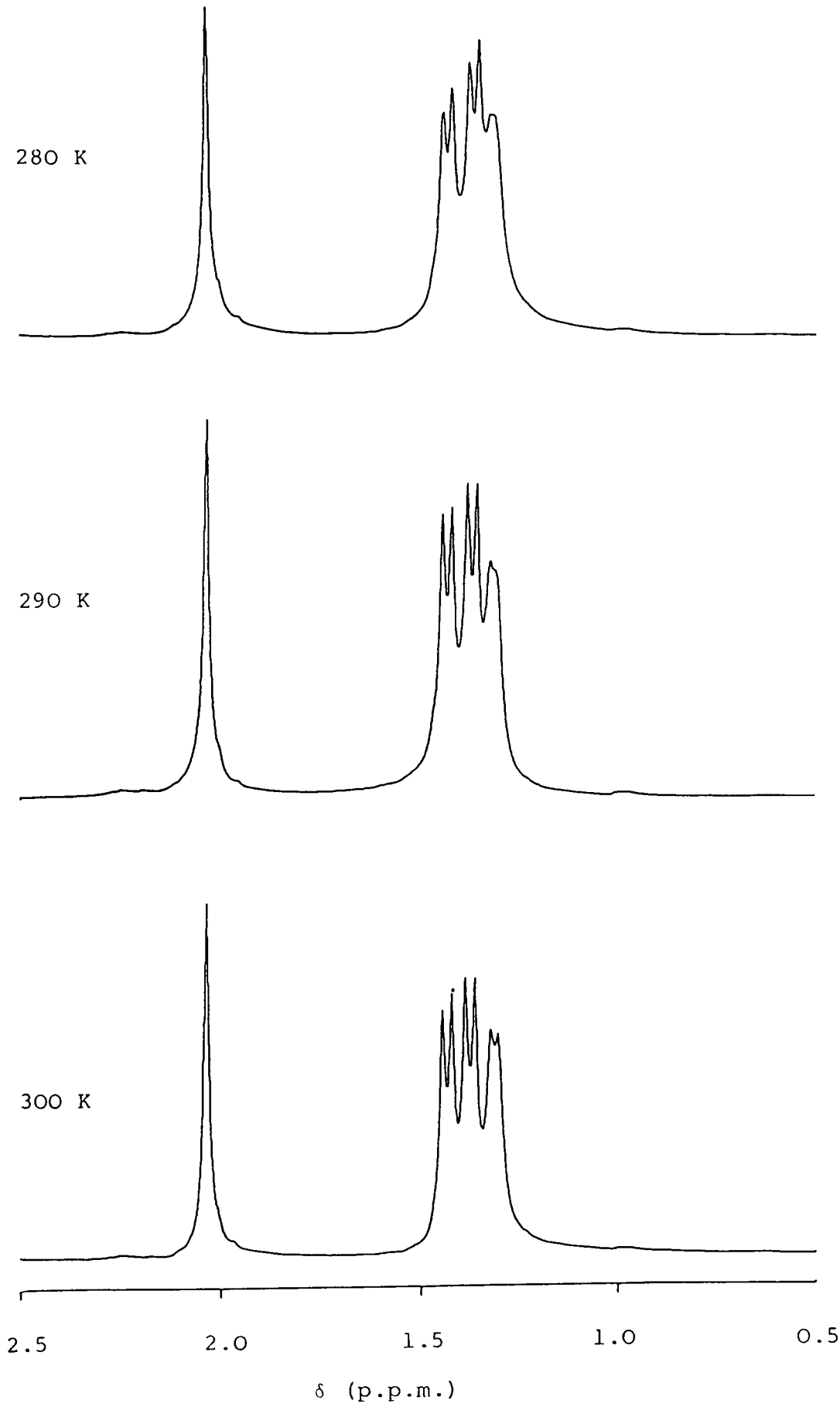

Figure 8.7

Temperature dependence of the antifreeze glycopeptide from fish plasma (continued)

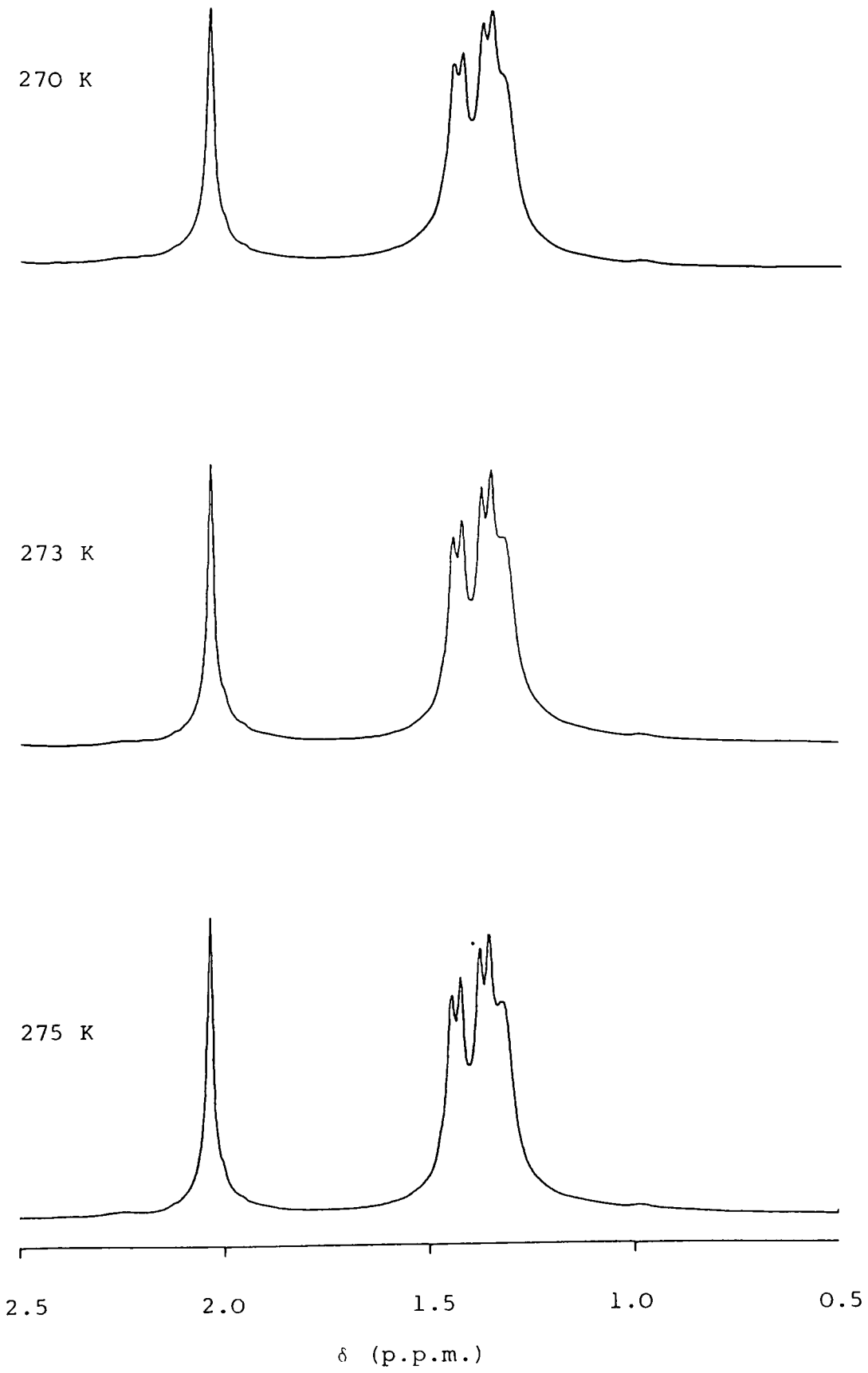

Figure 8.8

Temperature dependence of antifreeze glycopeptide

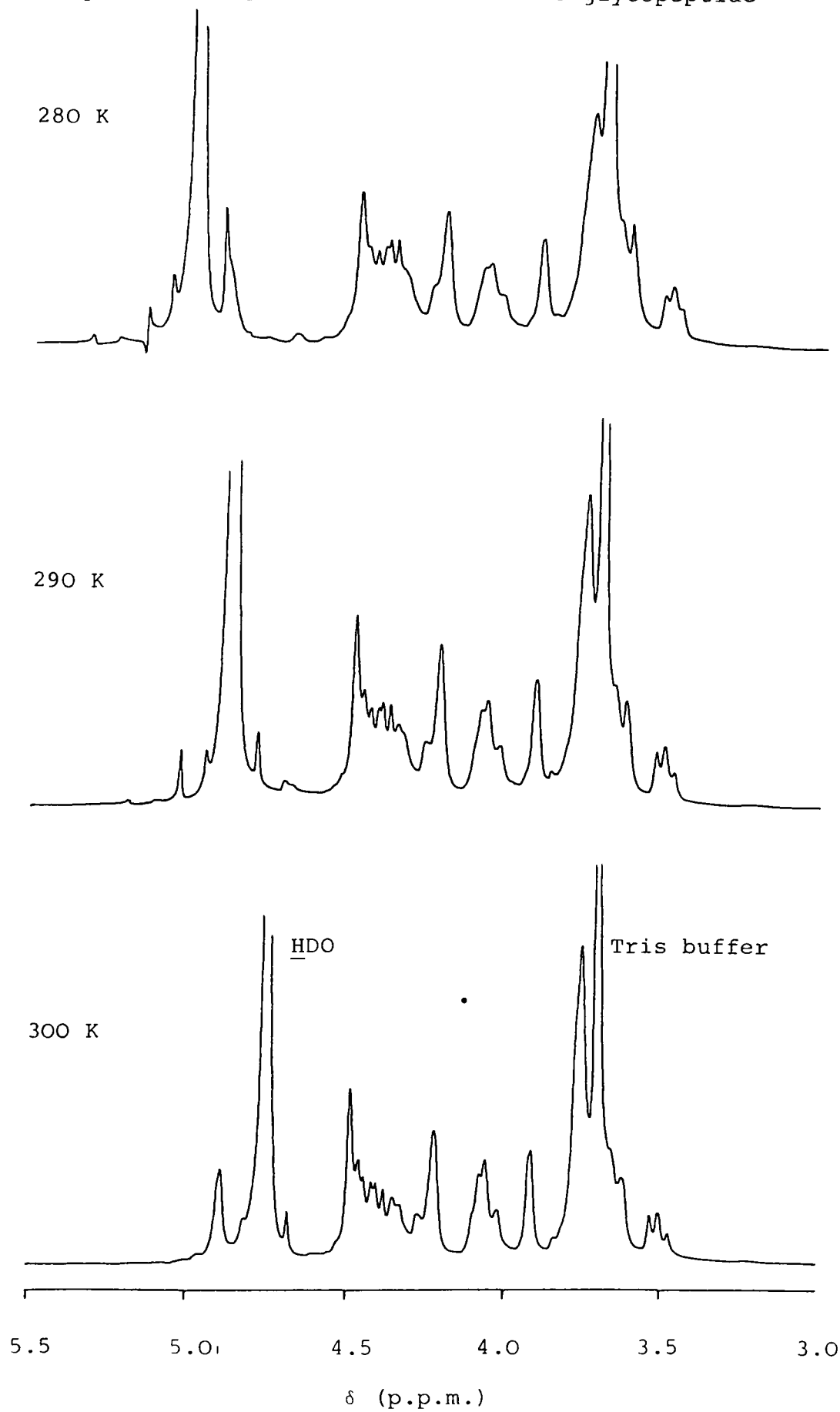

Figure 8.9

Temperature dependence of the antifreeze glycopeptide

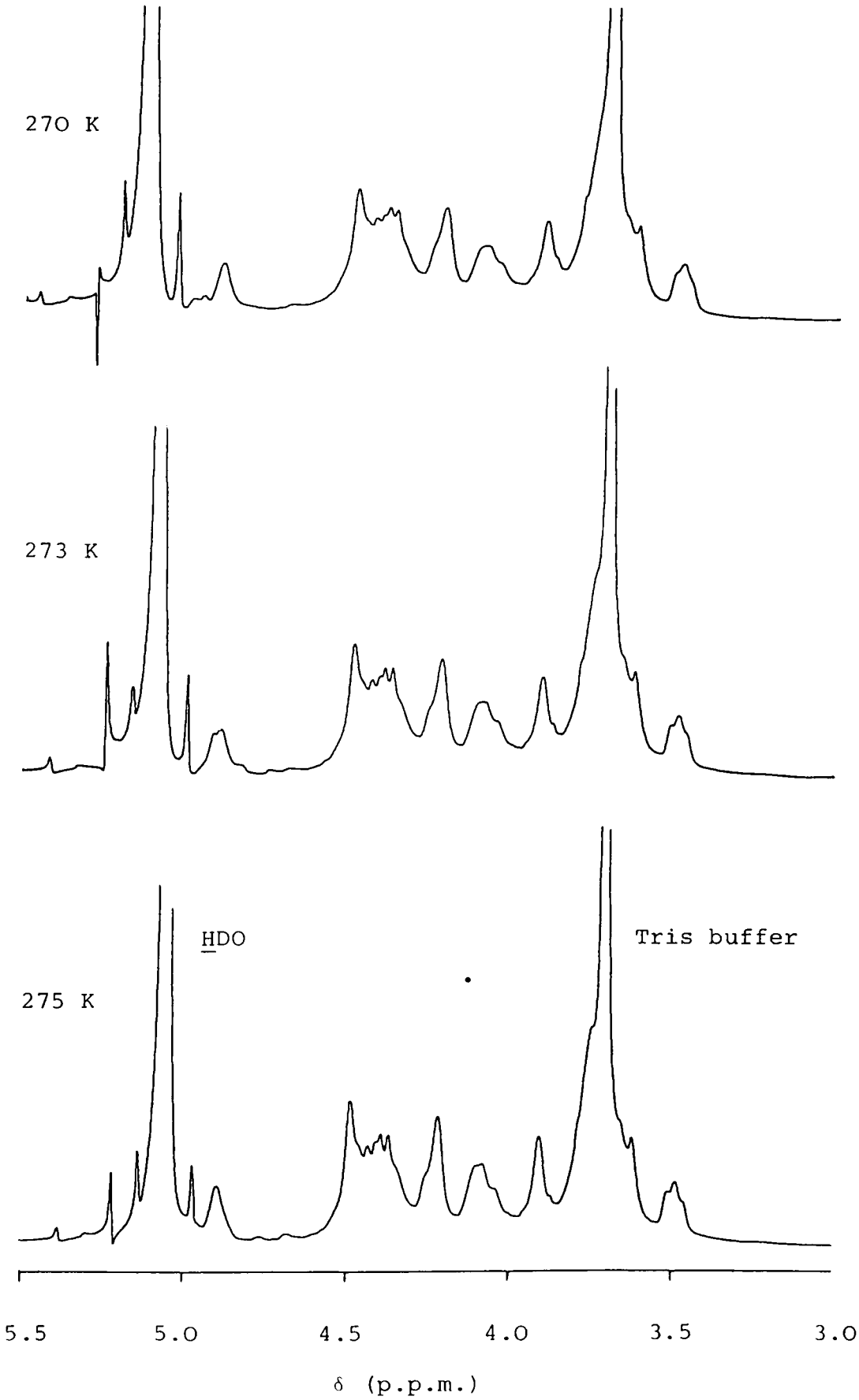

Table 8.II

Assignment of the Resonances Arising from the Disaccharide Fraction of the Glycopeptide

Assignment	Chemical Shift (ppm)
N-acetyl galactosamine	
1-H	4.90
2-H	4.25
3-H	4.02
4-H	3.74
Galactose	
1-H'	4.495
2-H'	3.22
3-H'	3.501
4-H'	3.62

Notes

1. These assignments are tentative due to the quantity of Tris buffer in the sample, which obscured several resonances.
2. All -OH protons are labile and exchange with the D_2O
3. Protons at carbons 5 and 6 of both saccharide rings are believed to lie under the Tris peak, but have small couplings, preventing their being observed in the COSY spectrum.

followed by the α-CH of the same residue. The saccharide resonances begin to be affected at 280 K, with gross broadening between 275 and 270 K. The alanine α-CHs remain comparatively sharp, indicating that they play little or no role in the inhibition process.

8.4 Discussion

The glycopeptide acts as the sum of each of its repeating units when observed by ^{1}H-nmr spectroscopy. This confirms the previous reports that it has little or no tertiary structure, having an extended conformation, which was confirmed by the random-coil positions of the α-Hs. The two alanines in the repeating sequence are not equivalent, each giving identifiable resonances. There also appears to be little interaction between the saccharides and the threonine at ambient temperature; when the temperature is lowered, however, the exchange processes in the threonine and then the saccharide are slowed, resulting in a broad, intermediate exchange spectrum. The only exceptions to this are the alanine residues, which remain in fast exchange throughout the experiment. One possible explanation for this behaviour is that the conformation adopted by the glycopeptide is the one required for binding and a lowering of the temperature brings about a restriction of movement of the saccharide through the ether linkage to the threonine. This could be brought about by the onset of hydrogen bonding via the N-acetyl carbonyl atom to the threonine; it should be noted, however, that the methyl from this group is not affected by the change.

It is apparent that the conformation is set in the solution phase and not just through adsorption to the ice crystallite since there is no appearance of signals due to a

'bound' versus 'free' system. It would be reasonable to assume that the greatest efficiency would arise from the adsorption of a preformed structure, rather than relying on the correct conformation forming once part of the molecule has bound to the crystallite.

This work is not able to determine a definitive mode of antifreeze action, but Haschemeyer et al (31) showed by nmr that the amount of water bound to the glycopeptide in solution is not great; indeed other work (32) has found that the glycopeptides bind only slightly more water than other proteins of equivalent size in solution. This indicates that the inhibition does not arise through immolisation of water but by binding to crystallites. If this is, indeed the case, then this work indicates that there is a preforming of the correct structure before binding takes place.

8.5 References

1. Mann, S. *Structure and Bonding* 54, 125-174, (1983)
2. Hay, D.I., Moreno, E.C. and Schlesinger, D.H. *Inorg. Perspectives Biol. Med.* 2, 271-285 (1979)
3. Price, P.A., Lothringer, J.W., Baukol, S.A. and Reddi, A.H. *J. Biol. Chem.* 256, 3781-3784, (1981)
4. Black, V.S. *Univ. Toronto Biol. Ser. 59* 71, 53-89, (1951)
5. Scholander, P.F., Vandam, L., Kanwisher, J.W., Hammel, H.T. and Gordon, M.S. *J. Cell Comp. Physiol.* 49, 5-24 (1957)
6. DeVries, A.L. and Lin, Y. in *"Adaptions within Antarctic Ecosystems"*. Ed. G.A. Llano. pp439-458, (1977). Pub. Gulf Publishing Co., Houston.
7. Andriashev , A.P. in *"Antarctic Ecology"*. Ed. M.W. Holdgate, Vol. 1, pp 297-304, (1970). Pub. Academic Press, London.
8. Gordon, M.S., Andur, B.N. and Scholander, P.F. *Biol. Bull.* 122, 52-62, (1962)
9. Potts, W.T.W. and Parry, G.*"Osmotic and Ionic Regulations in Animals"* 19, (1964). Pub. Pergamon Press, Oxford.
10. Fletcher, G.L. *Can. J. Zool.* 55, 789-795, (1977)
11. Fletcher, G.L. *Can. J. Zool.* 59, 193-201, (1981)
12. DeVries, A.L. *Comp. Ciochem. Physiol.* 73A, 627-640, (1982)
13. DeVries, A.L. in *"Biochemical and Biophysical Perspectives in Marine Biology"*. Eds. J.S. Sargent and D.W. Mallins. Vol. 1, pp289-330, (1974). Pub. Adademic Press, London.
14. DeVries, A.L. *Science, N.Y.* 172, 1152-1155, (1971)
15. DeVries, A.L. and Wohlschlag, D.E. *Science N.Y.* 163, 1074-1075, (1969)

16. O'Grady, S.M., Ellory, J.C. and DeVries, A.L. *J. Exp. Biol.* 98, 429-438, (1982)

17. O'Grady, S.M.,Ellory, J.C. and DeVries, A.L. *J. Exp. Biol.* 104, 149-162, (1983)

18. Lin, Y., Duman, J.G. and DeVries, A.L. *Biochem. Biophys. Res. Commun.* 46, 87-92, (1972)

19. Morris, H.R., Thompson, M.R., Osuga, D.T., Ahmed, A.I., Cham, S.M., Vanderheede, J.R. and Feeney, R.E. *J. Biol. Chem.* 253, 5155-5162, (1978)

20. Raymond, J.A., Lin, Y. and DeVries, A.L. *J. Exp. Zool.* 193, 125-130, (1975)

21. Fletcher, G.L., Addison, R.F., Slaughter, F. and Hew, C.L. *Arctic* (1983) in Press

22. Ananthanaryanan, V.S. and Hew, C.L. *Biochem. Biophys. Res. Commun.* 74, 685-689, (1977)

23. Raymond, J.A., Radding, W. and DeVries, A.L. *Biopolymers*, 16, 2575-2578, (1978)

24. Franks, F. and Morris, E.R. " *Biochim. Biophys. Acta* 540, 346-356, (1978)

25. Berman, E., Allerhand, A. and DeVries, A.L. *J. Biol. Chem.* 255, 4407-4410, (1980)

26. DeVries, A.L. and Lin, Y. *Biochim. Biophys. Acta* 495, 388-392 (1977)

27. Raymond, J.A. and DeVries, A.L. *Cryobiol.* 9, 541-547, (1972)

28. DeVries, A.L. *Proc. Roy. Soc. Lond. B.* (1983) In press

29. Raymond, J.A. PhD Thesis, University of California (1976)

30. Bundi, A. and Wuthrich, K. *Biopolymers* 13, 285-297, (1979)

31. Haschemeyer, A.E.V., Guschlbaur, W. and DeVries A.L. *Nature (Lond.)* 269, 87-88, (1977)

32. Duman, J.H., Patterson, J.L., Kozak, J.J. and DeVries, A.L. *Biochim. Biophys. Acta* 626, 332-336, (1980)

Appendix

Two-dimensional Correlated Spectroscopy

2D COSY spectra were run on the 470 MHz nmr spectrometer using the method of Jenner et al (1). 256 FIDs of 80 scans each were accumulated, each in a 2K block. The phase cycling used was timed to ensure N-type peak selection. The resulting spectrum is Fourier Transformed twice; for the first transform, a sine-bell resolution enhancement function was applied before the transform, whereas a trapezoidal function was used for the second transform. For the second transform, the width of the spectrum was reduced by zero-filling to obtain the best possible resolution. The results of the second transform were displayed in Magnitude Calculation mode.

Results were examined both in the form of contour plots and cross-sections in an attempt to detect relatively weak cross-peaks.

Reference

1. Jenner, J., Meier, B.H., Bachmann, P. and Ernst, R.R. *J. Chem. Phys.* 71, 4546-4553, (1979)

Chapter 9

Conclusions

9.1 The Biominerals

This work has shown that the minerals precipitated in biological systems are laid down in different structures to those in geological systems. The biominerals are aggregations of crystallites, controlled in direction of growth, polymorph and overall morphology by the organic matrix laid down before, or in conjunction with the mineral formation. The difference in the polymorphs in otoconia and otoliths can arise from very few substitutions of the amino acids in the organic matrix. It would be of great interest to isolate the organic matrix from normal otoconia and vaterite otoconia arising from pathological conditions in order to detect any substitutions that may have occurred. Evidence that the matrix controls the polymorph formation is also available from bivalve mollusc shells (see chapter 1) in which all three forms of calcium carbonate can be found in different regions of the shell.

It is apparent that a variety of mechanisms have evolved to form minerals most suited to their required purpose, which is chiefly one of support or defence. Thus the mechanism proposed for coccolith formation is different in many respects from that proposed for gastropod shell formation. There is an overall progression in these mechanisms which has become more apparent with discoveries in recent years. This progression may be traced back to the amorphous silica structures of diatoms and choanoflagellates. These structures are essentially formed by

pumping silica into preformed vesicles. This allows the required morphology to be formed by the liquid, which then sets into the solid structure. Such a mechanism is acceptable only for amorphous substances; the control necessary for a crystalline mineral is far greater, since a crystal will rapidly grow out of control once the free energy of crystallisation becomes favourable unless a tight control is placed upon the growth in some way. The first attempt at this arises in the calcite formation of the coccolith. This is an intracellular process carried out inside a vesicle, but with the addition of a basal plate and an acidic polysaccharide to control the growth.

Biomineralisation becomes an extracellular process as the evolutionary scale progresses. In bivalve molluscs, the mantle cells generate firstly the outermost proteinaceous periostracum (which plays no part in the mineralisation process) and then the mineralisation matrix layers discussed in chapter 5 above. These are laid down beneath the periostacum, which isolates the growing system from the seawater. The calcium carbonate is then precipitated at preformed sites onto this matrix. One refinement to this process is the formation of γ-carboxyglutamic acid (gla) to bind the calcium more tightly at key sites. This amino acid has not been unequivocably shown to be present in invertebrates, but is found in many vertebrate calcerous growths, both normal and pathological in phosphate systems. Bone itself contains very many proteins, only some of which contribute to the mineralisation process. Indeed, it is probably accurate to suggest that the major role of collagen, the most abundant of the organic components, is to import tensile strength and flexibility to the structure, rather than any mineralisation function it might perform.

9.2 The Organic Matrix

It has not been possible, as was originally hoped, to fully isolate and characterise any matrix protein from a mineralising system. However, certain important peripheral aspects have been investigated. It has been shown, by means of nucleation experiments, that the action of inhibition of calcium carbonate formation, seen from *in vitro* solutions of matrix proteins arises from the conformational change experienced when they are dissolved away from their insoluble matrix. This conformational change can be adjusted by immobilising the acidic matrix onto a support; the immobilised protein allows mineralisation to take place.

It can be seen from the studies on the ionophore Lasalocid-A that calcium is easily complexed by many oxygen atoms and it is apparent that this complexing of calcium is carried out by the mineral matrix. It should also be recalled that under such circumstances, calcium can be moved around the matrix by being passed from one carboxylate to another in much the same way as the oxygen ligands of lasalocid take turns to be complexed to the metal. It remains most important to fully characterise the matrix proteins; until this is achieved, model complexes involving increasing numbers of carboxylates would make an interesting and valuable study. A peptide containing the repeating unit -(asp-gly)- would be of interest in modelling the sequence determined for aragonite formation.

9.3 Epitaxial Growth

There has been a good deal of discussion in the biomineralisation field as to the importance of epitaxial growth and the likelihood of this mechanism being the method used to

achieve the required control over the mineral. It is my belief that biomineralisation is too broad a field to be encompassed by a single mechanism, but that crystalline minerals can best be controlled by epitaxial growth. This form of growth in the context of biomineralisation involves the binding of calcium (or carbonate) to ligands lying in a predetermined position in order to bring about the crystal formation of a specific polymorph of the required mineral. This would reduce the energy required to nucleate a crystal. Amorphous minerals have no need of such close control; indeed a possible reason why silica is selected over calcium carbonate (which is saturated in sea water) in the lowest forms of life that mineralise is that they have not evolved the required organic matrix to control crystal growth. The situation in bone is complicated by the cellular processes occurring in the matrix, but the mineralisation requirement remains essentially the same as that of calcium carbonate systems, which epitaxial control of growth can best provide.

Appendix 1

The Double Diffraction Phenomenon in Electron Diffraction

(Adapted from "Interpretation of Electron Diffraction Patterns" by K.W. Andrews, D.J. Dyson and S.R. Keown. Pub. Plenum Press, New York, 1971)

Double diffraction (double reflection) arises from the appearance of finite intensity at integral points on single crystal spot patterns which would otherwise have zero intensity. It arises from a ray being diffracted by one set of crystal planes, and then further diffracted by a second set of crystal planes of different d-spacing. The conditions for this phenomenon to arise are that the ray must be perpendicular to $(h_1k_1l_1)$, the first set of planes, which contain the vector $\underset{\sim}{d}^*_1$, and then that the ray between the two sets of planes, $\underset{\sim}{d}^*_2$, and the re-diffracted ray must also lie in a second plane not necessarily coincident with the first. In reciprocal species, this gives rise to a point P_1, lying $\underset{\sim}{d}^*_1$ from the origin for the singly diffracted ray and then a point P_3, $\underset{\sim}{d}^*_2$ from P_1. The angles involved are small (about 2^o) and thus it is possible that diffraction could also have occurred from the $(h_2k_2l_2)$ planes giving rise to a point P_2, where OP_2 is a vector $\underset{\sim}{d}^*_{2,P_2}$, which is a point on the reciprocal lattice of non-zero intensity. It follows that $OP_3 = \underset{\sim}{d}^*_3$ is also a reciprocal lattice vector. The relationship of these vectors to each other can be seen in Figure 1. It can thus be shown that for all cases,

$$h_3 = h_1 \pm h_2$$

$$k_3 = k_1 \pm k_2$$

$$l_3 = l_1 \pm l_2$$

(all plus or minus signs)

The intensity at P_3 will only be finite if it is finite at P_2. Hence, if P_2 is a point of zero intensity due to the lattice type (such as centred lattices), double diffraction will not produce a finite reflection at P_3. Thus face-centred and body-centred lattices will not produce additional spots by double diffraction, although certain intensities may be altered.

Figure A.1

Elements of double diffraction, showing the various vectors defined in the text.

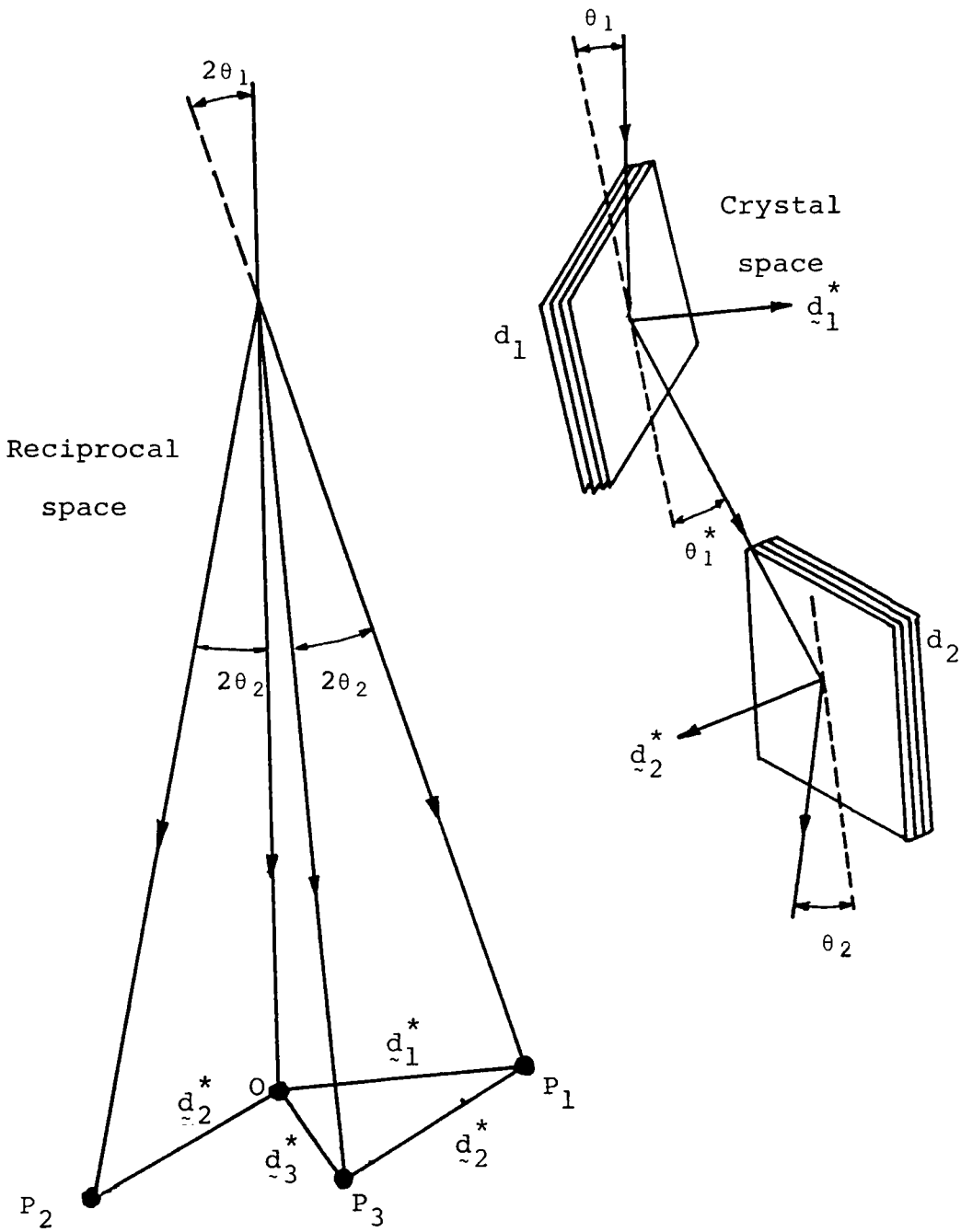

Appendix 2

Crystallographic Data of Minerals Studied in this Thesis

1. Aragonite (1)

Symmetry: Orthorhombic

Space group: Pmcn

Lattice parameters: a = 4.959 Å

b = 7.968 Å

c = 5.741 Å

$\alpha = 90^{\circ}$

$\beta = 90^{\circ}$

$\gamma = 90^{\circ}$

Volume of unit cell = 226.907 $Å^3$

2. Calcite (2)

Symmetry; Hexagonal

Space group: $R\bar{3}c$

Lattice parameters: a = 4.990 Å

b = 4.990 Å

c = 17.002 Å

$\alpha = 90^{\circ}$

$\beta = 90^{\circ}$

$\gamma = 120^{\circ}$

Volume of unit cell: 366.590 $Å^3$

3. Ice (3)

Symmetry: hexagonal

Space group: P^6_{3mmc}

Lattice parameters: a = 4.498 Å

b = 4.498 Å

c = 7.338 Å

$\alpha = 90^\circ$

$\beta = 90^\circ$

$\gamma = 120^\circ$

Volume of unit cell: 125.657 $Å^3$

4. Gold (4)

Symmetry: cubic

Space group: $O_H^5 - F_{m3m}$

Lattice parameters : a = 4.0786 Å

b = 4.0786 Å

c = 4.0786 Å

$\alpha = 90^\circ$

$\beta = 90^\circ$

$\gamma = 90^\circ$

Volume of unit cell: 67.818 $Å^3$

References

1. de Villiers, J.P.R. *Amer. Min.* 56, 758-767, (1971)

2. Chessin, H., Hamilton, W.C. and Post, B. *Acta Cryst.* 18, 689-693, (1965)

3. Bertie, J.E., Calvert, L.D. and Whalley, E. *J. Chem. Phys.* 38, 840-846, (1963)

4. Thomson, G.P. *Proc. Roy. Soc. Lond. A.* 128, 641-648, (1930)